ISSN - 0132-1447

GEORGIAN NATIONAL ACADEMY OF SCIENCES

საქართველოს მეცნიერებათა ეროვნული აკადემია

Bulletin

მოამბე

New Series
vol. 6, no. 3
SEPTEMBER-OCTOBER-NOVEMBER-DECEMBER

2012

ტ. 6, № 3
სექტემბერი-ოქტომბერი-ნოემბერი-დეკემბერი

GEORGIAN ACADEMY PRESS
TBILISI

«საქართველოს მეცნიერებათა ეროვნული აკადემიის მოამბე»
«BULLETIN OF THE GEORGIAN NATIONAL ACADEMY OF SCIENCES»
Scientific Journal Appearing in English & Georgian in Three Issues Annually

Founded in 1940

Publisher: Loudmila Gverdtsiteli ● *Text Editor:* Arrian Tchanturia

Bulletin of the Georgian National Academy of Sciences presents the Proceedings of the Georgian Academy in different fields of Science and Technology: Mathematical & Physical Sciences, Geology & Chemical Sciences, Biological & Medical Sciences, Engineering & Applied Sciences, Agricultural & Environmental Sciences, Humanities & Social Sciences, etc.

TABLE OF CONTENTS

შინაარსი

Mathematics & Physical Sciences
მათემატიკა & ფიზიკური მეცნიერებანი

საქართველოს მეცნიერებათა ეროვნული აკადემიის მოამბე, ტ. 6, №3, 2012
BULLETIN OF THE GEORGIAN NATIONAL ACADEMY OF SCIENCES, vol. 6, no. 3, 2012

Mathematics

Divergence of Fourier Series with Respect to Systems of Products of Bases

Giorgi Oniani

Faculty of Exact and Natural Sciences, Akaki Tsereteli State University, Kutaisi

(Presented by Academy Member Vakhtang Kokilashvili)

ABSTRACT. It is proved that the feature of function systems being products of quite general type bases is almost everywhere divergence of certain blocks (and consequently, almost everywhere divergence in Pringsheim sense) of Fourier series in integral classes wider than $L(\ln^+ L)^{d-1}$. © *2012 Bull. Georg. Natl. Acad. Sci.*

Key words: *multiple Fourier series, basis, complete orthonormal system, Haar system, divergence.*

Definitions and notation. Let a sequence $\varepsilon = (E_k^{(i)})$ $(k \in \mathbb{N},\ 1 \le i \le 2^k)$ of measurable subsets of $\mathbb{I} \equiv [0,1]$ be such that $|E_k^{(i)}| = 1/2^k$, $E_k^{(i)} = E_{k+1}^{(2i-1)} \cup E_{k+1}^{(2i)}$ and $E_k^{(i)} \cap E_k^{(j)} = \varnothing$ $(i \ne j)$. The Haar type system $H^{(\varepsilon)} = (h_n^{(\varepsilon)})_{n \in \mathbb{N}}$ corresponding to the sequence ε is defined as follows (see e.g. [1, Ch. 3, §4]):

$$h_n^{(\varepsilon)} = 2^{k/2} \chi_{E_{k+1}^{(2i-1)}} - 2^{k/2} \chi_{E_{k+1}^{(2i)}} \qquad (n = 2^k + i,\ \ k \in \mathbb{N},\ \ 1 \le i < 2^k),$$

where χ_A denotes the characteristic function of a set A. For the case $E_k^{(i)} = \left(\frac{i-1}{2^k}, \frac{i}{2^k}\right)$ the construction gives the ordinary Haar system $H = (h_n)$.

Denote by $L^0(\mathbb{I})$ the space of all measurable functions on $\mathbb{I}$ and by P_Φ denote the class of all polynomials with respect to a system of functions $\Phi = (\varphi_n)$.

Following [2, Ch. III, §1] let us say that a Banach space $B \subset L^0(\mathbb{I})$ satisfies the (*)-condition if $B \supset P_H$ and for every $F \in B^*$ there is a function $\psi_F \in L(\mathbb{I})$ such that

$$F(f) = \int_{\mathbb{I}} f\psi_F \qquad \text{for every} \qquad f \in P_H.$$

Let (φ_n) be a basis in a Banach space $B \subset L^0(\mathbb{I})$ satisfying the (*)-condition and (F_n) be the system of functionals dual to (φ_n). (ψ_{F_n}) will be called the system of functions dual to (φ_n).

Let $\Phi^{(1)} = (\varphi_n^{(1)}), \dots, \Phi^{(d)} = (\varphi_n^{(d)})$ be systems of functions on $\mathbb{I}$. Their product $\Phi^{(1)} \times \cdots \times \Phi^{(d)}$ is defined as the system of functions

$$\varphi_n(x) = \varphi_{n_1}^{(1)}(x_1) \cdots \varphi_{n_d}^{(d)}(x_d),$$

where $n = (n_1, \dots, n_d) \in \mathbb{N}^d$, $x = (x_1, \dots, x_d) \in \mathbb{I}^d$. Denote by $\Phi^{(d)}$ the d-th power of a system Φ.

Let for each $1 \le k \le d$: B_k be a Banach space satisfying the (*)-condition, $\Phi^{(k)}$ be a basis in B_k, and let $\Psi^{(k)}$ be the system of functions dual to $\Phi^{(k)}$. Suppose $\Phi = (\varphi_n)_{n \in \mathbb{N}^d}$ and $\Psi = (\psi_n)_{n \in \mathbb{N}^d}$ be the products of the systems $\Phi^{(k)}$ and $\Phi^{(k)}$, respectively. For a function $f \in L(\mathbb{I}^d)$ with $f\psi_n \in L(\mathbb{I}^d)$ $(n \in \mathbb{N}^d)$ the Fourier coefficients and series of f with respect to the system Φ are defined as follows:

$$c_n(f, \Phi) = \int_{\mathbb{I}^d} f\psi_n, \qquad \sigma(f, \Phi) \sim \sum_n c_n(f, \Phi)\varphi_n,$$

respectively.

For a system of functions $\Phi = (\varphi_n)$ and a class $A \subset L^0(\mathbb{I})$ we will write $\Phi \subset A$ if $\varphi_n \in A$ for each n.

Below the convergence and divergence of multiple series will be understood in the Pringsheim sense.

Following [3, Ch. 1, §4], an Orlicz space $M(L)$ is said to satisfy the Δ'-condition if there exist constants $t_0 > 0$ and $c > 0$ such that $M(t_1 t_2) \le cM(t_1)M(t_2)$ if $t_1, t_2 > t_0$.

Result. Olevskii developed the method of expanding the singularities of the Haar system to arbitrary complete orthonormal systems and bases in function spaces. The method is based on the following lemma (see e.g. [2, Ch. III, §1] or [1, Ch. 9, §1]).

Lemma A. *Let $B \subset L^0(\mathbb{I})$ be a Banach space satisfying the (*)-condition and let $\Phi = (\varphi_n)$ be a basis in B. Then there exist a Haar type system $(h_k^{(\varepsilon)})$ and a sequence of indices $n_k \uparrow \infty$ such that each $h_k^{(\varepsilon)}$ is representable in the form*

$$h_n^{(\varepsilon)}(x) = \sum_{n=n_k+1}^{n_{k+1}} a_n \varphi_n(x) + \alpha_k(x) \qquad (x \in \mathbb{I}),$$

where

$$\|\alpha_k\|_B < \frac{1}{2^k},$$

$$\sum_{i=1}^{k-1} \sum_{j=k+1}^{\infty} \left\| \sum_{m=n_j+1}^{n_{j+1}} c_m(\alpha_i, \Phi)\varphi_m \right\|_B < \frac{1}{2^k}.$$

Various applications of Lemma A to the problems of convergence of one-dimensional Fourier series can be found in [2, Ch. III, §1] and [1, Ch. 9, §1].

It is known that (see [4, 5]) $L(\ln^+ L)^{d-1}(\mathbb{I}^d)$ is the widest integral class in which the almost everywhere convergence of Fourier-Haar series is provided. In particular, T. Zerekidze [5] proved

Theorem A. *Let $M:[0,\infty)\to[0,\infty)$ be an increasing function such that $\lim_{t\to\infty}\frac{M(t)}{t(\ln t)^{d-1}}=0$. Then there exists a function $f\in M(L)(\mathbb{I}^d)$ whose Fourier-Haar series diverges almost everywhere.*

G. Karagulyan [6] extended Theorem A to complete orthonormal double systems of the type $\Phi\times\Phi$ with $\Phi\subset L^\infty(\mathbb{I})$. Namely, in [6] the following statement is proved.

Theorem B. *Let $\Phi\subset L^\infty(\mathbb{I})$ be a complete orthonormal system and let $f\in L(\mathbb{I}^2)$ be a function whose Fourier-Haar series diverges almost everywhere. Then there exists an equimeasurable with f function g on $\mathbb{I}^2$ whose Fourier series with respect to the system $\Phi\times\Phi$ diverges almost everywhere.*

In [6], by Theorem A, from Theorem B was derived

Theorem C. *Let $\Phi\subset L^\infty(\mathbb{I})$ be a complete orthonormal system. Then for every increasing function $M:[0,\infty)\to[0,\infty)$ with $\lim_{t\to\infty}\frac{M(t)}{t\ln t}=0$ there exists a function $f\in M(L)(\mathbb{I}^2)$ whose Fourier series with respect to the system $\Phi\times\Phi$ diverges almost everywhere.*

The result of [7, 8] implies

Theorem D. *For every $f\in L\setminus L(\ln^+ L)^{d-1}(\mathbb{I}^d)$ there exists an equimeasurable with f function g on $\mathbb{I}^d$ such that a general term of the Fourier-Haar series of g diverges unboundedly almost everywhere, i.e.*

$$\overline{\lim_{n\to\infty}}\left|c_n(g,H^d)h_n(x)\right|=\infty$$

for almost every $x\in\mathbb{I}^d$, where $H^{(d)}=\left(h_n\right)_{n\in\mathbb{N}^d}$ is a d-tuple Haar system. Consequently, the Fourier-Haar series of g diverges almost everywhere.

Note that before [7] R. Getsadze [9] established that in every integral class $M(L)(\mathbb{I}^2)$ with $\lim_{t\to\infty}\frac{M(t)}{t\ln t}=0$ there exists a function f for which $\overline{\lim_{n\to\infty}}\left|c_n(f,H^2)h_n(x)\right|=\infty$ on the set of positive measure.

The following generalization of Theorems A–D is true.

Theorem. *Let*

- $B_1,\dots,B_d\subset L^0(\mathbb{I})$ *be Banach spaces satisfying the* (*)*-condition;*
- $\Phi^{(1)},\dots,\Phi^{(d)}$ *be bases in* $B_1,\dots,B_d$, *respectively, and* $\left(\varphi_n\right)_{n\in\mathbb{N}^d}$ *be their product;*
- $\Psi^{(1)},\dots,\Psi^{(d)}$ *be systems of functions dual to* $\Phi^{(1)},\dots,\Phi^{(d)}$, *respectively;*
- $(n_k^{(1)}),\dots,(n_k^{(d)})$ *be sequences of indices corresponding to* $\Phi^{(1)},\dots,\Phi^{(d)}$, *respectively, according to Lemma A;*
- $M(L)(\mathbb{I}^d)$ *be an Orlicz space satisfying the* Δ'*-condition;*

- *spaces* $B_1,\dots,B_d$ *be continuously embedded in* $M(L)(\mathbb{I}^d)$;
- $\Psi^{(1)},\dots,\Psi^{(d)} \subset M^*(L)(\mathbb{I}^d)$, *where* $M^*(L)$ *is the space dual to* $M(L)$.

Then for every $f \in M(L)\setminus L(\ln^+ L)^{d-1}(\mathbb{I}^d)$ *there exists an equimeasurable with* f *function* g *on* $\mathbb{I}^d$ *such that*

$$\overline{\lim_{k\to\infty}}\left|\sum_{m\in\Gamma(k)} c_m(g,\Phi^{(1)}\times\cdots\times\Phi^{(d)})\varphi_m(x)\right| = \infty$$

for almost every $x\in\mathbb{I}^d$, *where the blocks* $\Gamma(k)$ *are defined as follows*

$$\Gamma(k)=\left(\left[n_{k_1}^{(1)}+1, n_{k_1+1}^{(1)}\right]\times\cdots\times\left[n_{k_d}^{(d)}+1, n_{k_d+1}^{(d)}\right]\right)\cap\mathbb{N}^d \qquad (k\in\mathbb{N}^d).$$

Consequently, the Fourier series of g *with respect to* $\Phi^{(1)}\times\cdots\times\Phi^{(d)}$ *diverges almost everywhere.*

Remark. Obviously, if $M(L)(\mathbb{I}^d)=L(\mathbb{I}^d)$, then the conclusion of Theorem valid for any $f\in L\setminus L(\ln^+ L)^{d-1}(\mathbb{I}^d)$. In particular, this is the case if $\Phi^{(1)},\dots,\Phi^{(d)}$ are complete orthonormal systems such that $\Phi^{(1)},\dots,\Phi^{(d)}\subset L^\infty(\mathbb{I})$.

მათმატიკა

ფურიეს მწკრივების განშლადობა ბაზისების ნამრავლის სახის სისტემების მიმართ

გ. ონიანი

აკაკი წერეთლის სახელმწიფო უნივერსიტეტი, ზუსტ და საბუნებისმეტყველო მეცნიერებათა ფაკულტეტი, ქუთაისი

(წარმოდგენილია აკადემიის წევრის ვ. კოკილაშვილის მიერ)

დამტკიცებულია, რომ საკმაოდ ზოგადი ტიპის ბაზისების გამრავლებით მიღებული ფუნქციათა სისტემებისათვის დამახასიათებელია $L(\ln^+ L)^{d-1}$-ზე ფართო ინტეგრალურ კლასებში ფურიეს მწკრივის გარკვეული ბლოკების თითქმის ყველგან განშლადობა (და შედეგად, პრინგსჰაიმის აზრით თითქმის ყველგან განშლადობა).

REFERENCES

1. *B.S. Kashin, A.A. Saakyan* (1984), Ortogonal'nye riady. M. (in Russian).
2. *A.M. Olevskii* (1975), Fourier Series with Respect to General Orthogonal Systems. Springer-Verlag, New York-Heidelberg.
3. *M.A. Krasnosel'skii, Ya.B. Rutitskii* (1958), Vypuklye funktsii i prostranstva Orlicha. M. (in Russian).
4. *O.P. Dzagnidze* (1964), Soobshch. Akad. Nauk Gruz.SSR, **34**: 277-282 (in Russian).
5. *T.Sh. Zerekidze* (1985), Trudy Tbiliss. Mat. Inst. Razmadze, **76**: 80-99 (in Russian).
6. *G.A. Karagulyan* (1989), Izv. Akad. Nauk Arm. SSR. Ser. Mat., **24**, 2: 147-159 (in Russian); translation in: (1989), Sovict J. Contemporary Math. Anal. **24**, 2: 44-56.
7. *G.G. Oniani* (2008), Dokl. Akad. Nauk Rossii, **419**, 2: 169-170 (in Russian); translation in (2008), Dokl. Math., **77**, 2: 203-204.
8. *G.G. Oniani* (2012), Anal. Math., **38**, 3: 227-247.
9. *R.D. Getsadze* (2006), Arch. Math., **86**: 331-339.

Received April, 2012

საქართველოს მეცნიერებათა ეროვნული აკადემიის მოამბე, ტ. 6, №3, 2012
BULLETIN OF THE GEORGIAN NATIONAL ACADEMY OF SCIENCES, vol. 6, no. 3, 2012

Mathematics

The Nonlinear Characteristic Goursat Problem for a Nonlinear Oscillation Equation

Rusudan Bitsadze* and Marine Menteshashvili**

* *Department of Theoretical Informatics, Georgian Technical University, Tbilisi*
** *Niko Muskhelishvili Institute of Computational Mathematics of Georgian Technical University, Tbilisi*

(Presented by Academy Member Nikoloz Vakhania)

ABSTRACT. The paper proposes a nonlinear analogue of the characteristic Goursat problem for a nonlinear oscillation equation, which makes it possible to simultaneously define regular solutions and extension domains. The structures of these domains up to the proximity of the points of degeneracy of degree of the equation are described. © *2012 Bull. Georg. Natl. Acad. Sci.*

Key words: *characteristic invariants, general integral, solution definition domain.*

In the works [1, 2] dedicated to linear non-strictly hyperbolic equations much attention is given to the well-known second order equation of nonlinear oscillations

$$u_y^4 u_{xx} - u_{yy} = 0,$$

which depending on the behavior and values of the first order derivative u_y of the sought solution $u(x, y)$ may generate parabolically. Its general integral is represented by means of the generator of groups of solutions which are based on contact transformations. However the question as to the solvability of problems was not considered. If the method proposed there is used for construction of a general integral for an equation with the non-zero right-hand part, then we are faced with great and even insurmountable difficulties.

In the present paper, an analogous question is considered for the equation

$$u_y^4 u_{xx} - u_{yy} = cx^{-2} u_y^4, \qquad c = const \tag{1}$$

which is interesting not only from the theoretical viewpoint, but also as having various practical applications [3-10].

Like in the case for general nonlinear hyperbolic equations, for equation (1) too, linear formulations of boundary value or characteristic problems, except for the Cauchy initial boundary value problem, are meaningless. This fact is caused by the dependence of characteristic families on yet unknown solutions.

The right-hand part of equation (1) along the ordinate axis is unbounded. This property makes it possible to attribute this equation to the class of Euler-Darboux equations [11-12]. By performing multiplication by a factor defining this unboundedness and making some assumptions, we can consider, instead of (1), an equation with the degeneration not only of hyperbolicity but of order, too. However, there may exist solutions along which equation (1) remains hyperbolic. In other words, these are solutions for which the characteristic directions defined by the characteristic roots

$$\lambda_1 = u_y^{-2}, \quad \lambda_2 = -u_y^{-2},$$

do not coincide anywhere. Naturally, the class of hyperbolic solutions of equation (1) is defined by the condition

$$0 \neq \left|u_y(x,y)\right| < \infty .$$

Before formulating a nonlinear analogue of the Goursat problem, let us clarify the general properties of hyperbolic solutions of equation (1). For this we will use the classical characteristic method [13].

As is known, the characteristic roots λ_1, λ_2 give the differential relations of characteristic directions

$$u_y^2 dy - dx = 0, \quad u_y^2 dy + dx = 0. \tag{2}$$

If equation (1) is considered with (2) taken into account, then we come to the following differential characteristic relations

$$x^2 u_y^4\, du_x - x^2 u_y^2\, du_y - c u_y^4\, u\, dx = 0, \quad x^2 u_y^4\, du_x + x^2 u_y^2\, du_y - c u_y^4\, u\, dx = 0.$$

The following theorem is valid.

Theorem 1. *Assuming that* $c > -\dfrac{1}{4}$, *each of the characteristic systems of equation* (1) *admits exactly two first integrals and they are defined in the explicit form*

$$\begin{cases} \xi \equiv \left(u_y^{-1} + u_x\right) x^{\alpha} - \alpha\, u\, x^{\alpha-1} \\ \xi_1 \equiv \left(u_y^{-1} + u_x\right) x^{1-\alpha} - (1-\alpha)\, u\, x^{-\alpha} \end{cases} \tag{3}$$

for the family of the root λ_1 *and*

$$\begin{cases} \eta \equiv \left(u_y^{-1} - u_x\right) x^{\alpha} + \alpha\, u\, x^{\alpha-1} \\ \eta_1 \equiv \left(u_y^{-1} - u_x\right) x^{1-\alpha} + (1-\alpha)\, u\, x^{-\alpha} \end{cases}, \quad \alpha = \frac{1}{2}\left(1 + \sqrt{4c+1}\right) \tag{4}$$

for the family of the root λ_2.

Due to these two pairs of first integrals (ξ, ξ_1) and (η, η_1) which are actually characteristic invariants, it follows that in the class of hyperbolic solutions we can construct two intermediate integrals

$$\xi_1 = \varphi'(\xi), \quad \eta_1 = \psi'(\eta)$$

of equation (1) [13]. In these integrals we denote by φ, ψ arbitrary functions smooth enough to ensure the differentiability of the sought solution up to second order.

Theorem 2. *If* $\varphi,\ \psi \in C^3(R_1)$, *then equation* (1) *is equivalent to a triple of the following relations*

$$x = \left(\frac{\varphi'(\xi) + \psi'(\eta)}{\xi + \eta} \right)^{\frac{1}{1-2\alpha}}, \tag{5}$$

$$y = \frac{1}{4(1-2\alpha)} \left[(\xi + \eta)(\psi'(\eta) - \varphi'(\xi)) + 2(\varphi(\xi) - \psi(\eta)) \right], \tag{6}$$

$$u = \frac{1}{1-2\alpha} \left[\xi \left(\frac{\varphi'(\xi) + \psi'(\eta)}{\xi + \eta} \right)^{\frac{1-\alpha}{1-2\alpha}} - \varphi'(\xi) \left(\frac{\varphi'(\xi) + \psi'(\eta)}{\xi + \eta} \right)^{\frac{\alpha}{1-2\alpha}} \right], \tag{7}$$

which in a certain sense can be taken as a general integral of equation (1), *whereas the invariants* ξ, η *play the role of characteristic variables.*

Thus, the invariants ξ, ξ_1 will be constant along each characteristic of the family of the root λ_1. The invariants η, η_1 will preserve constant values along the characteristics of the family of the root λ_2. This circumstance should be taken into consideration when formulating the problems with regard to the question whether characteristics are included in the data carrier. Based on this principle, we propose the following nonlinear variant of the Goursat problem.

Suppose we are given two arcs γ_1, γ_2 drawn from the common point $(a, f(a))$ and let them be given in the explicit form

$$\gamma_1 : y = f_1(x), \quad a \le x \le b, \quad a < 0, \quad b > 0$$

and

$$\gamma_2 : y = f_2(x), \quad a \le x \le d, \quad d > 0, \quad f_1(a) = f_2(a). \tag{8}$$

Assume that the functions f_1 and f_2 are three times continuously differentiable and the arc γ_1 monotonically ascends, whereas the arc γ_2, vice versa, monotonically descends.

The Goursat problem consists in constructing the solution of a hyperbolic equation using data whose carriers consist only of characteristics. In that case, the problem conditions will be the assumptions that the arc γ_1 is a characteristic of the family of the root λ_1, whereas the arc γ_2 is a characteristic of the family of the root λ_2. But since the characteristic directions of these families at every point are symmetrical with respect the abscissa axis direction, it immediately follows that the requirement

$$f_1'(a) = -f_2'(a)$$

is justified.

The Goursat Problem. Find a regular hyperbolic solution $u(x, y)$ of equation (1) and, simultaneously with it, a domain of its extension when the curves γ_1 and γ_2 are the arcs of the characteristics, and the values

$$u(a, f_1(a)) = \vartheta, \tag{9}$$

$$u_x\left(a, f_1(a)\right) = \delta \tag{10}$$

are given at the common point.

The assumption that the arcs γ_1 and γ_2 are drawn from the point $(a,0)$ does not cause the loss of generality. Therefore we assume

$$f_1(a) = f_2(a) = 0.$$

By the conditions of the problem we have

$$f_1'(x) = u_y^{-2}, \quad f_2'(x) = -u_y^{-2},$$

which define the values of the derivative u_y on γ_1 and γ_2. But they are defined non-uniquely:

$$u_y\big|_{\gamma_1} = \pm\frac{1}{\sqrt{f_1'(x)}}, \quad u_y\big|_{\gamma_2} = \pm\frac{1}{\sqrt{-f_2'(x)}}.$$

To obtain the continuity of the derivative, we should take the right-hand parts of the latter equalities of the same sign.

Let us first consider the case

$$u_y\left(a, f_1(a)\right) = \frac{1}{\sqrt{f_1'(a)}}. \tag{11}$$

Using (9)-(11) we calculate in a straightforward manner the values of all characteristic invariants at the point $(a,0)$ and introduce for them the notation

$$\xi\big|_{(a,0)} \equiv \xi^{[a]}, \quad \xi_1\big|_{(a,0)} \equiv \xi_1^{[a]}, \quad \eta\big|_{(a,0)} \equiv \eta^{[a]}, \quad \eta_1\big|_{(a,0)} \equiv \eta_1^{[a]}.$$

By the property of characteristic invariants that they are constant along the respective curves, we have

$$\xi\big|_{\gamma_1} \equiv \xi^{[a]}, \quad \xi_1\big|_{\gamma_1} \equiv \xi_1^{[a]} \tag{12}$$

and

$$\eta\big|_{\gamma_2} \equiv \eta^{[a]}, \quad \eta_1\big|_{\gamma_2} \equiv \eta_1^{[a]}. \tag{13}$$

Let us now turn to the general integral (5)-(7) defined in terms of the characteristic invariants ξ, η and, using (5), (7), establish the relation between the values x, u along the arc γ_1:

$$u\big|_{\gamma_1} = \frac{1}{1-2\alpha}\left[\xi^{[a]}x^{1-\alpha} - \xi_1^{[a]}x^{\alpha}\right]. \tag{14}$$

From the second relation (12) we obtain

$$u_x\big|_{\gamma_1} = \frac{1-\alpha}{1-2\alpha}\xi^{[a]}x^{-\alpha} - \frac{\alpha}{1-2\alpha}\xi_1^{[a]}x^{\alpha-1} - \sqrt{f_1'(x)}. \tag{15}$$

Substituting the derivative value

$$u_y\big|_{\gamma_2} = \frac{1}{\sqrt{-f_2'(x)}}$$

into the first equality (13), we express the relation between the values x, u, u_x on γ_2 as follows

$$u_x\big|_{\gamma_2} = -\eta^{[\alpha]}x^{-\alpha} + \alpha\, u x^{-1} + \sqrt{-f_2'(x)}\,. \tag{16}$$

Substituting the values u_x, u_y into the total differential

$$du = \left(u_x + f_2'(x)u_y\right)dx$$

taken along γ_2, we obtain

$$\left.\frac{du}{dx}\right|_{\gamma_2} = \frac{\alpha}{x}u\Big|_{\gamma_2} - \eta^{[\alpha]}x^{-\alpha}, \quad x\in[a,b]. \tag{17}$$

Let us consider relation (17) as an ordinary differential equation with respect to the trace $U(x) = u\left(x, f_2(x)\right)$ of the function u on γ_2

$$\frac{dU}{dx} - \frac{\alpha}{x}U = -\eta^{[\alpha]}x^{-\alpha}$$

and write explicitly the solution of the Cauchy problem with the initial condition $U(a) = \vartheta$. We obtain

$$u\big|_{\gamma_2} = \left(\vartheta a^{-\alpha} + \frac{a^{1-2\alpha}}{1-2\alpha}\eta^{[\alpha]}\right)x^{\alpha} - \eta^{[\alpha]}\frac{x^{1-\alpha}}{1-2\alpha}. \tag{18}$$

A pair of relations (13), (18) enables us to define the relation of the derivative u_x with the variable x along the arc γ_2 as follows

$$u_x\big|_{\gamma_2} = \frac{\alpha-1}{1-2\alpha}\eta^{[\alpha]}x^{-\alpha} + \alpha\left(\vartheta a^{-\alpha} + \frac{a^{1-2\alpha}}{1-2\alpha}\eta^{[\alpha]}\right)x^{\alpha-1} + \sqrt{-f_2'(x)}\,. \tag{19}$$

Thus the conditions of problem (1), (9), (10) make it possible to define along both characteristic arcs γ_1, γ_2 the interdependence between the argument x, the solution $u(x,y)$ of equation (1) and its first order derivatives. But the aim we pursue is to define the solution not only on the characteristics but also outside the data carrier. To this end, we will again try to use the general properties of characteristic invariants. On the arc γ_1, we can represent the invariants η, η_1 from the other family as functions of the argument x. This is done by substitution of (11), (14), (15) into (4). On the arc γ_2, the values ξ, ξ_1 are constructed in the same manner.

From an arbitrary point $P_2\left(x_2, f(x_2)\right)\in\gamma_2$ let us draw the characteristic γ_3 of the family of the root λ_1. The constants along will be the invariants ξ and ξ_1. Another point $P_1\left(x_1, f_1(x_1)\right)\in\gamma_1$ is treated analogously and the characteristic of the family of the root λ_2 drawn from it is denoted by γ_4. The values of the

invariants η, η_1 at the point P_1 are preserved all along the arc γ_4. According to the general theory, a set of points of intersection of the analogous characteristics γ_3, γ_4 defines the domain of solution extension. If there exits a point of intersection of the arcs γ_3, γ_4, we denote it by $M\left(x^0, y^0\right)$.

Let us introduce the notation

$$\xi\big|_{P_2} \equiv \xi^{[x_2]}, \quad \xi_1\big|_{P_2} \equiv \xi_1^{[x_2]}, \quad \eta\big|_{P_1} \equiv \eta^{[x_1]}, \quad \eta_1\big|_{P_1} \equiv \eta_1^{[x_1]}.$$

As has already been said, the following relations hold true

$$\xi\big|_{\gamma_3} = \xi^{[x_2]}, \quad \xi_1\big|_{\gamma_3} = \xi_1^{[x_2]}, \tag{20}$$

$$\eta\big|_{\gamma_4} = \eta^{[x_1]}, \quad \eta_1\big|_{\gamma_4} = \eta_1^{[x_1]} \tag{21}$$

and they are simultaneously fulfilled at the point $M\left(x^0, y^0\right)$ of intersection of the arcs γ_3, γ_4.

Thus we obtain the following system with respect to x^0, $u^0 = u\left(x^0, y^0\right)$, $u_x^0 = u_x\left(x^0, y^0\right)$, $u_y^0 = u_y\left(x^0, y^0\right)$:

$$\begin{cases} \left(u_y^{0^{-1}} + u_x^0\right) x^{0\alpha} - \alpha u^0 x^{0\alpha-1} = \xi^{[x_2]} \\ \left(u_y^{0^{-1}} + u_x^0\right) x^{01-\alpha} - (1-\alpha) u^0 x^{0-\alpha} = \xi_1^{[x_2]} \\ \left(u_y^{0^{-1}} - u_x^0\right) x^{0\alpha} + \alpha u^0 x^{0\alpha-1} = \eta^{[x_1]} \\ \left(u_y^{0^{-1}} - u_x^0\right) x^{01-\alpha} - (1-\alpha) u^0 x^{0-\alpha} = \eta_1^{[x_1]} \end{cases} \tag{22}$$

We have already dealt with a system of form (22) when constructing the general integral (7)-(8). Hence to solve system (22), we perform analogous actions with the only difference that (22) will be considered not with respect to the functions x, u, u_x, u_y, and $u\alpha$ but with respect to their concrete values at the point $M\left(x^0, y^0\right)$. The right-hand parts are also concrete constant values well defined by the conditions of problem (1), (9), (10).

To find $y^0 = y\left(x_1, x_2\right)$ we resort to relation (6). Taking into consideration the explicit equations of the arcs γ_1, γ_2, we finally define the value $y = y^0$ in terms of x_1, x_2. The values x^0, y^0, u^0 are expressed as follows

$$x^0 = \left(\frac{\xi^{[x_1]} + \eta_1^{[x_1]}}{\xi^{[x_1]} + \eta^{[x_1]}}\right)^{\frac{1}{1-2\alpha}}, \tag{23}$$

$$y^0 = f_1\left(x_1\right) + f_2\left(x_2\right) +$$

$$+ \frac{1}{4(1-2\alpha)}\left[\xi^{[x_1]}\eta_1^{[x_1]} - \eta^{[x_1]}\xi_1^{[x_1]} - \xi^{[a]}\eta_1^{[x_1]} + \eta^{[x_1]}\xi_1^{[a]} - \xi^{[x_1]}\eta_1^{[a]} + \xi_1^{[x_1]}\eta^{[a]} + \xi^{[a]}\eta_1^{[a]} - \eta^{[a]}\xi_1^{[a]}\right], \tag{24}$$

$$u^0 = \frac{1}{1-2\alpha}\left[\xi^{[x_2]}\left(\frac{\xi^{[x_2]}+\eta^{[x_2]}}{\xi^{[x_2]}+\eta^{[x_2]}}\right)^{\frac{1-\alpha}{1-2\alpha}} - \xi_1^{[x_2]}\left(\frac{\xi^{[x_2]}+\eta^{[x_1]}}{\xi^{[x_2]}+\eta^{[x_1]}}\right)^{\frac{\alpha}{1-2\alpha}}\right]. \tag{25}$$

We have obtained the definition domain D of the solution $u\left(x^0, y^0\right)$ of problem (1), (9), (10) for the current x_1, x_2. This domain is well defined by relations (23), (24), where the expressions of x^0, y^0 are presented depending on x_1, x_2. We consider the values of these functions as the current coordinates describing the domain D. Then, taking into consideration the expressions of invariants along the arcs γ_3, γ_4 and their values at $(a,0)$, we can represent the solution of the considered problem (1), (9), (10) by the following three equalities

$$x = F\left(x_1, x_2\right) \equiv \left(\frac{\sqrt{f_1'(x_1)}\, x_1^{1-\alpha} + \sqrt{-f_2'(x_2)}\, x_2^{1-\alpha} - \sqrt{f_1'(a)}\, a^{1-\alpha}}{\sqrt{f_1'(x_1)}\, x_1^{\alpha} + \sqrt{-f_2'(x_2)}\, x_2^{\alpha} - \sqrt{f_1'(a)}\, a^{\alpha}}\right)^{\frac{1}{1-2\alpha}}, \tag{26}$$

$$y = G\left(x_1, x_2\right) \equiv f_1(x_1) + f_2(x_2) + \frac{1}{1-2\alpha}\left[\left(\sqrt{f_1'(x_1)}\, x_1^{1-\alpha} - \sqrt{f_1'(a)}\, a^{1-\alpha}\right)\left(\sqrt{-f_2'(x_2)}\, x_2^{\alpha} - \sqrt{f_1'(a)}\, a^{\alpha}\right) + \right.$$

$$\left. + \left(\sqrt{f_1'(a)}\, a^{\alpha} - \sqrt{f_1'(x_1)}\, x_1^{\alpha}\right)\left(\sqrt{-f_2'(x_2)}\, x_2^{1-\alpha} - \sqrt{f_1'(a)}\, a^{1-\alpha}\right)\right], \tag{27}$$

$$u = \frac{1}{1-2\alpha}\left[\left(\delta a^{\alpha} - \alpha\vartheta a^{\alpha-1} + 2\sqrt{-f_2'(x_2)}\, x_2^{\alpha} - \sqrt{f_1'(a)}\, a^{\alpha}\right)\right]\times$$

$$\times\left[\left(\frac{\sqrt{f_1'(x_1)}\, x_1^{1-\alpha} + \sqrt{-f_2'(x_2)}\, x_2^{1-\alpha} - \sqrt{f_1'(a)}\, a^{1-\alpha}}{\sqrt{f_1'(x_1)}\, x_1^{\alpha} + \sqrt{-f_2'(x_2)}\, x_2^{\alpha} - \sqrt{f_1'(a)}\, a^{\alpha}}\right)^{\frac{1-\alpha}{1-2\alpha}} + \right.$$

$$+\left((\alpha-1)\vartheta a^{-\alpha} - \sqrt{f_1'(a)}\, a^{1-\alpha} + \delta a^{1-\alpha} + 2\sqrt{-f_2'(x_2)}\, x_2^{1-\alpha}\right)\times$$

$$\left.\times\left(\frac{\sqrt{f_1'(x_1)}\, x_1^{1-\alpha} + \sqrt{-f_2'(x_2)}\, x_2^{1-\alpha} - \sqrt{f_1'(a)}\, a^{1-\alpha}}{\sqrt{f_1'(x_1)}\, x_1^{\alpha} + \sqrt{-f_2'(x_2)}\, x_2^{\alpha} - \sqrt{f_1'(a)}\, a^{\alpha}}\right)^{\frac{\alpha}{1-2\alpha}}\right]. \tag{28}$$

They simultaneously define both the domain D and the sought solution.

Note that the characteristic of the family λ_1 lying in the domain $D \cap \left\{F\left(x_1, x_2\right) \le \varepsilon < 0\right\}$ and drawn from the fixed point $\left(x_2^0, f_2\left(x_2^0\right)\right)$ is parametrically represented by the equations

$$x = F\left(x_1, x_2^0\right), \quad y = G\left(x_1, x_2^0\right), \quad x_1 \in [a, \varepsilon].$$

The parametric equations of the characteristic of the family λ_2 drawn from the point $\left(x_1^0, f_1\left(x_1^0\right)\right)$ are given as follows

$$x = F\left(x_1^0, x_2\right), \quad y = G\left(x_1^0, x_2\right), \quad x_2 \in [a, \varepsilon].$$

For the characteristics of one and the same family not to intersect each other in the domain $D \cap \{F(x_1, x_2) \le \varepsilon < 0\}$, it is sufficient that the conditions

$$\left[F\left(x_1^0, x_2\right) - F\left(x_1', x_2\right)\right]^2 + \left[G\left(x_1^0, x_2\right) - G\left(x_1', x_2\right)\right]^2 \neq 0, \tag{29}$$

$$\left[F\left(x_1, x_2^0\right) - F\left(x_1, x_2'\right)\right]^2 + \left[G\left(x_1, x_2^0\right) - G\left(x_1, x_2'\right)\right]^2 \neq 0 \tag{30}$$

be fulfilled for any fixed values $x_1^0 \neq x_1'$ and $x_2^0 \neq x_2'$ from the interval $[a, \varepsilon]$ and for the parameters $x_1, x_2 \in [a, \varepsilon]$.

If

$$u_y\big|_{\gamma_1} = -\frac{1}{\sqrt{f_1'(x)}}, \quad u_y\big|_{\gamma_2} = -\frac{1}{\sqrt{-f_2'(x)}},$$

then by a reasoning analogous to that in the preceding case we see that problem (1), (9), (10) has, in addition to (26)-(28), one more solution represented by the formulas

$$\begin{aligned}
&x = F\left(x_1, x_2\right),\\
&y = G\left(x_1, x_2\right),\\
&u = \frac{1}{1-2\alpha}\left[\left(\delta a^{\alpha} - \alpha\vartheta a^{\alpha-1} - 2\sqrt{-f_2'\left(x_2\right)}\, x_2^{\alpha} + \sqrt{f_1'(a)}\, a^{\alpha}\right) F^{\frac{1-\alpha}{1-2\alpha}}\left(x_1, x_2\right) + \right.\\
&\left. + \left(\left(\alpha-1\right)\vartheta a^{-\alpha} + \sqrt{f_1'(a)}\, a^{1-\alpha} + \delta a^{1-\alpha} - 2\sqrt{-f_2'\left(x_2\right)}\, x_2^{1-\alpha}\right) F^{\frac{\alpha}{1-2\alpha}}\left(x_1, x_2\right)\right].
\end{aligned} \tag{31}$$

The definition domains of these solutions coincide since in both cases the arguments x and y are defined in the same manner.

The following theorem is true.

Theorem 3. *If conditions* (29), (30) *are fulfilled, then for any arbitrarily real branch of the multi-valued function* (26) *in the domain* $D \cap \{F(x_1, x_2) \le \varepsilon < 0\}$ *there exist regular hyperbolic solutions of problem* (1), (9), (10) *representable by formulas* (26)-(28) *and* (26), (27), (31).

მათმატიკა

გურსას არაწრფივი მახასიათებელი ამოცანა არაწრფივი რხევების განტოლებისათვის

რ. ბიწაძე*, მ. მენთეშაშვილი**

** საქართველოს ტექნიკური უნივერსიტეტი, თეორიული ინფორმატიკის დეპარტამენტი, თბილისი*
*** საქართველოს ტექნიკური უნივერსიტეტის ნ.ყ. მესხიშვილის სახელობის გამოთვლითი მათმატიკის ინსტიტუტი, თბილისი*

(წარმოდგენილია აკადემიკოს ნ. ვახანიას მიერ)

ნაშრომში არაწრფივი რხევების ცნობილი განტოლებისათვის შესწავლილია გურსას მახასიათებელი ამოცანის ერთი არაწრფივი ვარიანტი, რომლის მიხედვითაც ერთდროულად უნდა განისაზღვროს რგულარული ჰიპერბოლური ამონახსნი და მისი გავრცელების არე. აღწერილია ამ არეთა სტრუქტურული თვისებები განტოლების რიგის გადაგვარების წერტილთა სიახლოვემდე.

REFERENCES

1. *S. Kumei, G.W. Bluman* (1982), SIAM J. Appl. Math., **42**, 5: 1157-1173.
2. *P. Olver* (2000), Applications of Lie groups to differential equations. Springer-Verlag, N.Y.
3. *J. Hadamard* (1903), Leçons sur la propagation des ondes et les équations de l'hydrodynamique. Paris.
4. *A.V. Bitsadze* (1959), Uravneniya smeshannogo tipa, M. (in Russian).
5. *L. Bers* (1958), Surveys in Applied Mathematics, **3**: 1-208
6. *J.K. Gvazava* (2004), Proc. A. Razmadze Math. Inst., **135**: 79-96.
7. *R. Bitsadze* (1987), Soobshch. Akad. Nauk Gruzii, **128**, 3: 17-20 (in Russian).
8. *M.Z. Menteshashvili* (1993), Soobsh. Akad. Nauk Gruzii, **148**, 2: 190-193 (in Russian).
9. *G. Bagkaturia* (2006), Proc. A. Razmadze Math. Inst., **141**: 15-27.
10. *M. Klebanskaya* (2006), Georg. Math. Journal, **141**: 67-74.
11. *E. T. Whittaker, G.N. Watson* (1965), A Course of Modern Analysis, Cambridge University Press.
12. *F. Tricomi* (1957), Lectures on Partial Differential Equations. M. (Russian translation).
13. *E. Goursat* (1896-1898), Leçons sur l'intégration des équations aux dérivées partielles du second ordre, à deux variables indépendantes. Tome 2. Hermann, Paris.

Received February, 2012

Mathematics

On the Pseudo-Maximal Likelihood Estimation of the Parameters of an Exponential Distribution by Grouped Observations with Censoring

George Lominashvili* and Mzevinar Patsatsia**

* *Faculty of Exact and Natural Sciences, Akaki Tsereteli State University, Kutaisi*
** *Faculty of Mathematics and Computer Sciences, Sukhumi State University, Tbilisi*

(Presented by Academy Member Elizbar Nadaraya)

ABSTRACT. In the paper is studied the problem of estimating λ parameter of exponential distribution by the pseudo-maximum method for censoring observations. Existence and uniqueness of solution of the maximal likehood equation is shown. The solution is asymptotic consistence and effective estimator of λ parameter of exponential equation. © *2012 Bull. Georg. Natl. Acad. Sci.*

Key words: *pseudo-maximal likelihood, grouped observations, censoring incomplete observation.*

Let X be a random variable with the distribution function $F(x)=F(x,\theta)$ where $\theta\in\Theta$ is an unknown vector parameter in a finite-dimensional Euclidean space $\Theta\in R^{l}$. Assume that Θ is a compactum. We are to construct a consistent estimate θ using observations of the random variable X. The experiment is run so that we do not know the actual number of realizations and know only a part of these realizations.

Let the fixed points $-\infty\le t_1\le t_2\le\cdots\le t_k\le\infty$ be given on the straight line R (we do not exclude the case in which the first or the last point takes an infinite value). These points form intervals which can be of three categories:

(0) An interval (t_i,t_{i+1}) belongs to the zero category if in this interval we know neither individual values of the sampling nor the number of sample values of the random value X which occur in this interval.

(1) An interval (t_i,t_{i+1}) belongs to the first category if in this interval we do not know individual values of the sampling but know the number of sample values of the random variable X which occur in this interval. As usual this number will be denoted by n_i.

(2) An interval (t_i,t_{i+1}) belongs to the second category if in this interval we know individual values of the sampling.

We call a sampling of this type a partly grouped sampling with censoring.

The absence of information in the intervals of the zero category creates difficulties which we will try to overcome by assuming that we know the type of the distribution $F(x,\theta)$ and the number of sample values from the sampling which do not occur in the intervals of the zero category: $n=\sum_{(1),(2)} n_i$.

Let $A_i=(t_i,t_{i+1})$ be an interval of the zero category. Denote by m_i the number of sampling terms occurring in A_i. Then $r=n+\sum_{(0)} m_i$ is the total number of observations. Note that $\frac{m_i}{n+\sum_{(0)} m_i}$ is a relative frequency of occurrence of X in A_i.

If $\hat{F}_r(x)$ denotes an empirical distribution function, then

$$\frac{m_i}{n+\sum_{(0)} m_i}=\hat{F}_r(t_{i+1})-\hat{F}_r(t_i) \tag{1}$$

and, according to the strengthened Bernoulli law of large numbers, it converges to $p_i(\theta)=F(t_{i+1},\theta)-F(t_i,\theta)$ with probability 1.

By summation of equalities (1) over all intervals of the zero category we find

$$\sum_{(0)} m_i = n\frac{\sum_{\kappa(0)}\left[\hat{F}_r(t_{i+1})-\hat{F}_r(t_i)\right]}{1-\left[\sum_{\kappa(0)}\left[\hat{F}_r(t_{i+1})-\hat{F}_r(t_i)\right]\right]}.$$

Hence we obtain

$$m_i = n\frac{\hat{F}_r(t_{i+1})-\hat{F}_r(t_i)}{1-\left[\sum_{\kappa(0)}\left[\hat{F}_r(t_{i+1})-\hat{F}_r(t_i)\right]\right]}. \tag{2}$$

Let us apply the method of pseudo-maximal likelihood. Assume that the distribution density of the random variable X with respect to the Lebesgue measure is $f(x)=f(x,\theta)$. Then a likelihood function has the form

$$L_n(x;\theta)=\prod_{\kappa(0)}\left[F(t_{i+1})-F(t_i)\right]^{m_i}\prod_{\kappa(1)}\left[F(t_{i+1})-F(t_i)\right]^{n_i}\cdot\prod_{j=1}^{n_i} f(x_{ji}), \tag{3}$$

where m_i, $i\in(0)$, are defined by formulas (2).

The finding of points of a maximum of the function $L(x;\theta)$ is complicated because the study of the

smoothness properties of empirical functions is difficult. Therefore we consider the slightly corrected likelihood function

$$\overline{L}_n(x;\theta)=\prod_{i\in(0)}\left[F(t_{i+1})-F(t_i)\right]^{\frac{F(t_{i+1})-F(t_i)}{1-[F(t_{i+1})-F(t_i)]}}\prod_{i\in(1)}\left[F(t_{i+1})-F(t_i)\right]^{n_i}\cdot\prod_{j=1}^{n_i}f(x_{ji}). \tag{4}$$

Lemma [1]. *Let the following conditions be fulfilled:*

a) the distribution function $F(x,\theta)$ *is continuous with respect to both variables and has the continuous derivative* $f(x,\theta)=\dfrac{\partial F(x,\theta)}{\partial x}$;

b) the function $\overline{L}_n(x;\theta)$ *has the absolute maximum* $\theta=\overline{\theta}_n$.

Then $\overline{\theta}_n$ *is an asymptotically consistent and asymptotically effective estimate of the true value of the parameter* $\theta=\theta_0$.

Let X be an exponentially distributed random value with the density

$$f(x)=\begin{cases}\lambda e^{-\lambda x} & \text{if } x\geq 0\\ 0 & \text{if } x<0\end{cases}$$

where $\lambda>0$.

Assume that $[a,b]$ is an inaccessible interval for the observer and we do not know the number and individual observations in this zone. We, however, know the observations outside this interval: $X_1,X_2,\ldots,X_n$. It is required to estimate λ by means of these observations. For this, we use pseudo-maximal likelihood estimates.

To construct likelihood functions note that if we denote by k the number of terms from the general sampling which occur in $[a,b]$, then $\dfrac{k}{k+n}$ will be the frequency of occurrences in the interval $[a,b]$. Hence, by the Bernoulli-Kolmogorov theorem $\dfrac{k}{k+n}\to p$ a.s., where $p=F(b)-F(a)$

$$F(x)=\begin{cases}1-e^{-\lambda x} & \text{if } x\geq 0\\ 0 & \text{if } x<0\end{cases}.$$

Therefore, we define k as

$$\hat{k}=\frac{n\left[F(b)-F(a)\right]}{1-\left[F(b)-F(a)\right]}.$$

Since the probability that exactly k elements from the sampling will occur in the "black hole" is $\left[F(b)-F(a)\right]^k$, we can write the pseudo-likelihood function as follows:

$$L=\prod_{i=1}^{n}f(x_i;\lambda)\cdot\left[F(b)-F(a)\right]^{\frac{F(b)-F(a)}{1-[F(b)-F(a)]}}=\lambda^n\cdot e^{-\lambda\sum_{i=1}^{n}X_i}\left(F(b)-F(a)\right)^{\frac{F(b)-F(a)}{1-(F(b)-F(a))}}. \tag{5}$$

Note that in (5) the power may turn out to be a non-integer number, but it is always positive. Also note that in this formula the multiplication sign is used for the expression in front of the large bracket.

From (5) we write

$$\ln L = n\cdot\ln\lambda - \lambda\sum_{i=1}^{n} X_i + \frac{n\cdot\left(F(b)-F(a)\right)}{1-\left(F(b)-F(a)\right)}\cdot\ln\left(F(b)-F(a)\right),$$

$$\frac{d\ln L}{d\lambda} = \frac{n}{\lambda} - \sum_{i=1}^{n} X_i + n\cdot\left(\frac{\left(b\cdot e^{-\lambda b} - a\cdot e^{-\lambda a}\right)\cdot\ln\left(F(b)-F(a)\right)\left(1-\left(F(b)-F(a)\right)\right)}{\left(1-\left(F(b)-F(a)\right)\right)^2} + \right.$$

$$\left. + \frac{\left(b\cdot e^{-\lambda b} - a\cdot e^{-\lambda a}\right)\cdot\left(1-\left(F(b)-F(a)\right)\right)}{\left(1-\left(F(b)-F(a)\right)\right)^2} + \frac{\left(F(b)-F(a)\right)\cdot\ln\left(F(b)-F(a)\right)\cdot\left(b\cdot e^{-\lambda a} - a\cdot e^{\quad}\right)}{\left(1-\left(F(b)-F(a)\right)\right)^2}\right) =$$

$$= \frac{n}{\lambda} - \sum_{i=1}^{n} X_i + n\cdot\frac{\left(b\cdot e^{-\lambda b} - a\cdot e^{-\lambda a}\right)\cdot\left(1-\left(F(b)-F(a)\right)+\ln\left(F(b)-F(a)\right)\right)}{\left(1-\left(F(b)-F(a)\right)\right)^2}. \qquad (6)$$

Let us investigate expression (6) when $\lambda\to 0$. Note that when $\lambda\to 0$, we have $F(b)-F(a)=e^{-\lambda a}-e^{-\lambda b}\to 0$ and $\ln\left(F(b)-F(a)\right)\to-\infty$.

We obtain

$$\lim_{\lambda\to 0}\frac{d\ln L}{d\lambda} = \infty.$$

Indeed,

$$\lim_{\lambda\to 0}\frac{d\ln L}{d\lambda} = \lim_{\lambda\to 0}\frac{\dfrac{\left(1-\left(F(b)-F(a)\right)\right)^2}{n\left(b\cdot e^{-\lambda b}-a\cdot e^{-\lambda a}\right)\left(1-\left(F(b)-F(a)\right)+\ln\left(F(b)-F(a)\right)\right)} - \dfrac{\lambda}{n-\lambda\sum_{i=1}^{n}X_i}}{\dfrac{\left(1-\left(F(b)-F(a)\right)\right)^2\lambda}{n\left(b\cdot e^{-\lambda b}-a\cdot e^{-\lambda a}\right)\left(1-\left(F(b)-F(a)\right)+\ln\left(F(b)-F(a)\right)\right)\left(n-\lambda\sum_{i=1}^{n}X_i\right)}} =$$

$$= \lim_{\lambda\to 0}\frac{\left(1-\left(F(b)-F(a)\right)\right)^2\left(n-\lambda\sum_{i=1}^{n}X_i\right) - \lambda\cdot n\left(b\cdot e^{-\lambda b}-a\cdot e^{-\lambda a}\right)\left(1-\left(F(b)-F(a)\right)+\ln\left(F(b)-F(a)\right)\right)}{\left(1-\left(F(b)-F(a)\right)\right)^2\cdot\lambda} =$$

$$= \lim_{\lambda\to 0}\frac{\left(1-\left(F(b)-F(a)\right)\right)^2\left(n-\lambda\sum_{i=1}^{n}X_i\right)}{\left(1-\left(F(b)-F(a)\right)\right)^2\cdot\lambda} -$$

$$- \lim_{\lambda\to 0}\frac{n\left(b\cdot e^{-\lambda b}-a\cdot e^{-\lambda a}\right)\left(1-\left(F(b)-F(a)\right)+\ln\left(F(b)-F(a)\right)\right)}{\left(1-\left(F(b)-F(a)\right)\right)^2} = \infty.$$

Analogously, when $\lambda\to\infty$, we have

$$\lim_{\lambda\to\infty}\frac{d\ln L}{d\lambda}=-\infty .$$

The continuous function $\frac{d\ln L}{d\lambda}$ changes its sign and therefore there exists a point $\hat{\lambda}$ such that $\left.\frac{d\ln L}{d\lambda}\right|_{\lambda=\hat{\lambda}}=0$. Let us verify that at this point the second derivative is negative.

We write the second derivative in the form

$$\frac{d^2\ln L}{d\lambda^2}=-\frac{n}{\lambda^2}+\frac{n\cdot\left(a^2\cdot e^{-\lambda a}-b^2\cdot e^{-\lambda b}\right)\left(1-\left(F(b)-F(a)\right)+\ln\left(F(b)-F(a)\right)\right)\left(1-\left(F(b)-F(a)\right)\right)}{\left(1-\left(F(b)-F(a)\right)\right)^3}+$$

$$+\frac{n\cdot\left(b\cdot e^{-\lambda b}-ae^{-\lambda a}\right)\left(-\left(b\cdot e^{-\lambda b}-ae^{-\lambda a}\right)\right)+\frac{b\,e^{-\lambda b}-ae^{-\lambda a}}{F(b)-F(a)}}{\left(1-\left(F(b)-F(a)\right)\right)^2}+$$

$$+\frac{2n\cdot\left(b\cdot e^{-\lambda b}-ae^{-\lambda a}\right)^2\left(1-\left(F(b)-F(a)\right)+\ln\left(F(b)-F(a)\right)\right)}{\left(1-\left(F(b)-F(a)\right)\right)^3}. \tag{7}$$

Note that $x^2\cdot e^{-\lambda x}$, where $x>0$, is a decreasing function and therefore the first term and the second term in (7) are negative. Let us now show that the sum of the third term and the fourth term is negative. We have

$$\frac{2n\cdot\left(b\cdot e^{-\lambda b}-ae^{-\lambda a}\right)^2\left(1-\left(F(b)-F(a)\right)+\ln\left(F(b)-F(a)\right)\right)}{\left(1-\left(F(b)-F(a)\right)\right)^3}+$$

$$+\frac{n\cdot\left(b\cdot e^{-\lambda b}-ae^{-\lambda a}\right)^2\left(\frac{1}{F(b)-F(a)}-1\right)\cdot\left(1-\left(F(b)-F(a)\right)\right)}{\left(1-\left(F(b)-F(a)\right)\right)^3}=$$

$$=\frac{n\cdot\left(b\cdot e^{-\lambda b}-ae^{-\lambda a}\right)^2\left(2\left(1-\left(F(b)-F(a)\right)+\ln\left(F(b)-F(a)\right)\right)+\left(\frac{1}{F(b)-F(a)}-1\right)\cdot\left(1-\left(F(b)-F(a)\right)\right)\right)}{\left(1-\left(F(b)-F(a)\right)\right)^3}=$$

$$=\frac{n\cdot\left(b\cdot e^{-\lambda b}-ae^{-\lambda a}\right)^2\left(\frac{1}{F(b)-F(a)}-\left(F(b)-F(a)\right)+2\ln\left(F(b)-F(a)\right)\right)}{\left(1-\left(F(b)-F(a)\right)\right)^3}. \tag{8}$$

If we take the equalities $\frac{1}{x}-x+2\ln x\le 0$, where $0<x\le 1$, into consideration, then we can show the negativity of relation (8), which means that $\hat{\lambda}$ is the unique point of a maximum of the likelihood equality.

The following theorem is valid by virtue of Lemma.

Theorem. *Suppose that we have a sampling of exponential random values $X_1,X_2,\ldots,X_n$ with an unknown parameter $\hat{\lambda}$. The observation is carried out beyond the limits of the interval $[a,b]$ in which*

neither sampling terms nor their quantity are recorded. Then the estimate of a maximal pseudo-likelihood exists for λ and is the unique root of the equation

$$\frac{n}{\lambda}-\sum_{i=1}^{n}X_i+\frac{n\cdot\left(b\cdot e^{-\lambda b}-ae^{-\lambda a}\right)\left(1-\left(F(b)-F(a)\right)+\ln\left(F(b)-F(a)\right)\right)}{\left(1-\left(F(b)-F(a)\right)\right)^2}=0.$$

Moreover, this estimate is asymptotically consistent and effective.

მათმატიკა

დაჯგუფებული დაკვირვებების საფუძველზე ექსპონენციალური განაწილების პარამეტრების ფსევდომაქსიმალური დასაჯერობის შეფასების შესახებ

გ. ლომინაშვილი*, მ. ფაცაცია**

* აკაკი წერეთლის სახელმწიფო უნივერსიტეტი, ზუსტ და სამუნებისმეტყველო მეცნიერებათა ფაკულტეტი, ქუთაისი
** სოხუმის სახელმწიფო უნივერსიტეტი, მათმატიკისა და კომპიუტერულ მეცნიერებათა ფაკულტეტი, თბილისი

(წარმოდგენილია აკადემიის წევრის გ. ნადარაიას მიერ)

ნაშრომში შეფასების ფსევდომაქსიმალური მეთოდის გამოყენებით შესწავლილია ექსპონენციალური განაწილების λ პარამეტრის შეფასების ამოცანა ცენზურირებული დაკვირვებების საფუძველზე. ექსპონენციალური განაწილებისათვის ნაჩვენებია შესაბამისი ფსევდომაქსიმალური დასაჯერობის განტოლების ამონახსნის არსებობა და ერთადერთობა. ეს ამონახსნი წარმოადგენს ესპონენციალური განაწილების λ-პარამეტრის ასიმტოტურად ძალდებულ და ეფექტურ შეფასებას.

REFERENCES

1. *E. Nadaraya, M. Patsatsia, G. Sokhadze* (2009), Sokhumi State University Proceedings. VII, Mathematics and Computer Sciences Series. Tbilisi, 33-43.
2. *G. Kulldorf* (1966), Contributions to the theory of estimation from grouped and partially grouped samples. Translated from the English by N. A. Bodin. Edited by Ju. V. Linnik. Moscow, 176 pp. (in Russian).

Received January, 2012

საქართველოს მეცნიერებათა ეროვნული აკადემიის მოამბე, ტ. 6, №3, 2012
BULLETIN OF THE GEORGIAN NATIONAL ACADEMY OF SCIENCES, vol. 6, no. 3, 2012

Mathematics

Affine Isomorphisms of Power Groups

Tengiz Bokelavadze* and Alexander Lashkhi**

* *Faculty of Exact and Natural Sciences, Akaki Tsereteli State University, Kutaisi*
** *Department of Theoretical Informatics and Computer Modelling, Georgian Technical University.*

(Presented by Academy Member Hvedri Inassaridze)

ABSTRACT. In the present paper the lattice of cosets $\Re(G)$ is constructed for Hall's power group G over the ring W. This lattice is called the affine or coset lattice of G. Since in the lattice $\Re(G)$ only the elements of G cover $\varnothing$, the isomorphism $f:\Re(G)\to\Re(G_1)$ defines the bijection $f:G\to G_1$. Among all possible isomorphisms f we shall select in the sequel those for which $f(1)=1$. Such isomorphisms will be called the affine isomorphisms. We prove the following theorem: Let $f:\Re(G)\to\Re(G_1)$ be an affine isomorphism between the w-power groups G and G_1 over the fields W and W_1, respectively, if G is nilpotent of class 2 then f is either a semilinear isomorphism or a semilinear antiisomorphism with respect to the isomorphism $\sigma:W\to W_1$. The given example shows that the theorem is false for the class of nilpotency ≥ 3. © *2012 Bull. Georg. Natl. Acad. Sci.*

Key words: *affine geometry, coset lattice, power groups.*

Let L be a lattice and M a subset of L which is a lattice relative to the induced partial order. Clearly, M is not a sublattice of L; the subgroup lattice of a group G as a subset of the lattice of all subsets of G is an example. If $\cap$ and $\wedge$ denote the intersections in L and M, respectively, then for $x,y\in M$, $x\wedge y$ is a lower bound of $\{x,y\}$ in L and so $x\wedge y\leq x\cap y$. We call M a *meet-sublattice* of L if $x\wedge y\leq x\cap y$ for all $x,y\in M$. The lattice M is a *complete meet-sublattice* of L if M and L are complete lattices and for every subset $S\subset M$ the greatest lower bounds of S in M and L coincide.

Proposition. *If M is a subset of a complete lattice L such that for every subset S of M the greatest lower bound $\cap S$ of S in L is contained in M, then M is a complete meet-sublattice of L.*

Proof. For a subset S of M let S^* be the set of upper bounds of S in M. By hypothesis, $\inf S^*\in M$. Every $s\in S$ is a lower bound of S^*, hence $s\leq\inf S^*$. Thus $\inf S^*$ is an upper bound of S and then, certainly, the least upper bound of S in M. Clearly, $\inf S$ is the greatest lower bound of S in M. Hence M is a complete lattice

and the greatest lower bounds of S in M and L coincide.

If G is a group, the subgroup lattice $L(G)$ is an example of a complete meet-sublattice of the lattice of all subsets of G. We introduce two further lattices of this kind.

The notion of a discrete w-power group was introduced by Hall [1]. At the present time there are a number of works where the properties of w-power groups are studied. In [2] the fundamental theorem of projective geometry for w-power groups was proved for principal ideal domains which are not fields. For the relation problems in Lie algebras and groups see [3-6]. For affine geometry of modules and the fundamental theorem see [7]. In [8,9] the affine lattices and the fundamental theorem of affine geometry for Lie algebras and power groups are studied. Furthermore, G (and G_1) is Hall's power group over the ring W (the ring W_1).

Let $\Re(G)$ be the set of all right cosets of subgroups of G together with the empty set $\varnothing$. If $\mathcal{Y}$ is a nonempty subset of $\Re(G)$, then either $\cap\mathcal{Y}=\varnothing\in\Re(G)$ or there exists an element $x\in\cap\mathcal{Y}$. In the latter case, $\mathcal{Y}=\{H_i x \mid i\in I\}$ for certain subgroups H_i of G, and hence $\cap\mathcal{Y}=\left(\bigcap_{i\in I}H_i\right)x\in\Re(G)$. If $\mathcal{Y}$ is an empty subset of $\Re(G)$, then $\cap\mathcal{Y}=G\in\Re(G)$. The lattice $\Re(G)$ is a complete meet-sublattice of the lattice of all subsets of G. Since $Hx=x\left(x^{-1}Hx\right)$ for all $H\le G$ and $x\in G$, every right coset is a left coset, and conversely. So $\Re(G)$ is the set of all (right or left) cosets in G and we call $\Re(G)$ the *affine or coset lattice* of G. The subgroups of G are precisely the cosets containing the coset 1. Hence $L(G)$ is the interval $[G,1]$ in $\Re(G)$.

For the basic properties of affine lattice $\Re(G)$ see [4].

Affine lattices do not usually have nice lattice properties. For example, if $1<H<G$ and $a\in G/H$, then $\{\varnothing,\{a\},Ha,\langle H,a\rangle,H\}$ is a nonmodular sublattice (pentagon) of $\Re(G)$. Thus a group with a modular coset lattice is cyclic without proper subgroups; in this connection see [2-4, 6, 8, 9].

Thus the groups whose coset lattices have special properties, is not a very fruitful one: almost any interesting lattice property is satisfied by nearly all or by a very few coset lattices, or else it holds in $\Re(G)$ if and only if it holds in $L(G)$ [2, 4-6, 8, 9]. The study of isomorphisms between coset lattices is more interesting. Since the atoms of $\Re(G)$ are the one-element subsets of G and for any such atom $\{g\}$, the interval $[G,\{g\}]$ in $\Re(G)$ is isomorphic to $L(G)$, two groups with isomorphic coset lattices have the same order and isomorphic subgroup lattices. Nevertheless there are nonisomorphic groups with isomorphic coset lattices. An isomorphism $\sigma:\Re(G)\to\Re(\overline{G})$ can be regarded as a bijective map from G to $\overline{G}$ preserving cosets. We consider under which condition σ is a semilinear isomorphism from G to $\overline{G}$.

Let G and G_1 be w-power groups over the rings W and W_1, respectively. The bijection $f:G\to G_1$ will be called a semilinear isomorphism with respect to the isomorphism $\sigma:W\to W_1$ if the equality

$$f\left(x_1^{\alpha_1}x_2^{\alpha_2}\right)=f\left(x_1\right)^{\sigma(\alpha_1)}f\left(x_2\right)^{\sigma(\alpha_2)}$$

is fulfilled for any $x_1,x_2\in G$ and $\alpha_1,\alpha_2\in W$ and f will be called a semilinear antiisomorphism if the equality

$$f\left(x_1^{\alpha_1}x_2^{\alpha_2}\right)=f\left(x_2\right)^{\sigma(\alpha_2)}f\left(x_1\right)^{\sigma(\alpha_1)}$$

is fulfilled for any $x_1,x_2\in G$ and $\alpha_1,\alpha_2\in W$.

We say that the fundamental theorem of projective geometry is valid for w-power group G over the ring W, if the lattice isomorphism $\varphi: L(G)\to L(G_1)$ (where $L(G)$ and $L(G_1)$ are the lattices of all w-subgroups of G and G_1) implies the existence of a semilinear isomorphism $f: G\to G_1$ with respect to the isomorphism $\alpha: W\to W_1$ such that $f(A)=\varphi(A)$ for all $A\in L(G)$.

Since in the lattice $\Re(G)$ only the elements of G cover $\varnothing$, the isomorphism $f:\Re(G)\to\Re(G_1)$ defines the bijection $f: G\to G_1$.

Among all possible isomorphisms f we shall select in the sequel those for which $f(1)=1$. Such isomorphisms will be called affine isomorphisms. If $f:\Re(G)\to\Re(G_1)$ is an isomorphism, then the bijection φ defined by the equality

$$\varphi(x)=f(x)\left[f(1)\right]^{-1}$$

will be an affine isomorphism.

We say that the fundamental theorem of affine geometry is valid for a w-power group G if any affine isomorphism is either a semilinear isomorphism or a semilinear antiisomorphism.

Remark 1. If $a\in A$ is a fixed element and $f(a)=a_1$ then the mapping

$$\varphi(x)=f(ax)\left[f(1_a)\right]^{-1}$$

is an affine isomorphism. Indeed, φ will be a C-isomorphism defined by the element a_1^{-1} i.e. it will be an automorphism $\left[\bar{a}_1\right]^{-1}\in Aut\left[\Re(G)\right]$; since $\varphi(1)=f(a)a_1^{-1}$, we have that f_1 is an affine isomorphism.

Not each affine isomorphism (antiisomorphisms) is a semilinear isomorphism. Any one-dimensional vector space over Z_p admits $(p-1)!$ affine automorphisms while the group of all internal automorphisms of Z_p has order $p-1$. Therefore for $p>3$ a one-dimensional vector space over Z_p admits affine automorphisms different from ordinary ones.

Lemma 1. *Let $\Re(G)\to\Re(G_1)$ be an affine isomorphism. Then the following statements are true:*

(i) *f induces a lattice isomorphism $f: L(G)\to L(G_1)$;*

(ii) $f\left(\langle M\rangle\right)=\left\langle f(M)\right\rangle$ *for any subset $M\subseteq G$;*

(iii) $f\left(a\langle b\rangle\right)=f(a)\left\langle f(b)\right\rangle$ *for any $a,b\in G$.*

Assume that W is a commutative domain. The w-group G is called torsion-free if $x^\alpha=1$ $(\alpha\in W,\ x\in G)$ implies $\alpha=0$ or $x=1$.

Lemma 2. *Let $f:\Re(G)\to\Re(G_1)$ be an affine isomorphism between torsion-free w-power groups over the rings W and W_1, then*

(i) $Z(G_1)=Z\left(f(G)\right)$;

(ii) *the nilpotency classes on the subgroups coincide;*

(iii) *there exists an isomorphism* $\sigma : W \to W_1$ *such that* $f(a^\mu) = [f(a)]^{\sigma(\mu)}$, $\mu \in W$, $a \in G$.

Theorem (Fundamental theorem of affine geometry for *w*-power groups). *Let* $f : \Re(G) \to \Re(G_1)$ *be an affine isomorphism between the w-power groups* G *and* G_1 *over the fields* W *and* W_1, *respectively, if* G *is nilpotent of class* 2 *then* f *is either a semilinear isomorphism or a semilinear antiisomorphism with respect to the isomorphism* $\sigma : W \to W_1$.

Remark 2. Thus we have concluded that using the coset lattices the fundamental theorem of affine geometry can be proved for *w*-power groups over fields, while the fundamental theorem of projective geometry is false [2, 6, 8, 9].

The example below shows that the theorem is false for the class of nilpotency ≥ 3.

Example. Let G be *w*-power group over the field F generated by the elements a, b and have the defining relations

$$1 \neq [a,b] = z_1, \quad [a,z] = [b,z] = 1, \quad [a,z_1] = [b,z_1] = z.$$

It is clear that G is nilpotent of class 3 and $Z(G) = \langle [a,b] \rangle$. For an arbitrary element

$$l = a^\alpha b^\beta [a,b]^\gamma z^\mu \in G, \ \alpha, \beta, \gamma, \mu \in F$$

consider the map $f : G \to G$

$$f(l) = a^\alpha b^\beta ([a,b]z)^\gamma z^\mu.$$

We have

$$f([a,b])^\alpha f([a,b])^\beta = ([a,b]z)^\alpha ([a,b]z)^\beta = ([a,b]z)^{\alpha+\beta} =$$
$$= f([a,b])^{\alpha+\beta} = f([a,b]^{\alpha+\beta}) = f([a,b]^\alpha [a,b]^\beta).$$

So for any

$$l_1 = a^{\alpha_1} b^{\beta_1} [a,b]^{\gamma_1} z^{\mu_1}, \ \alpha_1, \beta_1, \gamma_1, \mu_1 \in F,$$
$$l_2 = a^{\alpha_2} b^{\beta_2} [a,b]^{\gamma_2} z^{\mu_2}, \ \alpha_2, \beta_2, \gamma_2, \mu_2 \in F.$$

Thus we have $f(l_1, l_2) = f(l_1) f(l_2)$, $f(l^\alpha) = [f(l)]^\alpha$. Therefore

$$f(l_1 \cup l_2) = f(l_1 \langle l_1 l_2^{-1} \rangle) = f(l_1) \langle (l_1 l_2^{-1}) \rangle = f(l_1) \langle f(l_1) [f(l_2)]^{-1} \rangle = f(l_1) \cup f(l_2).$$

Consequently, f is an affine automorhism of the lattice $\Re(G)$, which is not a semilinear automorphism of G.

Remark 3. For a similar example for Lie algebra see [8].

Remark 4. From this example we can conclude that the theorems from [2, 9] need correction, i.e. they are valid for class of nilpotency ≤ 2.

Acknowledgements. This work was supported by Shota Rustaveli National Science Foundation (Projects # GNSF/ST08/3-383 and # GNSF/ST08/3-396).

მათმატიკა

ხარისხოვანი ჯგუფების აფინური მესერები და მათი იზომორფიზმები

თ. ბოკელავაძე*, ა. ლაშხი**

* აკაკი წერეთლის სახელმწიფო უნივერსიტეტი, ზუსტ და სატუნებისმეტყველო მეცნიერებათა ფაკულტეტი, ქუთაისი
** საქართველოს ტექნიკური უნივერსიტეტი, თეორიული ინფორმატიკის და კომპიუტერული მოდელირების დეპარტამენტი, თბილისი

ნაშრომში ჰოლის ხარისხოვანი G ჯგუფისათვის W რგოლზე იგება მოსაზღვრე კლასების $\Re(G)$ მესერი. ასეთ მესერებს ეწოდება G ჯგუფის აფინური ან მოსაზღვრე კლასების მესერი. რადგანაც $\Re(G)$ მესერში მხოლოდ G-ს ელემენტები ფარავენ ცარიელ სიმრავლეს, იზომორფიზმი $f:\Re(G)\to\Re(G_1)$ განსაზღვრავს ბიექციას $f:G\to G_1$. ყველა შესაძლო f იზომორფიზმებიდან ჩვენ ავარჩევთ ისეთებს, რომელთათვისაც $f(1)=1$. ასეთ იზომორფიზმებს ვუწოდებთ აფინურ იზომორფიზმებს. მტკიცდება შემდეგი თეორემა: ვთქვათ, $f:\Re(G)\to\Re(G_1)$ აფინური იზომორფიზმია ჰოლის ხ-ხარისხოვან G და G_1 ჯგუფებს შორის, რომლებიც განსაზღვრულნი არიან W და W_1 ველებზე, თუ G არის 2 კლასის ნილპოტენტური, მაშინ f ან ნახევრადწრფივი იზომორფიზმია ან ნახევრადწრფივი ანტიიზომორფიზმი, რომელიც შეესაბამება $\sigma:W\to W_1$ ველების იზომორფიზმს. იგება მაგალითი, რომელიც გვაჩვენებს, რომ თეორემა არ არის სამართლიანი, როდესაც ნილპოტენტურობის კლასი ≥ 3.

REFERENCES

1. *Ph. Hall* (1969), The Edmonton Notes on Nilpotent Groups. Queen Mary College Mathematics Notes. London.
2. *T. Bokelavadze, A. Lashkhi* (2006), Bull. Georg. Natl. Acad. Sci., **173**, 1: 17-18.
3. *A.A. Lashkhi* (1986), J. Algebra, **99**, 1: 80-88.
4. *R. Schmidt* (1994), Subgroup Lattices of Groups. Berlin, New York: de Gruyter.
5. *T. Gelashvili, A. Lashkhi* (1999), Proc. A. Razmadze Math. Inst. **119**: 43-58.
6. *A. Lashkhi* (2007), Doklady Akademii Nauk Rossii, **417**, 3: 313-315 (in Russian).
7. *T. Kvirikashvili, A. Lashkhi* (2004), Sovrem. Mat. Prilozh., No. 22, Algebra i Geom., 126-138 (in Russian); English transl.: (2006), J. Math. Sci., **137**, 5: 5161-5173 (N. Y.).
8. *A. Lashkhi* (2011), Bull. Georg. Natl. Acad. Sci. New Series, **5**, 1: 21-30.
9. *T. Bokelavadze, A. Lashkhi* (2009), Doklady Akademii Nauk Rossii, **429**, 6: 1-4 (in Russian).

Received May, 2011

საქართველოს მეცნიერებათა ეროვნული აკადემიის მოამბე, ტ. 6, №3, 2012
BULLETIN OF THE GEORGIAN NATIONAL ACADEMY OF SCIENCES, vol. 6, no. 3, 2012

Physics

Quantized Chiral Soliton as an Alternative to the Skyrme Model and $\gamma N\Delta$ Vertex

Anzor Khelashvili

Academy Member, High Energy Physics Institute. I. Javakhishvili Tbilisi State University; St.Andrew the First-Called Georgian University of the Patriarchy of Georgia. Tbilisi

ABSTRACT. The problem of soliton stability in the chiral sigma model is investigated. After the brief introductory relations the relevant expression for the Hamiltonian appropriate to the quantization of rotational and vibrational modes as well as the pion mass term is presented. Corresponding equation of motion is exhibited, from which the effective potential is extracted. The existence of minimum of this potential is established and the energy of the ground state is found. It is shown that stability may be achieved only after the breaking of chiral symmetry by pion mass term. The profile function is constructed which guarantees the stability. Mass spectra of nucleon and its resonances are derived. This is analogous to WKB quantization formula.

$$E_n = m_\pi \left(\frac{c}{4a}\right)^{1/2} \left[W_{eff}(Y_0) + \sqrt{2W''_{eff}(Y_0)}\,(n+1/2)\right]$$

where expressions for entering here parameters are given in the main text, Eqs. (15).

Unfortunately the profile functions applied do not satisfy to the equation of motion, therefore their status is unclear. Nevertheless the existence of minimum is a remarkable property for this problem and it underlines the importance of quantum consideration. Therefore it is interesting to calculate appropriate profile function. In this purpose the calculation scheme is proposed for the profile function in the Skyrme anzatz, which then may be applied to delta – nucleon transition problem. The most profound task is a reconstruction of the profile function from the integral relations. For the present only phenomenological consideration shows that by choosing of appropriate test profile functions rather good description of nucleon resonance masses may be achieved. © *2012 Bull. Georg. Natl. Acad. Sci.*

Key words: *chiral soliton, Skyrme model, Skyrme anzatz, mass formula, nucleon-delta transition form factors.*

Skyrme model [1] is a possible effective field theory for quantum chromodynamics (QCD). It explains many static properties of Baryons – nucleons and its resonances [2].

From the view of global symmetries, the Skyrme model is based on $SU(2)\times SU(2)$ chiral sigma algebra and its effective Lagrangian

$$L_{sc} = \frac{F_\pi^2}{2} Tr\left[\partial_\mu U^+ \partial^\mu U\right], \qquad U \subset SU(2)\times SU(2) \tag{1}$$

As is well known [2] this Lagrangian does not provide for the stability of static solitonic solutions. It was found that to ensure stability the addition of various terms to Lagrangian (1) is necessary. But all of this is valid in the framework of classical field theory.

One of the widespread methods consists in addition of a new, so-called Skyrme term [1], which looks like this

$$L_{Sk} = \frac{1}{32g^2} Tr\left[U^+\partial_\mu U, U^+\partial_\mu U\right]^2 = \frac{\varepsilon^2}{4} Tr\left[L_\mu, L_\nu\right]^2, \tag{2}$$

where

$$L_\mu \equiv U^+\partial_\mu U, \tag{3}$$

by means of which the topological current may be constructed as

$$J_\mu = \frac{1}{24\pi^2}\varepsilon^{\mu\nu\lambda\rho} Tr\left(L_\nu L_\lambda L_\rho\right). \tag{4}$$

The topological charge is

$$Q = \frac{1}{24\pi^2}\varepsilon^{0ijk}\int d^3x Tr\left(L_i L_j L_k\right) \tag{5}$$

and it equals the winding number.

Skyrme [1] introduced the so-called "hedgehog" anzatz

$$U_0 = \exp\left\{i\tau\cdot x F(r)\right\}. \tag{6}$$

Where the profile function $F(r)$ must be imposed by definite boundary conditions. Namely, at infinity U has to turn into the unit matrix, or $F(\infty) = 2\pi n$. In particular, $F(\infty) = 0$ is also permissible.

On the other hand, at the origin $F(r)$ must be a well-defined function and must provide turning to unit matrix of U independently of direction, in which $r = 0$ point is approached. It means that we must have

$$\sin F(0) = 0, \quad i.e. \quad F(0) = n\pi \tag{7}$$

Accordingly, $Q = n$. The Skyrme term together with chiral one gives the following scale property for the energy functional

$$E = \frac{1}{\lambda}E^{(2)} + \lambda E^{(4)}, \qquad (x \to \lambda x) \tag{8}$$

and provides a minimum when $E^{(2)} = E^{(4)}$. At the same time the Energy is bounded from below by topological charge

$$E > 12\sqrt{2}\pi^2\varepsilon F_\pi |Q|. \tag{9}$$

Therefore corresponding configurations are stable.

With the aid of chiral angle $F(r)$ the energy (or mass) of static configuration is expressed as

$$M_{Ch} = 2\pi F_\pi^2 \int_0^\infty dr r^2 \left[\left(\frac{\partial F}{\partial r}\right)^2 + \frac{2}{r}\sin^2 F\right], \tag{10}$$

from which in accordance with the variation principle the equation of motion follows

$$r^2\frac{d^2F}{dr^2}+2r\frac{dF}{dr}=\sin 2F(r). \tag{11}$$

Explicit analytic solution of this equation is impossible; therefore one can investigate only the behavior at small and large distances accounting for corresponding boundary conditions and some symmetry properties, such as under the scale transformation

$$F(r)\to F\left(\frac{r}{\lambda}\right) \tag{12}$$

and under the translation $F(r\to 0)=\pi-\frac{r}{\lambda}$.

Numerical calculations, performed by us, show that all the solutions starting from the point $F(0)=\pi$ reach the same asymptotic value $\frac{\pi}{2}$ for different values of negative slope $dF/dr\big|_{r=0}$. However, it differs from the correct boundary behavior, mentioned above. Therefore we have proved by numerical analysis that there are no stable solitonic solutions.

To achieve stability of the chiral solution vector fields are often used as well [3] instead of Skyrme term. There are also many other generalizations of the Skyrme model [4].

One of attractive ideas was proposed in the 1990s [5]. This idea rests on the analogy with quantum mechanics, namely the hydrogen atom after quantization becomes stable, or the bottom of the classical well is a stable point, whereas in quantum mechanics the lowest level is non-trivial according to Heisenberg's uncertainty principle, and so on.

The natural question arises: if *something like this can occur in the chiral model?* It follows from our discussion below that in certain circumstances stability may be guaranteed. Not restricting generality, we consider chiral Lagrangian, taking into account quantization of rotational and vibrational modes and the mass term of the pion.

Quantization is performed by using the transformed chiral field $F\left(\frac{r}{\lambda}\right)$ and accounting for λ as a dynamical variable, i.e. $\lambda=\lambda(t)$. After this the matrix U is taken as follows

$$U=A(t)U_0\left(\frac{r}{\lambda(t)}\right)A^{-1}(t), \tag{13}$$

where U_0 is a Skyrme matrix (6) and $A(t)$ accomplishes quantization of rotational modes. Together with the pion's mass term we derive the following Schrödinger equation [6]

$$\left[-\frac{d^2}{dZ^2}+\left(\frac{b}{4a}\right)^{1/3}Z^{2/3}+\left(\frac{3}{4}+\frac{2a}{I}T(T+1)\right)\frac{1}{Z^2}+\frac{m_\pi^2\,c\,Z}{F_\pi^2\,4\,a}\right]\Phi=\frac{E}{F_\pi}\Phi, \tag{14}$$

where $Z=\sqrt{4a}\lambda^{3/4}$ and Φ is related to the true Schrödinger wave function Ψ according to the relation $\Phi=\Psi\lambda^{3/4}$. Other quantities are defined by

$$a=\frac{8}{9}\pi\int_0^\infty dy y^4\left(\frac{dF}{dy}\right)^2;\quad b=2\pi\int_0^\infty dy y^2\left[\left(\frac{dF}{dy}\right)^2+\frac{2}{y^2}\sin^2 F\right], \tag{15a}$$

$$c=8\pi\int_0^\infty dy y^2\sin^2\frac{F}{2};\quad I=\frac{8\pi}{3}\int_0^\infty dy y^2\sin^2 F. \tag{15b}$$

As the effective potential for this equation is

$$W_{eff}(Z)=\alpha Z^{2/3}+\frac{\beta}{Z^2}+\gamma Z^2, \tag{16}$$

where

$$\alpha=\left(\frac{b^3}{4a}\right)^{1/3};\quad \beta=\frac{3}{4}+\frac{2a}{I}T(T+1);\quad \gamma=\frac{m_\pi^2}{4F_\pi^2}\frac{c}{a} \tag{17}$$

This potential has a non-trivial minimum when one of the parameters α or γ is non-vanishing. Scale transformations now are

$$F\left(\frac{r}{\lambda}\right)=\lambda^3 F(r) \tag{18}$$

and α and γ are not changed in this case. Let us extract γ parameter from the equation by transformation $Y=\gamma^{1/4}Z$. Then the Schrödinger equation gets the form

$$\left[-\frac{d^2}{dY^2}+\alpha\gamma^{-2/3}Y^{2/3}+\frac{\beta}{Y^2}+Y^2\right]\Phi(Y)=\frac{E}{\gamma^{1/2}F_\pi}\Phi(Y) \tag{19}$$

and the ground state energy is written as

$$E=\gamma^{1/2}F_\pi\varsigma\left(\beta,\alpha\gamma^{-2/3}\right) \tag{20}$$

The effective potential has a minimum, which may be determined from the following equation

$$\frac{\beta}{Y_0^2}=\frac{\alpha\gamma^{-2/3}Y_0^{2/3}}{3}+Y_0^3. \tag{21}$$

The solution of this equation looks like this

$$Y_0^{4/3}=\left(-\frac{q}{2}+\sqrt{Q}\right)^{1/3}+\left(-\frac{q}{2}-\sqrt{Q}\right)^{1/3}, \tag{22}$$

where

$$-\frac{q}{2}=\frac{\beta}{2}-\frac{\left(\alpha\gamma^{-2/3}\right)^3}{9},\qquad Q=\left(\frac{\beta}{2}\right)^2-\frac{\beta\left(\alpha\gamma^{-2/3}\right)^3}{9}. \tag{23}$$

The energy spectrum in WKB approximation is

$$E_n=m_\pi\left(\frac{c}{4a}\right)^{1/2}\left[W_{eff}(Y_0)+\sqrt{2W''_{eff}(Y_0)}(n+1/2)\right]. \tag{24}$$

Here

$$W_{eff}(Y_0) = \frac{4}{3}\alpha\gamma^{-2/3}Y_0^{2/3} + 2Y_0^2, \tag{25a}$$

$$W''_{eff}(Y_0) = \frac{16}{9}\alpha\gamma^{-2/3}Y_0^{-2/3} + 8. \tag{25b}$$

Because β is positive, it follows that $Y_0 > 0$ and $W_{eff}(Y_0) > 0$, $W''_{eff}(Y_0) > 0$. Therefore limitation from below is guaranteed! Minimum of energy is achieved at $\alpha = 0$. In this case

$$E_n = \frac{m_\pi}{2}\left(\frac{c}{a}\right)^{1/2}\left(4n+2+2\sqrt{\beta}\right) = \frac{m_\pi}{2}\left(\frac{c}{a}\right)^{1/2}\left(4n+\sqrt{3+8\frac{a}{I}T(T+1)}\right). \tag{26}$$

The analytic solution of the Schrödinger equation gives practically the WKB form

$$E_n = \frac{m_\pi}{2}\left(\frac{c}{a}\right)^{1/2}\left(4n+2+\sqrt{4+8T(T+1)\frac{a}{I}}\right) = \frac{m_\pi}{2}\left[\left(4n+2\sqrt{\frac{c}{a}}+\sqrt{\frac{4c}{a}+8T(T+1)\frac{c}{I}}\right)\right]. \tag{27}$$

Estimation gives

$$\frac{c}{I} = 3\frac{\int dy y^2 \sin^2\frac{F}{2}}{\int dy y^2 \sin^2 F} = \frac{3}{4}\frac{\int dy y^2 \sin^2\frac{F}{2}}{\int dy y^2 \sin^2\frac{F}{2}\left(1-\sin^2\frac{F}{2}\right)} \geq \frac{3}{4} \tag{28}$$

This leads to the following inequality

$$E_0 \geq m_\pi\sqrt{\frac{3T(T+1)}{2}}. \tag{29}$$

It follows that in the chiral soliton stabilization a key role belongs to the chiral symmetry breaking by pion mass term and to the quantized rotational modes.

The above-obtained results can be summarized as follows:
The soliton mass is given by

$$M = M_{Ch} + E_{n,T}, \tag{30}$$

where

$$E_{n,T} = \frac{m_\pi}{2}\sqrt{\frac{c}{a}}\left(4n+2+\sqrt{3+\frac{8a}{I}T(T+1)}\right); \quad (n=0,1,...) \tag{31}$$

This is a mass formula for the nucleon $(T=1/2)$ and the delta resonances $(T=3/2)$.

We have elaborated these relations by numerical methods, using the following phenomenological profile functions

$$F_1(r) = \frac{2\pi}{1+\exp(0,15r)}; \qquad F_2(r) = \frac{\pi}{1+r+0,25r^2} \tag{32}$$

The obtained results are given in the Table

mass(GeV)	N	N'	N''	Δ	Δ'	$\sqrt{\langle r^2 \rangle}$ fm
exp	0.94	1.440	1.710	1.232	1.600	0.72
F_1	input	1.340	1.700	1.220	1.580	0.39
F_2	input	1.320	1.660	1.240	1.580	0.40

We see that these test functions describe experimental mass spectra sufficiently well with only one input parameter used – the nucleon mass, while they do not satisfy the equation of motion. Therefore their status is unclear.

It is interesting to clarify how these model-functions can be applied to other problems. Especially, in calculations of electromagnetic form-factors of nucleon resonances. We consider below delta to nucleon transition form-factors. A relevant electric form-factor of this problem is defined for spacelike momentum transfer $q^2 > 0$ as a Fourier transform of its electric charge

$$G_E^p\left(-q^2\right) = \frac{1}{2}\int_0^\infty dr B_0(r) j_0(qr) \tag{33}$$

with

$$B_0(r) = -\frac{2}{\pi}\sin^2 F\left(\frac{dF}{dr}\right). \tag{34}$$

It is evident from this relation that one needs profile functions of our model. Therefore we give a scheme for elaboration profile function founded on model relations derived above. This scheme is as follows: Our main relations are (30) and (31) for the masses of an isodublet (N, Δ) and their radial excitations. We have for the mass difference

$$N' - N = 2m_\pi\sqrt{\frac{c}{a}} \tag{35}$$

From experimental data one can determine the value of $\sqrt{c/a}$. Then construct the expression

$$N + N' = 2M_{cl} + 4m_\pi\sqrt{\frac{c}{a}} + m_\pi\sqrt{\frac{c}{a}} f_T\left(\frac{a}{I}\right), \tag{36}$$

where

$$f_T\left(\frac{a}{T}\right) \equiv \sqrt{3 + 8\frac{a}{I}T(T+1)}\,. \tag{37}$$

This function may be evaluated from the difference

$$\Delta - N = E_{0,3/2} - E_{0,1/2} = \left[f_{3/2}\left(\frac{a}{I}\right) - f_{1/2}\left(\frac{a}{I}\right)\right]\frac{m_\pi}{2}\sqrt{\frac{c}{a}} \tag{38}$$

Therefore from masses of N, N' and Δ one can calculate unknown quantities

$$\sqrt{\frac{c}{a}}, \qquad \frac{a}{I} \qquad and \qquad f_{a,T}\left(\frac{a}{I}\right)$$

After that we determine the chiral mass, M_{cl}. According to equation (10) we then restore the profile function $F(r)$, and then we'll have all ingredients for calculating other physical quantities, among them $N\Delta\gamma$ transition form-factors.

The Author acknowledges the financial support of the Rustaveli Foundation (Project DI/13/02).

ფიზიკა

დაკვანტული კირალური სოლიტონი, როგორც სკირმის მოდელის ალტერნატივა და γNΔ წვერო

ა. ხელაშვილი

აკად. ი. ვეკუას სახ. თბილისის სახელმწიფო უნივერსიტეტის მაღალი ენერგიების ინსტიტუტი; საქართველოს საპატრიარქოს წმინდა ანდრია პირველწოდებულის სახ. ქართული უნივერსიტეტი, თბილისი

ნაშრომში შესწავლილია კირალური სოლიტონის სტაბილურობის საკითხები მისი ბრუნვითი და ვიბრაციული მოდების დაკვანტვის შედეგად. მცირეოდენი შესაფასი თანაფარდობების შემდეგ მოცემულია ჰამილტონიანის გამოსახულება, რომელიც შეიცავს ბრუნვითი და ვიბრაციული მოდების დაკვანტვის პიონის მასურ წერტილ ერთად. მოყვანილია სათანადო განტოლებები, საიდანაც ადდგენილია ეფექტური პოტენციალი. დადგენილია ამ პოტენციალისთვის მინიმუმის არსებობა და ნაპოვნია ძირითადი მდგომარეობის ენერგია. ჩაჩვენება, რომ სტაბილურობა მიიღწევა მხოლოდ კირალური სიმეტრიის დარღვევის შედეგად პიონის მასური წერით. აგებულია პროფილური ფუნქცია, რომელიც უზრუნველჰყოფს სტაბილურობას. მიღებულია ნუკლონისა და მისი რეზონანსების მასური სპექტრი, რომელიც ანალოგიურია ეგზიკლასიკური დაკვანტვის ფორმულისა:

$$E_n = m_\pi \left(\frac{c}{4a}\right)^{1/2} \left[W_{eff}\left(Y_0\right) + \sqrt{2W''_{eff}\left(Y_0\right)}\left(n+1/2\right)\right]$$

აქ შემაფასი სიდიდების ცხადი გამოსახულებანი მოცემულია მთავარ ტექსტში (15). სამწუხაროდ, გამოყენებული სპექტრალური ფუნქციები არ აკმაყოფილებენ მოძრაობის განტოლებას, რის გამოც მათ სტატუსი ჯერჯერობით ნათელი არ არის. მიუხედავად ამისა, მინიმუმის არსებობა წარმოადგენს მნიშვნელოვან თვისებას ამ პრობლემაში. ამიტომაც სათანადო პროფილური ფუნქციის გამოთვლა საინტერესო ამოცანას წარმოადგენს. ამ მიზნით გადმოცემულია პროფილური ფუნქციის გამოთვლის შესაძლო სქემა სკირმის ჩასმისათვის, რომელიც შემდგომ შეიძლება გამოვიყენოთ დელტა-ნუკლონში გადასვლის ამოცანაში. პროფილური ფუნქციის აგება ანტტკრალური თანაფარდობებიდან წარმოადგენს ყველაზე რთულ პრობლემას. ამ მიზნით ჩვენ ჩაგატარეთ მხოლოდ ფენომენოლოგიური განხილვა, რომელიც გვიჩვენებს, რომ გარკვეული პროფილური ფუნქციის მისადაგებით ვღებულობთ საკმარისად კარგ აღწერას ნუკლონური რეზონანსების მასებისათვის.

REFERENCES

1. *T. Skyrme* (1961), Proc. R. Soc. London., A260: 127.
2. *G.S. Adkins, C.P. Nappi, E. Witten* (1983), Nucl.Phys., B228: 552.
3. *G.S. Adkins, C.P. Nappi* (1984), Phys.Lett., 137B: 251.
4. *I. Zahed,G.E. Brown* (1986), Physics Reports.,142:1.
5. *P. Jain, J. Schechter, R. Sorkin* (1989). Phys.Rev., D39: 998.
6. *A.A. Khelashvili, N.A. Kiknadze* (1992), Preprint TSU HEPI 03-92.

Received August, 2012

საქართველოს მეცნიერებათა ეროვნული აკადემიის მოამბე, ტ. 6, №3, 2012
BULLETIN OF THE GEORGIAN NATIONAL ACADEMY OF SCIENCES, vol. 6, no. 3, 2012

Physics

Quantum Properties of Scalar Fields with Broken *SU(2)* –Symmetry

Vakhtang Gogokhia* and Avtandil Shurgaia**

* *Research Institute for Particle and Nuclear Physics, Wigner Research Centre for Physics, Hungarian Academy of Sciences, Budapest, Hungary; Andria Razmadze Mathematical Institute of I. Javakhisvili Tbilisi State University, Tbilisi*
** *Andria Razmadze Mathematical Institute of I. Javakhisvili Tbilisi State University, Tbilisi*

(Presented by Academy Member Anzor Khelashvili)

ABSTRACT. We consider the simplest theoretical model of scalar fields in one spatial dimension with an internal symmetry. We apply the Schrödinger picture to describe the quantum properties of localized solutions. The use of the method of collective coordinates allows to develop a perturbation theory, which exactly describes the symmetry properties of the theory. As an example, we consider the theory of three scalar fields with a broken SU(2) symmetry, for which we derive the dependence of the energy spectrum on a quantum number corresponding to a charge symmetry. The energy of quantum bound states is the classical energy plus the energy of quantum excitations. The result does not depend on the specific form of the interaction potential. © *2012 Bull. Georg. Natl. Acad. Sci.*

Key words: *collective coordinates, charge symmetry, localized field configurations.*

Quantization of localized in space solutions has a long history. There are several approaches to this problem, mainly within the framework of a functional integration[1-8]. The method of collective coordinates, which indeed uses the parameters of a symmetry group as dynamical variables, is one of them. We apply in the present investigation the operator approach of this method for solving the Schrödinger equation. The advantage of this approach is the absence of an ambiguity related with the operator ordering. Besides, a perturbation theory can be constructed which is manifestly invariant with respect to the group of the symmetry of a theory under consideration in every order of the perturbation series.

We consider below the simplest model with internal symmetry, which is of interest even today, although many articles were devoted to this issue [3, 10-12]. The point is that it is possible in theories with internal symmetry to obtain stable field configurations in more than one space dimension. In papers [3, 10-12] the charge symmetry has been studied and contribution of the charge depending terms to the energy of the system has been evaluated. We want to focus our attention on [10]. In this article the charge symmetry is investigated in detail. It has been shown that there exist charged classical field configurations that are stable owing to the existence of a charge. The centrifugal term and its contribution to the energy have been calculated in the framework of the functional integration. The charge is *assumed* to take on integer values.

The approach used in the present article starts from the quantum theory and suggests the construction of a perturbation theory around the classical neutral field configuration (around charged configurations is also possible). The charge is quantized such that the exact dependence of the energy on the charge is represented. Besides, the operator ordering problem, which requires special treatment in the frame of a functional integration, does not arise in this approach.

The Model with the *U(1)* Symmetry

We consider the model of scalar triplet in one space dimension with a broken *SU(2)* symmetry. The Hamiltonian of the model is

$$H = \int dx\{\pi_\alpha(x)\pi_\alpha(x) + \frac{1}{2}\frac{\partial\varphi_\alpha(x)}{\partial x}\frac{\partial\varphi_\alpha(x)}{\partial x} + U(\varphi_1(x),\varphi_3(x),g)\} \tag{1}$$

with the following commutation relations between the field operators:

$$\left[\varphi_\alpha(x),\pi_\beta(y)\right] = i\delta_{\alpha\beta}\delta(x-y). \tag{2}$$

The Greek indices α, β, γ take on values 1, 2, 3 and Latin indices – 1, 2. The fields $\varphi_\alpha(x)$ form the charged and neutral fields. The potential $U(\varphi_1(x),\varphi_2(x),\varphi_3(x),g)$ is suggested to be breaking the *SU(2)* symmetry and obeys the condition:

$$U(\varphi_1(x),\varphi_2(x),\varphi_3(x),g) = g^2U(g\varphi_1(x),g\varphi_3(x),1). \tag{3}$$

Thus the model is *U (1)* invariant and, as a result, the charge of the system

$$Q = \int dx\{\varphi_1(x)\pi_2(x) - \varphi_2(x)\pi_1(x)\} \tag{4}$$

is conserved. We apply the method of collective coordinates to the Schrödinger equation

$$H\Psi(\varphi_1(x),\varphi_3(x)) = E\Psi(\varphi_1(x),\varphi_3(x)) \tag{5}$$

Mention that the operator $\pi_\alpha(x)$ is considered as $-\partial/i\partial\varphi_\alpha(x)$.

Let us introduce the transformations

$$\varphi_i(x) = D_{ij}(\vartheta)\left[g\delta_{1j}u(x) + \Phi_j(x)\right], \quad \varphi_3(x) = g\sigma(x) + \Phi_3(x) \tag{6}$$

in which the function $u(x)$ is a c-number and the parameter ϑ together with the fields $\Phi_\alpha(x)$ compose a new set of operators. The matrix $D_{ij}(\vartheta)$ is a two-dimensional matrix of rotation:

$$D_{ij}(\vartheta) = \begin{pmatrix} \cos\vartheta & -\sin\vartheta \\ \sin\vartheta & \cos\vartheta \end{pmatrix}. \tag{7}$$

In order to retain the total number of independent variables a subsidiary condition has to be imposed, namely

$$\int dx N(x)\Phi_\alpha(x) = 0. \tag{8}$$

The c-number $N(x)$ is normalized as follows:

$$\int dx N(x)u(x) = 1. \tag{9}$$

We must now express the momenta $\pi_\alpha(x)$ in terms of the new variables θ, $\Phi_\alpha(x)$.

This is done according to the ordinary rules of differentiation provided that the subsidiary condition (8) is taken into account. In addition to (8) we need to introduce the following projection operator $A_{ik}(x,y) = \delta_{ik}\delta(x-y) - \delta_{2i}\delta_{2j}N(x)u(y)$ with the properties:

$$\int dy A_{2i}(x,y)N(y) = \int dx u(x)A_{2i}(x,y) = 0, \quad \int dy A_{ij}(x,y)A_{jk}(y,z) = A_{ik}(x,z). \tag{10}$$

The fields $\Phi_\alpha(x)$ can be expressed as

$$\Phi_k(x) = \int dz A_{kj}(y,z)\overline{D}_{ji}(\vartheta)(\delta_{i1}u(z) - \Phi_i(z)) \tag{11}$$

in which $\overline{D}(\theta) = D^{-1}(\theta)$. Taking the functional derivative of (8) and (11) with respect to $\varphi_{i\sigma}(x)$, we obtain:

$$\pi_k(x) = \overline{D}_{ji}(\vartheta)\{\Pi_j(x) + \frac{N(x)\delta_{2k}}{g-F}(p_\vartheta + \overline{Q})\}, \tag{12}$$

$$\pi_3(x) \equiv \Pi_3(x) = \frac{\delta}{i\delta\Phi_3(x)}. \tag{13}$$

In this expression the following notations are used: $\overline{Q} = \overline{J}_{ik}\int dx\Phi_k(x)\Pi_i(x)$ is the charge of mesons (described by the fields $\Phi_j(x)$), the antisymmetric matrix

$$\overline{J}_{ik} = \frac{\partial\overline{D}(\vartheta)}{\partial\vartheta}|_{\vartheta=0}$$

is the element of the algebra of the group $U(1)$, $\Pi_i(x) = \int dy A_{ji}(y,x)\left(\frac{\delta}{i\delta\Phi_j(y)}\right)$, $F = \int dx N(x)\Phi_1(x)$. The new set of the variables of the system obey the following nonzero commutation relations:

$$[\vartheta, p_\vartheta] = i, \quad [\Phi_j(x), \Pi_k(y)] = iA_{ik}(x,y), \quad [\Phi_j(x), \Pi_k(y)] = i\delta(x-y). \tag{14}$$

We can now write down the kinetic energy in the new representation:

$$K = \int dx \frac{1}{2}\pi_\alpha(x)\pi_\alpha(x) = \int dx\left\{\frac{1}{2}\Pi_3^2(x) + [\Pi_k(x) + \frac{N(x)\delta_{2k}}{g-F}(p_\vartheta + \overline{Q})][\Pi_k(x) + \right.$$
$$\left.\frac{N(x)\delta_{2k}}{g-F}(p_\vartheta + \overline{Q})] - i\frac{N(x)}{g-F}\Pi_1(x)\right\}. \tag{15}$$

As we can see the kinetic energy does not contain the variable ϑ. It is easy to verify that in the new representation the charge operator Q is reduced to p_ϑ, so $Q = p_\vartheta$. Now, the equality (3) and the transformations (6) make it possible to expand the potential U in a series by inverse powers of g, namely

$$U = g^2U(u(x),\sigma(x)) + g\frac{\partial U(u(x),\sigma(x))}{\partial u(x)} + g\frac{\partial U(u(x),\sigma(x))}{\partial\sigma(x)} +$$
$$\frac{1}{2}\frac{\partial^2 U(u(x),\sigma(x))}{\partial u(x)^2} + \frac{1}{2}\frac{\partial^2 U(u(x),\sigma(x))}{\partial\sigma(x)^2} + \frac{\partial^2 U(u(x),\sigma(x))}{\partial u(x)\partial\sigma(x)} + ... \qquad (16)$$

Thus the variable ϑ is cyclic and the operator p_ϑ can be replaced with the c-number. Before doing this, we introduce the transformations, which eliminate the linear and cross terms in the operators $\Phi_j(x)$ and $\Pi_j(x)$ from the kinetic energy. First of all we assume $N(x) = \lambda u(x)$ such that owing to (9) $\lambda\int dxu^2(x) = 1$. The quantity F can now be rewritten as λh with $h = \int dxu(x)\Phi_1(x)$. Secondly, we change the wave functional $\Psi(\theta,\Phi_\alpha(x))$ as follows:

$$\Psi(\vartheta,\Phi_\alpha(x)) = \frac{1}{\sqrt{g-\lambda h}}\widetilde{\Psi}(\vartheta,\Phi_\alpha(x)).$$

Making use of this substitution we finally obtain for the Hamiltonian

$$H = \int dx\{\frac{1}{2}\frac{\partial}{\partial x}(\delta_{1i}u(x)+\Phi_i(x))\frac{\partial}{\partial x}(\delta_{1i}u(x)+\Phi_i(x)) +$$
$$\frac{1}{2}\frac{\partial}{\partial x}(\sigma(x)+\Phi_3(x))\frac{\partial}{\partial x}(\sigma(x)+\Phi_3(x)) + U + \frac{1}{2}\Pi_\alpha(x)\Pi_\alpha(x)\} +$$
$$\frac{\lambda}{2}[\frac{1}{g-\lambda h}(p_\vartheta+\widetilde{Q})\frac{1}{g-\lambda h}(p_\vartheta+\widetilde{Q}) - \frac{1}{4}] \qquad (17)$$

which acts on $\widetilde{\Psi}(\vartheta,\Phi_\alpha(x))$. We can now factor out the ϑ-dependence in the wave functional since ϑ is cyclic:

$$\widetilde{\Psi}(\vartheta,\Phi_\alpha(x)) = \exp(im\vartheta)\Psi'(\Phi_\alpha(x))$$

with $m = 0,\pm1,\pm2,\pm3...$ We now replace the operator p_ϑ by m. All calculations are so far accurate and we did not make any approximation. We have eliminated p_ϑ-dependence from the Hamiltonian and it is now the function of the quantum number m, thereby the charge has been quantized. One can now construct a perturbation theory (which will be manifestly $U(1)$-invariant in every order) by means of expanding the Hamiltonian, the energy and the $\Psi'(\Phi_\alpha(x))$ in terms of inverse powers of g as follows:

$$H = g^2H_0 + gH_1 + H_2 + g^{-1}H_3 + g^{-2}H_4 + ...$$
$$E = g^2E_0 + gE_1 + E_0 + g^{-1}E_3 + g^{-2}E_4 + ...$$
$$\Psi'(\Phi_\alpha(x)) = \Psi_1 + g\Psi_2 + g^2\Psi_2 + ... \qquad (18)$$

We next solve the system of equations:

$$(H_0 - E_0)\Psi_0 = 0,$$
$$(H_0 - E_0)\Psi_1 + (H_1 - E_1)\Psi_0 = 0,$$
$$(H_0 - E_0)\Psi_2 + (H_1 - E_1)\Psi_1 + (H_2 - E_2)\Psi_0 = 0, \qquad (19)$$
$$.....$$

We do not specify the potential U since we aim to quantize the charge and to obtain the exact dependence of the Hamiltonian on the charge. We shall only make some remarks regarding the equations (19). It is evident, that the leading equations of order g^2 and g reproduce the classical equations of motion with the zero charge solutions $u(x)$ and σ and classical energy of neutral field configurations. The equation of order g^0 is bilinear in field operators $\Phi_\alpha(x)$ and $\Pi_\alpha(x)$, which formally can be diagonalized. The result is infinite sum of oscillators and must be regularized. The charge dependence of the energy arises in the approximation of the order g^{-2} and is of the form:

$$E_4 = \frac{\lambda}{2}(m^2 + 2m < \overline{Q} >_0 + < \overline{Q}^2 >_0 - \frac{1}{4}).$$

The symbol $<>_0$ denotes the average over the ground states of oscillators. One can show that $< \overline{Q} >_0 = 0$. We see that the charge is quantized in a natural way and takes on integer values as a consequence of the periodicity of the wave functional in ϑ (and this is an exact result, which does not depend on any further approximation) as opposed to the article [10], in which the charge is *assumed* to be an integer.

In this article we were interested in the simplest case of internal symmetry. The realistic theories with higher symmetry in more than 2-dimensions are of more interest which is the subject of further investigation. Besides, application of our method to QCD at finite temperature [13, 14] is of great interest. We suggest studying the topological properties of the QCD ground state and phasing transitions due to the objects like periodic instantons.

Acknowledgements. The authors acknowledge support by the Hungarian National Fund OTKA - 77816 - P. Levai (V. Gogokhia) and by the Grant of the Georgian National Science Foundation GNSF/ST-08/ 4-405 (A. Shurgaia).

ფიზიკა

სკალარული ველების კვანტური თვისებები დარღვეული SU(2) სიმეტრიით

ვ. გოგოხია*, ა. შურღაია**

* უნგრეთის მეცნიერებათა აკადემია, ვიგნერის ფიზიკის კვლევითი ცენტრი, ნაწილაკთა და ბირთვული ფიზიკის კვლევითი ინსტიტუტი, ბუდაპეშტი, უნგრეთი; თბილისის ი. ჯავახიშვილის სახ. სახელმწიფო უნივერსიტეტი, ა. რაზმაძის სახ. მათემატიკის ინსტიტუტი

** თბილისის ი. ჯავახიშვილის სახ. სახელმწიფო უნივერსიტეტი, ა. რაზმაძის სახ. მათემატიკის ინსტიტუტი

(წარმოდგენილია აკადემიის წევრის ა. ხელაშვილის მიერ)

ნაშრომში განხილულია სკალარული შინაგანი სიმეტრიის მქონე ველების უმარტივესი მოდელი ერთგანზომილებიან სივრცეში. სივრცულად ლოკალიზებული კლასიკური ამოხსნების კვანტური

ფოფაქცვის შესასწავლად არჩეულია შრედინგერის სურათი. კლექტიური კოორდინატების გამოყენება შესაძლებელს ხდის აგებულ იქნას შეშფოთების თეორია, რომელიც ზუსტად აღწერს თეორიის სიმეტრიის თვისებებს. მაგალითის სახით განხილულია სამი ურთიერთმოქმედი სკალარული ველის თეორია დარღვეული SU(2) სიმეტრიით. მიღებულია ენერგეტიკული სპექტრის დამოკიდებულება დაკვანტულ მუხტზე, რაც შეესაბამება სისტემის მუხტურ სიმეტრიას. ბმული მდგომარეობების ენერგია არის კლასიკური ენერგიისა და კვანტური აგზნებების ენერგიების ჯამი. შედეგი არ არის დამოკიდებული ურთიერთქმედების პოტენციალის კონკრეტულ სახეზე.

REFERENCES

1. *R. Dashen, B. Hasslacher and A. Neveu* (1974), Phys.Rev., **D10**: 4114.
2. *R. Dashen, B. Hasslacher and A. Neveu* (1974). Phys.Rev., **D10**: 4130.
3. *E. Tomboulis and G. Woo* (1976), Nucl. Phys., **B107**: 21.
4. *J. Goldstone and R. Jackiw* (1975), Phys.Rev., **D11**: 1486.
5. *J.-L. Gervais and B. Sakita* (1975), Phys.Rev., **D11**: 2943.
6. *C.G. Callan and D. Gross* (1975), Nucl. Phys., **B93**: 29.
7. *N.H. Christ and T.D. Lee* (1975), Phys. Rev., **D12**: 1606.
8. *N.E. Tyurin and A. Shurgaia* (1973), Teor.Mat.Fiz., **16**: 197.
9. *A. Shurgaia and H.J. W. Müller-Kirsten* (2007), Int. J. Mod. Phys., **A22**: 3655.
10. *R. Rajaraman and E. Weinberg* (1975), Phys.Rev., **D11**: 2950.
11. *T.D. Lee* (1976), Phys. Rep., 23C. 254.
12. *R. Friedberg, T.D. Lee and A. Sirlin* (1976), Phys. Rev., **D13:** 2739.
13. *C. Montonen* (1976), *Nucl. Phys.*, **B112**: 49.
13. *G.G. Barnaföldi, V. Gogokhia* (2010), J. Phys. G: Nucl. Part. Phys., **37:** 025003; arXiv:0708.0163.
14. *V. Gogokhia, M. Vasuth* (2010), J. Phys. G: Nucl. Part. Phys., **37:** 075015; arXiv:0902.3901.

Received June, 2012

საქართველოს მეცნიერებათა ეროვნული აკადემიის მოამბე, ტ. 6, №3, 2012
BULLETIN OF THE GEORGIAN NATIONAL ACADEMY OF SCIENCES, vol. 6, no. 3, 2012

Physics

Azimuthal Correlations between Protons in the Backward and Forward Hemispheres in Nucleus-Nucleus Collisions at a Momentum of 4.2 GeV/c per Nucleon

Lida Chkhaidze*, Tamar Djobava*, Lali Kharkhelauri*

High Energy Physics Institute, I. Javakhishvili Tbilisi State University

(Presented by Academy Member Anzor Khelashvili)

ABSTRACT. Multiparticle azimuthal correlations between protons have been investigated in (d, He)C, CC, (d,He)Ta and CTa collisions at a momentum of 4.2 GeV/c and "back-to-back" correlations have been observed. Essentially, correlation function $C(\Delta\varphi)$ for protons from these collisions increases with $\Delta\varphi$ and reaches maximum at $\Delta\varphi = 180^0$ (the angle between the vector sums of the forward and backward emitted protons). The asymmetry coefficient $|\xi|$ decreases and the strength of correlation ς increases with increase of the projectile and target mass numbers. The dependence of the mean of the square transverse momentum in the reaction plane $\langle P_x^2 \rangle$ on $\Delta\varphi$ shows similar behaviour for all observed interactions.

The data stem from the propane bubble chamber (PBC-500) system utilized at JINR. The quark gluon string and the ultrarelativistic quantum molecular dynamics models satisfactorily describe the experimental results. © *2012 Bull. Georg. Natl. Acad. Sci.*

Key words: *multiparticle azimuthal correlations, collision, nucleus, proton.*

One of the main goals of relativistic heavy-ion collisions experiments is to study nuclear matter under extreme conditions of high densities and temperatures [1,2]. The most impressive results of high energy heavy ion research so far are the collective phenomena discovered in these reactions. Study of multiparticle correlations [3-6] offers unique information on the space-time evolution of the colliding system. Over the last years we have studied experimental data using the collective variables depending on the transverse momentum of all secondary particles in the azimuthal plane, to reveal nontrivial effects in nucleus-nucleus collisions [7-11].

In this paper we present the results of the analysis of multiparticle correlations in (d, He)C, CC, (d,He)Ta and CTa collisions (4.2 GeV/c). Azimuthal correlations between protons and the dependence of these correlations on the projectile (A_p) and target (A_t) nucleus mass numbers have been investigated.

Table 1. The number of experimental and generated events (N_{event}) and participant protons (N_{prot}), the asymmetry coefficient (x) and the strength of the correlation (V) in (d,He)C, CC, (d,He)Ta and CTa collisions.

A_P, A_T	N_{event}	ξ	ς
(d,He)C exp.	14318	-0.417±0.015	0.411 ± 0.015
UrQMDM	59218	-0.418± 0.009	0.410±0.009
CC exp.	15962	-0.369±0.013	0.461 ± 0.014
QGSM	36 457	-0.357±0.010	0.474±0.011
(d,He)Ta exp.	2956	-0.309 ±0.028	0.528±0.033
UrQMDM	17629	-0.321±0.022	0.514±0.025
CTa exp.	2469	-0.234±0.033	0.571±0.043
QGSM	42295	-0.242±0.010	0.610±0.013

Experimental data. The data of dC, HeC, CC, dTa, HeTa and CTa interactions have been obtained using 2 m Propane Bubble Chamber (PBC-500) of JINR (3.4 GeV/nucleon). The chamber was placed in a magnetic field of 1.5 T. Three Ta plates 140x70x1 mm in size mounted into the fiducial volume of the chamber at a distance of 93 mm from each other, served as a nuclear target. Protons with momentum p<150 MeV/c have not been detected within this chamber (as far as their track lengths l<2 mm) and protons with p<200 MeV/c are absorbed in Ta target plate (the detector biases).

The method of separation of dC, HeC and CC collisions in propane, the processing of the data, identification of particles and discussion of corrections is described in detail in [12]. Corrections by azimuthal angle distributions for protons were added. Because protons only with momentum p<750 MeV/c were identified, added identification of π^--mesons removal of their admixture from the positive charged particles was necessary. The identification was carried out by statistical methods, it had been assumed that π^- and π^+ mesons have similar distributions [10]. In order to increase the statistics, (d, He)C and (d, He)Ta collisions were combined for further analysis. In separating the so-called "participant proton" from fragmentation products, the following criteria were adopted: p > 3 GeV/c and $\vartheta < 4°$ (for C target), p > 3.5 GeV/c and angle $\vartheta < 3°$ (for Ta target) for projectile fragmentation and p < 0.3 GeV/c (for C target), p < 0.25 GeV/c (for Ta target) for target fragmentation. A sub-sample of "semicentral" collisions with the number of particles N ≥ 3 was selected for analysis from the whole ensemble of (d, He)C, CC, (d,He)Ta and CTa inelastic collisions (see Table 1).

Azimuthal correlations between protons The procedure for study of the correlations between groups of particles was developed in Refs. [5,6]. The azimuthal correlation function was defined by the relative opening angle between the transverse momentum vector sums of particles emitted forward and backward hemispheres in the target fragmentation region (y_i≈0.2). The data were obtained at 4.9, 60 and 200 GeV (BEVALAC, CERN/SPS).

We applied this method for our data, but the analysis was carried-out in the central rapidity region instead of the target rapidity range of Refs. [5, 6]. The analysis was performed event by event, in each event we denote the vectors $\vec{Q}_B = \sum_{y_i<(y)} \vec{P}_{z_i}$ and $\vec{Q}_F = \sum_{y_i\geq(y)} \vec{P}_{z_i}$, <y> was determined by two approaches: average rapidity in each event or in each colliding pair of nuclei. It was mentioned that the results coincide within statistical errors. Then the correlation function $C(\Delta\varphi)$ is constructed as follows $C(\Delta\varphi) = dN/d\Delta\varphi$, where $\Delta\varphi$ is the angle between these vectors:

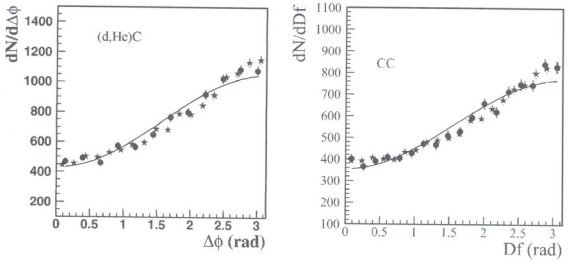

Fig. 1. Dependence of the correlation function $C(\Delta\varphi)$ on the $\Delta\varphi$ for protons from (d,He)C and CC collisions: • – experimental and ★ – generated (see text) data, respectively. The curves are the results of the approximation of the data (see text).

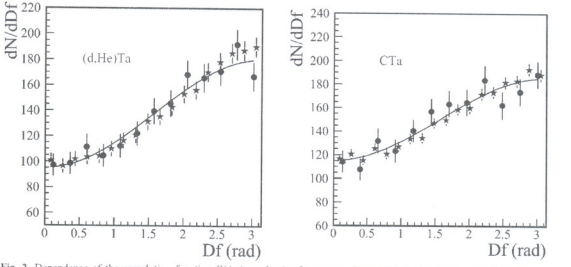

Fig. 2. Dependence of the correlation function $C(\Delta\varphi)$ on the $\Delta\varphi$ for protons from (d,He)Ta and CTa collisions: • – experimental and ★ – generated (see text) data, respectively. The curves are the results of the approximation of the data (see text).

$$\Delta\varphi = \arccos\frac{(\vec{Q}_B \cdot \vec{Q}_F)}{\left(|\vec{Q}_B|\cdot|\vec{Q}_F|\right)}. \qquad (1)$$

Essentially, $C(\Delta\varphi)$ measures whether the particles in the backward and forward hemispheres are preferentially emitted "back-to back" ($\Delta\varphi = 180^0$) or "side-by-side" ($\Delta\varphi = 0^0$).

Figs. 1, 2 show the experimental correlation function $C(\Delta\varphi)$ for protons from (d,He)C, CC, (d,He)Ta and CTa collisions. One can observe from the Figures a clear back-to-back correlation for protons (correlation increases with $\Delta\varphi$, reaches maximum at $\Delta\varphi = 180^0$). To quantify these experimental results, the data were fitted by $C(\Delta\varphi) = 1+\xi\cos(\Delta\varphi)$. Results of the fitting are listed in Table 1. The strength of the correlation is defined as:

$$\varsigma = C(0^\circ)/C(180^\circ) = (1+\xi)/(1-\xi) \qquad (2)$$

As can be seen from Table 1, the asymmetry coefficient $\xi<0$ and thus the strength of correlation $\varsigma<1$ for protons in these interactions.

We studied the dependence of the asymmetry coefficient (ξ) on mass numbers of projectile (A_P) and target (A_T) for protons. The absolute values of ξ

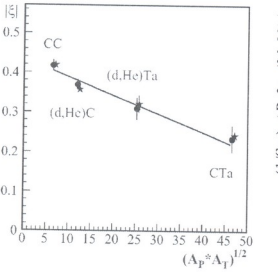

Fig. 3. Dependence of the asymmetry coefficient (□) on $(A_p{}^*A_T)^{1/2}$ for protons in (d,He)C, CC, (d,He)Ta and CTa collisions: • – the experimental and ★ – generated (see text) data.

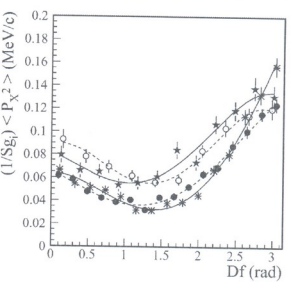

Fig. 4. Dependence of $< P_X{}^2 >$ on $\Delta\varphi$ (as described in the text) for protons in: * – (d,He)C, • – CC, o – (d,He)Ta, ★ – CTa collisions. Solid and dashed curves are the results of the approximation of the data by 4th order polynomal.

for protons decrease linearly with the increase of (A_p, A_T), from -0.417±0.014 for (d,He)C up to -0.234±0.028 for CTa (see Table 1, Fig. 3).

Back-to-back correlation was observed between protons or pions with the Plastic-Ball detector protons in p + Au collisions at energy of 4.9, 60 and 200 GeV/nucleon [5, 6, 13]. Because the azimuthal correlation function was defined in the target fragmentation region, the correlation parameters in the wide range of energy increases inappreciably.

In CC (2500 event) inelastic interactions at a momentum of 4.2 GeV/c per nucleon in the 2-meter propane buble chamber at the JINR [4] were the back-to-back azimuthal correlations observed between protons or pions, emitted in the forward and backward hemispheres in the c.m.s. of the collisions (-0.5 < y < 0.5). The absolute value of the asymmetry coefficient is $\xi = 0.26 \pm 0.01$ [4]. Since these results were obtained on the minor statistics of our data CC (15962 events), we determined $\xi = 0.24 \pm 0.01$ under the same conditions.

Several theoretical models have been proposed for nucleus-nucleus collisions at high energy. We used the Quark Gluon String Model (QGSM) [14, 15] and Ultra-relativistic Quantum Molecular Dynamics Model (UrQMDM) [16-18] for comparison with experimental data. The QGSM is based on the Regge and string phenomenology of particle production in inelastic binary hadron collisions. The UrQMD model is now widely applied for simulations of particle production and flow effects in various nucleus-nucleus interactions [19, 20], although its original design was directed towards high energies.

We generated CC (2.65 fm) and CTa (6.53 fm) interactions by QGSM and dC (2.79 fm), HeC (2.79 fm), dTa (5.31 fm) and HeTa (5.46 fm) interactions by UrQMDM, as well as 50000 events for dC, HeC, CC, CTa and 1000 events for dTa, HeTa collisions.

The experimental selection criteria were applied to the generated events and the protons with deep angles greater than 60–grad were excluded, because in the experiment the registration efficiency of such vertical tracks is low. From the generated events, events with two protons were selected for C-target p>150 MeV/c and for Ta-target p > 200 MeV/c (Table 1).

There is a fairly good agreement between the experimental and the theoretical distributions (Figs. 1÷3).

As obtained in our previous articles [7, 8, 21, 22], the dependence of the mean transverse momentum in the reaction plane $< P_X >$ on the rapidity

y showed the typical S-shape behaviour in collisions observed for protons and pions. In order to extend these investigations, we obtained the relation between $\langle P_x \rangle$ and the angle $\Delta\varphi$ (opening angle between $\mathbf{Q}_B$ and $\mathbf{Q}_F$ vectors). These distributions are normalised on the sum weights of all events (Fig. 4). One can see from this figure that the distributions show similar behaviour for protons for all pairs of nuclei.

In summary, a study of azimuthal correlations between protons in (d,He)C, CC, (d,He)Ta and CTa collisions has been carried out.

1. For protons ²back-to-back² correlations were observed in these interactions. The asymmetry coefficient |ξ| decreases and the strength of correlation ς (ς < 1) increases with increase of the (A_p, A_t).

2. The dependence of the mean of the square transverse momentum in the reaction plane $\langle P_x^2 \rangle$ on $\Delta\varphi$ (the angle between the vector sums of the forward and backward emitted protons) shows similar behaviour for all observed interactions.

3. The QGSM and UrQMDM satisfactorily describe azimuthal correlations of protons for all pairs of nuclei.

Acknowledgements

One of the authors (L. Ch) would like to thank the Board of Directors of the Laboratory of Information Technologies of JINR for the warm hospitality.

This work was partially supported by the Georgia Shota Rustaveli National Science Foundation under Grant GNSF/ST08/4-418.

ფიზიკა

წინა და უკანა ნახევარსფეროებში გამოსხივებულ პროტონებს შორის აზიმუტური კორელაციების შესწავლა 4.2 გევ/ც ნუკლონზე იმპულსის დროს

ლ. ჩხაიძე*, თ. ჯობაგა*, ლ. ხარხელაური*

* ი. ჯავახიშვილის სახ. თბილისის სახელმწიფო უნივერსიტეტის მაღალი ენერგიების ფიზიკის ინსტიტუტი

(წარმოდგენილი აკადემიის წევრის ა. ხელაშვილის მიერ)

გამოკვლეულია პროტონებს შორის მრავალნაწილაკოვანი აზიმუტური კორელაციები (d, He)-C, C-C, (d,He)-Ta, C-Ta დაჯახებებში 4.2 გევ/ც ნუკლონზე იმპულსის დროს და დამზერილია ე.წ. "back-to-back" კორელაციები. არსებითად, განხილულ დაჯახებებში პროტონებისათვის C(Δφ)-კორელაციის ფუნქცია იზრდება Δφ-კუთხის ზრდასთან ერთად და აღწევს მაქსიმუმს Δφ= 180⁰. |ξ| აზიმეტრიის კოეფიციენტი მცირდება, ხოლო ς კორელაციის პარამეტრი იზრდება დამცემი და სამიზნის მასური რიცხვების ზრდასთან ერთად. რეაქციის სიბრტყეში განივი იმპულსის გეგმილის კვადრატის საშუალოს Δφ-კუთხეზე დამოკიდებულება მსგავსია ყველა განხილული ბირთვული წყვილისთვის.

ექსპერიმენტული მასალა მიღებულია **JINR**-ის დანადგარზე პროპანის ბუშტოვანი კამერის (**PBC-500**) მეშვეობით. კვარკ-გლუონური სიმერი მოდელი (**QGSM**) და ულტრა რელატივისტური კვანტურ-მოლეკულური დინამიკური მოდელი (**UrQMDM**) დამაკმაყოფილებლად აღწერს ექსპერიმენტულ შედეგებს.

REFERENCES

1. *M. Jacob and Van Than Tran* (1982), Phys. Rept., **88**: 325.
2. *H. Stoecker, J.A. Maruhn, W. Greiner* (1979), Phys. Lett., **81B**: 303.
3. *H.A. Gustafsson, H.H. Gutbrod, B. Kolb, et al.* (1984), Phys. Lett., **142B**: 141.
4. *A.H.Vinitsky, M. Ezbasarov, I.Ya. Chasnikov, et al.* (1991), Yad. Fiz., **54**: 1636.
5. *H. R. Schmidt, R. Albrecht, T.C. Awes, et al.* (1992), Nucl. Phys., **544A**: 449.
6. *T.C. Awes, D. Bock, R. Bock, et al.* (1996), Phys. Lett., **381B**: 29.
7. *L. Chkhaidze, T. Djobava, G. Gogiberidze, L. Kharkhelauri* (1997), Phys. Lett., **411B**: 26.
8. *L. Chkhaidze, T. Djobava, L. Kharkhelauri* (2000), Phys. Lett., **479B**: 21.
9. *L. Chkhaidze, T. Djobava, L. Kharkhelauri, et al.* (2004), Phys. Atom. Nucl., **67**: 693.
10. *L. Chkhaidze, T. Djobava, L. Kharkhelauri* (2002), Phys. Part. Nucl., **2**: 393.
11. *L. Chkhaidze, T. Djobava, L. Kharkhelauri* (2002), Phys. Atom. Nucl., **65**: 1479.
12. *A.L. Bondarenko, R.A. Bondarenko, E.N. Kladnitskaya* et al. (1998), JINR P1-98-292, Dubna.
13. *Th. Lister, K.H. Kampert, H.H. Gutbrod, H.R. Schmidt* (1993), University of Munster, GSI and WA80 Collaboration,GSI-94-1.
14. *N.S. Amelin, E. F. Staubo, L. P. Csernai, et al.* (1991), Phys. Rev., **44C**: 1541.
15. *N.S. Amelin* (1986), JINR P2-86-837, Dubna.
16. *S.A. Bass, M. Belkacem, M. Bleicher, et al.* (1998), Prog. Part. Nucl. Phys., **41**: 225.
17. *L.V. Bravina, M. Brandstetter, M. I. Gorenstein, et al.* (1999), J. Phys., **25G**: 351.
18. *A.S. Botvina, A. S. Iljinov, I. N. Mishustin, et al.* (1987), Nucl. Phys., **475A**: 663.
19. *Md. Nasin, L. Kumar, P.K. Netrakanti, B. Mohanty* (2010), Phys. Rev., **82C**: 054908.
20. *Q. Li, Z. Li, S. Soff, M. Bleicher, H. Stoecker* (2006), J. Phys., **32G**: 151.
21. *L. Chkhaidze, T. Djobava, L. Kharkhelauri, M. Mosidze* (1998), Eur. Phys. J., **1A**: 299.
22. *L. Chkhaidze, P. Danielewicz, T. Djobava, et al.* (2007), Nucl. Phys., **794A**: 115.

Received June, 2012

საქართველოს მეცნიერებათა ეროვნული აკადემიის მოამბე, ტ. 6, №3, 2012
BULLETIN OF THE GEORGIAN NATIONAL ACADEMY OF SCIENCES, vol. 6, no. 3, 2012

Physics

The Tasks Related to the Decommissioning of Georgian Nuclear Research Reactor

Shukuri Abramidze*, Akaki Gigineishvili, Noe Katamadze**, Grigol Kiknadze*, Giorgi Nabakhtiani*, Malkhaz Razmadze*, Zaza Rostomashvili*, Zurab Saralidze****

* *E. Andronikashvili Institute of Physics, I. Javakhishvili Tbilisi State University*
** *Department of Physics, Georgian Technical University*

(*Presented by Academy Member Jumber Lominadze*)

ABSTRACT. The nuclear research reactor IRT-M belonged to the Institute of Physics and operated during the 1960-1988 period. All nuclear fuel (both fresh and spent) was sent out of Georgia after the reactor was shut down. The reactor decommission activity was conducted at different stages. Special activity plans were developed considering safety and security requirements, international experience and local circumstances. The developed decommissioning strategy was based on the idea on possible establishment of a new low power nuclear facility in the tank of the decommissioned reactor. At the first stage the reactor core together with some comparably high active waste was covered with special concrete. A special underwater concreting technology was developed for this purpose. Theoretical assessment of radiation was conducted before the activity. The results of theoretical assessment were in good correlation with data obtained at radiation monitoring during the concreting activity. During the second and third stages the reactor system inside and outside of the reactor building was dismantled. Lacking the capability to conduct full scale radioactive waste treatment, a special technology of waste packaging is developed to meet the safety requirements. The creation of a radioactive waste treatment facility was defined as a next stage of the activity. © *2012 Bull. Georg. Natl. Acad. Sci.*

Key words: *nuclear reactor, decommissioning, radioactive waste.*

The IRT-2000 Research Nuclear Reactor, having the heat power of 2MW, was commissioned in 1960. IRT–2000-type nuclear reactor, designed in the Soviet Union, belongs to the group of light water pool-type reactors, in which the light water is used as a moderator and a reflector of neutrons and as a coolant and a part of biological shielding of the reactor. Nuclear reactors of such type were also built in Russia (Moscow, Tomsk, Sverdlovsk), Byelorussia (Minsk) and Latvia (Riga). Besides, IRT–2000 type research nuclear reactors were constructed in Bulgaria (1961), China (1962), North Korea (1965) and Iraq (1967) [1, 2].

The pool of IRT–2000 reactor was a tank made of

6mm thick aluminum alloy sheets surrounded by 1.8 m thick biological shielding of reinforced concrete. The height of the pool was 7.6 m and the entire volume – about 60 m^3. The following units of the reactor were located on the bottom of the pool under a six-meter water layer: the reactor core, ejection pump and pipelines of the primary circuit of cooling system, loading and unloading devices, channels of control and emergency protection systems and 10 horizontal experimental channels of various diameters (100-150 mm), which bordered the core and served as an outlet of neutron beams to the experimental installations. The pool of the reactor was filled with distilled water up to the height of 7.2 m and was covered with a lid of organic glass. The reactor was also equipped with vertical experimental channels for irradiation of samples in the vicinity and within the core. At the reactor power of 2MW, the maximum flux of thermal neutrons measured in the center of the core was $2.5 \cdot 10^{13}$ n/cm^2·sec, in the water reflector of the core - $5 \cdot 10^{12}$ n/cm^2·sec and at the outlet of the horizontal experimental channels - $5 \cdot 10^{8} \div 1 \cdot 10^{9}$ n/cm^2·sec.

In 1967-1968 the research IRT-2000 nuclear reactor was subjected to the first large-scale refurbishment which was connected with the necessity of increasing reactor power (about two times) and of the possibilities of carrying out the experiments mainly in the reactor core. The refurbished reactor, named IRT-M (M-modernized), had the power of 4MW and it operated reliably till 1973. In 1973-1975 the IRT-M reactor was subjected to the second large-scale refurbishment with the following aims: to replace the aluminum tank and in-tank equipment of the reactor by a tank and the same equipment made of stainless steel - being the most corrosion protective material. The new IRT-2M - type fuel assemblies and the modification of the cooling system with the use of new circular pumps allowed to increase the reactor power to 8MW. Accordingly, the neutron flux was increased up to ~10^{14} n/cm^2·sec.

For 28 years (1960-1987) the nuclear reactor of the Institute of Physics operated more than 70,000 hours. More than 9 000MW·day heat energy was produced, which corresponds to the consumption of nuclear fuel - Uranium-235 in the amount of 11 kg. 201 fuel assemblies of various types were used, in which the total content of 90% enriched Uranium-235 was about 30kg.

In 1990 the Presidium of the Georgian Academy of Sciences, taking into account the limited life time and absence of further safe operation of the reactor, the decision was issued to shut down the reactor and start its decommissioning procedure. The decommissioning activity was based on the concept of transforming the reactor to a low power nuclear facility using the reactor infrastructure (mainly the reactor pool to install the new nuclear device in it).

Preliminary decommissioning activities

The prepared Preliminary Decommissioning Plan (PDP) considered the following activities:

- Unloading the spent fuel from the reactor core.
- Preparation of the spent fuel assemblies of all types accumulated at the reactor by the time of its shutdown for their transportation to the reprocessing plant, and to accomplish the measures for their transportation in accordance with the transport regulations.
- Return of the fresh nuclear fuel in the form of separate rod type fuel elements and assemblies of different design to the manufacturer (or shipment to another reactor).
- Preparation of a complete inventory of all kind radioactive waste accumulated at the reactor site during its long operation life.

According to the programme all fuel (both fresh and spent) under international control was sent out of Georgia. Special radiological characterization of the reactor structures was done. ^{60}Co radioanuclide was defined as the main contaminant with total amount ~2 TBq. The greatest part of contaminated devices contains auxiliary system pipes that are characterized by inner surface contamination.

Based on the obtained data a Detailed Decommissioning Plan (DDP) has been prepared in accordance with the International Atomic Energy Agency (IAEA) guidance [2,3] and advice provided by the IAEA via the relevant Technical Cooperation Project (GEO/4/002) - "Conversion of Research Reactor to a Low Power Facility"[4].

The plan considered three stages:

I – Concreting of the lower part of redundant Research Nuclear Reactor IRT-M and cumulated high radioactive waste;

II – Dismantling of the technological systems of the Reactor;

III – Dismantling of the external technological system of the low-temperature complex of the reactor.

Concreting of the lower part of the reactor pool

It was decided to make a special confinement for the reactor core by filling of the lower part of the reactor pool (where the core is situated) by shielding material [4]. This confinement should also include some comparable highly contaminated small parts of the reactor devices. It is foreseen that a new low power nuclear device can be installed on the confinement in the existing reactor pool. The decision was based on the following criteria:

- No radioactive waste storage facility existed at that time;
- Lack of appropriate financial and human resources and technical devices.

It was also considered that the proposed method:

- is radiologically and ecologically safe;
- is radiation resistant and seismically safe;
- achieves minimal generation of radioactive waste and hence, copes with the problem of their accumulation, conditioning and transportation;
- financially affordable;
- provides the possibility of installing a new low power facility in the radiation free part of the reactor tank.

Before carrying out the procedure of the confinement, a special theoretical estimation of gamma-radiation on the surface of the concrete was made, using computer code "MicroShield" [5]. First of all, the possibility of using different shielding materials was estimated. The analysis of the obtained results shows the preference of concrete, considering the financial resources and technical aspects of the planned work. It should be emphasized that, according to the calculations, the amount of concrete, necessary to reduce gamma dose rate to natural background is not very large, and there is enough free space in the reactor tank to install a low power nuclear facility, which can be used for medical purposes (producing of medical radionuclides or treatment exposure of medical patients).

In accordance with the elaborated plan, the whole activity was divided into the following ten steps:

1. Preparation of the reactor hall;
2. Preparation of the reactor tank with its internals;
3. Preparation of the experimental horizontal channels;
4. Preparation of the radioactive waste;
5. Preparation of the auxiliary systems and reactor equipment;
6. Concreting the reactor tank;
7. Concreting the 8 experimental horizontal channels;
8. Concreting the waste in the dry storage vertical channels;
9. Concreting the waste in the storage well;
10. Installation of the monitoring and surveillance system.

A special underwater concreting method was used for filling the reactor tank with special concrete. The method provides more efficient shielding for specialists engaged in concreting the tank. During the operation gamma dose rates were measured at different stages. A comparison of the measured data with the calculated values proved the acceptance of the conducted theoretical calculations. Thus, at the first stage the water was pumped out to the mark 2.85m above the tank bottom level. The gamma

dose rate measured on the surface of water was equal to 5μSv/h (Calculated value 8.75μSv/h). At the next stage the reactor tank was filled with the concrete (underwater concreting) up to the mark 1.75 m from the tank bottom. The measured value of the dose rate on the water surface was 0.4μSv/h (calculated value 0.2μSv/h). After the concreting the water was pumped out from the tank. According to the conducted measurement the gamma dose rate on the surface of the mortar was 25μSv/h (calculated value 26.6μSv/h). According to the theoretical estimations, to reduce the gamma dose rate on the surface of the protective concrete block in the reactor tank practically down to natural background, further concrete-covering of the tank from the mark 1.75m to the mark 2.9m was conducted. All activities were performed under the IAEA Technical Cooperation Project (GEO/4/002) - "Conversion of Research Reactor to a Low Power Facility".

Dismantling of the technological systems of the reactor

It proved possible to conduct the planned activity was due to the construction on the site of Applied Research Center (Reactor site) Centralized Storage Facility (CSF). All activities were conducted under IAEA TC project GEO/3/002 whose aim was "to decontaminate and to dismantle the remaining radioactive parts of the IRT-M research reactor and to manage safely the radioactive waste generated from the dismantling operations". The project scope was defined as a dismantling of all radioactive devices located inside the reactor building, including the following:

1) The dual-circuit cooling system of the reactor.

2) The system of mechanical and chemical purification of the coolant of the primary circuit of the reactor cooling system.

3) The part of the pipeline of the system of circulation of gaseous helium.

4) The system of filters intended for cleaning the air from radioactive gases and aerosols being ventilated from the above-reactor space and different special technological rooms prior to their release into the atmosphere.

5) Devices of mechanical and chemical purification of water of pools intended for temporary storage of the fuel assemblies and cassettes.

Before the dismantling activity a special decommissioning programme was developed. The programme elaboration was based on previously conducted radiological monitoring. Dosimetry and gamma-spectrometry measurements were made on pipelines under dismantling. The values of radioactive contamination of the internal surface of the pipes were estimated by using the data on the characteristics of the material of the pipes and the width of their walls. Another method was used: the pipes were screwed at defined places and smears were taken from internal surfaces of the tubes. The data obtained by both methods shows good correspondence. It was found that the devices are characterized by inner surface not fixable contamination. The main contaminant nuclide was defined as ^{60}Co and ^{137}Cs. According to the obtained results, the average contamination value was 20-30 Bq/cm^2 and dose rates near the contaminated surfaces were in the range 5-50 mSv/h. The total activity of the pipes under dismantling was 1.8×10^7 Bq. The clearance level for radionuclide ^{60}Co was defined as 1Bq/cm^2. Based on this value the pipes from secondary circuit were assigned as radiologically clean. So, secondary circuit tubes were released from radiation control after dismantling.

It should be stated that Georgia has not developed a special system for waste treatment. Therefore special tools and methods for waste processing were developed: All dismantled parts (pipes, valves etc.) were segmented, sealed hermetically and sent to CSF. Many parts of the pipes were screwed; others were cut, using abrasive cutting technique. The big pipes were used as containers (packages) for small ones. As a result, 34 large packages were prepared with the total weight of ~ 6,750 kg. Each package has a label indicating the number and weight of the package.

The special inventory contains detail explanation (including radiological characterization of each package). It is shown clearly that the proposed method creates acceptable safety conditions only for a temporary period of time (several years). Taking into account the possible corrosion and drying of ribbon materials, radionuclide leakage from the packages can appear after some years of storing.. Therefore it is very important to conduct routine radiological survey of the packages kept in CSF. A system for treatment of the waste should be developed to clean all dismantled pieces, which gives a satisfactory level of waste size reduction factor and, (which is most important) the safety level of the waste, taking into account its long-term storage and further opportunity of its disposal.

200l drums were used for conditioning comparably high active and small-size metallic parts, where the waste was covered with concrete. The same technique was used for ion exchange resins, which were placed in stainless steel boxes (4 pieces) and hermetically closed. The boxes were placed into 200l drums and covered with concrete. As the radiological monitoring showed, the dose rate on the surface in the case of opened boxes was: 125-130 μSv/h, and on the surface of closed boxes – 50-55 μSv/h. After concreting of drums with boxes containing resins, the dose rate decreased to 7-10 μSv/h.

Thus, 26 concreted drums were placed into CSF. During this stage all technological systems within the reactor building were dismantled and the following waste generated:

- Concreted waste in drums:
  $^{137}Cs - 1.013 \cdot 10^{10}$Bq and $^{60}Co - 6.2 \cdot 10^{8}$Bq;
- Sealed pumps:
  $^{137}Cs - 8.06 \cdot 10^{6}$Bq and $^{60}Co - 7.44 \cdot 10^{7}$Bq;
- Ion exchanger filter:
  $^{137}Cs - 2.3 \cdot 10^{9}$Bq and $^{60}Co - 7.2 \cdot 10^{8}$Bq;
- Sealed up pipes (packages):
  $^{137}Cs - 1 \cdot 10^{8}$Bq and $^{60}Co - 2.65 \cdot 10^{9}$Bq;
- Sealed heat exchangers:
  $^{137}Cs - 2.59 \cdot 10^{7}$Bq and $^{60}Co - 5.18 \cdot 10^{7}$Bq

Dismantling of the external technological system of the low-temperature complex of the reactor

During the operation of the reactor IRT-M a large number of physical experiments were carried out at low temperatures using liquid nitrogen and helium. The liquid nitrogen was provided to the reactor building from a cryogenic station situated at the reactor site by a special system of tubes. The conducted radiological survey confirms the existence of the same contaminants in the same condition as they were characterized for the reactor building tubes. The maximum contamination was fixed at 380 Bq/cm^2. All activities were conducted under the IAEA TC project GEO/3/004. The same method and tools were used for dismantling and waste treatment. As a result 27 395 kg pipes were dismantled with total activity of $^{60}Co - 1 \cdot 10^{9}$Bq. It was noted that free volume of CSF is not enough to keep all dismantled parts. Therefore dismantling of the cryogenic station was delayed until the waste treatment facility was established at the reactor centre. The facility should be designed to treat all waste generated during the reactor decommissioning and all other types of radioactive waste to reduce their size and convert them into a more safe condition.

ფიზიკა

ქართული ბირთვული საკვლევი რეაქტორის დეკომისიის ზოგიერთი ამოცანები

შ. აბრამიძე*, ა. გიგინეიშვილი**, ნ. ქათამაძე*†, გ. კიკნაძე*, გ. ნაბახტიანი*, მ. რაზმაძე*, ზ. როსტომაშვილი*, ზ. სარალიძე*†

* ა.ჯავახიშვილის სახ. თბილისის სახელმწიფო უნივერსიტეტი, ე. ანდრონიკაშვილის ფიზიკის ინსტიტუტი, თბილისი

** საქართველოს ტექნიკური უნივერსიტეტი, ფიზიკის დეპარტამენტი

(წარმოდგენილია აკადემიკოს ჯ. ლომინაძის მიერ)

ე.ანდრონიკაშვილის ფიზიკის ინსტიტუტის კუთვნილი ბირთვული კვლევითი რეაქტორი **IRT-M** ოპერირებდა 1960-1988 წლებში. რეაქტორის გაჩერების შემდგომ მთელი ბირთვული საწვავი (როგორც ახალი, ისე მოხმარებული) გატანილ იქნა საქართველოდან. რეაქტორის დეკომისია ხორციელდება ცალკეულ ეტაპებად. აქტივობისათვის შემუშავდა სპეციალური გეგმები, რომლებიც ეყრდნობიან ბირთვული უსაფრთხოების და უშიშროების მოთხოვნებს, ითვალისწინებენ საერთაშორისო გამოცდილებას და არსებულ ადგილობრივ სიტუაციას. დეკომისიის სტრატეგია ეყრდნობა იდეას მცირე სიმძლავრის ბირთვული დანადგარის რეაქტორის აზომი განთავსების შესახებ. დეკომისიის პირველ ეტაპზე განხორციელდა რეაქტორის აქტიური ზონის სხვა შედარებით მაღალ აქტიურ ნარჩენებთან ერთად დაბეტონება, რისთვისაც შემუშავდა სპეციალური წყალქვეშა ბეტონირების მეთოდი. სამუშაოების დაწყებამდე განხორციელდა რადიაციული ველების თეორიული შეფასება. მუშაობის დროს წარმოებულმა რადიაციულმა მონიტორინგმა დაადასტურა თეორიული შეფასების შედეგების სისწორე. დეკომისიის მეორე და მესამე ეტაპზე განხორციელდა რეაქტორის შენობის შიგნით და გარეთ მყოფი სისტემების დემონტაჟი. რადიოაქტიური ნარჩენების გადამამუშავებელი სიმძლავრეების არქონის გამო შემუშავდა ამ ნარჩენების შეფუთვის ახალი ტექნოლოგია, რომელიც უზრუნველყოფს რადიაციული უსაფრთხოების საჭირო დონეს. რადიოაქტიური ნარჩენების გადამამუშავებელი მცირე საწარმოს დაფუძნება განისაზღვრა როგორც დეკომისიის შემდეგი ეტაპი.

REFERENCES

1. Directory of Nuclear Reactors, vol. III: Research, Test and Experimental Reactors (Soviet Research Reactor IRT), IAEA, Vienna, 1960, pp. 29-45.
2. *V.V. Goncharov* (1986), Issledovatel'skie reaktory (Konstruktsiia i razvitie). Moscow, p. 13.
3. IAEA Technical Report Series TRS-351: Planning and Management for the Decommissioning of Research Reactors and Other Small Nuclear Facilities, Vienna, 1993.
4. *Sh. Abramidze* (1999), in: IAEA TECDOC-1124, Vienna, pp.38-42.
5. *Sh. Abramidze, N. Katamadze, G. Kiknadze, et al.*(2004), Bull. Georg. Acad. Sci., **169**, 3: 626-629.

Received July, 2011

საქართველოს მეცნიერებათა ეროვნული აკადემიის მოამბე, ტ. 6, №3, 2012
BULLETIN OF THE GEORGIAN NATIONAL ACADEMY OF SCIENCES, vol. 6, no. 3, 2012

Geophysics

Influence of Global Warming on the Near-Surface Air Temperature Field in Georgia

Kukuri Tavartkiladze*, Nodar Begalishvili, Tengiz Tsintsadze**, Antaz Kikava#**

* *Vakhushti Bagrationi Institute of Geography, I.Javakhishvili Tbilisi State University.*
** *Institute of Hydrometeorology, Georgian Technical University, Tbilisi*
\# *Department of Geography, Shota Rustaveli State University, Batumi*

(Presented by Academy Member Tamaz Chelidze)

ABSTRACT. Statistical analysis was conducted (data of 1906-2009) on the change of near-surface air temperature field for various geographical regions of Georgia. The analysis was fulfilled by the dynamical norm method. Data of 89 points existing in 1906-1995 and 28 points in 1996-2009 were used. Restoration of missing observation data with given accuracy and reduction of the data series to the same period of time were carried out by the method of expansion of the random function in natural orthogonal components in multidimensional space.

Natural variability of temperature anomalies, linear and nonlinear trends of the variability, density of space-time change probability are shown. Regional parameters corresponding to two periods of time are compared with each other. Schematic map of change of near-surface air temperature field on the territory of Georgia in 1906-2009 is given.

Facts of fall of temperature on the territory of Western Georgia and significant warming in Eastern Georgia in 1906-1995 have been proved. The data of 1906-2009 on warming in all regions under study have also been proved; tendency of the increase of the global warming intensity over the last 10-15 years within the temperature range 0.2-0.5 °C/100yr is shown. Maximal rate of temperature growth observed on the territory of Kvemo Kartli is defined. Results indicate increase of intensity of global warming on the whole territory of Georgia for last 10-15 years. *© 2012 Bull. Georg. Natl. Acad. Sci.*

Key words*: global warming, air temperature, observation stations, data series, statistical analysis, dynamics of temperature field.*

Study of regional near-surface air temperature field with high accuracy is one of the main problems of modern times since destruction of stable balance of the sun-atmosphere-earth energetic system and a gradual increase of the earth's energy level is doubtless. The first work in this direction for the territory of Georgia was fulfilled for the Initial National Communication and then published as a monograph [1]. In the work the total picture of the change of near-surface air temperature field made at 89 stations on the territory of Georgia in 1905-1995 was described. Unfortunately, it was modified in the Initial National

Communication [2]. As for the change in the near-surface air temperature field since 1996 numerous studies were carried out using various methods and different ways of solution of the problem.

An independent analysis of time series data, restoration of missing observation data, for different reasons, and verification of homogeneity were carried out by the method of expansion of the random function in natural orthogonal components in multi-dimensional space [1,3-8]. It should be noted here that this method is practically the only one which allows us to determine the accuracy of the restoration (error). Furthermore, using this method it is possible to determine time interpolation of series with the error order established *a priori*. The higher accuracy is required the more data are needed to construct a correlation function. Analysis, restoration and control of homogeneity were made with the use of the eigenvalues and eigenvectors of this function. After the building of a perfect database, which is a decisive factor in the climate change study, the change of near-surface air temperature described in [1] was determined by a linear approximation of multiyear oscillations using the method of the least squares. On the basis of the results of the mentioned study maps were compiled determining changes of the near-surface air temperature in Georgia in the 1906-1995.

It is interesting that global warming in the 20th c. in Georgia was revealed in different ways. It grew a bit colder (0.1-0.2°C/100 yr) in Western Georgia and got perceptibly warmer (0.5-0.6°C/100 yr) in Eastern Georgia [1,2].

Based on the above-said two tasks were marked:

- Determination of the air temperature with new approach (in particular introducing the "dynamical norm" [5]) and comparison of it with the results of earlier researches on the basis of the database existing in the last century (1906-1995) on the territory of Georgia;
- Compilation of a new database which includes the period of 1906-2009. The database consists of observation series of 28 meteorological stations, 14 of which are active at present and characterized by a complete observation period. Therefore restoration in the incomplete series of the remaining 14 points is carried out with minimum interference using the non-modified natural data and under control of restoration accuracy.

In order to study the first task, the location of 89 observation points on the territory of Georgia in the 20th c. was considered. For further analysis 4 regions (zones) were assigned: (1) – high mountainous zone of the southern slope of the Caucasus; (2) – Eastern Georgia's plain; (3) – Kolkheti lowland and foothills in Eastern Georgia; (4) – Kvemo Kartli and Meskheti-Javakheti highland. The number of observation stations in each zone is respectively (1) – 22; (2) – 22; (3) – 33; (4) – 12.

Statistical analysis is fulfilled according to the data of 89 stations in 1906-1995. The results show that in most parts of Georgia's territory century-long warming has taken place. In particular, mainly annual temperature increase ~0.5°C/100yr with a maximum 0.8°C/100yr was recorded in Eastern Georgia's region. In South Georgia the increase was 0.8°C/100yr with the maximum 0.8°C/100yr. In high mountainous zone warming and fall of temperature were represented equally, but warming concerned the eastern part of the zone and temperature fall – the western part. Increase of temperature there was ~0.3°C/100yr and cooling ~0.2°C/100yr. It must be noted that if the data of the warm and cold seasons are considered separately, it is evidence that in this zone temperature fall is more significant in the cold season: an average increase of temperature is 0.2°C/100yr, and an average decrease is 0.4°C/100yr. As for the western part of the high mountainous zone of the Caucasus, mainly warming is recorded in the cold season (0.2°C/100yr) and temperature practically does not fall in the warm season. It is natural that such a peculiarity of a temperature change promoted melting of nival glaciers of the Caucasus, which is continuing to the present [9, 10]. Fall of temperature in Western Georgia was confirmed again in the last century [1,2] – tempera-

ture fall was 0.4°C/100yr in average with the minimum 0.85° C/100yr.

Interestingly enough, temperature rise is observed in the warm season in all regions. It totals 0.15-0.62°C/100yr in average with the maximum 1°C/100yr.

Temperature variability within the year should be also noted. In Eastern Georgia the warming takes place almost during the whole year. In this respect only August is an exception: fall of temperature is recorded 0.1°C/100yr in average with the minimum 1°C/100yr, but in October-November the warming-temperature fall spreads equally for areas.

In Western Georgia almost all months were colder except January, February and April. In these three months warming took place on almost the whole territory of the region that finally determined the warming in the cold season of the year in the region.

Peculiarities of the temperature change in Eastern Georgia are repeated in Southern Georgia. August is a different case, temperature fall is registered: 0.5°C/100yr in average with the minimum 1.2°C/100yr.

As for the high mountainous zone of the Caucasus, warming takes place in February-July (6 months, average increase 0.3-1°C/100yr.), and in the other 6 months temperature fall is observed with the average decrease of temperature 0.4-1°C/100yr., which also points to warming in the cold season of year.

In order to study the second problem – dynamics of the air temperature field in 1906-2009, – 28 stations out of 89 were retained for the period of 1996-2009 - 7 stations in each zone. If we take into account that at present 14 stations out of the mentioned 28 are functioning, we can once more point to the minimal interference in the restoration of the observation data of the stations. In this case the restoration and also the reduction of the data of the eration stations to the same period of time were made by the methods of expansion of a random function in orthogonal components (vectors). According to the data of restoration stations in 1906-2009 the accuracy of the month average temperatures (in %) of 1996-2009 in most cases was 85-95%.

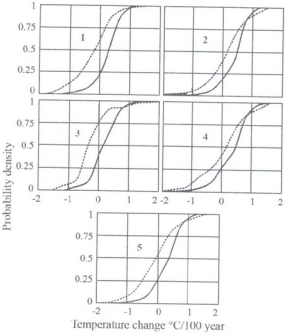

Fig. 1. Temperature change probability density according to 1906-1995 (dashed line) and 1906-2009. (1) – High-mountainous zone of the Caucasus range; (2) – Eastern Georgia's plain; (3) – Kolkheti lowland and foothills in Western Georgia; (4) – Kvemo Kartli and Meskheti-Javakheti highland; (5) – the whole territory of Georgia.

Fig.1 shows probability density of the air temperature change according to the 1906-1995 and 1906-2009 in each selected region. As seen from the figure, at the 0.05 probability level the value of temperature change in Eastern Georgian plain increased from 0.2°C/100yr to 0.5°C/100yr; on the Kolkheti lowland in Western Georgia and foothills - from -0.4°C/100yr to 0.2°C/100yr (temperature fall was replaced with weak warming); at the high mountainous zone of the southern slope of the Caucasus the temperature was increased from -0.2°C/100yr to 0.4°C/100yr (here temperature fall was also changed to warming); in Kvemo Kartli and Meskheti-Javakheti highland – it was increased from 0.2°C/100yr to 0.5°C/100yr.

Thus, the data of 1906-2009 confirm warming in all four regions with the value within the temperature range 0.2-0.5°C/100yr, which indicates the increase of the global warming intensity over the last 10-15 years.

In Fig.1 the same data are presented for the whole

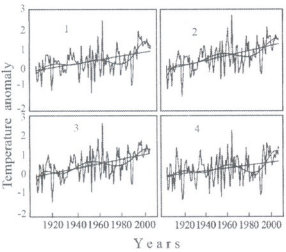

Fig. 2. Changes of temperature anomalies for 4 regions of Georgia (see Fig.1), their linear approximation (linear trend) and 7th order polynomial approximation (nonlinear trend).

territory of Georgia. In this case at the 0.05 probability level the rate of temperature change increased from ~-0.1°C/100yr to distribution of the temperature anomalies through the territory, which confirms intensification of the global warming on the territory of the country.

Fig. 2 shows natural changes in the temperature anomalies for 4 regions of Georgia, their linear approximation (linear trend) and 7th order polynomial approximation (nonlinear trend). It is of interest that in all regions increase of anomalies is recorded, which is confirmed with both linear and nonlinear trends. The fact should be considered that the nonlinear trend revealed significant decrease for the four regions approximately in 1965-1985, which began in 2004. When the nonlinear trend is considered some questions arise on trends of climatic system development change in Georgia, on continuing a decrease of temperature anomalies a decrease of global warming for the nearest decade, etc.

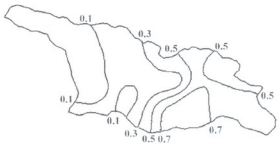

Fig. 3. Temperature field change in Georgia in 1906-2009.

Finally, Fig. 3 presents a schematic map of the changes in near-surface air temperature field in 1906-2009 in Georgia. Isolines depict distribution of the temperature anomalies through the territory.

The picture of temperature field change is homogenous: over the whole territory of Georgia warming is registered, the intensity of which increases from West to East. Maximal rate of temperature growth is observed on the whole territory of Kvemo Kartli where it exceeds 0.8 °C/100yr (Fig. 3).

გეოფიზიკა

გლობალური დათბობის გავლენა საქართველოში მიწისპირა ჰაერის ტემპერატურის ველზე

კ. თავართქილაძე*, ნ. ბეგალიშვილი**, თ. ცინცაძე**, ა. ქიქავა#

* ი.ჯავახიშვილის სახ. თბილისის სახელმწიფო უნივერსიტეტის ვახუშტი ბაგრატიონის გეოგრაფიის ინსტიტუტი, თბილისი
** საქართველოს ტექნიკური უნივერსიტეტის ჰიდრომეტეოროლოგიის ინსტიტუტი, თბილისი
# შოთა რუსთაველის სახელმწიფო უნივერსიტეტის გეოგრაფიის დეპარტამენტი, ბათუმი

(წარმოდგენილია აკადემიკოს წერეთლის მიერ)

ქვეყნის 4 გეოგრაფიული რეგიონისთვის – აღმოსავლეთი და დასავლეთი საქართველო, კავკასიონის მაღალმთიანი ზონა, ქვემო ქართლი და მესხეთ-ჯავახეთის ზეგანი, შესრულებულია ჰაერის ტემპერატურის მიწისპირა ველის ცვლილების სტატისტიკური ანალიზი "დინამიკური ნორმის" შემოტანის საფუძველზე. გამოყენებულია 1906-1995 და 1906-2009 წლებში არსებული შესაბამისად 89 და 28 დაკვირვების პუნქტის მონაცემი. დაკვირვების რიგებში გამოტოვებული ელემენტების დათქმული სიზუსტით აღდგენა და რიგების დაყვანა ერთი და იგივე პერიოდამდე შესრულებულია მრავალგანზომილებიან სივრცეში შემთხვევითი ფუნქციის ბუნებრივ ორთოგონალურ კვეტორებად დაშლის მეთოდით.

წარმოდგენილია ტემპერატურის ანომალიების ბუნებრივი ცვალებადობა, მისი წრფივი და არაწრფივი ტრენდები, ტემპერატურის სივრცით-დროითი ცვლილების ალბათობის სიმკვრივეები. ორი პერიოდის შესაბამისი რეგიონალური პარამეტრები შედარებულია ერთმანეთთან. მიღებულია 1906-2009 წლებში საქართველოს ტერიტორიაზე ჰაერის ტემპერატურის მიწისპირა ველის ცვლილების სქემატური რუკა.

დადასტურდა ვასსერ საუკუნეში (1906-1995) დასავლეთ საქართველოს ტერიტორიაზე მცირე აცივების, ხოლო აღმოსავლეთ საქართველოში შესამჩნევი დათბობის არსებობა. 1906-2009 წლების მონაცემებით დაფიქსირებულია დათბობა საქართველოს მთელ ტერიტორიაზე, რომლის ინტენსივობა იზრდება დასავლეთიდან აღმოსავლეთისკენ ინტერვალში 0.2-0.5°C/100წელი. ტემპერატურის მატების მაქსიმალური სიჩქარე დაიკვირვება ქვემო ქართლში, სადაც ის აჭარბებს 0.8°C/100წ. ეს შედეგი მეუთთებს ბოლო 10-15 წლის განმავლობაში საქართველოს ტერიტორიაზე გლობალური დათბობის ინტენსივობის გაძლიერებაზე.

REFERENCES

1. *K. Tavartkiladze, E. Elizbarashvili, D. Mumladze, J.Vachnadze* (199), Empirical model of the change of overground air temperature field. Tbilisi (in Georgian).
2. *Georgia's Initial National Communication under the United Nations Framework. Convention on Climate Change* (1999), UNPP/GET – Government of Georgia. National Climate Research Centre, Tbilisi, 137 p.
3. *K. Tavartkiladze, A. Kikava, R. Solomonidze, N. Gogatishvili* (2011), in: Proceedings of the Vakhushti Bagrationi Institute of Geography, 3: 35-38, Tbilisi (in Georgian).
4. *K. Tavartkiladze* (2011), in: Proceedings of the Vakhushti Bagrationi Institute of Geography, 3: 38-45, Tbilisi (in Georgian).
5. *K. Tavartkiladze, A. Kikava, R. Solomonidze* (2011), in: "Khandzta" – Periodical Scientific Journal, 5: 67-78 (in Georgian).
6. *N.A. Begalishvili, K.A. Tavartkiladze, D.I. Vachnadze* (2007), Sovremennoe izmenenie klimata v Gruzii. Vekovoe izmenenie vlagosoderzhaniia atmosfery i ego vliianie na vlagooborot. Tbilisi (in Russian).
7. *A.M. Bagrov* (1959), Trudy Tsentral'nogo Instituta Prognozov, 74: 3-24, M. (in Russian).
8. *A.M. Obukhov* (1960), Izvestiia AN SSSR, Ser. Geofizika, 3: 432-439 (in Russian)
9. Georgia's Second National Communication to the UNFCCC (2009), Ministry of Environmental Protection and Natural Researches – UNPP, Tbilisi, 237 p.
10. *L. Shengelia, G. Kordzakhia, G. Tvauri, et al.* (2012), Science and Technologies, 4-6: 67-78 (in Georgian).

Received July, 2012

საქართველოს მეცნიერებათა ეროვნული აკადემიის მოამბე, ტ. 6, №3, 2012
BULLETIN OF THE GEORGIAN NATIONAL ACADEMY OF SCIENCES, vol. 6, no. 3, 2012

Geophysics

Tropical Cyclone: Alignment Effect and Maximum Potential Intensity

Irakli Shekriladze

Department of Hydro Engineering, Georgian Technical University, Tbilisi

(Presented by Academy Member Tamaz Chelidze)

ABSTRACT. The analysis of some major tropical cyclones (TC) has been performed in the framework of the so-called model of equilibrium translation (MET) in order to eliminate the contradiction between the available field data and thermodynamic theory of maximum potential intensity (MPI). According to the MET, TC is an open dissipative system internally aimed at intensification. When this inner focus comes into a certain harmony with large-scale environmental wind, TC becomes particularly effective in the conversion of oceanic heat into kinetic energy of cyclonic motion and rapidly intensifies (alignment effect). Dimensionless Shekriladze number, incorporating integral thermal and dynamical parameters of the system ocean-cyclone-atmosphere (SOCA) acquires the role of a predictor of the character of TC development, including rapid intensification. The MET reveals negative feedback between hurricane heat potential (HHP) and TC translation speed during the alignment effect, leading to a constant mean sea surface temperature (SST) under acting TC, regardless of the initial HPP. In such circumstances, the constancy of real maximum intensities of TCs recorded in field observations at HHPs, exceeding 50 kJ×cm^{-2}, is in agreement with the thermodynamic theory. In addition, the approximate analysis of the field data specified in the regular forecast advisories shows linkage of the alignment effect to the critical value of Shekriladze number around 35. However, this important outcome needs further confirmation by analysis of more detailed field data. © *2012 Bull. Georg. Natl. Acad. Sci.*

Key words: *tropical cyclone, Shekriladze number, maximum potential intensity, equilibrium translation.*

Tropical cyclone (TC) is an extremely complex multiscale phenomenon, the description of which requires accounting for a wide variety of interrelated irreversible thermo-hydrodynamic processes. That is why numerical models have become a major tool in the investigation of TC. Currently, this "great numerical attack" comes with certain achievements, such as TC track forecasting [1-3].

However, progress in forecasting TC intensity is much slower [3-4]. Besides, prediction of TC rapid intensification remains a particular challenge.

Another, important related problem is assessment of maximum potential intensity (MPI). Comparative analysis [5] reveals difficulties with interpretation of the existing field data by a known thermodynamic theory [6-7] considering TC as Carnot heat engine.

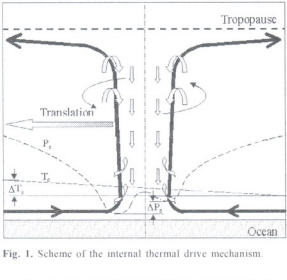

Fig. 1. Scheme of the internal thermal drive mechanism.

To some extent, all these challenges reflect a typical modern problem with proper combination of numerical methods with adequate physical models, including ignoring of the analysis at integral scales of the SOCA.

Model of equilibrium translation (MET) [8] attempts to bridge the gaps linking TC development to a degree of conformity dynamical and thermal fields of the SOCA. At that, dimensionless number, incorporating integral thermal and dynamical parameters of the SOCA [8] (named in [9] as Shekriladze number), acquires the role of the predictor of TC development, including the rapid intensification (alignment effect).

Below we consider the relationships between the alignment effect, MPI and the thermodynamic theory based on the analysis of 8 major TCs of more than 200 observed worldwide in 2003-2012.

Conceptual Basics of the Study

The MET considers sea upper layer as the only source of energy for the development of TC (the applicability of this approach is limited in the range of low HHPs and small diameters of TC, when energy of air inflow is also valuable). The MET also suggests that TC is always under the influence of a certain internal thermal drive mechanism caused by SST asymmetry at TC outer boundary.

Certain initial adaptation of dynamical and thermal fields always holds in the zones of TC development. In the main tropical zones background SST rise is oriented along the dominant environmental wind. In the area of trade winds, SST rise is of the order of 10^{-6}°C×m^{-1}.

At the same time, the internal drive is mainly due to more significant longitudinal gradient of SST, induced by TC translation which inevitably leads to a cooling of sea upper layer and gradual reduction of SST in the rear. According to existing data the resultant SST gradient is of the order of 10^{-5}°C×m^{-1}.

Further, aside from the fact that TC translation is mainly determined by large-scale environmental (steering) wind, the ideal case is considered in which TC moves only under the influence of the internal thermal drive mechanism.

According to the scheme (Fig. 1) SST jump (ΔT_s) results in more intense upstream in front of the eye wall cloud with a minimum air pressure. As eye wall cloud is a dynamic core of the whole system, a pressure drop between its front and rear (ΔP_s) can be assumed as a basis for the internal drive.

Heat and mass transfer from the sea to TC is only slightly dependent on TC translational speed. Here, the main role is played by much higher air tangent velocities. In this regard, slowdown of translation, resulting in the prolonging of the passage of the given sea area, intensifies the cooling of sea upper layer by TC, and on the contrary, the acceleration reduces cooling, all other things being the same.

This inverse dependence creates a rather strong negative feedback in the thermal drive mechanism: decrease of translational speed, along with increasing ΔT_s, leads to increased pressure drop ΔP_s, causing, in turn, TC acceleration. Conversely, increasing of the translational speed reduces ΔP_s, which is slowing down TC.

In such a manner, TC not only prefers to shift toward SST elevation, but it also tends to establish certain equilibrium between translational speed and heat inflow. Similar translation of TC is named as "equilibrium translation". Besides, it is equilibrium translation that is assumed to be a precondition for realization of the aforementioned internal tendency of TC

(rapid intensification and achieving maximum intensity, that is, the so-called alignment effect).

ΔT_s and, accordingly, ΔP_s depend on TC intensity and HHP in a given sea area. Besides, generation of the same driving force requires more slow TC translation at high HHP and vice-versa. This inverse relationship allows to assume, for the equilibrium translation, rough constancy of the so-called heat involvement factor equal to the share of HHP removed by TC through passage of a given area (most of the initial HHP goes down through upwelling [10]).

Then, returning to the dominant role of steering wind, the conclusion must be made that establishment of the equilibrium translation is possible only through favoring by large-scale environmental field. Only accurate inscribing of TC in the steering wind, in the sense of compatibility of the internal tendency with external dynamic field, can turn an "intended" equilibrium translation to the real one.

By the way, in accordance with the MET, later it was established that, in the western North Pacific, "very intense TCs and TCs with rapid intensification rate are found only to occur in a narrow range of translational speeds between 3 and 8 $m \times s^{-1}$" [11], that is, in the range of speeds of trade winds.

Within accepted assumptions, integral heat flow (sensitive and latent) removed from sea strip left behind TC (Fig. 2) can be written as follows:

$$A_{34} \cdot q = C_t \cdot \underline{Q} \cdot \delta S_c , \qquad (1)$$

where A_{34} is an area inside tangent wind velocity 34 knots (TC outer boundary is assumed at the minimum tangent wind specified in regular forecast advisories); q is integral heat flux (sensitive and latent) averaged inside A_{34}; C_t is heat involvement factor; $\underline{Q}$ is HHP averaged inside A_{34}; δS_c is increment of sea surface cooled by TC (cooled surface remaining behind TC during unit time).

Since the involvement factor, constancy of which determines the equilibrium translation, is much less than unity, for convenience, we use its reciprocal to characterize TC development. Accordingly, the following condition for the establishment of the equilibrium translation can be written:

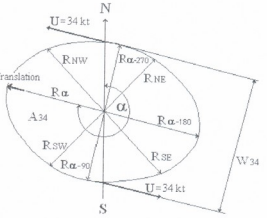

Fig. 2. Scheme of non-circular TC: R_{NE}, R_{SE}, R_{SW} and R_{NW} - TC radii at tangent velocity 34 knots in Northeast, Southeast, Southwest and Northwest quadrants, respectively; α - TC translation azimuth; W_{34} - TC transverse size at tangent velocity 34 knots.

$$Shk_{cr} = \frac{\underline{Q} \cdot \delta S_c}{A_{34} \cdot q} = Const , \qquad (2)$$

where Shk_{cr} is a critical value of Shekriladze number.

Accurate determination of Shk_{cr}, using equation (2), requires the availability of detailed continuous data on TC outer boundary translation and HHP field. Really we use restricted discrete data specified in forecast advisories and HHP maps which gives quite approximate estimates. At that, the following, equivalent to (2), within certain assumptions, relationship [12] is used:

$$Shk_{cr} = \frac{\underline{Q} \cdot U_{bb}}{R_{ef} \cdot q} = Const , \qquad (3)$$

where U_{bb} is translational speed of TC back boundary center; $R_{ef} = 2A_{34}/\pi W_{34}$ is effective radius of TC (it is equal to the radius in the case of circular TC).

Specific Mode of Heat Transfer Associated with Alignment Effect

Dynamic impact of TC involves intensive vertical stirring of sea water (upwelling) [10]. It is easy to show that new SST field that emerged below TC after vig-

orous stirring is much more dependent on the initial heat content of sea upper layer (that is, on the initial HHP) than on the initial SST field. In this regard, further, the initial HHP field (that existed before entering TC) is assumed as the main parameter characterizing, at the stage of forecasting, SST field below TC.

Of course, SST field below TC could most accurately be defined by direct measurements, but such data (leaving aside the technical feasibility) may not be available at the stage of forecasting.

In general, the complex problem of heat and mass transfer from sea surface to TC is far from being fully resolved needing further analytical and experimental studies.

The constancy of Shk_{cr} provides important features of heat transfer from sea surface to TC during equilibrium translation, which significantly simplify the analysis of this particular mode.

Removal by TC of constant share of HHP takes longer at high HHP and vice-versa. In this context, equilibrium translation is characterized by different combinations of translational speed, TC size and integral heat flux resulting in less intense cooling at low HHPs and more intense cooling at high HHPs.

Based on the above negative feedback between HHP and seawater cooling, it may be assumed that SST field below TC is roughly uniform during equilibrium translation, regardless of initial SST and HHP fields. Accordingly, in this mode, the average integral heat flux is approximately independent of the initial fields and becomes a unique function of tangent wind distribution.

At the same time it is clear that the subject matter reduces to near-equilibrium mode of translation, restricting the applicability of the simplified approach outside of this mode. However, such specializing is quite allowable at this stage in respect of our focusing on equilibrium translation.

Further, taking into account the structure of field data in regular forecast advisories, the three-zone model of heat transfer is offered. The first (outer) zone covers the area between tangential winds of 34 knots (17.5 m/s) and 50 knots (25.75 m/s). The second (intermediate) zone covers the area between tangential winds of 50 knots and 64 knots (33 m/s). The third (central) zone covers the area inside tangential wind of 64 knots.

Next, using available field data, the empirical formula is designed for the average integral heat flux from the sea surface during equilibrium translation:

$$q = \left[400\left(R_1^2 - R_c^2\right) + 600\left(R_2^2 - R_1^2\right) + \right.$$

$$\left. + 1,200\left(U_{max}/130\right)R_c^2\right]R_1^{-2}\ \mathrm{W\times m^{-2}}, \qquad (4)$$

where R_1, R_2 and R_3 are average outer radii of the first, second and third zones in meters determined as a quarter of the square root of the sum of squares of the radii of the above four quadrants; U_{max} is maximum tangential wind speed in knots; 130 is maximum tangential wind velocity of reference TC Opal (1995) in knots.

Characteristic zones reference averages 400 $\mathrm{W\times m^{-2}}$ and 600 $\mathrm{W\times m^{-2}}$ are determined based on analysis and rounding the data recorded by NDBC buoy 42001 during development of TC Opal in 1995 [10].

Characteristic of the central zone reference average (1,200 $\mathrm{W\times m^{-2}}$) is determined taking into account that buoy 42001 was located at around 25 km from Opal's center during its maximum intensity and recorded by the buoy maximum heat flux can be accepted as average for all central zone. At the same time, the possibility of a linear extrapolation of this parameter to other cases is assumed.

TC Geometrics and Translation of Back Boundary Center

Firstly, four radii R_{α}, $R_{\alpha-90}$, $R_{\alpha-180}$ and $R_{\alpha-270}$ are defined by simple trigonometric interpolation of the forecast advisory data (α is TC translation azimuth):

$$R_{\alpha} = R_{SW} - \frac{R_{SW} - R_{NW}}{90}\left(\alpha - 315\right) \qquad (5)$$

$$R_{\alpha-90} = R_{SE} - \frac{R_{SE} - R_{SW}}{90}\left(\alpha - 90 - 135\right) \qquad (6)$$

Table 1. Selected strongest TCs.

Q (kJ·cm^{-2})	TC (year), U_{max} (knots)	Q (kJ·cm^{-2})	TC (year), U_{max} (knots)
40	Ma-On (2004), 140	80	Nida (2009), 155
45	Celia (2010), 140	90	Chaba (2004), 155
50	Monica (2006), 155	100	Dianmu (2004), 155
60	Rick (2009), 155	120	Megi (2010), 155

$$R_{\alpha-180} = R_{NE} - \frac{R_{NE} - R_{SE}}{90}(\alpha - 180 - 45) \quad (7)$$

$$R_{\alpha-270} = R_{NW} - \frac{R_{NW} - R_{NE}}{90}(\alpha - 270 + 45) \quad (8)$$

Next TC transverse size (W_{34}), the average radii at the tangential winds of 34 knots, 50 knots and 64 knots (R_1, R_2 and R_3, respectively), the area inside tangential wind of 34 knots (A_{34}) and the coordinates of TC back boundary center (latitude – Lt_{bb}, longitude – Ln_{bb}) are defined:

$$W_{34} = R_{90} + R_{270} \quad (9)$$

$$R_1 = 0.25\left(R^2_{NE,34} + R^2_{SE,34} + R^2_{SW,34} + R^2_{NW,34}\right)^{0.5} \quad (10)$$

$$R_2 = 0.25\left(R^2_{NE,50} + R^2_{SE,50} + R^2_{SW,50} + R^2_{NW,50}\right)^{0.5} \quad (11)$$

$$R_3 = 0.25\left(R^2_{NE,64} + R^2_{SE,64} + R^2_{SW,64} + R^2_{NW,64}\right)^{0.5} \quad (12)$$

$$A_{34} = (\pi/4)\left(R^2_{NE,34} + R^2_{SE,34} + R^2_{SW,34} + R^2_{NW,34}\right) \quad (13)$$

$$Lt_{bb} = Lt_c \pm \left(R_{\alpha-180}/1.11\cdot 10^5\right)Cos\alpha \quad (14)$$

$$Ln_{bb} = Ln_c \pm \left[R_{\alpha-180}/\left(1.11\cdot 10^5 \cdot CosLt_{bb}\right)\right]Sin\alpha \quad (15)$$

Here Lt_c and Ln_c are coordinates of TC center specified in regular advisories; the lengths of degrees of latitude and longitude are accepted as 1.11×10^5 m and $1.11\times10^5\times\mathrm{Cos}Lt_{bb}$ m, respectively.

U_{bb} is defined by geographical coordinates of TC back boundary center as average of uniform straight translation at a track length prior to given position:

$$U_{bb} = \left[1/(\tau - \tau_{-1})\right]\left\{\left[(Lt_{bb} - Lt_{bb-1})\cdot 1.11\cdot 10^5\right]^2 + \left[(Ln_{bb} - Ln_{bb-1})\cdot 1.11\cdot 10^5 CosLt_{bb}\right]^2\right\}^{0.5}, \quad (16)$$

where τ is time of passing by TC given position; subscript -1 corresponds to the same parameter at TC position prior to given position at one track length.

Correlation of the Field Data

As follows from the logic of the above analysis, one must first confirm the linkage of the alignment effect to constant Shk_{cr} and then interpret the data on MPI. Below such an approach is realized relative to 8 TCs reached greatest intensity at a given initial HHP (Table 1).

Taking into account the above limitations with possibly valuable energy contribution of inflowing air at low HHP, only the cases at HHPs exceeding 40 kJ×cm^{-2} are considered. Specified in the forecast advisory maximum sustained wind based on one-minute average is accepted as TC intensity. The values of initial HHP are determined using HHP Maps.

In order to assess the accuracy of the correlation of the field data two values of Shekriladze number are used. The major value Shk_{cr} is based on U_{bb} (eq. (16)). The supplementary value Shk_s is based on the current translation speed of TC center specified in the forecast advisory.

It is assumed that the close agreement between the two values points to nearly uniform straight translation of TC with a nearly constant outer radius. In this case the accuracy of the calculation based on discrete in time and space data can be considered as satisfactory, and, conversely, a significant difference

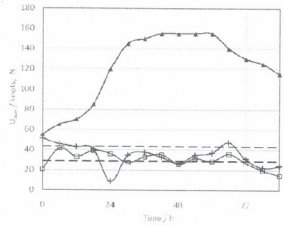

Fig. 3. Correlation of the field data on TC Dianmu: ▲ – maximum tangent wind; + – Shk_m; □ - Shk_v; dotted lines Shk=35±20%; the position 0 - 12:00 hour (UT) 14 JUN 2004.

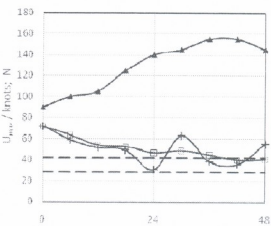

Fig. 4. Correlation of the field data on TC Megi: ▲ – maximum tangent wind; + – Shk_m; □ – Shk_v; dotted lines: Shk=35±20%; the position 0 - 00:00 hour (UT) 16 OKT 2010

between these two values calls into question the accuracy of the calculation procedure.

The calculations produce discrete values of Shk presented in the figures below by points. As for the smoothed curves, they are of purely conventional character.

Super typhoon Dianmu (Fig. 3) emerged in the zone with HHP 70-80 kJ/cm^2 in tropical western North Pacific. Further it translated through the zone with rather high HHP (90-110 kJ/cm^2) and rapidly intensified up to 155 knots. The record intensity of Dianmu, supposedly, is linked to the alignment effect at Shk_{cr}≈35. Besides, Shk_m and Shk_v are roughly the same at this stage.

Super typhoon Megi emerged in the zone with HHP 70-80 kJ/cm^2 in tropical western North Pacific. It translated through the zone with rather high HHP (90-130 kJ/cm^2) and rapidly intensified. According to Fig. 4, the record-breaking intensity of Megi also is linked to the alignment effect at Shk_{cr}≈35. The above correlations are common to most selected strongest TCs except Chaba and Celia the development of which was accompanied by tangible variations of translation speeds and outer radii (as reflected by large differences between Shk_m and Shk_v). As noted above, in this situation, the used approximate calculation procedure cannot provide sufficient accuracy of the correlation.

In general, the results of correlation show the validity of the MET at sufficiently high HHPs (50 kJ×cm^{-2} and more). Maximum intensification of TC (alignment effect) is linked to Shk_{cr} that can be refined as:

$$Shk_{cr} = 35 \pm 20\% \qquad (17)$$

By the way, the rapid intensification of TC Charley (2004), left out of sight prediction services, also took place at about the same Shk_{cr} [12].

Due differences in calculation schemes average heat flux, it is difficult to establish the equivalence of (17) with the previous evaluation Shk_{cr} ≈ 25 [8]. Since the critical value may vary somewhat depending on the assumptions (e.g., on the location of TC outer boundary) and the calculation procedure, the most refined values will be obtained from equation (2) based on continuous detailed field data.

Dependence of maximum intensities of selected strongest TCs on initial HHP is presented in Fig. 5.

The constancy of real maximum intensity in the wide range of HHP supports the MET along with all accepted assumptions and consequences, including the conclusion that alignment effect takes place at roughly constant average SST, irrespective of initial

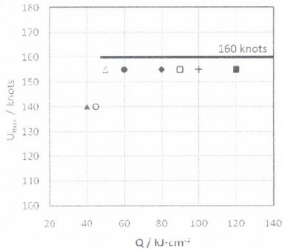

Fig. 5. Relationship between TC maximum intensity and initial HHP: ▲ – Ma-On; ○ – Celia; Δ – Monica; • – Rick; ◆ – Nida; □ - Chaba; + – Dianmu; ■ - Megi.

HHP and SST fields. It also can be concluded that MPI is roughly equal to 160 knots at HHP more than 50 kJ×cm^{-2}.

This removes the above-mentioned qualitative contradiction of the field data with the thermodynamic theory MPI. As for the quantitative agreement, it can be checked only after collection of reliable statistics on the average SST below rapidly developing TCs.

Finally, about TC development at very high HHP (150 kJ×cm^{-2} and more).

According to the MET, at very high HHP, the translational speed related to alignment effect falls significantly lower of characteristic range of dominant regional steering wind. This discrepancy strongly inhibits TC development and makes the development of strong TC unlikely in general, as evidenced by the vast field data, including above strong TCs.

In such a manner, as strange as it may seem, in some cases, increasing HHP and SST, caused, for example, by climate change, may lead even to preventing TC development detuning favorable thermo-hydrodynamic balance in OCAS. And, conversely, in some cases, reduction of HHP could step up TC development.

Concluding Remarks

The MET relates TC development to conformity of thermal and dynamical fields in the SOCA. When favored by large-scale environmental wind, TC tends to rapid intensification at the critical Shekriladze number (alignment effect).

The MET reveals negative feedback between HHP and TC translational speed during the alignment effect. This leads to roughly constant SST below TC and, equally, to rough constancy of MPI at sufficiently high HHP, removing qualitative contradiction of the field data with the thermodynamic theory MPI.

Analysis of the strongest tropical cyclones supports the MET along with accepted assumptions and the main consequences. The same analysis allows to refining the value of critical Shekriladze number to 35±20% and establishing roughly constant MPI (~160 knots) at HHP exceeding 50 kJ×cm^{-2}.

The presented results and conclusions require further refinement based on more detailed and continuous data on parameters of TC and sea upper layer. At the same time monitoring of Shekriladze number of acting TCs can be recommended as potential predictor of forthcoming developments.

გეოფიზიკა

ტროპიკული ციკლონი: თანადობის ეფექტი და მაქსიმალური პოტენციური სიმძლავრე

ი. შეყრილაძე

საქართველოს ტექნიკური უნივერსიტეტი, ატმოსფერული დეპარტამენტი, თბილისი

(წარმოდგენილია აკადემიის წევრის თ. ჭელიძის მიერ)

ტროპიკული ციკლონების საველე მონაცემებსა და მაქსიმალური პოტენციური სიმძლავრის თერმოდინამიკურ თეორიას შორის არსებულ წინააღმდეგობათა გარკვევის მიზნით, წონასწორული ტრანსლაციის მოდელის ჩარჩოებში, ჩატარებულია რამდენიმე მძლავრი ტროპიკული ციკლონის ანალიზი. დადასტურებულია თანადობის ეფექტის წამყვანი როლი ციკლონის განვითარებაში და, გარკვეულ მიახლოებაში, მძლავრი ციკლონების ქვეშ ოკეანის ზედაპირის საშუალო ტემპერატურის მუდმივობა, მიუხედავად განსხვავებებისა საწყის თბურ ველებს შორის. რეალურ მაქსიმალურ სიმძლავრეთა მუდმივობა ფიქსირდება ოკეანის ზედა ფენის საკმარისად მაღალი თბოშემცველობის დროს, რაც, ზედაპირის საშუალო ტემპერატურის ხსენებულ მუდმივობასთან ერთად, ხსნის თვისებრივ წინააღმდეგობას თერმოდინამიკურ თეორიასთან.

REFERENCES

1. *S.V. Poroseva , J. Letschert, M.Y. Hussaini* (2007), Meteorol. Atmos. Phys., **97**: 149-169.
2. *E.S. Blake, R.J. Pasch* (2010), Mon. Wea. Rev., **138**: 705-721.
3. *D.P. Brown, J.L. Beven, J.L. Franklin, E.S. Blake* (2010), Mon.Wea.Rev.,**138**: 1975-2001.
4. *M. DeMaria, J.A. Knaff, C. Sampson* (2007), Meteorol. Atmos. Phys., **97**: 19-28.
5. *L.I. Petrova* (2010), Meteorologiia i Gidrologiia, **6**: 16-25 (in Russian).
6. *K.A. Emanuel* (1988), J. Atmos. Sci., **45**: 1143-1155.
7. *K.A. Emanuel* (1997), J. Atmos. Sci., **54**: 1014-1026.
8. *I. Shekriladze* (2004), Bull. Georg. Acad. Sci., **169**: 298-302.
9. *A.I. Gvelesiani* (2005), J. Georg.Geophys. Soc., **10B**: 3-20.
10. *L.K. Shay, G.J. Goni, P.G. Black* (2000), Mon. Wea. Rev., **128**: 1366-1383.
11. *Z. Zheng, Y. Wang, C.C. Wu* (2007), Mon. Wea. Rev., **135**: 38-59.
12. *I. Shekriladze* (2009), J. Georg. Geophys. Soc., **13A**: 122-133.

Received September, 2012

საქართველოს მეცნიერებათა ეროვნული აკადემიის მოამბე, ტ. 6, №3, 2012
BULLETIN OF THE GEORGIAN NATIONAL ACADEMY OF SCIENCES, vol. 6, no. 3, 2012

Metallurgy

Determination of the Interrelation of Technological and Construction Characteristics of Direct Rolling Process

Giorgi Kevkhishvili*, Temur Namicheishvili*, Irakli Zhordania, Julietta Loria*, Zakaria Melashvili*, Vazha Ramishvili***

* *F. Tavadze Institute of Metallurgy and Materials Science, Tbilisi*
** *Academy Member, F. Tavadze Institute of Metallurgy and Materials Science, Tbilisi*

ABSTRACT. Traditional technology of rolling includes casting of primary billet of large cross-section and then producing thin sheets by hot rolling. Method of direct rolling, in contrast with the traditional technology, allows to obtain thin sheets (0.6-6 mm) by combining processes of continuous casting of liquid metal and rolling.

The method of direct rolling is fairly simple. Liquid metal is passed through a pair of rotating rolls, which are located in horizontal plane at a certain distance from each other equipped with cooling system. By varying rotation velocity of rolls it is possible to regulate metal solidification front which is necessary to establish required conditions for hot rolling process.

In the present paper mechanism of billet formation in the combined crystallizer is considered in detail. Method of theoretical determination of the main technological characteristics of direct rolling for both ferrous and nonferrous metals is conducted. Interrelation of these parameters with construction and energy-power characteristics of the casting-rolling mill is defined.

On the basis of the investigation results a pilot casting-rolling mill was designed and fabricated in metal. *© 2012 Bull. Georg. Natl. Acad. Sci.*

Key words: *crystallizer, billet, front of crystallization, meniscus of liquid metal, arc of deformation zone.*

The challenge of elaboration of new technologies and high effective modular plants for enterprises of low-productivity became topical for steel manufacturing companies of the world. This is partially caused by a sharp decrease of investment due to world economic crisis. To this point of view we developed a method of direct rolling, which means production of thin sheets by means of compact casting-rolling mills. The mentioned method allows to reduce costs of energy resources by 6-7 times and loss of metal by 5-7%; excludes 60-70% of expensive devices (rolling mills) out of technological cycle, which itself stimulates reducing of industrial areas and investment. If one takes into consideration high ecological indices, the actuality and availability of this direction becomes clear.

The method of direct rolling is fairly simple. Liquid metal is passed through a pair of rotating rolls, which are located in horizontal plane at a certain distance from each other and equipped with cooling

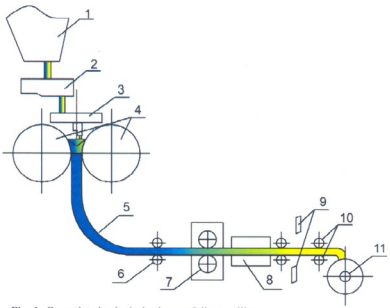

Fig. 1. General technological scheme of direct rolling process.

system. Rotation velocity is chosen in such a way that a billet solidifies after it leaves the rolls. At the same time, it is possible to move a metal solidification front above the interconnecting line of the rolls' centres and in this way regulate the process of hot rolling, which is necessary to produce a dense fine structure. The technological scheme of direct rolling additionally includes standard rolling mills, by means of which the obtained billet is reduced to sheets of needed thickness.

In Fig.1 a general technological scheme of direct rolling process is shown. Liquid metal from the casting ladle 1 goes to the intermediate ladle 2, from where through ladle nozzle 3 it gets to the crystallizer 4 (rotating rolls). After solidification partially rolled billet 5 with the help of guide sheaves 6 gets to the rolling mill 7, where it is rolled to needed thickness. Then, after thermal treatment in special chamber 8 with knives 9 it is cut into sheets of required length.

The method of "rolling without casting", i.e. direct rolling, combines continuous casting and rolling processes, but continuous casting in the classical sense is not carried out in this case, because we have a combined crystallizer (the space of the crystallizer is closed with rotating rolls and side closing plates). In terms of rolls it is the so-called crystallizer with moving walls, in which the billet and walls move synchronously. On the side closing plates it is slip crystallizer.

Let us consider the process of cast forming in the crystallizer (Fig.2).

By varying the rotating velocity (casting speed) it is possible to move the crystallization front (point C of billet complete solidification) towards the horizontal interconnecting line OO′ of the rolls' centres. It is clear from the scheme of rolling in the Fig. that the rolling process runs when the C point is placed above the line OO′, and the more γ-angle, the more relative stretching.

Intensive work has begun since 2009 at the Institute of Metallurgy and Materials Science on the technology of direct rolling. Following elaboration of detailed analysis of the available literature it was decided to design and construct a pilot casting-rolling mill.

When designing the device special attention is given to the correct determination of energy-power characteristics and interrelation between all main technological and construction characteristics of the process.

As the direct rolling process is a combination of two independent processes (continuous casting and

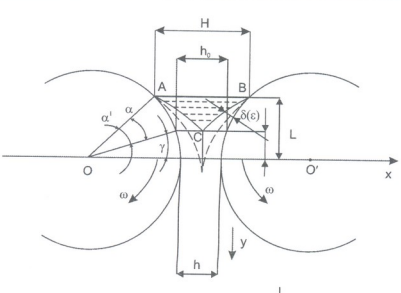

Fig. 2. Schematic view of billet forming in direct rolling process.

rolling), at calculating the driving actuator of an aggregate it is necessary to take into consideration forces taking a billet out of crystallizer and those occurring while rolling.

In the direct rolling process a combined crystallizer with two moving (rolls) and two static walls (side closing plates) are used. So, output of a cast out of crystallizer is impeded by sliding friction only, which occurs due to transverse deformation at casting tension and ferrostatic pressure at the side closing plates.

The ferrostatic pressure $F_f = 0.5\mu\gamma HS_f$ [1-3], where μ is friction coefficient; γ is specific weight of casting metal, kg/mm^3; H – height of liquid metal column, m (from the point C to AB line); S_f – a contact area of both side plates with liquid metal. The value of transversal deformation is calculated with Bakhtinov's formula [4]:

$$\Delta b = 1.15\frac{\Delta h}{2h_0}\left(r\Delta h - \frac{\Delta h}{2\mu}\right),$$

Δb is a linear extension, m; Δh – linear tension, m; h_0 – thickness of the billet at starting deformation, mm (at the point C); μ is friction coefficient; r – radius of rolls, mm. Both values are so small that they can be ignored in calculation of energy-power parameters.

The values of the forces occurring at billet tension depend on different technological and construction characteristics (tensile strain, cast's geometric dimensions, cross-section, temperature, chemical content, speed of drawing, roll's diameter, etc.).

As seen in the scheme of cast formation, the position of meniscus AB of liquid metal relative to OO' line defines the angle α. From points A and B on the roll's surface casting process starts with a thickness $\delta(\tau)$, where t is crystallization time. At $\tau = \tau_0$ moment two solid phases will meet at the point C ($\gamma = \gamma_0$). The angle γ concerns complete solidification of the cast section and is defined as follows:

$$[R + \delta(\tau_0)]\cos\gamma = R + 0.5h, \qquad (1)$$

where h is the final thickness of the cast (γ=0).

The corresponding crystallization time is

$$\tau_0 = \frac{\alpha - \gamma}{\omega}, \qquad (2)$$

where ω is angular velocity, rad/sec.

From point C the plastic deformation begins. Full length L of contact arc with metal rolls is

$$L = \sqrt{R(H-h)} = R\sqrt{2(1-\cos\alpha)} = 2R\sin\alpha/2, \quad (3)$$

and length of arc of deformation zone $l = \sqrt{R(h_c - h)}$, where $h_0 = 2\delta(\tau_0)$ and is defined from the equation (1), h_0 is billet thickness at point C when $y = y_0$.

Analysis of the literature data showed that the optimal values of α and γ angles are 20-30° and 2-5°, respectively. At that time the value of relative deformation varies within the range 10-30%, which is sufficient enough to get a high grade fine billet. At the same time costs for device exploitation are reduced on account of wear decrease of side closing plates of crystallizer.

As a rule, thickness of the crust formed at continuous casting is defined by the Stephany formula [1-3]:

$$\delta = K\sqrt{\tau}, \quad (4)$$

where K is a crystallization coefficient, mm/sec, τ – time of crystallization, sec.

Using this formula at the initial phase of crystallization, especially at casting thin sheets, when duration of the process is a mere 0.5-1 sec, does not give a real picture. In this case using the formula of Brovman and Tsariov is more reasonable [4]:

$$\delta(\tau) = \sqrt{x_0^2 + 2k\tau} - x_0, \quad (5)$$

where k and x_0 are constants for a given metal; k is quantity analogous to the crystallization coefficient, m²/sec; x_0 denotes the speed of crust thickness growth, m.

Substituting $\delta(\tau)$ in (1) and taking into account expression (2) we obtain

$$\alpha - \gamma = \frac{\omega R^2}{2K\cos^2\gamma}\left[\left(1+\frac{h}{2R}\right)^2 - \right.$$

$$\left. - \cos\gamma\left(2 + \frac{h}{R} - \frac{x_0}{R} - \frac{hx_0}{R^2}\right) + \cos^2\gamma\left(1 - \frac{x_0}{R}\right)\right], \quad (6)$$

from (6) the angular velocity of rolls' rotation is

$$\omega = \frac{(\alpha-\gamma)2K\cos^2\gamma}{R^2}\left[\left(1+\frac{h}{2R}\right) - \right.$$

$$\left. - \cos\gamma\left(2 + \frac{h}{R} - \frac{x_0}{R} - \frac{hx_0}{R^2}\right) + \cos^2\gamma\left(1 - \frac{x_0}{R}\right)\right]. \quad (7)$$

Knowing a optimal value of relative stretch allows to define the γ-angle for billets of different thickness. It is known that relative stretch for steels and nonferrous metals is

$$\varepsilon = \ln\frac{h_0}{h} = \ln\left[1 + \frac{2R(1-\cos\gamma)}{h}\right]. \quad (8)$$

Theoretical calculation of casting speed was carried out for the values $\alpha = 20\text{-}30°$, $\gamma = 2\text{-}5°$, $\varepsilon = 6\text{-}33\%$, $h = 2 \div 4\ 10^{-1}$ m using expressions (7),(8) and taking into consideration the diameter of rolls (D=0.42 m) (Figs.3-5).

On the basis of the data obtained power energy parameters of the device were determined.

As is known, in the rolling process the value of full load force is $P = pF$, where p is specific pressure on the roll's surface, kg/cm²; F – contact area of the deformation site. In its turn $p = \gamma n' n'' n''' n_\varepsilon \sigma_s$, where in our case, which presents a plate problem, $n''' = 1$; $n_\varepsilon = 1$;

$$n'' = 1; \quad \gamma = 1.15; \quad n' = 2, 3.$$

In its turn $\sigma_s = \sigma_{s_0} K_t K_v K_\varepsilon$, where for hot metal basis $\sigma_{s_0} = 30$ mPa; values of other coefficients depend on technological characteristics of the process and are defined with consideration of certain conditions [5, 6].

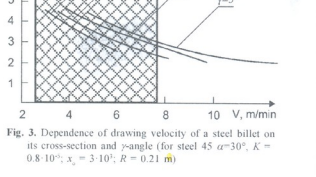

Fig. 3. Dependence of drawing velocity of a steel billet on its cross-section and γ-angle (for steel 45 $\alpha = 30°$, $K = 0.8 \cdot 10^{-2}$; $x_0 = 3 \cdot 10^{-3}$; $R = 0.21$ m)

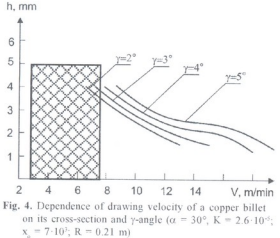

Fig. 4. Dependence of drawing velocity of a copper billet on its cross-section and γ-angle (α = 30°, K = 2.6·10^{-5}; x_c = 7·10^{-3}; R = 0.21 m)

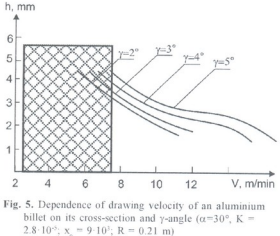

Fig. 5. Dependence of drawing velocity of an aluminium billet on its cross-section and γ-angle (α=30°, K = 2.8·10^{-5}; x_c = 9·10^{-3}; R = 0.21 m)

In our case K_1=const=0.5, values of K_n and K_d are given in Table 1. A contact area $F=Bl$, where B is roll's length (250 mm), l –length of deformation zone ($l=\sqrt{R(h_0-h)}$).

The calculated magnitudes of F are shown in Table. On their basis diagrams are constructed (Figs.3-5), where the shaded areas correspond to the optimum regime of the process.

The torsion moment on the motor shaft

$$M_{tmid} = 2P\Psi l.$$

In our case the coefficient of rolling moment arm Ψ=0.5, l is the length of deformation zone, mm.

A moment occurring due to torsion in roll neck and sliding bearing $M_{tor.1}=pd\mu$, where d is the diameter of the roll neck and equals 0.1 mm; torsion moment in the gear system driver-rolls (reduction gear, gear box) is equal to $M_{tor.2}$ = 0.01 tm = 10 kgm.

$$M_{dr} = M_{mid1} + M_{tor.1} + M_{tor.2}.$$

Finally, power of the engine

$$N_{dr} = M_{dr}\omega kW.$$

The angular velocity of the rolls' rotation $\omega = \frac{2v}{D}$, where v is linear velocity of billet drawing, m/sec., D – diameter of rolls.

The required power of the engine is chosen for maximum values of pressures on the rolls at γ= 5° and α=30° (Table).

Table. Interrelation of energy-power parameters of the casting-rolling mill and technological characteristics of the billet (steel 45).

NN	Thickness of the billet before rolling, h_0, mm	Deformation value, Δh, mm	Thickness of the billet after rolling, h, mm	Relative stretch, ε, %	Specific pressure on the rolls' surface, p, kg/mm^2	Force of full load, P, t.f.	Length of the deformation arc, l, mm	Power necessary to motor, N, kW	Angular velocity of rolls' rotation, ω, rad/min	Angle corresponding to the metal solidification, γ^0	Linear velocity of the billet drawing, V, m/hr
1	2.26	0.26	2	11.5	12.4	22.543	7.27	1.9	0.97	2	12.280
2	3.26	0.26	3	8.0	9.68	17.634	7.27	0.96	0.62	2	7.812
3	4.26	0.26	4	6.1	8.8	15.998	7.27	0.6	0.49	2	6.159
4	2.58	0.58	2	22.5	15.07	41.670	11.11	4.3	0.84	3	10.628
5	3.58	0.58	3	16.2	12.43	34.447	11.11	2.3	0.55	3	6.935
6	4.58	0.58	4	12.7	10.84	30.002	11.11	1.5	0.4	3	5.004
7	3.02	1.02	2	33.8	15.6	56.737	14.54	6.2	0.7	4	8.870
8	4.02	1.02	3	25.4	13.2	48.008	14.54	3.5	0.473	4	5.973
9	5.02	1.02	4	20.3	11.9	43.280	14.54	2.4	0.347	4	4.388
10	3.60	1.60	2	44.4	15.6	71.385	18.3	7.9	0.57	5	7.185
11	4.60	1.60	3	34.8	13.7	62.691	18.3	3.9	0.4	5	5.009
12	5.60	1.60	4	28.6	12.4	56.742	18.3	3.1	0.35	5	3.758

მეტალურგია

უსხმულო გლინვის პროცესის ტექნოლოგიური და კონსტრუქციული პარამეტრების ურთიერთკავშირის განსაზღვრა

გ. ქევხიშვილი*, თ. ნამიჩეიშვილი*, ი. ჟორდანია**, ჯ. ლორია*, ზ. მელაშვილი*, ვ. რამიშვილი*

** ფ.თაყაიშვილის მეტალურგიისა და მასალათმცოდნეობის ინსტიტუტი, ლითონური მასალების წნევით დამუშავების ლაბორატორია, თბილისი*

*** აკადემიკოსი, ფ.თაყაიშვილის მეტალურგიისა და მასალათმცოდნეობის ინსტიტუტი, ლითონური მასალების წნევით დამუშავების ლაბორატორია, თბილისი*

უსხმულო გლინვის მეთოდი განსხვავებით ტრადიციული ტექნოლოგიისა, რაც ითვალისწინებს დიდი კვეთის პირველადი ნამზადის ჩამოსხმას და შემდგომში მისი ეტაპობრივი ცხლად გლინვის ტექნოლოგიის ხარჯზე თხელი ფურცლების წარმოებას, საშუალებას იძლევა თხილი ლითონიდან უწყვეტი ჩამოსხმისა და გლინვის პროცესის შერწყმის გზით თხელი ფურცლების (0,6-6) მმ-ის მიღებას.

მეთოდის არსი საკმაოდ მარტივია. ჰორიზონტალურ სიბრტყეში განლაგებულ, გარკვეული მანძილით დაცილებულ ორ მბრუნავ გლინს შორის მიეწოდება თხიერი ლითონი. გლინების ბრუნვის სიჩქარის ვარირებით შესაძლებელია თხევადი ლითონის გამყარების ფრონტის რეგულირება, რაც აუცილებელი პირობაა ცხლად გლინვის პროცესის საწყისი რეჟიმის დასამყარებლად.

ნაშრომში დეტალურად არის განხილული კომბინირებულ კრისტალიზატორში ნამზადის ფორმირების მექანიზმი. შემუშავებულია მეთოდიკა ჩამოსხმის ძირითადი ტექნოლოგიური პარამეტრების თეორიულად განსაზღვრისათვის და ამ პარამეტრების დამოკიდებულება როგორც ფურცელი ასევე შუა ლითონებისათვის საჩამოსხმო სიგანეზე დანადგარის კონსტრუქციულ და ენერგომახლეურ პარამეტრებთან.

კვლევების შედეგად მიღებული მონაცემები საფუძვლად დაედო საცდელი ტიპის საჩამოსხმო-საგლინავი დანადგარის დაპროექტებასა და ლითონში დამზადებას.

REFERENCES

1. *M.Ya. Brovman, I.K. Marchenko, Yu.E. Kan* (1976). Usovershenstvovanie tekhnologii I oborudovaniia mashin nepreryvnogo lit'ia zagotovok. Kiev, 136 p. (in Russian).
2. *Sh.D. Ramishvili, N.D. Tkhelidze, U.Sh. Kevkhishvili* (1984), in: N.Khutsishvili (Ed.), Protsessy lit'ia i nepreryvnoi razlivki metallov. Tbilisi, p.70 (in Russian).
3. *Sh.D. Ramishvili* (1985). Nepreryvnoe lit'e polykh chugunnykh zagotovok. Tbilisi, 107 p. (in Russian).
4. *M.Ya. Brovman* (2007). Nepreryvnaia razlivka metallov. M. 482 p. (in Russian).
5. *A. Nozadze, B. Ramishvili, P. Doborjginidze* (1974), Theory of Rolling. Tbilisi, 153 p. (in Georgian).
6. *A.I. Tselikov, A.D. Tomlenov, V.I. Ziuzin, A.V. Tret'iakov, G.S. Nikitin* (1982). Teoriia prokatki. M., 335 p. (in Russian).

Received October, 2012

საქართველოს მეცნიერებათა ეროვნული აკადემიის მოამბე, ტ. 6, №3, 2012
BULLETIN OF THE GEORGIAN NATIONAL ACADEMY OF SCIENCES, vol. 6, no. 3, 2012

Geology

New Data on the Formation and Age of Orthoclase Gabbro of the Dzirula Crystalline Massif (Georgia)

David Shengelia*, Lasha Shubitidze, Sun-Lin Chung**, Han-Yi Chiu**, Peter Treloar§**

* *Academy Member; A. Janelidze Institute of Geology, I.Javakhishvili Tbilisi State University, Tbilisi*
A. Janelidze Institute of Geology, I. Javakhishvili Tbilisi State University, Tbilisi
** *Department of Geosciences, National Taiwan University, Taipei 106, Taiwan*
§ *Centre for Earth and Environmental Science Research, Kingston University, London, GB*

ABSTRACT. Orthoclase gabbro of the Dzirula crystalline massif incorporates the rocks of different genetic groups: protolith of the gabbroic intrusion, hybrid rock – orthoclase gabbro and leucocratic quartz-feldspar bearing formation. The rocks of all three genetic groups are dated by the U-Pb LA-ICP-MS zircon age method. The apparent age of zircon in the protolith of gabbroic intrusive and in hybrid orthoclase gabbro, respectively wt.mean 221±1.9 and 221.9±2.2Ma, records the time of crystallization of the intrusive and the apparent age of zircons (wt.mean 323±2.9Ma) from leucocratic quartz-K-feldspar formations, as well as the inherited Late Variscan age (323±9, 329±8.3, 332±10 and 335±11Ma) of zircons of hybrid orthoclase gabbro corresponds to the age of formation of Late Variscan granitoids widespread in the Dzirula crystalline massif. © *2012 Bull. Georg. Natl. Acad. Sci.*

Key words: *the Dzirula massif, orthoclase-gabbro, U-Pb zircon age.*

In the Eastern part of the Dzirula crystalline massif stock-like body of orthoclase gabbro (OG), known as "rikotites" is spread. The primary intrusive contact of OG is complicated by Mesozoic-Cenozoic tectonic events. Generally, the contact of the intrusive with the Baikalian quartz-diorite gneisses is tectonic, though locally the contact effects are observed. During the tectonic movements, the country rocks were insignificantly dislocated.

Views of researchers on the genesis and age of OG considerably differ. Some researchers believe that these OG are pre-Variscan or Early Variscan basites, reworked under the influence of Late Variscan [1-3] or Jurassic [4] granitoids. Others associate their formation with the assimilation of Paleozoic granitoids with ultrabasite magma, considering the latter to be a Late Paleozoic formation [5,6].

According to the scheme of I. Khmaladze [7] the OG formed as a result of deep assimilation and belongs to a group of Bathonian intrusions. Khmaladze's assumption is based on the following facts: a massive structure of OG; OG are considerably less (cataclased) broken down in comparison with the Paleozoic granitoids and gabbroids of the Dzirula

massif; presence of anorthoclase in OG that are missing in the pre-Jurassic rocks of the Dzirula massif; absence of vein facies of Paleozoic granitoids in the intrusive body of OG; presence of transformed (assimilated) granitoid xenoliths and also of veins of pyroxenites in OG; occurrence of active contacts of OG with quartz-diorite gneisses.

O.Dudauri [8] related the OG intrusive body to the Khevi-Chalvani intrusive complex. In his opinion, formation of OG was induced with the activity of basic magma of the first phase of Middle Jurassic magmatic processes. He considers that granite material was delivered into the OG by hydrothermal and pneumatolite solutions from the Khevi-Chalvani intrusive that was formed in the Middle Jurassic.

According to A.Okrostsvaridze et al. [9] the Σ_{Nd} parameter of OG varies within the limits of 0.4485 – + 0.36936 (mean figure – + 0.05870; and I_{sr} parameter shows the mantle source of magma (I_{sr} =0.7049476-0.7053333). From the above mentioned they consider that the main source of OG magma is an unexhausted mantle reservoir, from where the K-enriched magma intruded into the Precambrian quartz-diorites.

The age of OG biotite by K-Ar dating was determined by [10] as 163±11Ma, but according to [11] it is 179±6Ma. Isotope-geochemical determinations obtained by [9] is worth mentioning: the $^{40}Ar/Ar^{39}$ dating shows 219±4 Ma for hornblendes and 217±11Ma for biotites. Rb-Sr isochrone for 6 samples of OG drawn by the same authors corresponds to 211±11Ma (MSWO=0.83).

Thus, the age and formation of OG on the basis of the above facts is difficult to solve definitively.

Petrographic Model of Orthoclase Gabbro Formation

In the process of OG formation tectonic layering of the Earth's crust of the Black Sea – Central Transcaucasian terrane played a significant role.

According to geological [12-15] and geophysical [16] data in the Black Sea–Central Transcaucasian terrane in the Saurian phase of tectogenesis horizontal tectonic layering of the Earth'crust took place. Tectonic layering covers deeper horizons of the Earth's crust. Tectonic doubling of the Earth's crust of the Black Sea–Central Transcaucasian microcontinent takes place (Fig. 1). Thick tectonic nappe of mafic (second layer) and sialic (first layer) layers overlap the sialic basement (third "inversion" layer).

On the basis of the above-mentioned, in the present paper the questions of the formation of OG (original rocks of exotic composition) of the Dzirula massif are considered in a new light [15, 17-19].

The authors deem that the initial magma of OG is high temperature basite-ultrabasite magma. Crystallization products of the latter are represented by pyroxenite and pyroxene-bearing gabbro (with mineral composition – labradorite, bytownite and clinopyroxene). Petrochemical parameters of basite-ultrabasite magma [9, 17-19], most likely attest to its formation in the upper mantle and, perhaps, partially in the "crustal astenolayer", where the protolite of OG was formed. A newly formed high temperature and overheated dry magma with phenocrysts of clinopyroxene and also of basic plagioclase intruded into the third "inversion" sialic layer. From the new realm, it took the volatile components causing the selective fusion of leucocratic material of quartz-feldspar composition and at the same time provoking the intensive transformation of pyroxene to hornblende in the basite magma. The basic magma was admixed to the newly formed acid magma, or it remained partially unmixed. Granitic and partly decrystallized basaltic magmas intruded first into the allochthonous basite (second) layer, apparently, without substantial changes and then into the sialic (first) layer crystallizing at a depth of 7-10 km. The leucocratic granite magma, newly formed in the "inversion" sialic layer, belongs to the S type granites, but its mixing with the initial basite magma enables to include the products of its crystallization in the special hybrid H type granites distinguished by Spanish researchers [20]. At the final stage of magmatic process the gabbroic rock was saturated (impregnated) with high temperature

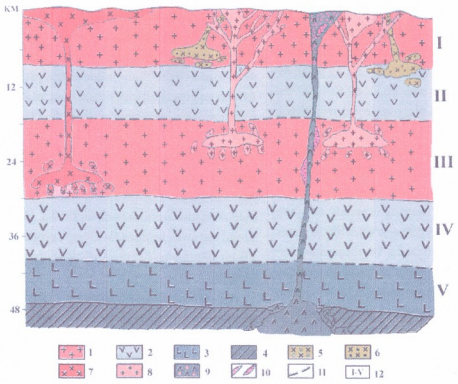

Fig. 1. Scheme of the principle of the formation of magmatic rocks of the Dzirula crystalline massif [15]
1 – sialic layer; 2 – mafic layer; 3 – "crustal astenolayer"; 4 – upper mantle; 5 – gabbro – gabbro-diorite of the Gezrula river gorge; 6 – granitoids of plagiogranite-granite series of the Kvirila and Macharula river gorges; 7 – the Rkvia intrusion; 8 – microcline granite; 9 – orthoclase gabbro (OG); 10 – quartz-feldspar anatectite; 11 - surfaces of tectonic displacement; I-V – geophysical layers.

feldspar material forming anorthoclase or orthoclase.

Thus, the OG unites the rocks of various genetic groups: 1) protolith of the gabbroic intrusion, 2) hybrid rocks - K-feldspar gabbro and 3) leucocratic quartz-feldspar bearing formation.

Protolith of the gabbroic intrusion is a massive, coarse-grained, mainly anchimonomineral (clinopyroxene-bearing diopside enriched with salite molecules) rock; brown hornfels and plagioclase of labradorite-bytownite series is also recorded. Frequently, ingrowths of clinopyroxene with reaction rims of brown hornfels are observed.

Hybrid rock – K-feldspar bearing gabbro also is a coarse-grained massive rock. Its main rock-forming minerals are: K- and Na-bearing feldspar of orthoclase-anorthoclase series, clinopyroxene, brown hornfels and plagioclase of labradorite-bytownite series; secondary biotite occurs as well. K- and Na-bearing feldspar was crystallized (-2VC – 42-60°; Dp – 0.06-0.5; Do – 0.4) [19, 21] at the final stage of rock formation. It is recorded as xenomorphic grains and fills the space between the minerals.

In the anchimonomineral pyroxenite and in the K-Na-bearing feldspar gabbro the amount of SiO_2 is within the limits of 42.4-56.3, K_2O – 0.5-2.5, Na_2O – 0.5-3%. Geochemical and petrochemical data on hybrid OG and on the protolith of gabbro differ. The hybrid OG is enriched with REE and with other petrogenic elements. The amount of high radius lithosphere elements Ba and Rb is high in them. $(La/Sm)_n$ and $(La/Yb)_n$ ratios in the hybrid OG are 3.21 and 11.16 respectively, that is twice as high as norm ratios of the same elements in the protolith of the OG. Variations of abundance ratios of slightly incompat-

ible elements (Hf/Sm, Ti/Y, Ti/P, Ti/Eu) are also high. Almost the same abundance ratios occur for some noncoherent elements (La/Th, La/Hf, Zr/Y, Ti/Zr). The abundance ratios of some indicator elements (Th/La, Th/Sm, Th/Yb, Zr/Y) are also increased. Eu/Eu* minimum in hybrid OG exceeds 1.0, pointing to the enrichment of this rock with Eu. Total REE in "the protolith" varies within 91.01-96.16 and in the hybrid OG it is 177.0.

In the OG mainly heterogenous leucocratic quartz-feldspar vein bodies of different thickness (from one cm to 2m) or accumulations of various shape spread widely. The rock is mainly fine- and medium-grained, rarely coarse-grained that in places passes into the pegmatitic areas. The main rock-forming minerals are: K-feldspar and acid plagioclase, sometimes quartz. In the K-feldspar (25-70%) grain size reaches 2cm; micropegmatitic aggregates of quartz- and K-feldspar occur. In the rock (12 samples were analyzed) the amount of SiO_2 is 61-70 mass%, K_2O – 5.4-11 mass%, Na_2O – 3.5-5.3 mass%. Heterogenous character of the leucocratic formations is conditioned mainly by the variation of partial pressure of water and rate of leucocratic acid and basic magma miscibility [19]. In all three characterized rocks, zircon is observed. Its maximum amount does not exceed 6.3 g/t. Two types of zircons are ascertained [22].

The zircon of first type, generally recorded in pyroxene gabbros, is represented by well faceted crystals of long-prismatic habitus. In their facet pattern tetragonal prism (110) and tetragonal dipyramid (111) occur. The facets of prism (100) and sharp dipyramid (311) are rarely developed. Zircon crystals are fine (0.05-0.1mm), transparent with light pink coloring; they are fissured and corroded. Elongation is within the limits of 4-5.

Zircon of the second type, being a mineral of hybrid and quartz-feldspar bearing rocks, is represented by metamictic diversity – citrolite. Unlike the zircons, citrolite is larger (0.1-0? mm); it forms dark brown non-transparent crystals of short prismatic habitus with the facets of tetragonal prism (100) and dipyramid and with elongation – 2-2.5.

New data on the U-Pb zircon age of orthoclase gabbro of the Dzirula massif

The results of LA-ICP-MS U-Pb dating of zircons in the protolith of the gabbroic intrusive (sample #1-98), in the hybrid rock (K-feldspar gabbro; samples ##10-06 and GEO127) and in quartz-feldspar bearing formations give significant information for the identification of the petrogenic model of the OG formation.

LA-ICP-MS U-Pb dating was performed at the laboratories of the Department of Geosciences of National Taiwan University, Institute of Earth Sciences of Academia Sinica (samples ##1-98, 10-06 and 12-06) and at the Institute für Geowissenschaften of Johann-Wolfgang-Goethe University (sample # GEO127).

Age determinations performed in 18 zircon crystals (sample # 1-98) of gabbroic intrusive protolith show 216-226±4Ma (wt. mean ≈221.4±1.9Ma; 2σ) (Table 1, Fig. 2). Th/U ratios in the analyzed zircons are high and vary from 2.273 to 0.730, mainly positive value of $\varepsilon_{Hf}(T)$ is from +6.4 to –0.1 (its negative value is fixed in two cases: -0.2 and -1.2) and T_{DM}^{C} vary from 1266 to 847Ma. The crystals are homogenous – in the core and in the peripheral part similar ages were obtained. These data are higher to some extent than those obtained by A.Okrostsvaridze et al. [9] with the Rb-Sr method for OG (211±11Ma) and are nearer to the results of measurements of OG hornfels (219±4Ma) and biotites (217±3Ma) performed by the same authors with $^{40}Ar/^{39}Ar$ dating. From the above it follows that the age of the OG protolith is ≈ 220Ma.

Two samples of hybrid K-feldspar gabbro were analyzed: ##GEO127 and 10-06. In the sample #GEO127 4 zircon crystals were studied (Fig. 3), where the Late Variscan age (323±9; 325±8.3; 332±10 and 335±11Ma) was received. In the fourth crystal, on the edge the Late Variscan age (327±12Ma) and in the core an inherited age (779±21Ma) was ascertained. To our mind, the inherited age of zircon determined in the core, corresponds to the early stage of the Grenville regional metamorphism manifested in

Table 1. U-Pb and Lu-Hf isotopic data of magmatic zircons from orthoclase gabbro of the Dzirula massif

Spot	Th/U	$^{207}Pb/^{206}Pb$	±1σ	$^{206}Pb/^{238}U$	±1σ	$^{207}Pb/^{235}U$	±1σ	error corr.	$^{206}Pb/^{238}U$ age (Ma ± 1σ)		$^{176}Hf/^{177}Hf$	±1σ	$^{176}Lu/^{177}Hf$	±1σ	$\varepsilon_{Hf}(T)$	±1σ	T_{DM}	T_{DM}^{C}
1-98	wt. mean = 221.4 ± 1.9 Ma (2σ)																	
1-98-01	1.266	0.05459	0.00052	0.03409	0.00060	0.25654	0.00553	0.815	216.0	4.0	0.282803	13	0.002644	4	5.6	0.5	665	899
1-98-02	1.235	0.05513	0.00048	0.03463	0.00061	0.26318	0.00529	0.876	219.0	4.0	0.282769	12	0.002462	15	4.4	0.4	713	976
1-98-03	1.818	0.05157	0.00042	0.03454	0.00060	0.24560	0.00451	0.946	219.0	4.0	0.282793	9	0.004949	20	4.9	0.3	727	943
1-98-04	0.909	0.05138	0.00041	0.03497	0.00061	0.24774	0.00450	0.960	222.0	4.0	0.282650	13	0.005102	14	-0.2	0.5	956	1266
1-98-05	1.124	0.05200	0.00045	0.03346	0.00062	0.25423	0.00500	0.889	225.0	4.0	0.282813	14	0.003115	64	5.9	0.5	659	881
1-98-06	1.587	0.05165	0.00052	0.03450	0.00062	0.24564	0.00552	0.800	219.0	4.0	—	—	—	—	—	—	—	—
1-98-09	1.724	0.05429	0.00043	0.03380	0.00059	0.25302	0.00455	0.971	214.0	4.0	—	—	—	—	—	—	—	—
1-98-10	1.667	0.05127	0.00042	0.03459	0.00060	0.24450	0.00458	0.926	219.0	4.0	0.282734	11	0.003599	6	3.0	0.4	789	1065
1-98-12	0.667	0.04970	0.00233	0.03453	0.00067	0.23661	0.01487	0.309	219.0	4.0	—	—	—	—	—	—	—	—
1-98-13	2.275	0.05118	0.00041	0.03490	0.00061	0.24621	0.00455	0.946	221.0	4.0	0.282696	12	0.006256	7	1.3	0.4	915	1174
1-98-15	0.840	0.05312	0.00047	0.03544	0.00063	0.25954	0.00571	0.886	225.0	4.0	0.282693	16	0.002896	8	1.7	0.5	833	1150
1-98-16	2.128	0.05063	0.00042	0.03511	0.00062	0.24503	0.00464	0.933	222.0	4.0	0.282839	11	0.005687	10	6.4	0.4	669	847
1-98-17	1.111	0.05081	0.00047	0.03508	0.00062	0.24572	0.00513	0.847	222.0	4.0	0.282764	10	0.002705	36	4.2	0.4	724	988
1-98-18	1.000	0.04633	0.00232	0.03551	0.00067	0.22687	0.01435	0.298	225.0	4.0	—	—	—	—	—	—	—	—
1-98-19	1.408	0.05161	0.00043	0.03523	0.00062	0.25071	0.00482	0.915	223.0	4.0	0.282710	12	0.002093	26	2.4	0.4	790	1104
1-98-20	1.754	0.05173	0.00042	0.03568	0.00063	0.25446	0.00471	0.954	226.0	4.0	0.282725	10	0.002605	6	2.8	0.3	780	1075
1-98-22	0.730	0.05095	0.00278	0.03566	0.00079	0.25051	0.01844	0.301	226.0	5.0	0.282605	15	0.001094	7	1.2	0.5	918	1332
1-98-23	1.163	0.05237	0.00053	0.03534	0.00067	0.25513	0.00586	0.825	224.0	4.0	0.282647	16	0.002531	9	0.1	0.6	892	1250
N12-06	wt. mean = 323.1 ± 2.9 Ma (2σ)																	
N12-06-02	0.195	0.05198	0.00086	0.04929	0.00097	0.35323	0.01137	0.611	310.0	6.0	—	—	—	—	—	—	—	—
N12-06-03	0.980	0.05453	0.00050	0.05091	0.00093	0.38269	0.00808	0.865	320.0	6.0	0.282531	10	0.003056	20	-2.1	0.3	1079	1464
N12-06-06	0.402	0.05209	0.00136	0.05117	0.00091	0.36746	0.01470	0.445	322.0	6.0	—	—	—	—	—	—	—	—
N12-06-07	0.301	0.05269	0.00044	0.05167	0.00093	0.37533	0.00712	0.949	325.0	6.0	0.282483	7	0.001769	5	-3.5	0.2	1109	1554
N12-06-09	0.336	0.05369	0.00044	0.05122	0.00092	0.37913	0.00701	0.971	322.0	6.0	0.282487	8	0.002708	8	-3.6	0.3	1134	1559
N12-06-10	0.565	0.05310	0.00045	0.05116	0.00093	0.37451	0.00726	0.938	322.0	6.0	0.282500	9	0.002212	40	-3.0	0.3	1098	1522
N12-06-14	0.365	0.05533	0.00046	0.05211	0.00095	0.39749	0.00738	0.982	327.0	6.0	0.282536	8	0.003386	27	-2.0	0.3	1082	1459
N12-06-15	0.389	0.05458	0.00046	0.05144	0.00094	0.38702	0.00732	0.966	323.0	6.0	0.282552	8	0.002249	28	-1.2	0.3	1024	1406
N12-06-16	0.455	0.05456	0.00046	0.05109	0.00093	0.38431	0.00738	0.948	321.0	6.0	0.282484	7	0.001688	10	-3.4	0.2	1106	1552
N12-06-17	0.671	0.05181	0.00242	0.05061	0.00109	0.36148	0.02311	0.337	318.0	7.0	—	—	—	—	—	—	—	—
N12-06-18	0.433	0.05447	0.00048	0.05114	0.00094	0.38402	0.00773	0.913	322.0	6.0	0.282504	7	0.001216	14	-2.6	0.3	1064	1500
N12-06-19	0.526	0.05343	0.00045	0.05172	0.00094	0.38099	0.00726	0.954	325.0	6.0	0.282479	7	0.001337	6	-3.5	0.3	1102	1557
N12-06-20	0.562	0.05309	0.00046	0.05179	0.00095	0.37909	0.00745	0.933	326.0	6.0	0.282494	7	0.002297	24	-3.2	0.2	1109	1536
N12-06-21	0.775	0.05815	0.00050	0.05127	0.00096	0.41096	0.00810	0.950	322.0	6.0	0.282455	23	0.004364	47	-5.0	0.8	1236	1652
N12-06-22	0.490	0.05546	0.00048	0.05162	0.00097	0.39468	0.00780	0.951	324.0	6.0	0.282392	16	0.001405	9	-6.6	0.6	1228	1753
N12-06-23	0.057	0.09764	0.00084	0.10069	0.00191	1.35546	0.02928	0.878	618.0	11.0	0.282318	15	0.001477	15	-3.0	0.5	1335	1749
N12-06-24	0.275	0.05371	0.00046	0.05339	0.00100	0.39532	0.00773	0.958	335.0	6.0	0.282430	16	0.002018	15	-5.4	0.6	1194	1678
N12-06-25	0.815	0.05459	0.00048	0.05222	0.00099	0.39295	0.00785	0.949	328.0	6.0	0.282421	12	0.002600	13	-5.9	0.4	1226	1705
10-06*	wt. mean = 221.9 ± 2.2 Ma (2σ)																	
10-06-01	1.408	0.05079	0.00048	0.03406	0.00064	0.23848	0.00513	0.874	216.0	4.0	0.282673	15	0.001871	18	1.1	0.5	840	1187
10-06-02	1.538	0.05229	0.00047	0.03464	0.00065	0.24970	0.00510	0.919	220.0	4.0	0.282635	13	0.002100	10	-0.3	0.5	901	1275
10-06-03	1.613	0.05153	0.00046	0.03536	0.00067	0.25116	0.00519	0.917	224.0	4.0	0.282637	14	0.001121	13	-0.1	0.5	874	1260
10-06-04	1.408	0.05311	0.00051	0.03410	0.00065	0.24972	0.00550	0.865	216.0	4.0	0.282623	17	0.002475	39	-0.7	0.6	926	1303
10-06-05	2.174	0.05146	0.00046	0.03491	0.00066	0.24768	0.00510	0.918	221.0	4.0	0.282653	14	0.001747	9	0.4	0.5	865	1230
10-06-06	1.471	0.05111	0.00048	0.03545	0.00067	0.24979	0.00538	0.878	225.0	4.0	0.282641	20	0.002137	34	-0.1	0.7	892	1260
10-06-08	1.695	0.05167	0.00048	0.03537	0.00068	0.25194	0.00542	0.894	224.0	4.0	0.282652	21	0.001860	40	0.3	0.7	870	1234
10-06-09	1.010	0.05271	0.00055	0.03471	0.00067	0.25226	0.00594	0.820	220.0	4.0	0.282650	25	0.003191	73	0.1	0.9	905	1250
10-06-10	1.587	0.05102	0.00049	0.03633	0.00070	0.25551	0.00560	0.879	230.0	4.0	0.282627	23	0.002172	65	-0.6	0.8	913	1293
10-06-11	1.333	0.05477	0.00058	0.03470	0.00068	0.26203	0.00625	0.822	220.0	4.0	0.282657	16	0.001185	18	0.6	0.6	846	1215
10-06-13	2.273	0.05247	0.00048	0.03521	0.00067	0.25472	0.00529	0.916	223.0	4.0	0.282679	13	0.002400	24	1.2	0.5	843	1177
10-06-14	1.136	0.05102	0.00050	0.03528	0.00068	0.24820	0.00551	0.868	224.0	4.0	0.282613	15	0.001083	7	-0.9	0.5	906	1313
10-06-15	1.695	0.05126	0.00047	0.03506	0.00067	0.24778	0.00521	0.909	222.0	4.0	0.282733	17	0.002142	7	3.2	0.6	759	1054

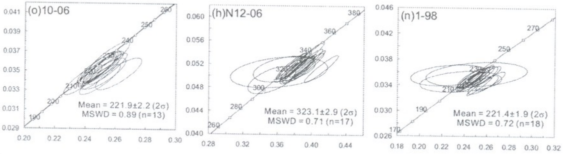

Fig. 2. Concordia diagrams of zircon U-Pb LA-ICP-MS dating results for the protolith of gabbro intrusive (sample #1-98), hybrid K-feldspar gabbro (sample # 10-06) and leucocratic quartz-potassium-feldspar formations (sample #12-06)

the Dzirula massif that is verified by the age of zircon in the Neoproterozoic gneiss-migmatitic complex dated by the La-ICP-MS U-Pb method [23, 24]. In the sample #10-06 13 crystals of zircon were analyzed. The obtained age – 221.9±2.2Ma (σ) corresponds to the zircon age of protolith of the gabbroic intrusive (sample #1-98) (see Fig.1). In the zircon crystals of sample #10-06 the Th/U ratio varies from 2.273 to 1.01, values of $\varepsilon_{Hf}(T)$ in seven cases are positive (3.2-0.1) and in six cases are negative (-0.1- -0.9) and T_{DM}^{C} varies from 1313 to 1054Ma.

18 zircon crystals from the quartz-K-feldspar leucocratic nests of OGs (sample #12-06) have been analyzed. The age of 17 crystals vary within 310-

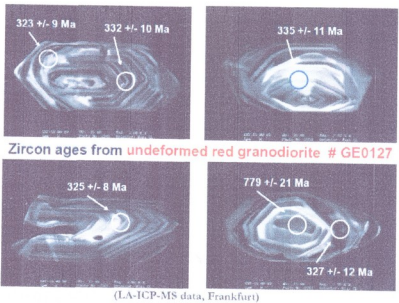

Fig. 3. Zircons from orthoclase gabbro (sample #GE0127) of the Dzirula massif

335±6Ma (wt. mean=323±2.9Ma) (2σ) (see Table 1 and Fig.2), where (Th/U is in the interval of 0.980-0.195, $\varepsilon_{Hf}(T)$ varies from -1.2 to -6.6 and T_{DM}^{C} – from 1753 to 1406 Ma) the inherited age 618±11 Ma (Th/U=0.057, $e_{Hf}(T)$ =-3.0 and T_{DM}^{C} =1749Ma) only in one crystal is fixed. It corresponds to the crystallization age of the Baikalian quartz-diorite orthogneisses widespread in the Dzirula massif. The age of the last one is also corroborated by the findings of La-ICP-MS U-Pb zircon dating [23, 24].

Conclusions

OG integrates the rocks of different genetic groups: 1 – protolith of gabbroic intrusive, 2 – hybrid rock (K-feldspar gabbro) and 3 – leucocratic quartz-feldspar bearing formations.

In the protolith of the gabbroic intrusive and in the zircons of hybrid K-feldspar gabbro the Th/U ratios are high and insignificantly differ from each other. $\varepsilon_{Hf}(T)$ value is mainly positive, though its negative value is also recorded and T_{DM}^{C} is almost identical. Th/U ratio is fairly high in the zircons of quartz-K-feldspar bearing rocks but lower than in the zircons of two previous genetic types of rocks. T_{DM}^{C} value is comparatively high and $\varepsilon_{Hf}(T)$ is always negative in all crystals of the zircon.

The apparent age of zircon in the protolith of gabbroic intrusive and in hybrid K-feldspar gabbro, respectively wt.mean 221±1.9 and 221.9±2.2Ma, records the time of crystallization of the intrusive and the apparent age of zircons from leucocratic quartz-K-feldspar formations wt.mean 323±2.9Ma, as well as the inherited Late Variscan age (323±9, 329±8.3, 332±10 and 335±11Ma) of zircons of hybrid K-feldspar gabbro corresponds to the age of formation of Late Variscan granitoids widespread in the Dzirula crystalline massif.

Thus, the age of formation of the OG of heterogenous composition is not defined explicitly. The Late Variscan age of zircons from orthoclase gabbro and leucocratic quartz-K-feldspar formations reflect the age of zircon of hard-to-melt relic mineral from the formations appearing as a result of selective melt during the injection of gabbro intrusive into the sialic crust.

გეოლოგია

ახალი მონაცემები ძირულის კრისტალური მასივის (საქართველო) ორთოკლაზიანი გაბროს ფორმირებისა და ასაკის შესახებ

დ. შენგელია*, ლ. შუბითიძე*, ს.-ლ. ჩუნგი**, ჰ.-ი. ჩიუ**, პ. ტრელუარი§

* აკადემიის წევრი, ა.ჯავახიშვილის სახ. თბილისის სახელმწიფო უნივერსიტეტი, ა. ჯანელიძის გეოლოგიის ინსტიტუტი, თბილისი
* ა.ჯავახიშვილის სახ. თბილისის სახელმწიფო უნივერსიტეტი, ა. ჯანელიძის გეოლოგიის ინსტიტუტი, თბილისი
** ტაივანის ეროვნული უნივერსიტეტი, თაიპეი, ტაივანი
§ კინგსტონის უნივერსიტეტი, ლონდონი, დიდი ბრიტანეთი

ძირულის კრისტალური მასივის ორთოკლაზიანი გაბრო (რიკოთიტი) აერთიანებს სხვადასხვა გენეტური ჯგუფის ქანს: გაბროული ინტრუზიის პროტოლითს, ჰიბრიდულ ქანს - კალიშპატიან გაბროს და ლეიკოკრატულ კვარც-მინდვრისშპატიან წარმონაქმნებს. სამივე გენეტური ჯგუფის ქანი დათარიღებულია ცირკონების **U-Pb LA-ICP MS** მეთოდით. გაბროული ინტრუზივის პროტოლითში და ჰიბრიდულ კალიშპატიან გაბროში განვითარებული ცირკონების ასაკი, შესაბამისად 221.4±1.9 Ma და 221.9±2.2 Ma აფიქსირებს ინტრუზივის კრისტალიზაციის დროს, ხოლო ლეიკოკრატული კვარც-მინდვრისშპატიანი წარმონაქმნების ცირკონების ასაკი 323±2.9 Ma, ასევე ორთოკლაზიანი გაბროს ცირკონების შემკვიდრეობითი გვიანვარისკული ასაკი - 323±9, 329±8.3, 332±10 და 335±11 Ma უპასუხებს ძირულის კრისტალურ მასივში ფართოდ წარმოდგენილი გვიანვარისკული გრანიტოიდების ფორმირების ასაკს.

REFERENCES

1. *G.M. Zaridze, N.F. Tatrishvili* (1953). Trudy Geologicheskogo Instituta AN GSSR, **3**: 33-79 (in Russian).
2. *Sh.A. Adamia* (1984). Trudy Geologicheskogo Instituta AN GSSR. Novaia seriia, **86**: 3-104 (in Russian).
3. *O.D. Khutsishvili* (1991), Trudy Geologicheskogo Instituta AN Gruzii. Novaia seriia, 103, 154 s. (in Russian).
4. *G.M. Zaridze* (1938), Biulleten' Geologicheskogo Instituta Gruzii, **4**, 1: 1-112 (in Russian).
5. *G.M. Smirnov, N.F. Tatrishvili, T.G. Kazakhashvili* (1938), Trudy KIMS, 2: 5-47, Tbilisi (in Russian).
6. *D.S. Belyankin, V.P. Petrov* (1945), Petrografiia Gruzii. Petrografiia SSSR, Ser.1. Regional'naia Petrografiia,11, 394 s. (in Russian).
7. *I. Khmaladze* (1969), Izv. AN Gruz.SSR. Ser. Geol., **6**, 1,2: 44-51 (in Russian).
8. *O.Z. Dudauri* (2003). Doctoral Thesis, Tbilisi: 326 s. (in Russian).
9. *A. Okrostsvaridze, B. Klark, P. Reynolds, D. Bluashvili* (2002), Bull. Georg. Acad. Sci., **166**, 3: 78-82.
10. *M.M. Rubinstein* (1967), Trudy Geol. Inst. AN Gruzii. Novaya seria, 11, 239 s. (in Russian).
11. *T. Mchedlishvili, M.G. Togonidze* (1985). Vyiavlenie petrologo-geokhimicheskikh osobennostei Yurskikh granitoidov dzirul'skogo massiva. Fondy Geol. Inst. AN GSSR, 204 s. (in Russian).

12. *D.M. Shengelia, A. Okrostsvaridze* (1996), Bull. Georg. Acad. Sci., **14**, 1: 93-95.
13. *D.M. Shengelia, A. Okrostsvaridze* (1998), Doklady RAN, 6: 801-803.
14. *I.P. Gamkrelidze, D.M. Shengelia* (1999), Bull. Georg. Acad. Sci., **159**, 1: 51-56.
15. *I.P. Gamkrelidze, D.M. Shengelia* (2005), Dokembriisko-paleozoiskii metamorfizm, granitoidnyi magmatizm i geodinamika Kavkaza, M., 458 s. (in Russian).
16. *M. Ioseliani, V. Chichinadze, Sh. Diasamidze, et al.* (1989), Stroenie litosfery Gruzii po seismicheskim dannym, Tbilisi, 150 s. (in Russian).
17. *I.P. Gamkrelidze, D.M. Shengelia* (2001), Geotectonics, **5**, 1: 51-61.
18. *L. Shubitudze, V. Pirmisashvili* (2004), Materials of the 32nd International Geological Congress (32 IGC), Florence, Italy, p. 32.
19. *L. Shubitidze* (2005), Candidate Thesis. Tbilisi, 132 p. (in Georgian).
20. *A. Castro, J. Moreno-Ventas, I.D. De La Rosa* (1991), Earth Sci. Rev., **31**, 3/4: 237-253.
21. *L. Shubitidze* (1999), Proceedings of the Geol. Inst. Acad. Sci. of Georgia. New ser., **114:** 314-317 (in Georgian, English Summary).
22. *K.S. Chikhelidze, L. Shubitidze* (2002), Proceedings of the Geol. Inst. Acad. Sci. of Georgia. New ser. **117**: 199-203 (in Russian, English Summary).
23. *D.M. Shengelia, O.Z. Dudauri, K.S. Chikhelidze* (2010), Proceedings of the Geol. Inst. of Georgia, New ser., **125**: 51-61.
24. *I.P. Gamkrelidze, D.M. Shengelia, T.N. Tsutsunava* (2011), Bull. Georg. Natl. Acad. Sci. **5**, 1: 64-76.

Received April, 2012

საქართველოს მეცნიერებათა ეროვნული აკადემიის მოამბე, ტ. 6, №3, 2012
BULLETIN OF THE GEORGIAN NATIONAL ACADEMY OF SCIENCES, vol. 6, no. 3, 2012

Petrology

First Evidence of Hyaloclastites at Madneuli Deposit, Bolnisi District, Georgia

Nino Popkhadze

A. Janelidze Institute of Geology of I. Javakhishvili Tbilisi State University

(Presented by Academy Member David Shengelia)

ABSTRACT. The Madneuli copper-gold polymetallic-deposit is a major deposit in Southern Georgia, which is still under development. It is located in the Artvin-Bolnisi zone, which is part of the Late Cretaceous Tethyan metallogenic belt. Several lithofacial units were outlined in the Madneuli open pit and their depositional setting was interpreted as submarine. The presence of rhyodacitic hyaloclastites in the host rocks is one of the supporting evidence of this setting. The hyaloclastite rocks represent the host rocks of the Madneuli upper Cretaceous rocks (Mashavera suite). Two types of hyaloclastite are recognized at the Madneuli deposit: hyaloclastite with pillow-like forms and hyaloclastite with glassy like selvages. The petrographic description shows a different nature: hyaloclastite with glassy like selvages represented by devitrification of volcanic glass, which is replaced by quartz-K-feldspar overgrowth crystals in the groundmass and elongated k-feldspar porphyry phenocrysts. Classical perlitic cracks were identified during thin section observation. The hyaloclastite with pillow-like forms consists of relicts of volcanic glass, large pumice clasts – surrounded by phyllosilicate and it still is possible to identify the fluidal nature of groundmass.

Silicified rhyodacitic hyaloclastite is interpreted as a result of water-rock interaction, in response to rapid chilling and quench fragmentation of lava. © *2012 Bull. Georg. Natl. Acad. Sci.*

Key words: *hyaloclastite, lobe hyaloclastite, pillow like form, glassy selvage.*

The identification and interpretation of major facial units, based on detailed field and petrographic descriptions is a powerful tool for determining paleogeography and geotectonic environment of volcanic successions, which in turn is a key for determining the depositional environments of ore deposits. The Madneuli deposit lacked such modern and detailed studies of volcano and volcano-sedimentary facies architecture based on physical volcanology aspects. The Madneuli deposit is described as volcanogenic massive sulfide (VMS) deposit with transitions to epithermal type deposit. According to current classification schemes based on host rock compositions, the Madneuli deposit can be classified as bimodal-felsic VMS type [1]. The upper Cretaceous Rhyodacitic hyaloclastic facies unit is the part of the host rock succession of the Madneuli deposit attributed to the Mashavera suite and represented by lavas, pyroclastics, volcanogenic-sedimentary and sedimentary rocks of rhyodacitic compositions [2].

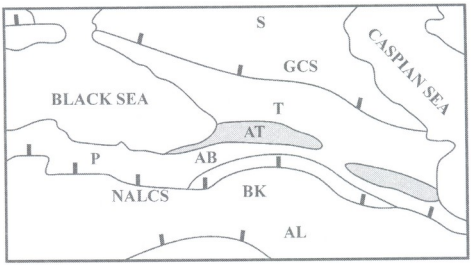

Fig. 1. Location map of the Madneuli deposit (adapted from Yilmaz et al. 2000). Abbreviations: S – Scythian Platform; GCS – Greater Caucasus Suture; T – Transcaucasus; AT – Southern Black Sea Coast-Achara-Trialeti Unit; AB – Artvin-Bolnisi Unit; P – Pontides; BK – Bayburt-Karabakh Imbricated Unit; NALCS – North Anatolian-Lesser Caucasian Suture; AI – Anatolian-Iran Platform.

Field and petrographic evidence presented in this paper shows that rhyodacitic hyaloclastites are hydrothermally altered and strongly silicified, and are evidence of a submarine depositional environment. The hyaloclastite is lobe hyaloclastite, which is one of the important characteristic facial units of the rocks hosting VMS deposits. In the open pit the periphery part of the lava lobe is still observed, which has a ring structure with internal columnar joints (Fig.2a).

Regional geological setting

The Bolnisi ore district is located in the Artvin-Bolnisi tectonic zone, which is continuing to the West into the Turkish Pontides and farther West to the Bulgarian Srednegoria tectonic zone (Fig. 1). The Artvin-Bolnisi Unit is bordered to the North by the Adjara-Trialeti unit (Santonian-Campanian back-ark) and the Imbricated Baiburt-Karabakh unit to the South (Upper Cretaceous fore-arc). It represents the northern part of the southern Transcaucasus and the central part of the Eastern Pontides, which formed the active margin of the Eurasian continent.

The Artvin-Bolnisi unit is characterized by a Hercinian basement, which consists of Precambrian and Paleozoic granites-gneisses and plagiogranites and late Variscian granits [3] overlain by Carboniferous volcano-sedimentary rocks [4] (Adamia et al.). Within the Bolnisi volcanic-tectonic depression, there are Cretaceous, Paleogene, Pliocene and Quaternary sedimentary rocks. Three main formations are distinguished within the Albian-Upper Cretaceous volcano-sedimentary unit: 1) terrigenous-carbonate (Albian-Senomanian), 2) volcanogenic (Turonian-Santonian) and 3) carbonate (Campanian-Maastrichtian) units [4]. Jurassic and Cretaceous rocks consist of volcaniclastic rocks, limestones and calc-alkaline magmatic arc rocks (andesite, dacite, rhyolite, and basalt and volcaniclastic rocks intruded by granitoids). The sequence is unconformably overlain by Maastrichtian – Paleocene limestone and turbidite. The Lower Eocene formation consists of terrigenous clastic rocks. Middle Eocene volcanic rocks overlie unconformable older rocks and are conformably overlain by Upper Eocene shallow-marine clastic rocks. The youngest rocks in the region are Quaternary volcanic rocks and alluvial sedimentary rocks.

Hyaloclastites

Field and petrographic descriptions

a. Glassy-like selvages hyaloclastite type. The best-exposed section of the hyaloclastite rock formations is in the eastern part of the Madneuli open pit. It is charac-

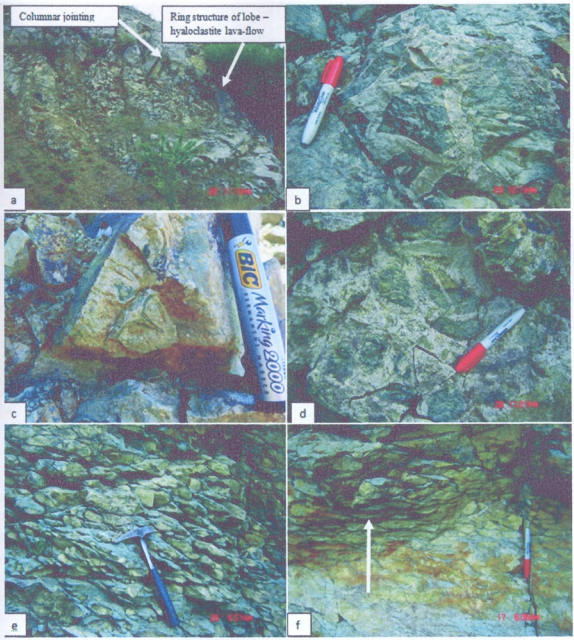

Fig. 2. Representative examples of hyaloclastite outcrops at Madneuli open pit. a. The margins of a lobe hyaloclastite flow with internal columnar joints, b. Carapace breccia, c. The alteration process in the coherent intrusive, d. Glassy-like selvage hyaloclastite-pseudo-breccia, with whitish and grayish-greenish parts, e.Pillow-like shapes in hyaloclastite, f.Transition zone from massive to pillow parts in pillow-like hyaloclastite.

terized by intense silicification-devitrification and chloritization. At the outcrop scale, the hyaloclastite gives the apparent impression of a breccia flow body with whitish rims around grey-greenish rock fragments. In fact, this apparent breccia texture is the result of weathering and alteration. The quenching process begins in the coherent part of the intrusive and increases toward the peripheral part of the flow (Fig. 2c). The whitish "rims"- within the flow are 1to-3 cm-thick, and in thin section they have the same texture as the grey-greenish "cores" (Fig. 2d), the difference is that the whitish part consists of a less amount of the phenocrysts than the greenish part. It is concluded that formation of such whitish zones, giving to the rock an apparent breccia

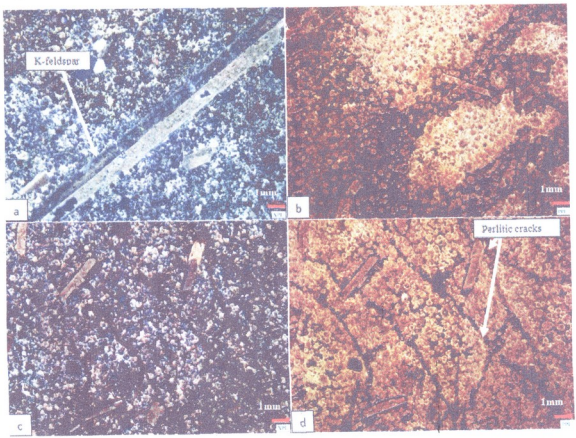

Fig. 3. Petrographic observations of glassy-like selvage type of the hyaloclastite. a. Elongated phenocryst of K-feldspar, b. The alteration processes: whitish and gray-brownish colors (crossed nicols), c. Perlitic cracks in glassy groundmass (crossed nicols), d. the perlitic cracks go around the edges. (plane-polarized light)

texture in the distal part of the hyaloclastite flow is a product of quench fragmentation during lava – water interaction. The chaotic character of the carapace breccia (Fig. 2b), their local distribution at the flow top, the absence of bedding and grading and lack of broken crystals suggest an origin predominantly due to autobrecciation [5] .This type of hyaloclastite rock is characterized by perlitic texture, which usually is recognizable with a hand lens or otherwise in thin section, in some exceptional cases macro-perlitic texture can be recognized at the outcrop scale within the Madneuli open pit. This hyaloclastite type contains round and oval-shaped amygdalae filled with quartz-chlorite or a fine-grained carbonate – clay mass.

b. The hyaloclastite with pillow-like forms are exposed on three bench levels in the eastern part of the open pit where typical small pillow shapes occur (Fig.2e). Along the same section, here is also a gradational transition from massive lava to the pillow-like shaped part (Fig.2f). Moreover, pillow-like forms occur within the massive rhyodacitic lava flow. The matrix surrounding the pillows is a bluish-colored altered rock of the same rhyodacitic composition as the pillow. The thickness of local outcrops is small and varies within 5-8 m.

Petrographic description

a. Glassy-like selvages type of hyaloclastite. This hyaloclastite contains less than 30% of phenocrysts. The matrix consists of devitrified volcanic glass with a mosaic texture, radial-shaped crystals of K-feldspar and spherules of quartz. Plagioclase microlites fill the spaces between spherulites and look like an overgrowth around them (Fig 3b, d). Porphyry phenocrysts include quartz, plagioclase and K-feldspar of different size. In some

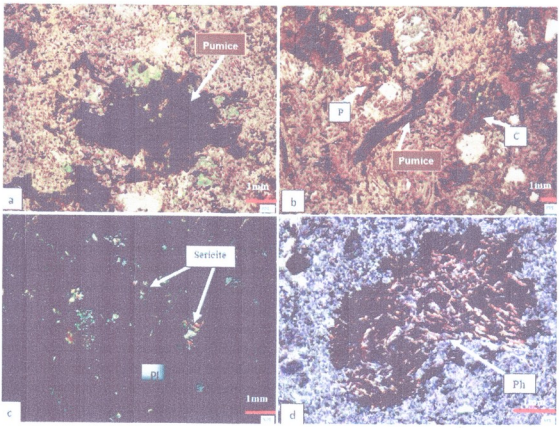

Fig. 4. Petrographic observations of pumice hyaloclastite. a. axiolitic devitrification of glass, b. remnants of platy and cuspate shapes of volcanic glass and pumice, c. sericite microcrystals along plagioclase crystal, d. phyllosilicate-rich pumice clast (Ph)

places they are associated in glomeroporphyric textures. Large and elongated sanidine crystal shapes are distinguished (Fig. 3a). Sericite alteration is developed in K-feldspar and plagioclase crystals. Spherulites with fine-grained quartz and feldspar are products of high-temperature devitrification of silicic volcanic glass. Subsequent recrystallisation of mosaic quartz-feldspar can destroy or modify such original devitrification textures [6].

The groundmass contains perlitic cracks, identified during thin section observation. Perlitic cracks develop in response to hydration of the glass. Hyaloclastite with glassy-like selvages has a classical perlitic texture, where the cracks are distinctly arcuate and concentrically arranged around spherical cores. Hydration occurs after emplacement and during the later cooling history of the glass, or after complete cooling to surface temperature. In some thin sections perlitic cracks cut the elongated K-feldspar phenocrysts, but sometimes instead of cutting across the crystals, the perlitic cracks just go around the edges (Fig.3 c, d). The conclusion is that the first stage was devitrification of volcanic glass followed by crystallization of porphyry crystals and finally formation of perlitic cracks.

b. The hyaloclastite with pillow-like shapes. In thin section pillow-like hyaloclastite has a rhyolitic nature. The massive part of pillows has similar composition, though with some differences. The rock has a porphyritic structure while the groundmass consists of relicts of volcanic glass replaced by finely disseminated quartz and K-feldspar. Large pumice clasts are also present. Locally, the groundmass has a fluidal nature. Shards of volcanic glass have preserved their platy and cuspate shapes (Fig.4b). In some places, the matrix displays a vitriclastic texture

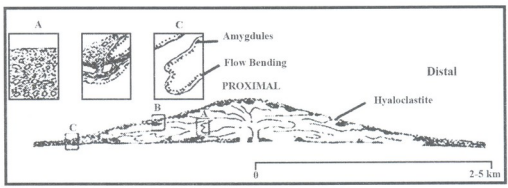

Fig. 5. Idealized cross-section through a rhyolitic lobe-hyaloclastite flow illustrating flow morphology and structures typical of proximal and distal facies (after Gibson et al., 1990)

accentuated by axiolitic devitrification of glassy components. The center of Fig.4a shows a relict pumice clast with destroyed internal vesicular microstructure. The brown rims of matrix shards are affected by axiolitic devitrification [6]. Crystals of biotite are present, with rare muscovite. The margins of K-feldspars are partly desorpded. In some places only crystal relicts are present filled by chlorite. Sericite alteration overprints plagioclase crystals (Fig.4c). In the massive part of the pillow hyaloclastite, phenocrysts are rare; they are concentrated in the mass between the pillows (pseudo cement). The pumice clast is surrounded by phyllosilicate (Fig.4d).

Interpretations

Subaqueous felsic lavas are typically divided into lobe-hyaloclastite flows, blocky subaqueous lavas and domes, cryptodomes, and regionally extensive felsic lavas. Volcanogenic-hosted massive sulphide deposits can be associated with the first three flow types [5]. Fig. 3 is an idealized cross-section through a rhyolitic lobe-hyaloclastite flow, which illustrates the flow morphology and structures typical of proximal and distal facies.

This paper describes two types of rhyodacitic hyaloclastite, which are exposed in the open pit of the Madneuli deposit: (1) hyaloclastite with pillow-like forms and (2) hyaloclastite with glassy-like selvages. They correspond to the section B in Fig.5. Hyaloclastite with glassy-like selvages refers to a breccia facies, morphologically associated with carapace breccias and occur along the upper surface of the distal part of flows. By contrast hyaloclastite with pillow-like forms is pumiceous hyaloclastite, which consists of pumice fragments and volcanic glass. The lobe-hyaloclastite flow is inflated by successive pulses of new magma, which feeds its large lobes. They generally follow a very irregular path to the flow front, where they form smaller lobes and locally they have small sized pillow-like shapes [5]. The Madneuli lobe-hyaloclastite flow is massive in general, though locally ribbed, flow laminated and columnar jointed.

As documented by reference 6, lobe-hyaloclastite flows are mostly fissure-fed flows, associated with seafloor spreading and are emplaced in both deep water and shallow (<500m) water environments." In the open pit lobe-hyaloclastite flows are associated with turbiditic volcanoclastic deposits and peperites, which clearly documents that hyaloclastite was formed in submarine environment, however there is no evidence to constrain the exact water depth during hyaloclastite formation.

Conclusions

- Spherulites in the hyaloclastite are strong evidence for the high temperature devitrification of volcanic glass, which is replaced by quartz-K-feldspar overgrowth crystals in the groundmass and columnar jointing, which occur inside the lobe flow in the open pit.

- Rapid quenching forms a glassy-like selvage along the edge of the lobe. It is constantly broken and spalled to produce more hyaloclastite.

- Both types of hyaloclastite with different textures are lobe hyaloclastite. The formation processes took place in one lobe body, which was inflated by successive pulses of new magma. In some places the ring structure of lobe hyaloclastite lava-flow with columnar jointing inside part of the lobe is presented.

- The lobe hyaloclastites, described in this paper, resemble other hyaloclastites from well-known deposits in the world, common in submarine felsic successions, is one of the important characteristic facial units of the rocks hosting VMS deposits.

- Two types of rhyodacitic lobe hyaloclastite flows are described in the open pit: hyaloclastite with glassy-like selvages and hyaloclastite with pillow like forms. Absence of different resedimented rock fragments, the gradational contact with coherent lavas, their laterally discontinuos character, absence of bedding suggests their in situ hyaloclastite nature.

Acknowledgements. The research was supported by the Georgia National Science Grant 204 and Swiss National Science Foundation through the research grant SNF 200020-113510 and SCOPES Joint Research Projects IB7320-111046 and IZ73Z0-128324. The author would like to thank the participants of the project and the staff of the "Madneuli Mine" for arranging access to the mine and sharing geological information.

პეტროლოგია

ჰიალოკლასტიტები მადნეულის საბადოს შემცველ წყებაში

ნ. ფოფხაძე

ი. ჯავახიშვილის სახ. თბილისის სახელმწიფო უნივერსიტეტის ა.ჯანელიძის გეოლოგიის ინსტიტუტი, თბილისი
(წარმოდგენილია აკადემიის წევრის დ.შენგელაიას მიერ)

მადნეულის ოქრო-სპილენძ-პოლიმეტალური საბადო სამხრეთ საქართველოში ერთ-ერთი უმთავრესი საბადოა, რომელიც კლავე ათვისების პროცესშია. ის განლაგებულია ართვინ-ბოლნისის ზონაში, რომელიც თავის მხრივ ტეთისის გვიანცარცული სარტყელის ნაწილს წარმოადგენს. მადნეულის კარიერის ფარგლებში გამოფენილი იქნა რამდენიმე ლითოფაციალური ერთეული და მათი დალექვის გარემო განისაზღვრა როგორც წყალქვეშა. საბადოს შემცველ ქანებში რიოდაციტური შედგენილობის ჰიალოკლასტიტების არსებობა ამ დებულების ერთ-ერთ უტყუარ მტკიცებულებად არის მიჩნეული. ჰიალოკლასტიტები საბადოს შემცველი მაშაერას წყების შემადგენელი ნაწილია.

საბადოზე გამოიყო პიალოკლასტიტების ორი ტიპი: პიალოკლასტიტები ბალიშისებრი ფორმებით და პიალოკლასტიტები მინისებრი არშიებით. სილიციფიცირებული რიოდაციტური პიალოკლასტიტების წარმოშობა განაპირობა წყლისა და ქანის ურთიერთქმედებისას ლავის მყისიერმა გაცივებამ და, შედეგად, მისმა ფრაგმენტაციამ.

REFERENCES

1. *N. Popkhadze, T. Beridze, R. Moritz, et al.* (2010), in: The Challenge of Finding New Mineral resources, SEG Conference, Keystone, Colorado, U.S.A., October 2010, Abstract volume, p. 128-129.
2. *N. Popkhadze, T. Beridze, R. Moritz, et al.* (2009), Bull. Georg. Natl. Acad. Sci., **3**, 2: 107.
3. *I.E. Gamkrelidze, D.M. Shengelia* (2005), Precambrian-Paleozoic Regional Metamorphism, Granitoid Magmatism i Geodynamics of the Caucasus. Moscow, p.458 (in Russian).
4. *A. Yilmaz, Sh. Adamia, Al. Chabukiani, et al.*(2000), in: E. Bozkurt, J.A. Winchester and J.D.A. Piper (Editors), Tectonics and Magmatism in Turkey and the Surrounding Area. Geological Society, London, Special Publications, **173**: 171-182.
5. *R.L. Morton, H.L. Gibson, G.J. Hudak* (1999), Reviews in Economic Geology, **8**: 13-48.
6. *J. McPhie, M. Doyle, R. Allen* (1993), Volcanic Textures. A guide to the interpretation of textures in volcanic rocks. Centre for Ore Deposit and Exploration Studies, University of Tasmania, 198 p.

Received July, 2012

საქართველოს მეცნიერებათა ეროვნული აკადემიის მოამბე, ტ. 6, №3, 2012
BULLETIN OF THE GEORGIAN NATIONAL ACADEMY OF SCIENCES, vol. 6, no. 3, 2012

Palaeogeography

Palaeogeography of the Sarmatian of Eastern Georgia

Kakhaber Koiava[*], Lamara Maissuradze[**], Andreas Strasser[§], Irina Shatilova[**], Lia Kvaliashvili[§§], Vakhtang (Bacho) Glonti[†]

[*] *Ivane Javakhishvili State University, Alexandre Janelidze Institute of Geology, Tbilisi*
[**] *The Georgian National Museum, L. Davitashvili Institute of Paleobiology, Tbilisi*
[§] *Department of Geosciences, University of Fribourg, Fribourg, Switzerland*
[§§] *LTD "GeoEngService", Tbilisi*
[†] *LTD "Frontera Eastern Georgia", Tbilisi*

(Presented by Academy Member Abesalom Vekua)

ABSTRACT. The limits of the Kura bay and of the adjoining tectonic high zones and depressions were inherited from the Middle Miocene and continued to exist. They had an important role in controlling the distribution of the sedimentary facies. The poorness in marine faunas of the Early Sarmatian deposits, together with the character of thickness and facies, suggest that these sediments formed in a big brackish basin. Towards the north and south from this basin, great mountain ranges of sublatitudinal direction existed. At the beginning of the Middle Sarmatian there were no important changes in the palaeogeographical and geotectonical situation. The basin expanded slightly towards the north, which is reflected by transgressive deposits of the Middle Sarmatian age on the northern Kakheti range (Chailuri, Manavi, Burdiani). The relatively homogeneous facies allows to suppose that the palaeogeographical and sedimentary conditions did not change for a long time. The orogenic movements, which began at the end of the Middle Sarmatian, reached their maximum in the Late Sarmatian (the Attic orogenic phase) and on the whole territory of Eastern Georgia a continental regime was established. Extension and depth of water bodies were significantly reduced: in the late Sarmatian the sea on the territory of Eastern Georgia was divided into isolated or semi-isolated comparatively small basins – lakes, lagoons. © *2012 Bull. Georg. Natl. Acad. Sci.*

Key words: *Eastern Paratethyan, Caucasus, Upper Miocene, foraminifera.*

Beginning with the Late Eocene, to the Early Pliocene, the geological development of the Caucasus was closely connected with the history of the Paratethys Sea (Fig. 1). In that period, the whole Paratethys underwent complicated paleogeographical changes [1, 2], including the territory of Georgia.

During the whole Early Miocene the territory of Georgia was involved in orogenic processes of the Alpine cycle, although in separate areas subsidence also occurred. These sites accumulated thick argillaceous sandstones. On the territory of Eastern Georgia, the Sarmatian stage (covering the Late Middle

Fig. 1. Outline of the Paratethys-Mediterranean region during Late Miocene (according to Müller et al, 1999).

Miocene and the Early Late Miocene) is divided into three substages: Early (Volhynian), Middle (Bessarabian), and Late (Khersonian).

Early Sarmatian (Fig. 2). For the Early Sarmatian, the tendency of subsidence of the Transcaucasus, inherited from Konkian time, is characteristic. This was followed by a widening of the basin that on the northern border and on the periphery of the Dzirulian massifs is confirmed by transgressive beds of the Sarmatian [3, 4]. In Early Sarmatian time, a large part of the Dzirulian massifs was dry land. To the west it was bordered by the Okribian land area. These two land masses were separated by a shallow sea or were connected with the Rioni bay on the western part and the Kura bay to the east.

The outlines of the Kura bay practically coincided with the borders of the Eastern zone of sinking of Transcaucasian intermountain area. To the south, the Kura bay bordered the Trialetian range. Passing on from the eastern side of the Trialetian range, the Kura bay formed the Yalgudgi bay. Towards the southeast, the Kura bay extended to the right bank of the river Kura. To the west it reached the eastern periphery of the Dzirulian massif and farther in the north joined with the Rioni bay, through the Djava-Tedeletian strait. The northern border of the Kura bay extended towards the Cretaceous flysch deposits of the Greater Caucasus range.

The limits of the Kura bay and of the adjoining tectonic high zones and depressions were inherited from the Middle Miocene and continued to exist. They had an important role in controlling the distribution of the sedimentary facies.

The poorness in marine faunas of the Early Sarmatian deposits, together with the character of thickness and facies, suggest that these sediments formed in a big brackish basin. Towards the north and south from this basin, great mountain ranges of sublatitudinal direction existed.

In the eastern part of the Dzirulian massif, the Early Sarmatian transgressively overlies Palaeozoic, Mesozoic, and Cenozoic deposits. At the base it is represented by conglomerates, which pass into quartz-sandstones with intercalations of clay [3]. The thickness of these deposits is 50-90 m. On the northern border of the Kartlian depression, the Early Sarmatian lies concordantly on the Konkian regiostage and consists of sandstone – clay marine deposits. Towards the east of the Dzirulian massif the quantity of clay material increases. There, the maximum thickness of the Early Sarmatian is 250-300m.

In the southern part of the Kartlian depression, the Early Sarmatian is represented by coastal deposits: microconglomerates, sandstones, and clays. Towards the east the clay content increases. The thickness is variable (60-170 m). Between the rivers Kura and Iori, the Early Sarmatian is built by deposits of deeper water (clays and intercalations of sandstones),

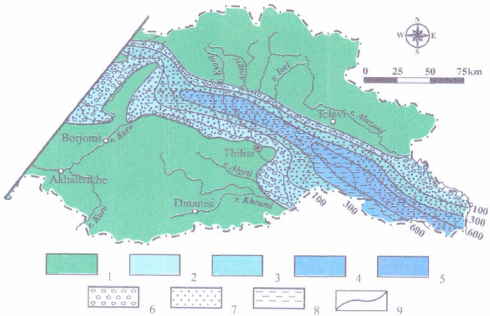

1. land; 2. shoreface facies; 3. shallow-water facies; 4. transition facies; 5. deep-water facies; 6. conglomerate; 7. sandstone; 8. clay; 9. borders the same thickness.

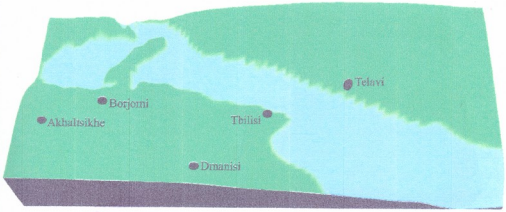

Fig. 2. Early Sarmatian lithofacies, thickness and paleogeographical map of Eastern Georgia.

and the thickness there reaches 250-350 m. To the south-east the Early Sarmatian is represented by sandstones with intercalations of microconglomerates and clays (40-70 m).

The fauna is mainly represented by euryhaline and eurythermal molluscs and benthic foraminifera that point to a shallow, fresh-water influenced basin. Two different assemblages of foraminifera are distinguished, indicating the existence of both shallow and deeper sites in the basin. The shallow-water fauna consists of representatives of the genera *Elphidium, Porosononion*, and *Nonion* which are characterized by coarsely sculptured tests. The fauna of the deeper basin is represented by forms with thin, nearly transparent tests of the so-called "miliolidian" complex [5, 6].

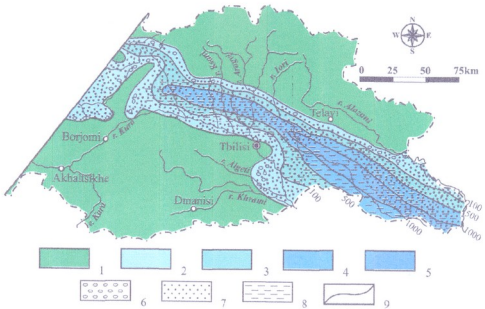

1. land; 2. shoreface facies; 3. shallow-water facies; 4. transition facies; 5. deep-water facies; 6. conglomerate; 7. sandstone; 8. clay; 9. borders the same thickness.

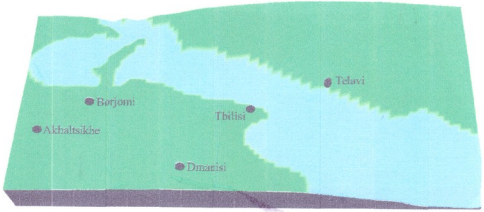

Middle Sarmatian (Fig.3). At the beginning of the Middle Sarmatian there were no important changes in the palaeogeographical and geotectonical situation. The basin expanded slightly towards the north, which is reflected by transgressive deposits of the Middle Sarmatian age on the northern Kakheti range (Chailuri, Manavi, Burdiani) [3].

In the area between Koda and Tsnelisi, the Middle Sarmatian transgresses over the Bajocian porphyritic series and the granitoids of the Dzirulian massif, and in the territory of Tsablovani-Nabakhtevi it is deposited on the Middle Miocene sandstones. The Middle Sarmatian there is represented by quartz-feldspathic sandstones with intercalations of clays and conglomerates. The thickness is 160-180 m.

On the northern border of the Karthlian depression, the Middle Sarmatian concordantly overlies the Early Sarmatian. The lower part of the Middle

Sarmatian there is represented by sandstones and clays with so-called "cryptomactrian" layers, which can be seen in many sections [4]. The upper part of the Middle Sarmatian is represented by sandstones, clays and conglomerates [5]. The thickness ranges from 350 to 1000 m.

On the southern border of the depression, the Middle Sarmatian consists of sandstone-clay deposits with intercalations of limestones, lumachelles and conglomerates [7]. The thickness there is 100-350 m.

In southern Kakheti, the Middle Sarmatian is represented by two lithofacies. The first is composed of thick, comparatively deep basin clays and sandstones, but the second one is represented by deposits of shallow-water sandstones and clays with intercalation of oolitic limestones, conglomerates, and coloured clays [8].

The relatively homogeneous facies allows to suppose that the palaeogeographical and sedimentary conditions did not change for a long time: as in the Early Sarmatian, accumulation of mainly conglomerates took place in the coastal zone, and of argillaceous sandstones in the deeper areas of the basin. The thickness there ranges from 600 m to 1000 m. The intensity of sedimentation was compensated by subsidence [3]. The absence of gypsum, anhydrite, and salt coupled with the occurrence of hydromica and carbonate as well as the poorness in marine fauna indicate the existence of a warm, low-salinity basin. The warm and humid climate of the Sarmatian is indicated by data of plant macrofossils [9] and palynological assemblages [10]: evergreen thermophilic plants dominated at this time.

The Middle Sarmatian assemblage of foraminifera is distinguished by abundant species and by numerous forms. Of great interest are typical Middle Sarmatian forms such as *Dogielina*, *Meandroloculina*, and *Sarmatiella*. Also large sizes, nearly 1 mm, of some representatives of *Elphidium* are to be mentioned [5,6].

The flourishing of the Middle Sarmatian fauna indicates favorable biotic and abiotic conditions - good aeration, sufficient quantity of food, and adequate temperature conditions in the basin.

The abundance of foraminifera, their diversity, and the thickness of sediments allow us to suppose that the main structural elements established in the Early Sarmatian continued to develop.

Beginning with the second half of the Middle Sarmatian, tectonical movements were active and produced some changes in palaeogeography, erosion processes, and differentiation of facies. In depressions these processes were especially well developed: shallowing of the water, increasing of grain sizes, and changes in clay facies. The coarse-grained material (conglomerates) on the northern side of the Kartli depression in the Djava-Tedeletian strait and on the Tsivgomborian range became more abundant.

In sections of the Kura bay coloured clays including fresh-water and land fauna occur. This indicates the existence of dry-land conditions on the periphery of the basin during the second part of the Middle Sarmatian. The retreat of the sea was so quick that the Djava-Tedeletian strait ceased to exist and full isolation of the Kura and Rioni bays took place.

Later the sea retreated towards the south-east, and at the beginning of the Late Sarmatian Kartli depression, Southern slopes of Tsiv-Gombori range and a significant part of Gare-Kakheti was the region of accumulation of fresh-water, continental sediments. Marine facies are preserved only near the Iori river.

Late Sarmatian (Fig. 4). The orogenic movements, which began at the end of the Middle Sarmatian, reached their maximum in the Late Sarmatian (the Attic orogenic phase) and on the whole territory of Eastern Georgia a continental regime was established. Extension and depth of water bodies were significantly reduced: in the late Sarmatian the sea on the territory of Eastern Georgia was divided into isolated or semi-isolated comparatively small basins – lakes, lagoons. The increasing orogenic processes promoted the widening of the hydrographical network, and a large amount of eroded sediment was transported by rivers. The river mouths formed deltas in the lakes, composed of conglomerates, clays and sandstones.

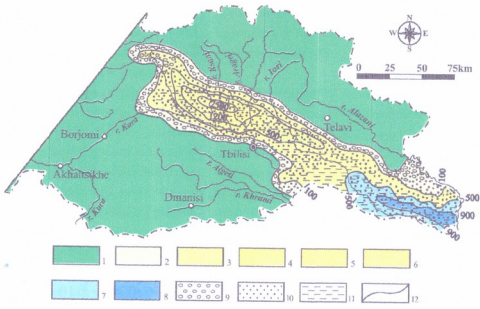

1. land; 2-6. continental facies; 7-8. marine facies;
9. conglomerate; 10. sandstone; 11. clay; 12. borders the same thickness.

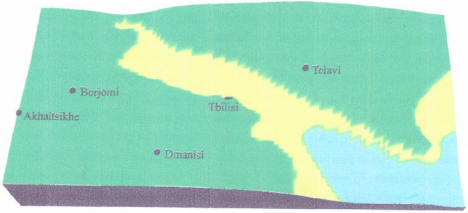

Fig. 4. Late Sarmatian lithofacies, thickness and paleogeographical map of Eastern Georgia.

In the Late Sarmatian, the Kartlian depression and part of Kakheti turned into an important depocenter. In the Karthlian depression, the Late Sarmatian is represented by fresh-water deposits and continental clays and sandstones with intercalation of micro-conglomerates and conglomerates. The sediment thickness ranges between 1000-2500 m.

The boundary between Middle and Late Sarmatian is drawn where the Middle Sarmatian layers containing fauna disappear and are replaced by thick, so-called "dumb" continental deposits, the Natskhorian suite [3, 11].

In the Late Sarmatian, the southern wing of the Tsivgomborian range began to subside and like the Kartlian depression the argillaceous sandstones of the Natskhorian suite began to accumulate here. The main source of the terrigenous material was the southern slope of the Caucasus

Range, but towards the southern edge of the Transcaucasian depression the amount of the terrigenous material decreased and the depression was finally filled with material from the Adjaro-Trialetian range [12].

South-east of the Kakhetian range, the Natskhorian suite is replaced by the Eldarian suite. In southern Kakheti, the Late Sarmatian starts with marine deposits that gradually change into continental sediments. Their lower part (thickness 150-350 m) is represented by clay-sandstone facies with poor microfauna, characteristic of the Late Sarmatian [3, 4]. The upper part is represented by colored clays of the Eldarian suite.

In the regions along the Iori River, marine sediments of so-called "marine thickness" appear. This is proven by the consistency of the material from the boreholes of Taribana and Eldari [8].

Towards the end of the Sarmatian, the sea had completely retired from the eastern part of the Transcaucasian intermountain region and the long-term regression of the Miocene sea was completed.

პალეოგეოგრაფია

აღმოსავლეთ საქართველოს სარმატული დროის პალეოგეოგრაფია

კ. ქოიავა*, ლ. მაისურაძე**, ა. სტრასსერი§, ი. შატილოვა**, ლ. კვალიაშვილი§§, ვ. ღლონტი†

* ი. ჯავახიშვილის სახელმწიფო უნივერსიტეტი, ა. ჯანელიძის გეოლოგიის ინსტიტუტი, თბილისი
** საქართველოს ერონული მუზეუმი, ლ. დავითაშვილის პალეობიოლოგიის ინსტიტუტი, თბილისი
§ ფრიბურგის უნივერსიტეტი, დედამიწის შემსწავლელ მეცნიერებათა განყოფილება, ფრიბურგი, შვეიცარია
§§ შპს "გეოინჟსერვისი", თბილისი
† შპს "ფრონტერა ისთერნ ჯორჯია", თბილისი

(წარმოდგენილია აკადემიკოს წერეთლის მიერ)

აღრესარმატულ დროში მტკვრის უბის ფარგლებში ნალექების ფორმირება ხდებოდა საკმაოდ ღრეცელ მარნხი ზღვის გამტკნარებულ აუზში, რომლის ჩრდილოეთით და სამხრეთით მდებარეობს ხუბანეიდური მიმართულების მაღალი ქედები. მარნხი ზღვის გამტკნარებულ აუზზე მიგვანიშნებს ნალექებში განამარხებული ფაუნაც, რომელშიც უპირატესად ვერიპალური და ვერითრიფული მოლუსკები და ბენტოსური ფორამინიფერები გვხვდებიან.

შუა სარმატულის დასაწყისში რაიმე მნიშვნელოვანი ცვლილებები პალეოგეოგრაფიული და გეოტექტონიკური თვალსაზრისით არ მომხდარა. ამ პერიოდის ფორამინიფერები გამოირჩევიან სახეობათა მრავალფეროვნებით და სიმრავლით. ფაუნის გაფურჩქვნა მიუთითებს ხელსაყრელ ბიოტურ და ბიოიტურ პირობებზე, პირველ რიგში საკვების საკმაო სიუხვეზე, აუზის კარგ აერაციაზე და თბილ ჰავაზე.

შუა სარმატულის მეორე ნახევრიდან გაიდგნება ტექტონიკური მოძრაობების გააქტიურება, რომლებმაც პალეოგეოგრაფიულ ვითარებაში ზოგიერთი გარდაქმნა გამოიწვია, რაც ასახა გადარეცხვის პროცესების გაძლიერებაში, ფაციესების დიფერენციაციასა და მათ მრავალფეროვნებაში.

მტკვრის უბის ხვადასხვა მონაკვეთზე შუა სარმატულის მიწურულში წნდება ფერადი თიხები, რომლებიც შეიცავს მტკნარი წყლის და ხმელეთის ფაუნას, ეს კი იმაზე მიგვანიშნებს, რომ შუა სარმატულის მიწურულს აუზის პერიფერიულ ნაწილში კონტინენტური რეჟიმი ჩამოყალიბდა.

შუა სარმატულის ბოლოს დაწყებული ტექტონიკური მოძრაობის ინტენსივობა ზედა სარმატულში მაქსიმუმს აღწევს (დანაოჭების ატიკური ფაზა) და აღმოსავლეთ საქართველოს მთელ ტერიტორიაზე კონტინენტური რეჟიმი მყარდება. ამ დროისთვის მკვეთრად შემცირდა წყლის აუზის ფართობი და მისი სიღრმე. ფაქტობრივად შეიძლება ითქვას, რომ აღმოსავლეთ საქართველოში გვიან სარმატულში ზღვა დანაწევრდა მეტ-ნაკლებად დაკავშირებულ ან იზოლირებულ, შედარებით მცირე ზომის აუზებად – ტბებად, ლაგუნებად.

REFERENCES

1. *F. Rögl* (1999), Geologica Carpathica, **4**: 339-349.
2. *M. Harzhauser, W. Piller, F. Steininger* (2002), Palaeogeography, Palaeoclimatology, Palaeoecology, **183**: 103-133.
3. *D. Buleishvili* (1960), Geologiia i neftegazonostnost' mezhgornoi vpadiny vostochnoi Gruzii. Leningrad: 238 p. (in Russian).
4. *K. Gruzinskaia* (1966), Abstract of Ph. D. thesis, Tbilisi (in Russian).
5. *K. Koiava* (2006), Abstract of Ph. D. thesis, Tbilisi (in Georgian).
6. *L. Maissuradze, K. Koiava, S. Spezzaferri, I. Shatilova, N. Mchedlishvili, A. Strasser* (2008), Proceedings of the Georgian Academy of Sciences. Biological series, **B**, **1-2**, 6: 57-71.
7. *K. Koiava* (2006a), Oil and Gas in Georgia, **17**: 38-43 (in Georgian).
8. *L. Maissuradze, K. Koiava* (2006a), Oil and Gas in Georgia, **19**: 50-62 (in Georgian).
9. *M. Uznadze* (1965), Neogenovaia flora Gruzii. Tbilisi,180 pp (in Russian).
10. *I. Shatilova, N. Mchedlishvili, L. Rukhadze, E. Kvavadze* (2011), The history of the flora and vegetation of Georgia (South Caucasus). Tbilisi, 200p.
11. *K. Chubinishvili* (1982), Neogenovye kontinental'nye molassy vostochnoi Gruzii. Tbilisi, 314 p. (in Russian).
12. *D. Buleishvili* (1964). Geologiia SSSR. **10**: 284-308 (in Russian).

Received March, 2012

Biochemistry

Phenolic Compounds of Wines from Georgian Autochthonous Grapes, Rkatsiteli and Saperavi, Prepared by Georgian (Kakhetian) Technology

Armaz Shalashvili*, Devi Ugrekhelidze, Teimuraz Mitaishvili*, Iraida Targamadze*, Natela Zambakhidze***

** Durmishidze Institute of Biochemistry and Biotechnology of Georgian Agrarian University, Tbilisi*
***Academy Member, Georgian National Academy of Sciences, Tbilisi*

ABSTRACT. The qualitative composition and the quantitative content of phenolic compounds of wines from the Georgian autochthonous grapes, white Rkatsiteli and red Saperavi, prepared by Kakhetian technology are studied. According to the obtained data, in white wine Rkatsiteli the content of catechines is the following: (+)-catechine (32.6 mg/l), (-)-epicatechine (58.6 mg/l), (-)-gallocatechine (43.7 mg/l), and in red wine Saperavi: (+)- catechine (115.4 mg/l), (-)-epicatechine (29.5 mg/l), (-)-gallocatechine (174.4 mg/l), respectively. It is shown that a significant difference in the contents of catechines is observed between white and red wines. Red wine Saperavi contains 3.4 times and 4 times more (+)-catechine and (-)-gallocatechine, and 2 times less (-)-epicatechine than the white wine Rkatsiteli. Out of flavonols kaempferol (13.2 mg/l), quercetin (11.2 mg/l) and rutin (2.6 mg/l) were found in red wine Saperavi, while in white wine Rkatsiteli those compounds are absent. The white wine Rkatsiteli does not contain resveratrol, while in red wine Saperavi its amount is equal to 1.47 mg/l. Out of hydroxybenzoic acids the protocatechuic acid and gallic acid were not found in white wine Rkatsiteli, while in red wine Saperavi their amount is equal to 14.5 mg/l and 21.8 mg/l. Of hydroxycinnamic acids, in red wine Saperavi caffeic acid in the amount of 7.4 mg/l, and o-coumaric acid and syringic acid as traces were found. These acids were not found in the white wine Rkatsiteli. Thus, in qualitative composition and quantitative contents of phenolic compounds the red wine Saperavi considerably surpasses the white wine Rkatsiteli. © *2012 Bull. Georg. Natl. Acad. Sci.*

Key words: *phenolic compounds, Georgian (Kakhetian) wines, catechines, flavonols, stilbenes, hydroxybenzoic acids, hydroxycinnamic acids, HPLC.*

A major challenge in human health over the next 50 years will be in the area of chronic diseases, many types of cancer, type 2 diabetes and obesity [1]. For protection against the cited diseases phenolic compounds, ubiquitously distributed in vascular plants, have on important value. The molecules of phenolic compounds have several biological effects, including inhibition of LDL oxidation *in vitro* and *in vivo* and protection of DNA from oxidative damage; they also have antithrombotic, antimutagenic properties

[2]. In addition, phenolic compounds are characterized by extremely high antioxidant properties [3]. Proceeding from this, identification of such foodstuffs which are rich in phenolic compounds having medical activity is extremely important. In this aspect interest attaches to white and red wines prepared by Kakhetian technology which contain phenolic compounds in the amount of 1.330-2.430 mg/l and 2.898-4.416 mg/l, respectively [4]. The purpose of this research is studying the qualitative composition and the quantitative content of phenolic compounds of Kakhetian white and red wines prepared in clay vessels (*kvevri*) by means of a method of high-pressure liquid chromatography.

Materials and methods. Analyzed samples were prepared by us in autumn 2010 from autochthonous grapes (*Vitis vinifera L)*, cultivated in Georgia white Rkatsiteli and red Saperavi. Grapes Rkatsiteli and Saperavi were collected in Kakheti region, respectively in villages Chumlaki and Velistsikhe of Gurjaani municipality. Grapes Rkatsiteli (80 kg) and Saperavi (70 kg), together with other parts of grape cluster (stem, skin, seeds), were crushed in juicer and were placed in clay vessels (kvevri) dug in the ground.In the case of Rkatsiteli, the fermentation took place in a closed cap (t = 21 °C) and at the further ripening of wine on husks of grapes within 120 days.In the case of Saperavi the fermentation occurred with an open cap (t = 23 °C) within 9 days, at regular agitation (daily) of emerged on surface of the husks of grapes, submerging the cap by hand with wooden paddle. In both cases natural yeasts were used. The fermented wines were drained into a glass vessel and stored in a cellar (t = 14 °C).

In the analyzed wines Rkatsiteli and Saperavi the sum of phenolic compounds is 2160 mg/l and 4320 mg/l, respectively [5]. A method of extraction of liquid/liquid was used for fractionation of phenolic compounds of the analyzed wines [6]. For this purpose, alcohol was removed from 1000 ml of each wine sample (dealcoholization) on the rotational evaporator at 40°C.The dealcoholized wine, pH of which was brought up to 2 (pH = 2), was extracted by ethyl acetate, after evaporation of ethyl acetate in vacuum (t = 30°C), the residue was dissolved in water, pH was brought up to 7 (pH = 7) and extracted again by ethyl acetate. The organic phase which substantially contains flavanols and flavonols, and a water phase was obtained. The organic phase was evaporated in vacuum (t = 30 °C), dissolved in methanol and marked as fraction X1 of Rkatsiteli white wine (RWWF X1) and fraction X3 of Saperavi red wine (SRWF X3). The pH of water phase was brought up to 2 (pH = 2) and extracted again by ethyl acetate. Extract of ethyl acetate was evaporated in vacuum (t = 30 °C), the residue was dissolved in methanol and marked as RWWF X2 and SRWF X4. These two fractions contain phenolic acids and flavonols. Identification of phenolic compounds from the obtained fractions was carried out by means of the high-pressure liquid chromatograph "Gilson 116", with UV detector. Chromatographic separation was carried out on "Zorbax ODS" column (25 cm x 4.6 mm); system of solvents: methanol - 4% acetic acid; 0.2 ml/min, at 280 nm, and 24 °C; injected volume 20 µl. Identification of compounds was carried out by comparison with retention time of authentic phenolic compounds. As authentic samples were used: (+)-catechine, (-)- epicatechine, (-)-gallocatechine, kaempferol and gallic acid (Sigma), quercetin and rutin (Chemapol), protocatechuic acid, o-coumaric acid and caffeic acid (Reachim), resveratrol (Bio-Tech Co.).

Results and discussion. According to the obtained data (Table), in white wine Rkatsiteli (fraction X1), the content of catechines is the following: (+)-catechine (32.6 mg/l), (-)-epicatechine (58.6 mg/l), (-)-gallocatechine (43.7 mg/l), and in red wine Saperavi (fraction X3): (+)- catechine (115.4 mg/l), (-)-epicatechine (29.5 mg/l), (-)-gallocatechine (174.4 mg/l), respectively. It is visible that under the contents of catechines, between white and red wines a significant difference is observed. Red wine Saperavi contains 3.4 times and in 4 times more (+)-catechine and (-)-gallocatechine, and 2 times less (-)-

Table. The contents of phenolic compounds in wines of grapes Rkatsiteli and Saperavi (mg/l)

Authentic phenolic compound	Retention time (min)	Fractions of white wine Rkatsiteli		Fractions of red wine Saperavi	
		X1	X2	X3	X4
(+)-Catechine	19.7	32±0.169		115.4±0.292	
(-)-Epicatechine	32.3	58.6±0.365		29.7±0.438	
(-)-Gallocatechine	9.1	43.7±0.204		174.5±0.432	
Kaempferol	57.5	not found		13.2±0.373	
Quercetin	53.9	not found		7.3±0.279	3.9±0.274
Rutin	50.6	not found		2.6±0.392	
Resveratrol	51.8	not found		1.47±0.323	
Protocatechuic acid	14.4		12.8±0.219		14.5±0.396
Gallic acid	9.2		26.7±0.288		21.8±0.287
O-coumaric acid	37.7		not found		traces
Caffeic acid	25.1		not found		7.4±0.357
Syringic acid	29.8		not found		traces

epicatechine than the white wine Rkatsiteli. Of flavonols (Table), in red wine Saperavi (fraction X3) were found kaempferol (13.2 mg/l), quercetin (11.2 mg/l) and rutin (2.6 mg/l), and in white wine Rkatsiteli (fraction X1), these compounds are absent.It is necessary to note that a certain amount (3.9 mg/l) of quercetin was revealed in fraction X4 of red wine Saperavi.

The white wine Rkatsiteli (fraction X1) does not contain resveratrol, while in red wine Saperavi (fraction X3) its amount is equal to1.47 mg/l. Of hydroxybenzoic acids (Table), in white wine Rkatsiteli (fraction X2) the protocatechuic acid and gallic acid were not found, while in red wine Saperavi (fraction X4) their amount is respectively equal to 14.5 mg/l and 21.8 mg/l. Of hydroxycinnamic acids (Table), in red wine Saperavi (fraction X4) the caffeic acid in the amount of 7.4 mg/l, o-coumaric acid and syringic acid as traces were found . These acids were not found in the white wine Rkatsiteli (fraction X2). Thus, in qualitative composition and the quantitative contents of phenolic compounds, the red wine Saperavi considerably surpasses the white wine Rkatsiteli. Exclusive interest attaches to a comparison of the quantitative contents of phenolic compounds of wines from grapes of white Rkatsiteli and red Saperavi, and wines prepared in the various countries. In particular, in the French white wines the quantitative contents of (+)-catechine and (-)-epicatechine on the average makes 9.8 mg/l and 5.3 mg/l, respectively, while in the French red wines the quantitative contents of (+)-catechine changes within the limits of 22.1-130.7 mg/l, and the quantitative contentsof (-)-epicatechine changes within the limits of 7.8-39.1 mg/l [7]. In wines prepared from red varieties of grapes (Tempranillo, Graciano, Cabernet, Merlot), cultivated in Spain, (+)-catechine content is equal to 16.01, 32.78, 41.76 and 27.09 mg/l, respectively [8], whereas the red wine Saperavi contains this compound in the amount of 115.4 mg/l (Table). The red wine Saperavi contains 11.2 mg/l of quercetin, whereas, in the above-mentioned red wines, the contents of this compound re-

spectively is equal to 1.88, 6.90, 5.00 and 4.67 mg/l. Red wine Saperavi contains 1.47 mg/l of resveratrol (Table), red wines Tempranillo, Graciano and Merlot contain this compound respectively in the amount of 0.73, 1.36 and 0.21 mg/l, and in red wine Cabernet it is detected as traces. Red wine Saperavi contains gallic acid and protocatechuic acid in amounts of 21.8 mg/l and 14.5 mg/l (Table), while in red wines of grapes Tempranillo, Graciano, Cabernet and Merlot the contents of these acids respectively varies in the limits of 12.20 - 14.5 mg/l and 0.81 - 1.52 mg/l. It is interesting that in red wine Saperavi, syringic acid was found as traces, however, in the above-cited Spanish four red wines this compound was found in the amount of 2.60 - 5.76 mg/l. According to our data, in white wine Rkatsiteli (the harvest of 2010), kaempferol, quercetin and rutin were not found (Table), however, in a commercial wine from grapes of the variety Chardonel cultivated in China (the harvest of 2005), these compounds were identified in the amount of 0.01, 0.06 and 0.17 mg/l, respectively. In commercial wine from the same variety of grapes, from the 2004 harvest, kaempferol was not found, however the contents of quercetin and rutin were equal to 0.25 mg/l and 0.40 mg/l, respectively [9]. Also it is interesting to compare the quantitative contents of flavonols of wine from grapes of Saperavi (the harvest of 2010) and of commercial wines from 5 varieties of red grapes cultivated in China [9]. Red wine Saperavi contains kaempferol 13.2 mg/l, quercetin 7.3 mg/l and rutin 2.6 mg/l (Table), however, in commercial red wine from grapes of varieties Cabernet Souvignon, Cabernet Franc, Merlot, Marselan and Petit Verdot, cultivated in China (the harvest of 2005), these compounds were identified in the amount of 0.01-0.04 mg/L., 0.2-0.94 mg/l and 0.49-0.72 mg/l, respectively. Apparently, the qualitative composition and the quantitative contents of phenolic compounds in wines are influenced by the variety of grapes and the geographical environment.

Conclusion. In this paper we have shown that the wines from the Georgian autochthonous grapes, white Rkatsiteli and red Saperavi, prepared by Georgian (Kakhetian) technology, in kvevri, contain biologically active phenolic compounds in abundance: catechines, flavonols, hydroxybenzoic acids hydroxycinnamic acids also are the best medical and preventive means.

ბიოქიმია

საქართველოს ავტოქტონური ვაზის ჯიშების რქაწითელის და საფერავის ყურძნიდან ქართული (კახური) წესით დაყენებული ღვინის ფენოლური ნაერთები

ა. შალაშვილი*, დ. უგრეხელიძე**, თ. მითაიშვილი*, ი. თარგამაძე*, ნ. ზამბახიძე*

* საქართველოს აგრარული უნივერსიტეტის ს. დურმიშიძის ბიოქიმიისა და ბიოტექნოლოგიის ინსტიტუტი, თბილისი
** აკადემიის წევრი, საქართველოს მეცნიერებათა ეროვნული აკადემია, თბილისი

შესწავლილია საქართველოს ავტოქტონური ვაზის ჯიშების თეთრი რქაწითელისა და წითელი საფერავის ყურძნიდან კახური წესით ქვევრში დაყენებული ღვინიების ფენოლური ნაერთების თვისებრივი შედგენილობა და რაოდენობრივი შემცველობა. რქაწითელის ყურძნიდან დაყენებულ ღვინოში იდენტიფიცირებულია: (+)-კატექინი (32.6 მგ/ლ), (-)-ეპიკატექინი (58.6 მგ/ლ), (-)-გალოკატექინი (43.7 მგ/ლ), პროტოკატექინმჟავა (12.8 მგ/ლ) და გალმჟავა (26.7 მგ/ლ); საფერავის ყურძნიდან დაშაქებულ ღვინოში - (+)-კატექინი (115.4 მგ/ლ), (-)-ეპიკატექინი (29.5 მგ/ლ), (-)-გალოკატექინი (174.4 მგ/ლ), კემპფეროლი (13.2 მგ/ლ), კვერცეტინი (11.2 მგ/ლ), რუტინი (2.6 მგ/ლ), რესვერატროლი (1.47), პროტოკატექინმჟავა (14.5 მგ/ლ), გალმჟავა (21.8 მგ/ლ) და ყავამჟავა (7.4 მგ/ლ).

REFERENCES

1. *C. Martin, E. Butelli, K. Petroni, Ch. Tonelli* (2011), Plant Cell, **23,** 5: 1685.
2. *J.M. Lopez-Nicolas, F. Garcia-Carmona* (2010), In: Fruit and Vegetable Phytochemicals: Chemistry, Nutritional Value and Stability. Eds. L. A. de la Rosa, E. Alvarez-Parrilla, G. A. Gonzalez-Aguilar. John Wiley & Sons.
3. *F. Shahidi, M. Naczk* (2004), Phenolics in Food and Nutraceuticals. Boca Raton, Florida, USA.
4. *A. Shalashvili, D. Ugrekhelidze, I. Targamadze, N. Zambakhidze, L. Tsereteli* (2011), Journal of Food Science and Engineering, **1**, 5: 361-365. Illinois, USA.
5. *V.L. Singleton, J.A. Rossi, Jr* (1965), Am. J. Enol. Vitic., 16:144-158.
6. *I.G. Roussis, I. Lambropoulos, K. Souliti* (2005), Food Technol. Biotechnol., **43,** 4: 351-358.
7. *S. Carando, P.L. Teissedre, L. Pascual-Martinez, J.C. Cabanis* (1999), J. Agric. Food Chem., **47,** 10: 4161-4166.
8. *M. Monagas, R. Suarez, C. Gomez-Cordoves, B. Bartolome* (2005), Am. J. Enol. Vitic., **56**, 2:139-147.
9. *F. Favg, J.M. Li, P. Zhang, Ke Tang, W. Wang, O.H. Pan, W.D. Huang* (2008), Food Research International, **41**, 1: 53.

Received August, 2012

საქართველოს მეცნიერებათა ეროვნული აკადემიის მოამბე, ტ. 6, №3, 2012
BULLETIN OF THE GEORGIAN NATIONAL ACADEMY OF SCIENCES, vol. 6, no. 3, 2012

Human and Animal Physiology

Some Effects of Mustard Oil and Cinnamaldehyde on Spinal Neuronal Responses to Cutaneous Stimuli in Male Rats

Merab G. Tsagareli[*], Austin W. Merrill[**], Nana Tsiklauri[*], Mirela Iodi Carstens[**], Ivliane Nozadze[*], Gulnaz Gurtskaia[*], Elene Abzianidze[§], Earl E. Carstens[**]

[*] *Dept of Neurophysiology, Ivane Beritashvili Experimental Biomedicine Center, Tbilisi*
[**] *Section of Neurobiology, Physiology and Behavior, University of California, Davis, CA, USA*
[§] *Department of Molecular and Medical Genetics, Tbilisi State Medical University, Tbilisi*

(Presented by Academy Member Tengiz Oniani)

ABSTRACT. Transient receptor potential (TRP) channels are being ardently pursued as targets for pain therapies. They play an important role in transducing thermal, mechanical and chemical stimuli for somatic sensation. Several TRP channels exhibit sensitivity to increases or decreases in temperature as well as chemical ligands that elicit similar thermal or painful sensations; these include mustard oil, cinnamaldehyde from cinnamon, menthol from mint, gingerol, camphor, capsaicin from chili peppers, eugenol from cloves, and others.

Mustard oil [allyl isothiocyanate (AITC)] and cinnamaldehyde (CA), agonists of the ion channel TRPA1 expressed in sensory neurons, elicit a burning sensation and heat hyperalgesia. In this work, we tested whether these phenomena are reflected in the responses of lumbar spinal wide-dynamic range (WDR) neurons recorded in anesthetized male rats. Responses to electrical and graded mechanical and noxious thermal stimulation were tested before and after cutaneous application of AITC or CA. Repetitive application of AITC initially increased the firing rate of 52% of units followed by rapid desensitization that persisted when AITC was reapplied 30 min later. Responses to noxious thermal, but not mechanical, stimuli were significantly enhanced irrespective of whether the neuron was directly activated by AITC. These findings indicate that AITC produced central inhibition and peripheral sensitization of heat nociceptors. CA did not directly excite WDR neurons, and significantly enhanced responses to noxious heat while not affecting responses to skin cooling or mechanical stimulation, indicating a peripheral sensitization of heat nociceptors.

Overall, the presented data with our behavioral results support the idea that thermo-sensitive TRPA1 channel represents a promising target for the development of analgesic drugs in relief of pain. *© 2012 Bull. Georg. Natl. Acad. Sci.*

Key words: *desensitization, dorsal horn, nociception, noxious heat, skin cooling, sensitization, spinal cord.*

The transient receptor (TRP) cation channels have been among the most intensively pursued drug targets for pain relief over the past few years. Pioneering research in the field of pain has established that a subset of TRP channels which are activated by temperatures (the so-called thermoTRP channels) are capable of initiating sensory nerve impulses following the detection of thermal and chemical stimuli [1-3]. Although pain is currently the most advanced TRP channel-related field, an increasing number of gene deletion studies in animals and genetic association investigations in humans have demonstrated that the pathophysiological roles of TRP channels extend well beyond the sensory nervous system [4].

The TRP cation channel superfamily is a diverse family of 28 cation channels that have varied physiological functions, including thermal sensation, chemo- and mechanosensation, magnesium and iron transport. Several TRP channels exhibit sensitivity to increases or decreases in temperature as well as chemical ligands that elicit similar thermal or painful sensations; these include mustard oil, cinnamaldehyde from cinnamon, menthol from mint, gingerol, camphor, capsaicin from chili pepper, eugenol from cloves, and others. The TRPA subfamily has only one known member (TRPA1) and its name refers to unusually high number of ankyrin repeats at the amino terminus of the channel protein [3-5].

It is known that mustard oil [allyl isothiocyanate (AITC)] and cinnamic aldehyde (CA) are agonists of the TRPA1 channel [6-8]. When applied to skin, they elicit burning pain, thermal hyperalgesia, and mechanical allodynia [9]. In the oral or nasal mucosa, AITC and CA elicit burning irritation that decreases (desensitizes) across trials of repeated application [10-12]. Lingual application of AITC or CA excites neurons in the trigeminal subnucleus caudalis (Vc) [13-15]. AITC excitation of Vc neurons exhibits a desensitizing temporal pattern while sensitizing responses to noxious heat [14].

Here we tested whether spinal wide-dynamic range (WDR) type dorsal horn neuronal responses to repeated cutaneous application of AITC or CA similarly exhibit a desensitizing pattern and whether their responses to mechanical and noxious thermal stimuli are enhanced after application of these chemicals, consistent with human psychophysical observations [9,11,12]. We presently focused on WDR neurons for two reasons. First, WDR neurons respond to innocuous mechanical as well as noxious thermal stimuli, allowing assessment of the effects of AITC and CA on both types of responses within the same neuronal population, which would not be possible with nociceptive-specific (NS) neurons. Second, available evidence indicates that WDR neurons are sufficient for pain perception and they are well suited to encode the intensity of noxious heat [16].

Methods

Animals and Surgery. Adult male Sprague–Dawley rats (450-600 g) were used. The experimental protocol was approved by the UC Davis Animal Use and Care Committee. Rats were housed in a room with controlled temperature (22±1°C) and lighting with unrestricted access to food and water.

Rats were anesthetized with sodium pentobarbital (65 mg/kg, intraperitoneal injection). A tracheostomy tube was implanted, the jugular vein or lateral tail vein was cannulated with PE-50 tubing for maintenance of pentobarbital anesthesia. Core body temperature was monitored rectally using a BAT-12 thermometer (Physitemp, Clifton, NJ) and maintained at 37±0.2°C with a lamp and heating pad. During recording, anesthesia was maintained by intravenous (iv) pentobarbital pump infusion. The L6–S1 intervertebral space was identified by palpation of the spinous processes and the posterior superior iliac spine, and a midline skin incision was made from approximately L6 to T11 spinous processes. The paraspinous muscles were dissected free from the L2–T12 spinous processes on both sides, and the transverse processes were exposed by scraping off attached connective tissue. L1 and T13 spinous processes were cut and

removed, and a bilateral laminectomy was performed at both levels under a dissection microscope. The dura was removed and warm agar was poured over the spinal cord. Vertebral clamps on the transverse processes of T12 and L2 were used to stabilize the animal in a stereotaxic frame (Kopf Instruments, Tujunga, CA). Needle electrodes were placed in both forelimbs to monitor electrocardiographic (ECG) activity. In 21 rats the sciatic nerve was exposed for electrical stimulation. A 3.5-cm midline incision was made in the postero-lateral upper hindlimb at the level of the biceps femoris muscle. The semitendinosus and biceps femoris muscles were separated using blunt dissection techniques and the semimembranosus muscle was reflected with fine forceps and microscissors. The left sciatic nerve was isolated above the bifurcation of the tibial and common peroneal nerve and a strip of paraffin wax was wrapped beneath the nerve. After placement in the stereotaxic frame, the sciatic nerve was positioned onto a hooked parallel bipolar electrode (FHC, Bowdoinham, ME) and bathed in warmed mineral oil intestinal lubricant. During trials with electrical stimulation a neuromuscular blocker (pancuronium, 0.1 mg iv) was administered and the animal was ventilated using a positive-pressure pump (Harvard Apparatus, Holliston, MA). End-tidal CO_2 was monitored by a Datex 254 gas analyzer (Datex-Ohmeda, Tewksbury, MA) and maintained between 3.0 and 4.0% by adjustment of tidal volume and/or respiratory rate.

Stimulation and recording. An 8-11-MΩ Teflon-coated tungsten microelectrode (FHC) was advanced into the dorsal horn of the spinal cord using a hydraulic microdrive to record single-unit activity of dorsal horn neurons. Units isolated for study were always at depths <1 mm. Action potentials were amplified and displayed by conventional means, and sent to a computer for storage and analysis using a Powerlab interface and Chart 5.0 software (AD Instruments, Oxford, UK).

Single units were searched for and isolated using innocuous mechanical stimulation of the plantar surface of the ipsilateral hindpaw. Units were chosen with receptive field areas on the plantar surface of the toes, corresponding to approximately L5 spinal cord. Only units that responded to graded non-noxious (brushing, 4–12 g von Frey) and noxious (76 g von Frey, pinch) mechanical and noxious thermal (42, 46, and 50°C) stimuli were considered for further study (WDR neurons). For mechanical stimulation, a series of graded von Frey filaments (4, 12, and 76 g) were applied in ascending order. Each stimulus was applied for 10 s at a 1.5-min interstimulus interval to the center of the receptive field.

Thermal stimuli were delivered to the center of the receptive field using a Peltier device (Physitemp NTE-2A) mounted to a micromanipulator. The thermode temperature was controlled by computer, and stimuli were delivered at a rate of about 12.5°C/s from an adapting temperature of 35°C with an accuracy of ±0.1°C. In the initial studies with AITC (n=27 rats), 46°C and 50°C stimuli were used, whereas in later studies with CA (n=14 rats), 42, 46, and 50°C stimuli were used. In several experiments, a cooling stimulus (from 35°C to 10°C over a 30 sec period) was also delivered.

Chemical application. Ten minutes after completion of the mechanical and thermal (and electrical, if included) stimulation series, 60 s of baseline activity was recorded before application of either AITC, CA, or mineral oil (vehicle control). AITC (allyl isothiocyanate; 2 µl, 75% in mineral oil; Fluka, St. Louis, MO), cinnamaldehyde (CA; in mineral oil; Sigma–Aldrich), or mineral oil was then topically applied to the center of the receptive field area at 1 min intervals for 10 min using a Hamilton microsyringe attached to PE-50 tubing. Eleven minutes after the last AITC or CA droplet was applied, the von Frey and thermal stimulation series were repeated. The thermal probe was replaced at the same hindpaw location using millimeter coordinates on the micromanipulator to which the thermal probe was mounted. Thermal stimulation was always initiated 2 min after

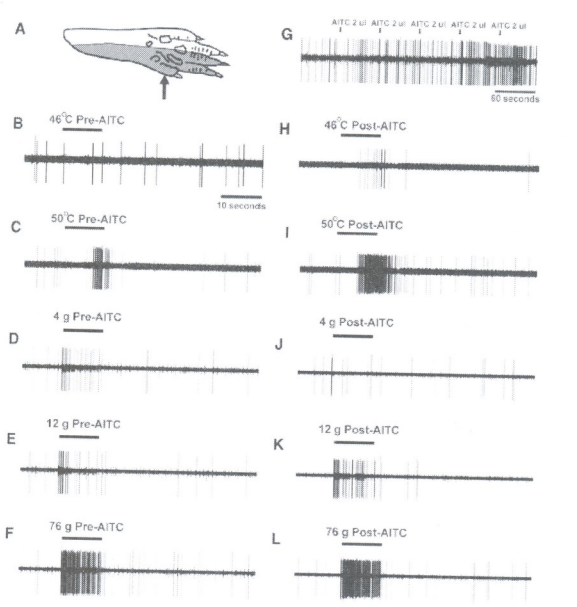

Fig. 1. Example of allyl isothiocyanate (AITC) sensitive lumbar spinal wide dynamic range (WDR) neuron. *A*: shaded area shows extent of mechano-sensitive receptive field on lateral hindpaw. Arrow: site of AITC application. *B* and *C*: raw spike traces of response to 46°C and 50°C heat stimuli before AITC application. *D–F*: responses to graded mechanical stimulation at indicated von Frey bending forces. *G*: spike trace of activity during repeated application of AITC (75%, 2 µl droplets) at 1 min intervals (arrows). *H–L*: spike traces of responses to graded noxious heat (*H, I*) and mechanical stimulation (*J–L*) after sequential application of AITC.

replacement of the thermal probe. Application of AITC or CA was repeated after a 10 min wait period. Thus, 30 min had passed between the last AITC or CA application of trial 1 and the first AITC or CA application of trial 2. On completion of the experiment the animal was killed by overdose of pentobarbital, administered intravenously.

In 14 experiments electrical stimulation of the sciatic nerve was performed. In these plus an additional 5 experiments, the hindpaw receptive field was also stimulated electrically by percutaneous needle electrodes. Constant-current stimulus trains of 16 pulses (0.7 ms duration) at 1 Hz were delivered with an S48 stimulator (Grass, West Warwick, RI). We presently

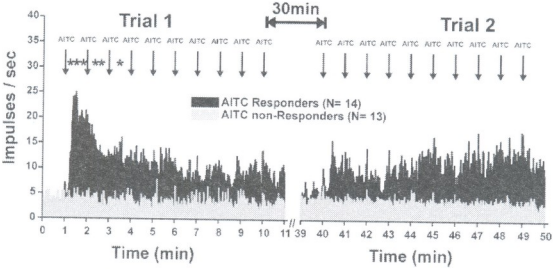

Fig. 2. Desensitization of responses to repeated application of AITC. Shown are averaged peristimulus time histograms (PSTHs, 1-s bin width) of unit firing during repeated application of AITC (75%, 2 µl droplets) at 1-min intervals (arrows) for 10 min to the center of the receptive field area on the ipsilateral hindpaw. Black PSTHs: 14 WDR units that exhibited increased firing during the initial applicatıon of AITC. Gray PSTHs: 13 units unresponsive to AITC. Error bars are omitted for clarity. Left-hand PSTHs: responses to the first trial of sequential AITC application. Right-hand PSTHs: responses to second trial of sequential AITC application starting 30 min after the end of the first trial. *, **, ***: significantly different compared with the initial 60 s baseline period before the first application of AITC ($P<0.05$, $P<0.005$, $P<0.0005$, respectively).

counted all C-fiber and after-discharge activity occurring in the 100- to 1,000 ms latency period. The stimulus intensity was adjusted for each unit to be threefold that of the C-fiber threshold.

Data analysis. The spontaneous firing rate was calculated as the sum of the total number of action potentials that occurred for 30 or 60 s before each stimulus. Responses to von Frey and thermal stimuli were quantified by summing the total number of action potentials recorded during the 10 s stimulus period, and subtracting the spontaneous firing rate per 10 s (30 s total/3). The after-discharge was quantified as the total number of action potentials during the 30 s after the offset of the stimulus. Spontaneous firing, evoked responses, and after-discharge to each mechanical and thermal stimulus were compared pre- versus post-treatment for each treatment group (AITC, CA, and mineral oil) using paired *t*-test. Responses to AITC, CA, and mineral oil were quantified by summing the total spikes during the 60 s interval after each application. Each sum was compared with the sum of the total spikes during the 60 s preceding the first application (baseline) using univariate ANOVA with post hoc Dunnett's two-sided *t*-test. A P value of <0.05 was taken to be significant. Statistical analyses were performed using SPSS 9.0 software. All data are means ±SE unless otherwise noted.

Results

Response to AITC application. In the first series of experiments, 27 units were tested for responses to repeated application of AITC and 14 (52%) responded. The example in Fig. 1*G* shows a buildup of firing to the initial AITC stimuli. The mean responses are shown in Fig. 2 for units excited by repeated application of AITC [Fig. 2, left, black peristimulus time histograms (PSTHs)] and for those unaffected by AITC (gray PSTH). For the responsive units, the mean firing rate during the first three stimulus applications was significantly greater compared with pre-AITC baseline but then declined to a level that was not significantly different from baseline (Fig. 2, left). After a 30-min rest period, AITC

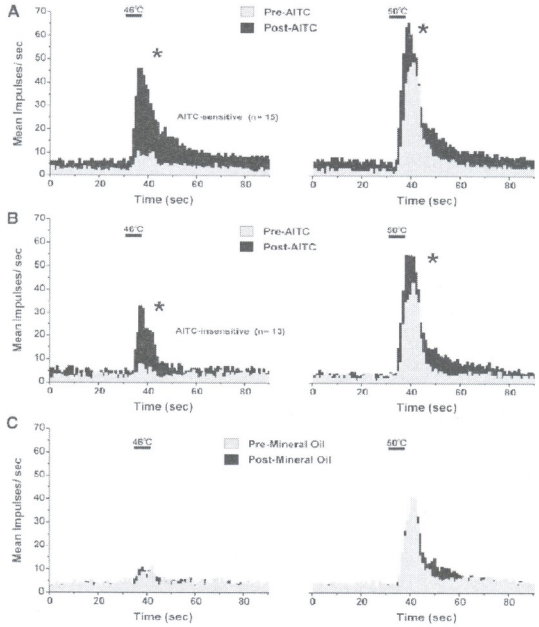

Fig. 3. AITC sensitization of WDR responses to noxious heat stimulation. *A*: responses to 46°C and 50°C heat stimuli, before (gray PSTHs) and 11 min after the end of sequential application of AITC (black PSTHs) for AITC-sensitive WDR units. Pre and post-AITC responses are aligned to the heat stimulus (indicated by horizontal bars). Error bars omitted for clarity. *: post-AITC response significantly different from pre-AITC ($P<0.05$). *B*: format as in *A* for 13 AITC-insensitive WDR units. *C*: format as in *A* for 10 separate WDR units receiving sequential application of mineral oil (vehicle control).

was reapplied in the same manner. Although there was a trend toward an increased firing rate, this did not reach statistical significance relative to pre-AITC baseline (Fig. 2, right).

All units were tested for responses to graded (46°C and 50°C) heat before and after AITC. Figure 1 shows one unit's responses before AITC (Fig. 1, B and C) and their marked enhancement post-AITC (Fig. 1, *H* and *I*). Figure 3*A* shows averaged responses to heat stimuli before (gray PSTHs) and after AITC (black PSTHs) for units that were directly activated by AITC. Responses to both 46 and 50°C were sig-

nificantly enhanced post-AITC. Units unresponsive to AITC similarly exhibited a significant enhancement of heat-evoked responses post-AITC (Fig. 3B). Vehicle (mineral oil) application had no effect on heat-evoked responses in a separate group of 10 units (Fig. 3C).

The WDR units typically exhibited graded responses to increasing bending forces of punctate von Frey stimuli (Fig. 1, D–F), which were minimally affected post-AITC (Fig. 1, J–L). Figure 4 shows averaged responses to graded mechanical stimuli before (gray PSTHs) and about 11 min after AITC (black PSTHs), for AITC-sensitive (Fig. 4A) and AITC-insensitive units (Fig. 4B). There were no significant differences in responses pre-versus post-AITC. Similarly, responses pre- and post-vehicle (mineral oil) application were not significantly different (Fig. 4C). Finally, responses of units to low-threshold brushing of skin in the center of the mechano-sensitive receptive field with cotton were not significantly different pre-versus post-AITC application.

Response to CA application

In a separate group of 14 units, repeated application of CA did not significantly affect any unit's firing rate. Similar to AITC, responses to graded noxious heating were significantly enhanced post-CA applications. Figure 5 shows an individual example (compare A–C with D–F), and Fig. 6A shows averaged responses that are overlaid to emphasize the progressive increase after the first (light gray PSTHs; post-CA 1) and second applications of CA (black PSTHs; post-CA 2) compared with pre-CA (dark gray PSTH). Mean responses after both the first and second trials of CA application were significantly different from pre-CA at each stimulus temperature (paired *t*-test, $P<0.05$).

At the same time, Figure 5 shows a typical example in which responses to graded von Frey stimuli were similar before (Fig. 5, G–I) and after CA (Fig. 5, J–L). Figure 6B shows averaged rs sponses to graded von Frey stimuli with no significant change after the first or second application of CA compared with pre-CA.

Discussion

A main finding of this study is that both AITC and CA sensitized dorsal horn WDR neuronal responses to noxious heat while not significantly affecting their responses to other stimuli. This heat sensitization was observed irrespective of whether the AITC or CA directly excited the neuron. Furthermore, electrically evoked responses of the WDR units were either unaffected, or reduced, after application of the irritant to the skin. These data therefore support a peripheral site of heat sensitization by the TRPA1 agonists and argue against a central sensitizing action.

Roughly, 50% of WDR dorsal horn units responded directly to topical application of AITC with an initial increase in firing that desensitized over a 3-min period despite continued application of AITC. A previous study reported a similar fraction (53%) of mainly WDR dorsal horn neurons to be directly activated by 4% AITC applied adjacent to the mechanosensitive receptive field in decerebrate spinalized rats [17]. The desensitizing response pattern observed presently was similar to that of responses of neurons in trigeminal subnucleus caudalis (Vc) to lingual application of AITC [14-15], as well as the desensitizing temporal pattern of irritancy ratings elicited by lingual AITC in humans [12]. The lack of response of the other half of the WDR units to topical AITC suggests that our application strategy using a high concentration (75%) and low volume (2 µl) did not have non-specific excitatory or toxic effects. On reapplication, AITC did not evoke a significant increase in WDR neuronal firing, consistent with self-desensitization reported for AITC irritancy on the tongue that lasts >10 min in humans [12]. However, Vc neurons overcome AITC self-desensitization more quickly [14], possibly due to a more rapid clearance rate in the oral mucosa compared with hindpaw skin. Consistent with this, it was shown that a 10-fold higher concentration of capsaicin is required on facial skin versus

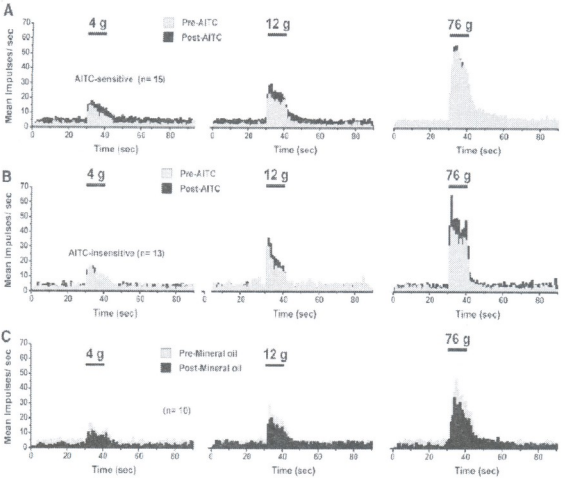

Fig. 4. Averaged responses to mechanical stimuli after application of AITC or mineral oil (control) to the receptive field area. *A*: averaged PSTHs of responses of AITC-sensitive neurons to stimulation with von Frey filaments with bending forces of 4, 12, and 76 g stimuli, from left to right, pre- (gray PSTHs) and 10-min post application of AITC (black PSTHs). Error bars omitted for clarity. *B*: format as in *A* for mechanically evoked responses of AITC-insensitive neurons pre- and post-AITC application. *C*: format as in *A* for mechanically evoked responses of 10 different WDR neurons pre- and post application of mineral oil (vehicle control).

tongue to elicit equivalent burning sensations and that the time course of desensitization was much slower on the face than on the tongue [18].

The mechanism underlying AITC self-desensitization could involve a peripheral or central site of action. Peripherally, repeated application of AITC may lead to desensitization of TRPA1 expressed in nociceptive endings. AITC self-desensitization was recently reported to occur by a calcium- and calcineurin-independent mechanism in an *in vitro* assay of peptide release from skin–nerve biopsies [19]. Alternatively, central inhibition might contribute to the reduced response of WDR neurons to repeated application of AITC. However, such a proposed central inhibition was insufficient to prevent AITC and CA enhancement of WDR neuronal responses to noxious heat.

CA did not directly excite the WDR units recorded presently, whereas lingual application of CA readily excited Vc neurons [15], presumably due to the lower diffusion barrier presented by the lingual epithelium compared with hindpaw skin. It is likely that the amount of CA that reached the sensory nerve endings in the hindpaw epithelium was insufficient to elicit action potentials, although it was sufficient to induce heat sensitization, presumably

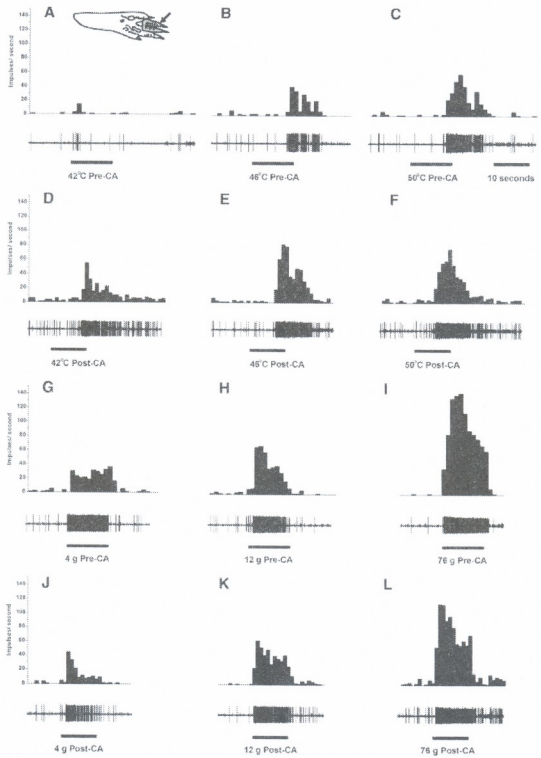

Fig. 5. Example of cinnamaldehyde (CA) heat sensitization of individual WDR neuron. A–C: spike traces (*bottom*) and PSTHs (1-s bin width) above, of responses to 42°C (A), 46°C (B), and 50°C (C) before CA. Inset in *A* shows receptive field on toes 3 and 4. Arrow: site of CA application. D–F: responses to same series of graded noxious heat stimuli post-CA. G–I: responses to graded mechanical von Frey stimuli: 4 g (G), 12 g (H), and 76 g (I), respectively, pre-CA. J–L: responses to graded mechanical von Frey stimuli post-CA.

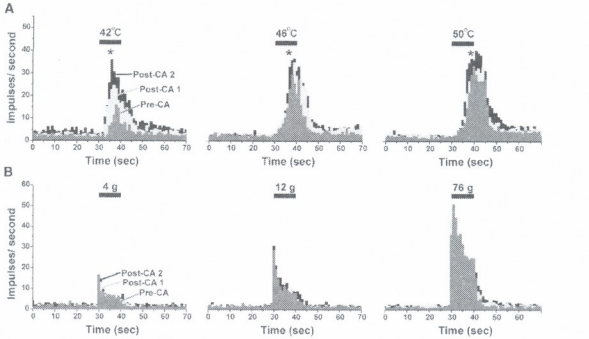

Fig. 6. CA sensitization of WDR responses to noxious heat but not mechanical stimuli. *A*: averaged PSTHs of responses of 13 units to 42°C (*left*), 46°C (*middle*), and 50°C (*right*) heat stimuli (black bars), before (dark gray PSTH) and after the first (post-CA 1; light gray PSTH) and second (post-CA 2; black PSTH) application of CA. Error bars omitted for clarity. *: significant difference between pre-CA and both post-CA 1 and post-CA 2 ($P<0.05$). *B*: averaged PSTHs of same units in *A* to 4 g (*left*), 12 g (*middle*), and 76 g (*right*) mechanical stimuli (black bars), before and after CA (format as in *A*).

by the same peripheral mechanism as suggested for AITC. In contrast, AITC strongly excited about 50% of WDR cells, with a resultant depression of electrically evoked neuronal responses presumably by activation of spinal inhibitory circuits by the stronger afferent drive.

Furthermore, AITC sensitized WDR neuronal responses to noxious heat, irrespective of whether AITC directly activated the unit. CA also sensitized responses to heat even though it did not directly excite WDR units. Previous studies of WDR neurons in lamina V of mice, reported significant enhancement of neuronal responses to 40°C (but not 45°C or 49°C) [20,21], and a significant enhancement of after-discharge responses to 41°C and 45°C [22] after application of AITC (10%, 60 µl) to the hindpaw. Lamina I nociceptive-specific (NS) neuronal responses to heat were also enhanced post-AITC [20,21]. Our results are generally consistent, in that AITC more strongly enhanced rat WDR neuronal responses to the lower stimulus temperatures (42°C and 46°C) compared with the highest (50°C). Two previous studies reported no change in noxious heat-evoked responses of rat and mouse WDR neurons after AITC (50 or 100%) was applied adjacent to the receptive field [23-24]. AITC sensitizes responses of mechanoheat- sensitive C-fiber afferents to noxious heating [25]. Because AITC did not enhance WDR neuronal responses to mechanical or electrical C-fiber stimuli, the most parsimonious explanation is that AITC applied within the cutaneous receptive field sensitized peripheral nociceptors to result in primary hyperalgesia. TRPA1 is coexpressed with the heat-sensitive channel TRPV1 in primary sensory neurons [26], so AITC enhancement of nociceptor responses to noxious heat might involve a cellular mechanism by which activation of TRPA1 enhances the thermal sensitivity of TRPV1. Another possibility is that AITC causes release of inflammatory mediators that in turn lower the thermal activation threshold of TRPV1 [27,28], resulting in

the observed enhancement of responses, particularly to 42°C and 46°C.

Neither AITC nor CA affected WDR neuronal responses to graded pressure or light brushing of the mechanosensitive receptive field. This is partially consistent with recent studies showing that AITC significantly enhanced murine deep dorsal horn WDR neuronal responses to only the weakest mechanical stimulus while having no significant effect on responses to stronger stimuli [21]. However, other studies have shown significant enhancement of neuronal responses to innocuous mechanical stimuli, and expansion of receptive fields, in rats and mice after application of AITC adjacent to the mechano-sensitive receptive field of spinal WDR or NS neurons [17,23,24,29]. Such enhancement was seen in decerebrate spinalized rats [17], although another study reported the AITC-induced mechanical enhancement to be significantly attenuated in spinalized rats [23], implicating involvement of descending facilitatory pathways. The present lack of effect of AITC or CA on mechanically evoked responses of WDR neurons indicates that our method of intermittent application of small (2 μl) volumes of these agents did not produce sufficient afferent drive to engage segmental or suprasegmental pronociceptive networks.

Our recent behavioral investigations showed that unilateral intraplantar injection of CA (5–20%) induced a significant, concentration-dependent reduction in latency for ipsilateral paw withdrawal from a noxious heat stimulus in mail rats (heat hyperalgesia). The highest dose of CA also significantly reduced the contralateral paw withdrawal latency. CA significantly reduced mechanical withdrawal thresholds of the injected paw (mechanical allodynia) and was more profound, with no effect contralaterally. Bilateral intraplantar injections of CA resulted in a significant cold hyperalgesia (cold plate test) and a weak enhancement of innocuous cold avoidance (thermal preference test) [30,31]. These results support a role for TRPA1 in cold detection, as the TRPA1 agonist CA enhanced cold sensitivity in two behavioral assays [32].

However, these behavioral findings are inconsistent with presented here electrophysiological data showing that neither CA nor AITC had any significant effect on mechanical sensitivity of spinal WDR neurons. The mismatch between our behavioral observation of a CA-induced increase in mechanosensitivity and lack of CA effect on neuronal mechanosensitivity may involve the route of administration of this substance [30-32].

Acknowledgements. This study was supported by grants from Shota Rustaveli National Science Foundation, Georgia (1/6-27), and National Institutes of Health (DE-13685 to E.C. and DE-13685-09S1 to M.T.).

ადამიანისა და ცხოველთა ფიზიოლოგია

მდოგვის ზეთისა და დარიჩინის ალდეჰიდის ზოგიერთი ეფექტი მაძრი ვირთაგვების ზურგის ტვინის ნეირონების პასუხებზე კანის გაღიზიანებისას

მ. ცაგარელი*, ო. მერილი**, ნ. წიკლაური*, მ. ი. კარსტენსი**, ი. ნოზაძე*, გ. ღურწკაია*, ე. აბზიანიძე#, ე. კარსტენსი**

* ფარე პატიაშვილის ექსპერიმენტული ბიომედიცინის ცენტრი, თბილისი
** კალიფორნიის უნივერსიტეტი, დევისი, აშშ
# მოლეკულური და სამედიცინო გენეტიკის დეპარტამენტი, თბილისის სახელმწიფო სამედიცინო უნივერსიტეტი

(წარმოდგენილია აკადემიკოს წერეთლის მიერ)

უკანასკნელი წლების გამოკვლევათა თანახმად გარდამავალ რეცეპტორულ პოტენციალთა (ვრპ- TRP) არხები მოიწვეთან ტკივილის სამკურნალო სამიზნეებად. ეს არხები მნიშვნელოვან როლს ახორციელებენ თერმული, მექანიკური და ქიმიური ტკივილის შეგრძნებების აღმოცენებაში. ზოგიერთი TRP არხი მგრძნობელობას ავლენს მაღალი ან დაბალი ტემპერატურის, ისევე როგორც რიგი ქიმიური ნივთიერებების მიმართ, რომლებიც აღძრავენ თერმულ ან ტკივილის შეგრძნებას. მათ მიეკუთვნები მდოგვის ზეთი, დარიჩინის ალდეჰიდი, პიპნის შემცველი მენთოლი, კაპსაიცინი (შეიცავს ცხარე წიწაკა), მიხაკის ზეთი და სხვა.

მდოგვის ზეთის შემცველი აქტიური ნივთიერება ალილ-იზოთიოციანატი (აითც) და დარიჩინის ალდეჰიდი (და) წარმოადგენენ TRPA1 იონური არხის აგონისტებს. ექსპერიმენტებიან რა სენსორულ ნეირონებში, ისინი იწვევენ მწველ შეგრძნებასა და სითბურ ჰიპერალგეზიას. წარმოდგენილ შრომაში ჩვენ შევისწავლეთ თუ როგორ აისახება ეს რეაქციები ზურგის ტვინის ე.წ. ფართო დიაპაზონის დინამიური (wide dynamic range-WDR) ნეირონების პასუხებზე მაძრ ვირთაგვებში. ელექტრული, ზრდადი მექანიკური და მტკივნეული სითბური სტიმულაციის შედეგად აღძოცენებული პასუხები შესწავლილ იქნა კანზე აითც-სა და და-ის მოქმედებამდე და მოქმედების შემდეგ. აითც-ის განმეორებითი აპლიკაცია თავდაპირველად იწვევდა ნეირონების განშტოცვა სიხშირის ზრდას, რომელსაც მოსდევდა სწრაფი დესენსიტიზაცია. ეს უკანასკნელი შენარჩუნებული იყო აითც-ის ზელაბალი აპლიკაციის შემდეგაც 30 წუთის ინტერვალით. პასუხები მტკივნეულ სითბურ, მაგრამ არა მექანიკურ სტიმულებზე სარწმუნოდ იყო გაზრდილი, მოუხედავად იმისა, იყო თუ არა ნეირონი პირდაპირ აქტივირებული აითც-ის ზემოქმედებით.

მიღებული შედეგები მიუთითებენ, რომ აითც იწვევს ცენტრალურ შეკავებას ზურგის ტვინის დონეზე და თერმული ნოციცეპტორების პერიფერიულ სენსიტიზაციას. დარიჩინის ალდეჰიდი არ იწვევს WDR ნეირონების უშუალო აგზნებას, თუმცა სარწმუნოდ ზრდის პასუხებს მტკივნეულ გაღიზიანებაზე. ამასთან ერთ არ რეაგირებს გაცივებასა და მექანიკურ სტიმულებზე. ეს უკანასკნელი ფაქტები მიუთითებენ სითბური ნოციცეპტორების პერიფერიულ სენსიტიზაციაზე.

ამრიგად, წარმოდგენილი მონაცემები, ჩვენი ქცევითი ექსპერიმენტების შედეგების გათვალისწინებით, ამყარებენ მოსაზრებას, რომ თერმო TRPA1 იონური არხი წარმოადგენს იმედის მომცემ პერიფერიულ სამიზნეს ახალი ტიპის ანალგეზიური პრეპარატების სინთეზისთვის.

REFERENCES

1. *M.M. Moran, M.A. McAlexander, T. Biro, A. Szallasi* (2011), Nature Rev. Drug Discov., **10**: 601-620.
2. *A. Patapoutian, S. Tate, C.J. Woolf* (2009), Nature Rev. Drug Discov., **8**: 55-68.
3. *A. Szallasi* (2010) In: Vanilloid Receptor TRPV1 in Drug Discovery. A. Gomtsyan & C.R. Faltynek (eds.), John Wiley & Sons, pp. 68-100.
4. *L.J. Wu, T.B. Sweet, D.E. Clapham* (2010), Pharmacol. Rev., **62**: 381-404.
5. *A.P. Christensen, D.P. Corey* (2007), Nature Rev. Neurosci., **8**: 510-21.
6. *M. Bandell, G.M. Story, S.W. Hwang, et al.* (2004), Neuron, **41**: 849-857.
7. *D.M. Bautista, S.E. Jordt, T. Nikai, et al.* (2006), Cell, **124**: 1269-1282.
8. *S.E. Jordt, D.M. Bautista, H.H. Chuang, et al.* (2004), Nature, **427**: 260-265.
9. *B. Namer, F. Seifert, H.O. Handwerker, C. Maihofner* (2005), Neuroreport, **16**: 955-959.
10. *G. Brand, L. Jacquot* (2002), Chem. Senses, **27**: 593-598.
11. *J. Prescott, N. Swain-Campbell* (2000), Chem. Senses, **27**: 593-598.
12. *C.T. Simons, M.I. Carstens, E. Carstens* (2003), Chem. Senses, **28**: 459-465.
13. *E. Carstens, T. Mitsuyo* (2005), Chem. Senses, Suppl., **1**: 203-204.
14. *C.T. Simons, S. Sudo, M. Sudo, E. Carstens* (2004), Pain, **110**: 64-71.
15. *K.L. Zanotto, A.W. Merrill, M.I. Carstens, E. Carstens* (2007) J. Neurophysiol., **97**: 966-978.
16. *W. Maixner, R. Dubner, M.C. Bushnell* (1986) Brain Res., **374**: 385-388.
17. *C.J. Woolf, A.E. King* (1990), J. Neurosci., **10**: 2717-2726.
18. *B.G. Green* (1998), Physiol. Behav., **65**: 517-523.
19. *N.B. Ruparel, A.M. Patwardhan, A.N. Akopian, K.M. Hargreaves* (2008), Pain, **135**: 271-279.
20. *W.A. Eckert, D. Julius, A.I. Basbaum* (2006), Pain, **126**: 184-197.
21. *J. Mazario, A.I. Basbaum* (2007), J. Neurosci., **27**: 762-770.
22. *W.J. Martin, Y. Cao, A.I. Basbaum* (2004), J. Neurophysiol. **91**: 1945-1954.
23. *A. Pertovaara* (1998), Exp. Neurol., **149**: 193-202.
24. *H.R. Weng, H. Mansikka, R. Winchurch, et al.* (2001), Anesthesiol., **94**: 1105-1112.
25. *P.W. Reeh, L. Kocher, S. Jung* (1986), Brain Res., **348**: 42-50.
26. *G.M. Story, A.M. Peier, A.J. Reeve, et al.* (2003), Cell, **112**: 819-829.
27. *H.H. Chuang, E.D. Prescott, H. Kong, et al.* (2001), Nature, **411**: 957-962.
28. *T. Sugiura, M. Tominaga, H. Katsuya, K. Mizumura* (2002), J. Neurophysiol., **88**: 544-548.
29. *C.J. Woolf, P. Shortland, L.G. Sivilotti* (1994), Pain, **58**: 141-155.
30. *M.G. Tsagareli, N. Tsiklauri, K.L. Zanotto, et al.* (2010), Neurosci. Letters, **473**: 233-236.
31. *M.G. Tsagareli* (2011), Neurophysiol., **43**: 309-320.
32. *E. Carstens, A. Klein, M.G. Tsagareli et al.* (2010), In: Reports of "The 9th Gagra Talks", International conference on fundamental questions of neuroscience Tbilisi, 13-16 October, 2010, p. 267-280.

Received June, 2012

Human and Animal Physiology

The Maximum Heart Rate as a Parameter of Sport-Age Functioning

Giorgi Zubitashvili

Ilia State University, Tbilisi

(Presented by Academy Member Nodar Kipshidze)

ABSTRACT. The maximum heart rate is the variable that is very important in determining the training quality as well as to avoiding unnecessary loading on the body. In spite of the known fact that heart rate depends on age, gender, sportive qualification, type of sport, load intensity and other environmental factors - it is still unknown exactly how much its value is affected by the factor of training. Aforementioned determined the research aim: to study the maximum heart rate value dependence on the age and training level on an example of different ages of judokas(8-20 year).

The maximum heart rate was measured by palpation during one minute. In order to achieve a maximum heart rate value in judokas developed fast durability test (fast throws) was used by the author, lasting for 100 seconds.

Quantitative heart rate data received after completing the test were depicted as minimum, average and maximum values ($p < 0.05$).

The study compared the data of untrained persons and judokas (20-22 years of age). It was found that on the one hand training factor somewhat increases this index and the difference makes 7.1 beats per minute. On the other hand, it is proved that the maximum heart rate is affected by the age factor, and therefore this index from 8 to 20-years of age decreases annually on average by1.2 beats (from 212 to 196).

The obtained results show that on the example of the heart rate the functional development for judokas extends well beyond the general biological characteristic regulations and makes standards specific for it. © *2012 Bull. Georg. Natl. Acad. Sci.*

Key words: *functional system, the limit of detection, biological determination, training factor.*

The heart rate is one of the best indicators for determining the naturalconditions of the body. In sports research practice it holds a special place in the evaluation of the training quality. Its precise definition is important not only because sportsman's body could get the maximum beneficial effect as a result of exercise, but also in order to eliminate unnecessary loading of the heart.

Taking into account the aforesaid, the sportsman necessarily needs to know what maximum value of heart rate he has. It should be noted that in general there is no precisely determined, optimal heart rate,

and according to one author [1] it depends on age, gender, qualification, type of sport, load intensity and other environmental factors.

The data obtained on this issue [2] confirm that the maximum heart rate primarily depends on age: it is higher in children than in adults and decreases linearly with age. Maximum heart rate of children under the age of 10 is often more than 210 beats, while for a 20-year-old man this value makes 195 beats per minute. Longitudinal studies show that after the adulthood age heart rate decreases by 1 - 0.5 units every year.

There are contradicting opinions about interrelations between the training level and maximum heart rate: the data obtained by a number of researchers [3-7] prove that the training and exercise factors do not cause the maximum heart rate reduction, and along with the physical training its value remains unchanged or slightly decreases.

Different data are provided by other authors' [8] survey results, according to which the maximum heart rate value really changes with the factor of training and its maximum value may change from 3 - to 7% as a result of aerobic exercise or detraining.

Review of this information shows that it is still not really determined precisely whether the maximum heart rate is affected by training factor. The aforesaid fact determined our goal.

The aim was to study maximum heart rate value dependence on the age and training level.

Objectives: 1. Registration of maximum heart rate in conditions of standard physical load on the example of judokas.

2. Review of maximum heart rate in different ages.

3. Determination of influence of training level factor on maximum heart rate. (Maximum heart rate value comparison between judokas and untrained persons).

Material and Methods

The study was conducted on 8-20 year old judokas. At least 60 judokas were recruited in each age group.

The maximum heart rate was measured by palpation for a minute. In order to achieve a maximum heart rate value in judokas use was made of a fast durability test developed by the author, when a person under experiment without resistance from a partner performed throws at maximum speed for 100 seconds.

Statistical Analysis. Data were processed by the computer program SPSS 19. The ANOVA test was used in order to determine the dependence of the

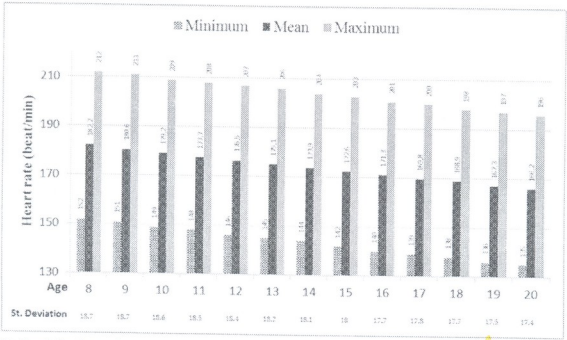

Fig. Descriptive data on the maximum heart rate of judokas.

maximum heart rate on age. Quantitative data are presented in the minimum, average and maximum values. Reliability level was $p < 0.05$.

Results and Discussion

The obtained results are presented in the Figure.

The data, presented in the Figure show that the maximum heart rate varies significantly at different ages after loading completion. From 8 - to 20-years of age the heart rate minimum values decrease from 152 - to 135, and the maximum values from 212 - to 196. In this age range percentage assessment of the minimum and maximum value dispersion shows the opposite picture: at the age of 8 the lower value is fixed - 39.5% (152 and 212) than at the age of 20 - 45.2% (135 and 196).

The average values of maximum heart rate in standard loading conditions clearly show an example of the highest functional shifts for the younger children, as far as the obtained values are less for each of the next age. During one minute after loading completion the determined maximum heart rate average value reaches 182.2 at the age of 8. This mark decreases by 16 units (up to 166.2) and 9.6% by 20-year-old age. This issue may be explained by the following circumstances: at teen age the initial heart rate value (at rest) is still quite high, and training levels are low and therefore despite performing even fewer throws compared with older age (at 8 years of age on average 30.2 throws; at 20 years on average 45.1 throws), which was expressed in less volume of performed work - the body gets more loaded.

In order to solve the issue, set in the third objective of the research, maximum heart rates were compared between untrained persons and judokas. Our data (20 years - 196 beats per minute) were compared with the results of study of one of the researchers, [8] conducted on untrained persons of 22 years of age (188.9 beats per minute). The comparison showed that the training factor in judo at the older age causes maximum heart rate increase by 7.1 units (3.8%).

In order to determine whether the data obtained by us corresponded to the already existing information on this question - obtained in our study by the continuous registration method results of maximum heart rate at the age of 20 (196 beats per minute) was compared to the data obtained in trained persons of the same age, [3], according to which the maximum heart rate amounts to the same value- 196 beat per minutes. On the one hand, this fact highlighted the tendency of maximum heart rate decrease together with the age increase (in our study 212 beats per minute were recorded in 8-year-old children), and on the other hand, in judokas of adult age (20 years) the specific result for maximum heart rate: 196 beats per minute.

The data obtained show that the maximum heart rate from 8 - to 20 years (during 13 years) reduces by 16 units (212-196), i.e. decreases in average by 1.2 units (16/13) each year. At the same time, according to the other author [2] the maximum heart rate from adult age decreases from1 to 0.5 units each year. Based on the comparison of these data with the results of our study show that the maximum heart rate reduction occurs not only in adults, but in youths as well, and here the process is characterized by relatively higher intensity.

Conclusions

The mean value of maximum heart rate from 8 to 20 years of age decreases by 16 units (182.2-166.2). This fact confirms that the value of this variable is especially affected by the age factor.

The maximum heart rate is also subjected to the influence of the training factor: its maximum value for the age of 20-22 years as a result of the judo training is in average by 7.1 units higher (196-188.9) compared with that of untrained persons.

The maximum heart rate from 8 - to 20-years of age decreases by 16 units (from 212 to 196). It means that it decreases in average by 1.2 units in each subsequent year. After 20 years of age it decreases with less intensity: from 1 - to 0.5 units per year.

The obtained results show that on the example of the heart rate the functional development for judokas extends well beyond the general biological characteristic regulations and makes standards specific for it.

ადამიანის და ცხოველთა ფიზიოლოგია

გულისცემის მაქსიმალური სიხშირე, როგორც სპორტულ-ასაკობრივი ფუნქციონირების პარამეტრი

გ. ზუბიტაშვილი

ილიას სახელმწიფო უნივერსიტეტი, სპორტის ფაკულტეტი, თბილისი

(წარმოდგენილია აკადემიკოს ნ. ჯოფშიძის მიერ)

სტატიაში შესწავლილია გულისცემის მაქსიმალური სიხშირის მაჩვენებელი სხვადასხვა ასაკის მოგალითზე. კვლევაში მოხდა უვარჯიშებელი და ძიუდოისტი პირების მონაცემთა შედარება და დადგინდა, რომ წვრთნის ფაქტორი ამ მაჩვენებელს რამდენადმე ზრდის. მეორე მხრივ დადასტურდა, რომ გულისცემის მაქსიმალურ სიხშირეზე მოქმედებს ასაკის ფაქტორიც და ამის გამო, ეს მაჩვენებელი 8-დან 20 წლამდე ყოველწლიურად საშუალოდ 1.2 ერთეულით მცირდება.

REFERENSES

1. *D. Chitashvili* (2005). Functioning of cardio-respiratory and muscle systems during physical loading. Tbilisi, 191p. (in Georgian).
2. *J. Wilmore, D. Costill, W. Larry Kenney* (2008). Physiology of Sport and Exercise (Fourth edition). Human Kinetics,UK, 592p.
3. *M. Houvenaeghel, C. Bizzari, D. Giallurachis, J. Demelas* (2005). Science & Sports, **20**, 1: 27-32.
4. *M. Fitzgerald, H. Tanaka, Z. Tran, D. Seals* (1997). Journal of Applied Physiology, **83**: 160-165.
5. *H. Engels, W. Zhu, R. Moffatt* (1998). Research Quarterly for Exercise and Sport, **69**, 1: 94-98.
6. *P. Stein, A. Ehsani, P. Domitrovich, et al.* (1999), American Heart Journal, **138**, 3: 567-576.
7. *H. Tanaka, K. Monahan, D. Seals* (2001), Journal of the American College of Cardiology, **37**, 1: 153-156.
8. *G. Zavorsky* (2000), Sports Medicine, **29**, 1: 13-26.

Received June, 2012

საქართველოს მეცნიერებათა ეროვნული აკადემიის მოამბე, ტ. 6, №3, 2012
BULLETIN OF THE GEORGIAN NATIONAL ACADEMY OF SCIENCES, vol. 6, no. 3, 2012

Microbiology

Helicobacter pylori Urease Activity and Spread of *Candida spp* in Patients with Gastric Cancer

Shorena Khetsuriani*, Zurab Khetsuriani, Muralidhasan Thanigaivasan§, Chandran Kulasekar§§**

* *Scientific Skills Center of Tbilisi State Medical University, Tbilisi*
** *National Cancer Center, Tbilisi*
§ *Government Stanley Hospital, Chennai, Tamilnadu, India; Scientific Skills Center of Tbilisi State Medical University, Tbilisi*
§§ *CSI Hospitals, Kancipuram, Tamilnadu, India; Scientific Skills Center of Tbilisi State Medical University, Tbilisi*

(Presented by Academy Member Giorgi Kvesitadze)

ABSTRACT. Nowadays, more than 50% of the world population are infected with *Helicobacter pylori*. It is a well-known fact that this microorganism is of a great danger for people in 20-30% cases. It is also known that the index of infection, caused by *H. pylori*, depends on geographic areas, ethnics and race, factors of habits, sex, age and social environment. It is especially common in economically under-privileged countries. This infection is mainly spread in the kind of gastroduodenal diseases: chronic gastritis, peptic ulcer disease, MALT-lymphoma, gastric cancer. According to certain literature the mentioned bacterium causes diseases of other visceral organs of humans.

The aim of our research was to study *H. pylori* urease activity, spread and coexistence of *Candida spp* and *H. pylori* in patients with gastric cancer. 24 patients with gastric cancer (GC) were involved in the study (National Cancer Center, Tbilisi). Identification of strains *H. pylori*, *Candida spp* and other gram-negative rods and gram-positive cocci were performed by established methods, on the basis of morphological, tinctorial, cultural and biochemical properties. Ages of patients ranged from 50-73 years with a male:female ratio of 1:3. Gc was more frequent in *antrum* (58.33±10.07%). Microorganisms were isolated both in monocultures and in associations. There were 19 *H. pylori*+ patients (35.84±9.78%). *Candida spp* were isolated in 30.18±9.35% cases. Other organisms were in a small amount (gram-negative rods, gram-positive cocci.). Correlation of *H. pylori* and *Candida spp* was higher in comparison with other species. The highest urease activity of *H. pylori* was revealed within 24h (42.10±10.07%). © *2012 Bull. Georg. Natl. Acad. Sci.*

Key words: *Helicobacter pylori, Candida spp, gastric cancer, microflora.*

Microbes induce an estimated 20% of all fatal cancers in humans, suggesting the tremendous potential of controlling microbe-related processes for cancer prevention [1].

Helicobacter pylori (*H. pylori*) is the first formally recognized bacterial carcinogen and is one of the most successful human pathogens, as over half of the world's population is colonized with this gram-

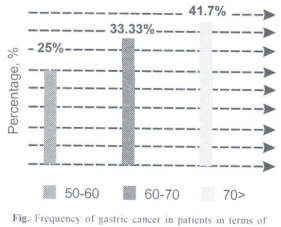

Fig. Frequency of gastric cancer in patients in terms of ages

negative bacterium. Unless treated, colonization usually persists lifelong. *H. pylori* infection represents a key factor in the etiology of various gastrointestinal diseases, ranging from chronic active gastritis without clinical symptoms to peptic ulceration, gastric adenocarcinoma, and gastric mucosa-associated lymphoid tissue lymphoma [2-4]. Although infection may be beneficial in some cases [5,6], its pathological consequences outweigh currently projected beneficial roles. Antibiotic resistance and compliance problems significantly reduce treatment efficacy [7,8]. In developing countries, reinfection is common, and current treatment options are inadequate for control as *H. pylori* is the most frequent infection of the stomach [9].

Gastric pathology can be caused by other infectious agents, including fungi, other bacteria, parasites, and viruses. These infectious agents frequently are part of a systemic process in which the resulting gastric pathology is one of the manifestations. Other microorganisms cause primary gastric pathology. Lots of interesting facts confirm that *Candida spp* is accompanied by gastric malignancy. Analysis of relationship between selected disorders of the upper gastrointestinal tract and infection with *H.pylori* and/or *Candida spp* revealed a link between the coexistence of *H. pylori* with *Candida spp* and gastric ulcers suggesting synergysm of those microorganisms in pathogenesis of the disease [10]. Study of the aggravating impact of this infection is under a great attention of the scientists.

Considering the above said, the aim of our study was to identify some cultural, biochemical characteristics of *H.pylori*, especially rapid urease test and coexistence of *Candida spp* and *H. pylori.*

24 patients with gastric cancer (GC) were included in the study. The resection materials and biopsy specimens were taken during the operation or endoscopy procedures. Identification of strains *H.pylori, Candida spp* and other gram-negative rods (G-rods/ and gram-positive cocci (G+cocci) was performed by established methods on the basis of morphological, tinctorial, cultural and biochemical properties [10,11].

The age of patients ranged from 50-73 years with a male:female ratio of 1:3 (Fig.).

Gc was more frequent in *antrum* (58.33±10.07%) than in *corpus* (29.16±9.26%) in comparison with the body and proximal part of *gaster* (29.16±9.26% and 12.5 ±6.75%, respectively).

Microorganisms were isolated both in monocultures and in associations. There were 19 *H.pylori*+ patients (35.8±9.78%). *Candida spp* were isolated in 30.18±9.35% cases. Other organisms were in a small amount (gram- rods, gram+ cocci.).

Table 1. Microflora of patients with GC (N=24)

N	Microflora	Number of patients	%
1	*H.pylori*	2	8.33±5.63
2	*Candida spp*	1	4.17±4.0
3	*H.pylori+ Candida spp*	6	25.0±8.83
4	*H.pylori+ Candida spp+ G+ cocci*	5	20.84±8.33
5	*H.pylori+ G+ cocci*	5	20.84±8.31
6	*Candida spp+ G+ cocci*	3	12.5±6.75
7	*H.pylori+ Candida spp+ G-rods*	2	8.33±5.63

Table 2. Urease Activity of *H.pylori* (%)

20 min.	3 h	18 h	24 h
10.52 ±6.25	26.31± 18.95	21.05±8.31	42.10±10.07

Correlation of *H.pylori* and *Candida spp* was higher in comparison with other species. As shown in the Table 1, *H.pylori* was in monoculture in 8.33±5.63%, *Candida spp* - in 4.1±54.0% cases. Other bacteria were in associations. *H.pylori*+*Candida spp*+G+cocci (20.84±8.33%). *H.pylori*+G+cocci (20.84±8.31%), *Candida spp*+ G+cocci (12.56±6.75%), *H.pylori*+ *Candida spp*+G-rods (8.33±5.63%).

The highest urease activity of *H.pylori* was revealed in 24h. (42.10±10.07%) in comparison with 3, 18 h and 20 minutes (26.3 ±18.95%, 21.05±8.31%, 10.52±6.25%, respectively) (Table 2).

Results of our study show high prevalence and coexistence of *H. pylori* and *Candida spp* in patients with Gc. Correlation of *H. pylori* and *Candida spp* was higher in comparison with other genera. *H. pylori* urease activity was very high as well. The highest urease activity was revealed in 24h (42.10%) in comparison with 3, 18 h and 20 minutes.

მიკრობიოლოგია

Helicobacter pylori-ს ურეაზული აქტივობა და *Candida* spp-ს გავრცელება კუჭის კიბოს მქონე პაციენტებში

შ. ზეცურიანი*, ზ. ზეცურიანი**, თ. მურალიდჰასანი§, კ. ჩანდრანი§§

** თბილისის სახელმწიფო სამედიცინო უნივერსიტეტის სამეცნიერო უნარ-ჩვევების ცენტრი,*
***ონკოლოგიის ნაციონალური ცენტრი, თბილისი*
§ სტერლის სახელმწიფო ჰოსპიტალი, ჩენაი, თამილნადუ, ინდოეთი; თბილისის სახელმწიფო სამედიცინო უნივერსიტეტის სამეცნიერო უნარ-ჩვევების ცენტრი
§§ GSI ჰოსპიტალი, კარჩაურამი, თამილნადუ, ინდოეთი; თბილისის სახელმწიფო სამედიცინო უნივერსიტეტის სამეცნიერო უნარ-ჩვევების ცენტრი

(წარმოდგენილია აკადემიკოს გ. კუსტანის მიერ)

ამჟამად მოსახლეობის 50% ინფიცირებულია *Helicobacter pylori*-თი. კარგადაა ცნობილი, რომ იგი 20-30% შემთხვევაში დიდი ზიანის მომტანია. *H. pylori*-ინფექციის ინდექსი დამოკიდებულია გეოგრაფიულ არეებზე, ეთნიკურობასა და რასაზე, წყეს-წეულებებზე, სქესზე, ასაკზე და სოციალურ გარემოზე. იგი განსაკუთრებით გავრცელდა დაბალი ეკონომიკური გარეთარების ქვეყნებში. ეს ინფექცია გავრცელებულია გასტროდუოდენური დაავადებების — ქრონიკული გასტრიტის, ჰეპტიური წყლულოვანი დაავადების, MALT-ლიმფომის, კუჭის კიბოს მქონე პაციენტებში. ზოგიერთი სამეცნიერო წყარის მიხედვით, იგი ასევე სხვა ორგანოების დაავადებებსაც იწვევს.

კვლევის მიზანი იყო შეგვესწავლა *H.pylori*-ს ურეაზული აქტივობა, *Candida* spp-ს გავრცელება და მისი თანაარსებობა კუჭის კიბოს (კკ) მქონე პაციენტებში.

კვლევას დაექვემდებარა კკ-ს მქონე 24 პაციენტის ბიოფსიური და რუზექციული მასალა (ონკოლოგიის ნაციონალური ცენტრი, თბილისი). *H.pylori-ს, Candida* spp-ს, სხვა გრამდადებითი კოკების და გრამუარყოფითი ჩხირების შტამების იდენტიფიკაცია ხდებოდა მორფოლოგიური, ტინქტორიული, კულტურალური, ბიოქიმიური ნიშნების მიხედვით.

პაციენტთა ასაკი მოიცავდა 50-73 წლებს. მამაკაცებისა და ქალების თანაფარდობა იყო 1:3. სიმსივნის ლოკალიზაცია უფრო ხშირი იყო ანტრუმში (58.33±10.07%). მაკროორგანიზმები გამოიყო როგორც მონოკულტურების, ასევე მიკრობთა ასოციაციების სახით. *H.pylori-* დადებითი იყო 19 პაციენტი (35.84±9.78%). *Candida* spp გამოიყო 30.18±9.35% შემთხვევაში. სხვა მიკროორგანიზმები იყო უმნიშვნელო რაოდენობით (გრამუარყოფითი ჩხირები, გრამდადებითი კოკები). *H.pylori-ს* და *Candida* spp-ს თანაარსებობა ბევრად მაღალი იყო სხვა მიკროორგანიზმებთან შედარებით. *H.pylori-ს* ურეაზული აქტივობა ყველაზე მაღალი იყო 24 საათში (42.10±10.07%).

REFERENCES

1. *M.J. Blaser* (2005), Sci. Am., **292**: 38–45.
2. *J.G. Kusters, A.H.van Vliet, E.J. Kuipers* (2006), Clin. Microbiol. Rev., **19**, 3: 449-490.
3. *K.L. McColl* (2010), NEJM, **362**(17): 1597-1604.
4. *I.M. Toller, et al.* (2011), Proc. Natl. Acad. Sci. USA, **108**:14944, Sep 6.
5. *Y. Chen, M.J. Blaser* (2007), Arch. Intern. Med., **167**: 821-827.
6. *P.B. Ernst, B.D. Gold* (2000), Annu. Rev. Microbiol., **54**: 615-640.
7. *D.H. Bergey, J.G Holt, et al.* (1994), Bergey's Manual of Determinative Bacteriology. 9th ed. Baltimore.
8. *E. Rimbara, L.A. Fischbach, D. Graham* (2011), Nat. Rev. Gastroenterol. Hepatol., **8**, 2: 79-88.
9. *Y. Nakayama, DY. Graham* (2004), Expert Rev. Anti Infect. Ther., **2**: 599-610.
10. *E. Karvzewska, I. Wojtas, E. Sito* (2009), J. Physiology and Pharmacology Suppl., **6**: 33-39.
11. *N.Z. Minaeva, U.M. Nesvizhsky, V.I. Minaev, L.V. Kudriavtseva, S.V. Zaitseva, K.I. Chekalina, B.L.Cherkasskii, P.L. Shcherbakov* (2001), Mikrobiologicheskaia diagnostika zabolevanii, vyzvannykh mikroaerofil'nymi izognutymi bakteriiami. M., 42 p. (in Russian).

Received August, 2012

საქართველოს მეცნიერებათა ეროვნული აკადემიის მოამბე, ტ. 6, №3, 2012
BULLETIN OF THE GEORGIAN NATIONAL ACADEMY OF SCIENCES, vol. 6, no. 3, 2012

Medical Sciences

Effect of some Pyrrole Derivatives on the Brain Cortex during Hemorrhagic Shock

Grigol Sulaberidze*, Murman Ghvaladze*, Eka Chkonia*, Tamar Gegeshidze*, Teona Buachidze*, Mamuka Chkhaidze*

* *Departments: Functional Morphology; Pathology and Cytopathology; Medical Pharmacology; Infectious Diseases; Psychiatry and Narcology; Tbilisi State Medical University*

(Presented by Academy Member Fridon Todua)

ABSTRACT. During hemorrhagic shock (HS), in which the destructive process develops, the brain cortex sharply reacts to hypoxia. The pyrrole derivative PV-88 is characterized by Ca^{2+} slow L channel blocking effect. Subsequently, it protects the brain cortex cells from overloading by Ca^{2+} ions. Possibly, it also affects T channels due to the cerebral-protective effect of this class of preparations.

The experiments were carried out on male cats. In total three series of experiments were conducted with 5 animals in each: one series in conditions of HS, the second series at the 80th minute of HS against the background of verapamil action, and the third series as a result of PV-88 effect.

Modeling of the hemorrhagic shock development was maintained up to 40 mm Hg the mean arterial pressure (MAP), gradually decreasing during 1 hour (HS60). The blood exfusion at 40 ml/kg was done against the background of artificial ventilation, which made 130-150 ml/min. The arterial blood pH was maintained at 7.35-7.45, and PO_2 - 90 mm Hg and more. The cat's body temperature stability varied between 37.8° C and 38.2° C. In the right femoral artery MAP was measured invasively, and from the left one the blood exfusion was done. Verapamil at the dose of 0.25 mg/kg and PV-88 at the dose of 3.0 mg/kg dissolved in normal saline, the volume of which did not exceed 1/20 of the exfused blood, were administered into the cat's right femoral vein. The animal's death was caused by putting it asleep at the 80th minute from the start of blood exfusion. We took the left frontal lobe (*Lobus frontalis*) of the brain cortex for examination by the electron microscope. Our research shows that PV-88, which is an acidic citrate 1-3(diethylamine) propyl-3(n-fluorophenyl-3-oxopropen)pyrrol, is characterized by more marked protecting ability to astrocytes and neurocytes, than preparation verapamil. © *2012 Bull. Georg. Natl. Acad. Sci.*

Key words: *hemorrhagic shock, cerebral cortex, verapamil, PV-88.*

Hypoxia, developed during the hemorrhagic shock, significantly affects the cerebral cortex functioning. At a sharp decrease of the activity of cardiovascular system a significant increase of Ca^{2+} ion amount is observed in the cerebral cortex cells, causing destruction of cell membrane of the astrocytes and neurocytes. The basis of this process is the depletion of the cell energy stock and profound destruction of microcirculation, which ultimately ends in irreversible process development. Ca^{2+} L slow chan-

nel blockers are used for acute functional disorders of cerebral blood circulation and homodynamic disorders. In this aspect, nimodipin is characterized by a marked efficacy in the treatment of subarachnoidal hemorrhage [1-2]. Based on the position of the functional activity, the central nervous system (CNS) viability is provided by *feed-back* type cycles as a unified ensemble. Centripetal striving for a state of shock from the middle of the brain reticular formations is subjected to modulated control. The cerebral cortex functioning is reflected at this level, which dramatically affects afferent ways; this process is stimulated by positive *feed-back* startup. Rapid manifestation of morphological damage to the neurons, organized in this entire microsystem, and their incompatibility with life indicates that the central nervous system is a crucial organ in the moment of the death occurrence. The *ensemble* of shock-producing information runs around the cerebral cortex once again and causes sharp, fulminant damage of central encephalic formations; in this direction the Ca^{2+} slow channel blockers completely change the gravity of irreversible process development. Their ability can be used in polymorphous manner toward the damage of other genes. This group of preparations and in particular PV-88 may be used effectively for prevention of dementias. Studies, conducted on animals, demonstrated that L-type Ca^{2+} blockers weaken β-amyloid oligomer toxicity, tau protein destructive effect and improve the autophagy (the basic process of abnormal protein liquidation). Frequent, repeated craniocerebral trauma significantly contributes to the development of dementia, (e.g. boxers' dementia), which is explained by the extra- and subdural hemorrhage and anoxia. Supposedly PV-88 due to its mechanism of action will have an important role in studies and may be used in treatment of dementia, which becomes more topical for the increase in the average age of life [3,4].

Materials and Methods. The experiments were carried out on male cats weighing 2.5-3.5 kg., which were not given food for 24 hours (receiving unlimited amount of water). General anesthesia was done with nembutal 35-40 mg/kg. Through the catheter, inserted in the left femoral artery the blood flowed into a glass vessel (cylinder), MAP was decreased to 40 mm Hg during 1 hour. The anesthetized animal was connected to the oxygen–air artificial breathing apparatus "Дала", the air ventilation was 130-150 ml / min/kg in a way that the arterial blood pH was 7.35-7.45 and PO_2 - 90 mm/Hg and more. Gas levels were monitored on the analyzer "Corning" (Great Britain). During the experiment the cat's body temperature was measured rectally, which amounted to 37.8-38.2°C. Temperature regime was maintained constant because its change significantly affects the homeostasis of the cerebral cortex [5]. The blood exfusion was done with the catheter, inserted in the right femoral artery and made 40 ml/kg, while MAP was measured in the left femoral artery. Heparin 2000 ED/kg was intravenously administered before blood exfusion; when MAP was stabilized to 40 mm/Hg, the experimental animal was disconnected from the apparatus and verapamil administered intravenously at the dose of 0.25 mg/kg, and PV-88 3.0 mg/kg, dissolved in normal saline, the amount of which did not exceed 1/20 of the blood exfusion.

Three series of experiments with 5 animals in each series (n=5)were conducted: 1. Control when frontal lobe of the brain cortex at HS60 was examined; 2. The series of examination against the background of a comparably standard preparation verapamil after 20 minutes of its intravenous administration; 3. In the same conditions the examination was done against the background of PV-88 effect.

The animal's death occurred at the 80th minute of blood exfusion, and the brain frontal lobe was immediately examined. The material for electron microscopy was fixed in 2% osmium acid on 0.1 molar phosphate buffer and on 3.5% glutaraldehyde on the same buffer. The preparation casting was carried out in the epoxy mass by conventional method. Ultrathin sections were made on the ultramicrotom "ЛКБ", and after contrasting with uranic acetate and lead, were examined with the electron microscope JEM-100B (Japan).

Verapamil represents an isochinoline derivative, while PV-88 is the acidic citrate 1-3(diethylamine) propyl-3(n-fluorophenyl-3-oxopropen)pyrrol, where the fluorine is introduced into electronic acceptor domain. This original structural modification significantly increased Ca^{2+} slow channel blocker effect compared with its predecessor compounds. Both preparations block myocardial L channels, but they may also affect the CNS channels as well.

Results and discussion. Hypoxia in hemorrhagic shock causes significant morphological changes in the CNS cortex. All ultrastructural deviations are caused by discirculation. Morphological changes in the brain frontal lobe cortex develop only in acute ischemia. The cell intactness to a certain extent is maintained for a limited time interval. The reason of destruction, developed in the next period, is sharp decrease of pH and activation of lysosome ferments.

Our data show that rapid development of hemorrhagic shock causes sharp swelling and aggregation of mitochondria and cell chromatin marginalization, first of all, in the astrocytes (Fig .1), which indicates the start of the brain edema. These changes of all the blood erythrocytes point to the reaction of the brain peripheral blood vessels to decrease the circulated blood amount, caused by the blood capillary stasis (Fig .2).

In the hemorrhagic shock verapamil caused marked protective effect on the frontal lobe of the brain cortex. Astrocytes and neurocytes were mainly maintained. Mitochondria swelling was observed in some astrocytes. There were some vacuoles, indicating the start of mild brain edema (Fig .3).

PV -88 cerebral-protective effects are like the above-described effects of verapamil activity. In the animals, treated with verapamil and against the background of PV -88, practically intact astrocytes were observed. (Fig .4). Rarely there were observed singular vacuoles with electro-transparent mass, indicating mild edema of the brain.

PV-88 is Ca^{2+} slow channel blocker, characterized by cerebral-protecting effect as well, caused also by its ability to stop calcium ion damaging activity to cell membranes. This process was caused by hypoxia, the reason for which was a serious homodynamic disorder, therefore, such damage is characteristic of all parenchyma cells. If we consider the fact that calcium slow L channel blockers are characterized by hypotensive effect due to decrease of general peripheral resistance, then it could be used in pathologies, such as portal hypertension with encephalopathy. β adrenergic blockers are used in portal hypertension, but they have no cerebral-protective effect and belong to the agents affecting the vegetative nervous system. Verapamil and PV-88, similar to it, L are calcium slow channel blockers with hypotensive effect, in addition, they are characterized by cerebral-protective effects. Therefore, they can be used for liver severe damage of various etiology (viral hepatitis, cirrhosis, malignant growth, alcohol damage), also in portal hypertension with ammonia genesis encephalopathy. It should be noted that the preparation of this group nimodipin is used in subarchnoid hemorrhages. Their main pharmacodynamics is reduction of oxygen consumption. The hemorrhagic shock in cats is characterized by liver protecting effect of verapamil, the liver lobule cell structure is maintained. The membrane integrity is maintained, acini do not experience significant pathological changes, and the liver metabolism is significantly improved, manifested in obvious rearrangement of anaerobic respiration to aerobic one. These positive changes are more obviously manifested for PV-88 compared with the reference preparation verapamil. Verapamil and PV-88 as calcium slow L channel blocker may be effectively used for dementia prevention. It is known that among the causes of dementia the leading one is Alzheimer's disease (50-60% of cases) and cerebral vascular dementia (20-25%), yet acetylcholinesterase inhibitors used for its treatment have only an insignificant effect and represent palliative treatment only. Cognitive impairment in different parts of the brain is associated with $\acute{a}$-amyloid deposit, which in turn, by acting on calcium channels, of membrane located in the plasma of

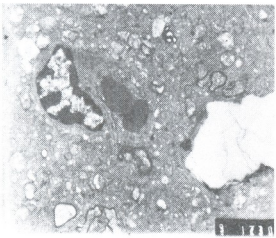

Fig. 1. Astrocyte of cerebral cortex. Swelling and aggregation of mitochondria and cell chromatin marginalization. Hemorragic shock. Electronogram x 12,000.

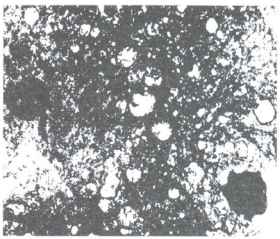

Fig. 2. Blood capillary of cerebral cortex. Blood capillary stasis. Start of the brain edema. Hemorragic shock. Electronogram x 12,000.

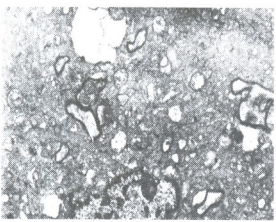

Fig. 3. Astrocyte of cerebral cortex. Hemorragic shock against the background of verapamil's action. Mitochondria swelling was observed in astrocyte. Electronogram x 13,000.

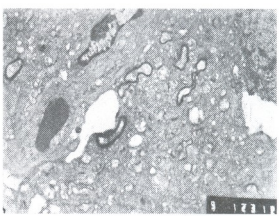

Fig. 4. Astrocyte of cerebral cortex. Hemorragic shock against the background of PV-88's action. Intact astrocytes were observed. Electronogram x 13,000.

somato-dendrites and axons, located in the cortex and hippocampus, causes its deregulation in cells. Studies conducted on animals have demonstrated that L-type calcium blockers weaken β-amyloid oligomer toxicity, tau protein destructive effect and improve autophagy. The L channel blocking and cerebral-protecting effect of PV-88 of the pyrrol group, studied by us, allows us to suppose its potential ability to block T channels as well. This requires further definition. Treatment of portal hypertension symptom (especially if it progresses with the picture of encephalopathy) by β blockers [6-14] which do not have cerebral-protecting effect and for β2 lysis properties in bronchial obstructive pathologies (bronchial asthma, atelectasis) cannot be used. In this regard, it is possible to use Ca^{2+} slow L channel blocker verapamil and other medications similar to it [15], and also PV-88, because at this time the frontal lobe of the brain cortex is significantly damaged [16,17], which requires further research.

Animal Handling. All experiments reported in this paper were carried out according to Institute National de la Santé et de la Recherche Medicale and Pasteur Institute animal welfare quidelines.

სამედიცინო მეცნიერებანი

პიროლის ზოგიერთი ნაწარმის მოქმედება თავის ტვინის ქერქზე ჰემორაგიული შოკის დროს კატებში

გრ. სულაბერიძე*, მ. ღვალაძე*, ე. ჭყონია*, თ. გეგეშიძე*, თ. ბუაჩიძე*, მ. ჩხაიძე*

* თბილისის სახელმწიფო სამედიცინო უნივერსიტეტი, ფარმაკოლოგიური ფარმაცევტიკის, ფიზიოლოგიის და ციტოპათოლოგიის, საქმიანი ურთიერთობის, ინფექციური დაავადებების, ფსიქიატრიისა და ნარკოლოგიის

(წარმოდგენილია აკადემიკოს ფ. თოდუას მიერ)

ჰემორაგიული შოკის დროს განვითარებულ ჰიპოქსიაზე განსაკუთრებით რეაგირებს თავის ტვინის ქერქი, რომელშიც ადგილი აქვს დესტრუქციული პროცესების განვითარებას. პიროლის ჯგუფის ნაწარმი PV-88 ხასიათდება Ca^{2+} ნელი L არხის მაბლოკირებელი ეფექტით, ეს უკანასკნელი კი ქერქის უჯრედებს იცავს Ca^{2+} იონების გადატვირთვისაგან. ამიტომ შეიძლება ვფიქრობდით, რომ ის მოქმედებს T არხებზეც.

ცდები ტარდებოდა მამრ კატებზე. სულ ჩატარებულ იქნა ექსპერიმენტის სამი სერია, თითოეულში 5 ცხოველი; I სერია – ჰემორაგიული შოკით (ჰშ); II სერია – ჰშ შესადარებელი ეტალონური პრეპარატ ვერაპამილის გამოყენების ფონზე და III სერია – ჰშ პიროლის ნაწარმებიდან PV-88-ის მოქმედების ფონზე.

ჰემორაგიული შოკის მოდელირება ხდებოდა საშუალო არტერიული წნევის (საწ) 40 mm/Hg-მდე თანდათანობით, ერთი საათის განმავლობაში დაქვეითებით. (ნარკოზი ნემბუტალი 40 მგ/კგ-წონაზე. სისხლის ექსფუზია შეადგენდა 40 მლ/კგ-ზე ხელოვნური სუნთქვის ფონზე 130-150 მლ/წთ-ში, არტერიული სისხლის pH შენარჩუნებული იყო 7.35-7.45, ხოლო PO_2 90 mm/Hg და მეტი. კატის სხეულის ტემპერატურის მუდმივობა შენარჩუნებული იყო 37.8-38.2°C-ზე. მარჯვენა ბარძაყის არტერიაში ანგიზიურად იზომებოდა საწ, მარცხნიდან – ხდებოდა სისხლის ექსფუზია, ხოლო გამოსაკვლევი პრეპარატები შეგვყავდა კატის მარჯვენა ბარძაყის ვენაში: ვერაპამილი დოზით 0.25 მგ/კგ-ზე და PV-88 3 მგ/კგ-ზე გახსნილი ფიზიოლოგიურ ხსნარში ამ უკანასკნელის მოცულობა არ აღემატებოდა გამოღებული სისხლის 1/20-ს.

ცხოველს ვაძინებდით სისხლის გამოშვებით და 1 სთ-ის შემდეგ ვიღებდით თავის ტვინის ქერქის მარცხენა შუბლის (Lobus frontalis) წილს ელექტრონული მიკროსკოპიისთვის სტანდარტული მეთოდით.

როგორც ჩვენი გამოკვლევიდან ირკვევა, მეცნიერებაში 1-(დეოთილამინ)პროპილ-3(n-ფტორფენილ-3-ოქსოპროპენ)პიროლი შიფრით PV-88-ს ახასიათებს ასტროციტებისა და ნეიროციტების დაცვის უნარი. მხოლოდ ასტროციტების გარკვეული ნაწილის მიტოქონდრიაში შეინიშნებოდა ვაკუოლები ელექტრონული გამჭვირვალე მასის სახით და ის თავისი პროტექტორული ეფექტით მნიშვნელოვნად აღემატებოდა ეტალონურ პრეპარატ ვერაპამილს.

ჭეშმარიტი ექსპერიმენტი ცხოველებზე ჩატარებულია პასტერის ინსტიტუტის რეკომენდაციების გათვალისწინებით.

REFERENCES

1. *A. Biondi, G.K. Ricciardi, L. Ruybasset, et al.* (2004), AJNR, **25,** 6: 1067-76.
2. *C.M. Sayma, J.K. Liu, W.T. Couldwell* (2006), Neurosurg Focus, **21,** 3: E12.
3. *L.R. Marco-Contelles* (2011), Curr. Med. Chem., **18,** 4: 552-576.
4. *K. Ritchie, S. Lovestone* (2002), Lancet, **360,** 9347: 1750-1766.0020
5. *H. Abdali, R.F. Fard, M. Mahmoudi, et al.* (2007), JRMS, **12,** 6: 282-285.
6. *H. Al-Chamdi* (2011), Saudi J. Gastroenterol., **17,** 2: 155-158.
7. *W.S. Cho, H.S. Kang,J.E. Kim, et al.* (2011), Interv. Neuroradiol., **17,** 2: 169-78.
8. *H.J. Gelmers, K. Gortez, C.J. de Weerdt, et al.* (1988), Engl. J. Med., **318**: 203-207.
9. *J.D. Lefrandt, J. Heitmann, K. Sevre, et al.* (2001), Br. J. Clin. Pharmacol., **52,** 6: 687-692.
10. *M. Ghvaladze, T. Gegeshidze, Gr. Sulaberidze* (2010), Collected Papers Dedicated to the 80th Aniversary of TSMU, XLIV: 112-114 (in English).
11. *M. Ghvaladze, T. Gegeshidze, Gr. Sulaberidze, et al.* (2010), Science and Technologies, **7-9:** 117-121 (in Georgian).
12. *Gr. Sulaberidze, M. Ghvaladze, G. Didava, et al.* (2011), Georg. Med. News, **1**: 65-69.
13. *R.J. Groszmann, G. Garcia-Tsao, J. Bosch, et al.* (2005), N. Engl. J. Med., **353**: 2254-2261.
14. *D. Tripathi, C. Graham, P.C. Hayes* (2007), Eur. J. Gastroenterol. Hepatol., **19,** 10: 835-845.
15. *S. Wolf, H. Martin, J.F. Landscheidt, et al.* (2010), Neurocrit Care, **12,** 3: 346-351.
16. *G.N. Kryzhanovskii, G.F. Leskova, V.I. Vdovichenko* (1996), Bull. Exp. Biol. Medic., **121,** 4: 352-355. DOI: 10.1007/BF0244
17. *G.F. Leskova, V.K. Lutsenko* (2002), Bull. Exp. Biol. Medic., **134,** 9: 263-266.

Received July, 2012

Medical Sciences

Statistical Characteristics of Blood Pressure and Heart Rate Variation in Different Blood Pressure Categories

Manana Janiashvili

M. Tsinamdzgvrishvili Institute of Cardiology, Tbilisi

(Presented by Academy Member Nicholas Kipshidze)

ABSTRACT: In this work different data sets of the blood pressure and heart rate characteristics of persons from different blood pressure categories have been investigated. In particular, the systolic, diastolic and heart rate time series obtained from 24h ambulatory monitoring were recorded. These data have been collected from 160 persons (91 men and 69 women) residents of Tbilisi. The age of patients for the present investigation was in the range of 30–70 years. Blood pressure and heart rate variability data in these patients have been recorded in the standard calm sitting conditions. Together with these, recorded during the investigation data sets, additionally we have carried out analysis of calculated data sets. Namely time series, such as the pulse pressure and the mean arterial pressure data sets have been analyzed. Patients have been grouped into four different blood pressure categories according to the guidelines of the European Society of Hypertension and the European Society of Cardiology.

Statistical features of these data sets, both measured and calculated, for patients from different blood pressure categories were calculated and compared. Standard statistical test was used and coefficients of variation of heart rate and blood pressure time series were calculated.

It was shown that there is clear correlation between statistical properties of the analyzed characteristics and level of blood pressure in different categories. Normal and high normal blood pressure categories of patients from different blood pressure categories reveal a clear difference in terms of the statistical features of blood pressure and heart rate characteristics. © *2012 Bull. Georg. Natl. Acad. Sci.*

Key words: *hypertension, blood pressure categories, heart rate, statistics.*

Today association between elevated systolic as well as diastolic blood pressure (SBP and DBP, respectively) and the risk of cardiovascular disease is well established [1, 2]. Therefore, classification of hypertension and identification of different blood pressure categories is recognized as an important prerequisite for risk assessment and prophylactic measures. Correct classification helps to make decisions concerning the blood pressure thresholds and appropriate treatment strategies at different forms of hypertension [3]. In 2007 the European Society of Hypertension (ESH) and the European Society of Cardiology (ESC) produced updated guidelines on the diagnosis and treatment of hypertension. In this guidelines blood pressure levels are defined corresponding to 7 categories: optimal (SPB <120 mmHg,

DBP <80 mmHg), normal (SPB in range 120–129 mmHg, DBP in range 80–84 mmHg), high normal (SPB in range 130–139 mmHg, DBP in range 85–89 mmHg) and grade 1 hypertension (SPB in range 140-159 mmHg, DBP in range 90-99 mmHg) categories (see Table 1 in ESH-ESC 2007 guidelines [3]. Such division, in itself, does not necessarily mean that variation of analyzed characteristics of patients from various blood pressure categories could differ by their statistical or distributive features. Moreover, reliability of the above division of blood pressure groups has not been accepted unambiguously because there is discrepancy with The USA Joint National Committee Guidelines (JNC 7) on hypertension published in 2003 [4] in which the normal and high normal blood pressure categories are unified into a single entity termed "prehypertension".

Materials and methods. In the present research we aimed to investigate the question of similarity or dissimilarity between normal, high normal blood pressure categories. To this end we compare the statistical features of measured and calculated blood pressure characteristics of patients, groups from optimal, normal, high normal blood pressure categories as well as of first grade hypertension. Study was performed at the Department of Hypertension of the Institute of Cardiology in Tbilisi, Georgia on appropriate data sets obtained from 160 persons (91 men and 69 women) residents of Tbilisi (of the age of 30 to 70). Additional details about the data bases used can be seen in [5]. We analyzed SBP, DBP and RR interval time series obtained from 24h ambulatory monitoring recordings at 15 min sampling time. Patients have been grouped in four blood pressure categories according to ESH guidelines [3] (Fig. 1). We also considered data sets of pulse pressure (PP), defined as SBP minus DBP, and the mean arterial pressure MAP, defined as 1/3(SBP)+ 2/3(DBP) data sets.

Results and discussion. We showed that differences between mean values in different categories are significant for all groups ($P<0.001$). Moreover, the mean

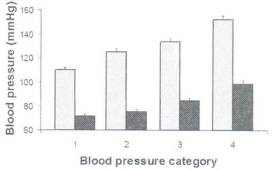

Fig. 1. Mean values with standard errors of systolic (grey columns) and diastolic (dark columns) blood pressures of patients from groups of optimal (1), normal (2), high-normal (3) and grade 1 hypertension categories (4).

values of diastolic blood pressure data, the sorting of which according to ESC guidelines was not perfect, also differring significantly ($P<0.001$) in different categories. These results seem to provide arguments to assume that normal and high normal groups, targeted in this work, can be statistically different.

At the same time contrary to measured SBP, DBP and heart rate data, time series of calculated MAP and PP characteristics do not always differ statistically in normal and high normal categories.

In order to exclude incorrect conclusions about the difference between normal and high normal blood pressure categories, we accomplished dispersion testing of blood pressure time series. Calculated values of dispersion characteristics, Cv, are presented in Fig. 2. It is understandable that Cv, calculated for averaged data is smaller than for pooled ones, where individual differences between patients from the same blood pressure category predominate. Results for both pooled as well as averaged, by consecutive 15 min intervals data, show that observed differences in the dispersion features are mainly connected with the type of the analyzed blood pressure data rather than with the blood pressure category. Indeed, it follows from Figs. 2*a* and 2*b*, that data sets of measured blood pressure characteristics, such as SBP and DBP, reveal much lower variability as compared to RR intervals time series. Data sets of calculated blood pressure characteristics, PP and MAP, also show

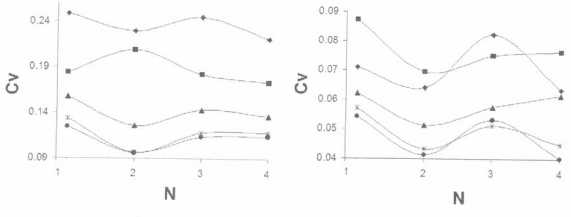

Fig. 2. Coefficient of variation vs. blood pressure category for pooled (a) and averaged (b) blood pressure data sets: SBP (circles), DBP (triangles), RR intervals (squares), PP (diamonds) and MAP (asterisks). On the x axis blood pressures categories are shown: optimal (1), normal (2), high-normal (3) and hypertension (4).

clearly different dispersion features; pulse pressure reveals much more variability than mean arterial pressure.

At the same time it should be pointed out that there are also smaller but still detectable changes which can be related to certain blood pressure categories. Namely, in Fig. 2*a*, we observe some changes in the Cv values at normal blood pressure category. It is worth mentioning that these are results obtained for long, pooled data sets described in methods section, which account for features of the individual blood pressure variation of patients grouped in a certain blood pressure category. In the case of averaged time series of the same characteristics presented in Fig. 2 *b*, we also discern some changes which are mostly similar to pooled ones, excluding RR data. In this last case changes at normal category for averaged data persist, though they are in opposition to what was observed for pooled ones. These results possibly indicate increased scatter of the considered characteristics for individuals at transition from optimal to normal blood pressure category.

At the same time, as follows from Fig. 2, in terms of deviation from dispersion features found in optimal blood pressure category, normal category is not an exception and that some changes take place for other categories too. Most important for the present research purposes is that all these small changes in dispersion features of the analyzed characteristics mostly occur between normal and high normal categories, notwithstanding unavoidable individual deviations or averaging effects throughout the category groups.

It should be underlined that, aiming at comparison of statistical features of blood pressure and heart rate characteristics of patients from different guidelines categories, we studied the representative groups with no regard for frequently used criteria such as ethnicity, gender or age. Thus the findings presented in this research indicate clear references between statistical properties of different blood pressure characteristics and changes occurring at transition from healthy to hypertension condition in persons from different blood pressure categories. According to these results normal and high normal blood pressure categories are clearly different in terms of the analyzed statistical and distributional properties.

სამედიცინო მეცნიერებანი

სისხლის წნევისა და გულის რიტმის ცვლილებათა სტატისტიკური მახასიათებლები არტერიული წნევის სხვადასხვა კატეგორიაში

მ. ჯანიაშვილი

მ. წინამძღვრიშვილის კარდიოლოგიის ინსტიტუტი, თბილისი

(წარმოდგენილია აკადემიის წევრის ნ. ჯოფშოძის მიერ)

ნაშრომის მიზანს წარმოადგენდა შეგვედარებინა ნორმალური და მაღალი ნორმის კატეგორიის პაციენტების სისტოლური სისხლის წნევის, დიასტოლური სისხლის წნევის, გულის რიტმისა და პულსური წნევის სტატისტიკური მახასიათებლები. ანათვალებს ვიღებდით 15 წუთიან ინტერვალში არტერიული წნევის 24 სთ-იანი მონიტორირების ჩანაწერების მიხედვით. ჯგუფები წარმოდგენილი იყო ევროპის კარდიოლოგთა ასოციაციის გაიდლაინის მიხედვით. გამოკვლეული იქნა 160 ადამიანი. აქედან 91 იყო მამაკაცი და 69 ქალი, რომელთა წლოვანება მერყეობდა 30-დან 70 წლამდე.

კვლევის შედეგებმა გვიჩვენა, რომ მიუხედავად საშუალო სიდიდეების სიახლოვისა, არტერიული წნევის ორი განხილული კატეგორიის სტატისტიკური მახასიათებლები სარწმუნოდ განსხვავდება.

REFERENCES

1. *M. Ezzati, A.D. Lopez, A. Rodgers, et al.* (2002). Lancet, **360**: 1347-1360.
2. *H. D. Sesso, M. J. Stampfer, B. Rosner, et al.* (2000), Hypertension, **36**: 801-807.
3. *G. Mancia, G. Backer, A. Dominiczak, et al.* (2007). Hypertension, **25**: 1105-1187.
4. *A.V. Chobanian, G.L. Bakris, H.R. Black, at al.* (2003), Hypertension, **42**: 1206-1252.
5. *M. Janiashvili* (2011), International Scientific Conference "Physical Research Methods in Medicine", Tbilisi, 27-29 October, 114-117.

Received July, 2012

საქართველოს მეცნიერებათა ეროვნული აკადემიის მოამბე, ტ. 6, №3, 2012
BULLETIN OF THE GEORGIAN NATIONAL ACADEMY OF SCIENCES, vol. 6, no. 3, 2012

Ecology

Vegetative Propagation of Ornamental Shrubs Using Hormodin-2 Solution in Batumi Botanical Garden

Nino Lomtatidze* and Eter Machutadze*

Shota Rustaveli State University, Batumi

(Presented by Academy Member Avtandil Korakhashvili)

ABSTRACT. Introduction and propagation of plants are considered to be one of the most important problems in plant biology. Successful introduction of plants depends on the conservation of the reproduction ability of plants in the new environmental conditions. During acclimatization of plants inner biological processes transform with respect to the new environmental conditions, such as soil and climate. Introduction and adaptation of plants is a complex and long process. Knowledge of the native habitat of plants, their transfer to a new area and propagation is not enough for introduction of alien species. It is necessary to conduct multi-year observation to determine the degree of habitation of some introduced specimens. In the present work the factors conditioning successful introduction of new species at the Ajara seaside are studied, prediction of the adaptation of alien plants under changed environmental conditions is made and the general mechanisms of introduction are determined.

In the humid subtropical zone of Ajara a fairly large group of aliens is distinguished for fast growth, high productivity and aesthetic value. They reveal a fairly high potential which is one of the significant factors of successful introduction. © *2012 Bull. Georg. Natl. Acad. Sci.*

Key words: *hormodin-2, ornamental plants.*

Ornamental shrubs introduced in the Batumi Botanical Garden such as *Abelia grandiflora* (Andre) Rhed, *Aucuba japonica* Thunb, *Gardenia jasminoides* Ellis, *Mahonia japonica* (Thunb.) DC, *Forsythia viridissima* Lindl, *Pieris japonica* Thunb. D., *Chaenomeles japonica* (Thunb) Lindl. ex Spach *A* under the local soil&climatic conditions are distinguished for abundant flowering and diversity of forms. Our aim was to study their biological peculiarities and work out prospective methods of their propagation.

The problem of propagation of the mentioned shrubs provokes more interest due to the circumstance that this problem is little-studied for Black Sea shore conditions Ajara. The experiments carried out by us allow to clarify the question of the propagation of the introduced ornamental shrubs that will help in future transplanting and propagating the mentioned plants.

Methods and Results. With a view to wide implementation of hitherto unused species in landscape planting in the Ajara moist subtropical zone study was

Table 1. Rooting of cuttings of ornamental shrubs (control)

№	Species	Date of cutting	Amount of cuttings	Amount of rooted cuttings	Duration of rooting (days)	Percent of rooting
1	*Abelia grandiflora* (Andre) Rhed	1.11.09	100	85	37	85
2	*Aucuba japonica* Thunb	1.11.09	100	65	35	65
3	*Mahonia japonica* (Thunb). DC.	2.11.09	100	7	41	7
4	*Pieris japonica* Thunb. D.	2.11.09	100	5	45	5
5	*Forsythia viridissima* Lindl	1.11.09	100	90	33	90
6	*Gardenia jasminoides* Ellis	1.11.09	100	75	34	75
7	*Chaenomeles japonica* (Thunb) Lindl. ex Spach A	2.11.09	100	25	38	25
	LSD 05			2.7	8.2	

made of the potentialities of propagation by stem cuttings. In the case of deciduous species from yearling woody stems we took cuttings 15-25 long, from evergreen species – 15-20 cm cuttings with 2-3 stem nodes. We removed the leaf from the lower node. On the upper node the leaf was shortened by 1/3 or 1/2 in order to lessen transpiration or eliminate intershading. Solution of hormodin-2 was prepared on the day the cuttings were taken. The cuttings were set in the solution with 1/3 of the length up to 1/2 of woody length, with 24 hour exposure. Cuttings were taken from the stems of relatively young specimens. Cuttings treated with the solution were transferred to the greenhouse planting. The substrate consisted of soil&sand mix. The cuttings were planted at 1.5-2 cm depth in slightly leaning position, the distance between rows was 3-4 cm. Control untreated cuttings were planted in order to compare how the growth stimulator influences the rooting process.

In the greenhouse temperature regime, light conditions, air and substrate humidity were kept normal. The most favourable temperature to root was 18-30 °C, air humidity 80%. Light is an important factor for cuttings treated with heteroaux in solutions since rooting begins fast and needs in food increase and photosynthesis in organic matters

As a result of the experiment it was revealed that out of ornamental plants untreated with 2%-solution of hormodin-2 *Forsythia* and *Abelia grandiflora* were characterized by high rooting index – 90 and 85%, respectively; with medium index - *Gardenia jasminoides* and *Aucuba japonica* 65 and 75% ,respectively). Especially low indices were shown by *Pieris japonica* and *Mahonia japonica* (5 and 7%, respectively). Duration of rooting of cuttings varied within the 33-45 days range (Table 1).

Table 2. Rooting of cuttings treated with 2% solution of hormodin-2

№	Species	Date of cutting	Amount of cuttings	Amount of rooted cuttings	Duration of rooting (days)	Percent of rooting
1	*Abelia grandiflora* (Andre) Rhed	1.11.09	100	95	33	95
2	*Aucuba japonica* Thunb	1.11.09	100	97	31	97
3	*Mahonia japonica* (Thunb). DC.,	2.11.09	100	17	40	17
4	*Pieris japonica* Thunb. D.	2.11.09	100	15	43	15
5	*Forsythia viridissima* Lindl	1.11.09	100	90	29	90
6	*Gardenia jasminoides* Ellis	1.11.09	100	75	31	75
7	*Chaenomeles japonica* (Thunb) Lindl. ex Spach *A*	2.11.09	100	25	35	25
	LSD 05			2.4	11.3	

Table 2 shows data on rooting of the treated cuttings with 2%-solution of growth hormone hormodin-2. As seen from the Table the duration of rooting of cuttings varied within the 29-35 days range. *Aucuba japonica* had the highest rooting index (97%), and *Pieris japonica* had the lowest one (15 and 17%, respectively).

The study of propagation peculiarities showed that treatment with rhizogenous hormone – hormodin-2 is especially effective for some plants. Rooting indices of *Abelia grandiflora, Pieris japonica and Mahonia japonica* increased by 10%, index of *Aucuba japonica* increased 1.5 times (Table 2).

Thus, our researches showed that among the ornamental plants, in all cases, whether they are treated with the growth stimulator hormodin-2 or not, *Abelia grandiflora, Forsythia, Aucuba japonica* differ with high indices at vegetation propagation whereas *Mahonia japonica* and *Pieris japonica* are characterized by low indices.

Based on the results of the study, one can conclude that it is possible to use 2%-solution of hormodin-2 in propagation of the studied decorative aliens of high quality. Due to high growth rate and abundant flowering of the above-mentioned ornamental shrubs in the Black Sea humid subtropical zone they can be used in planting up of the Ajara seaside parks and gardens.

ეკოლოგია

დეკორატიული ბუჩქების ვეგეტაციური გამრავლების მიზნით ჰორმოდინ-2-ის ხსნარის გამოყენება ბათუმის ბოტანიკურ ბაღში

ნ. ლომთათიძე*, ე. მაჭუტაძე*

შოთა რუსთაველის სახელმწიფო უნივერსიტეტი, ბათუმი

(წარმოდგენილია აკადემიის წევრის ა.კორახაშვილის მიერ)

მცენარის ბიოლოგიაში ერთ-ერთ მნიშვნელოვან საკითხად ითვლება გამრავლება, რადგანაც სწორედ გამრავლების უნარზეა დამოკიდებული სახეობის სიცოცხლე თუ გადაშენება, არეალის გაფართოება თუ შემცირება. მცენარის ინტროდუქციის წარმატება დამოკიდებულია ახალ გარემო პირობებში გადატანისას მცენარის გამრავლების უნარის შენარჩუნებაზე. მცენარეთა აკლიმატიზაციის დროს მიმდინარეობს ორგანიზმის შინაგანი პროცესების გარდაქმნა შეცვლილ საარსებო გარემო პირობების შესაბამისად. ამასთანავე, აუცილებელია მცენარე შეგუოს ნაადაგს, რომელიც არანაკლებ როლს ასრულებს მცენარეთა ინტროდუქციის პროცესში, ვიდრე კლიმატი. მცენარეში არსებული სასიცოცხლო ფიზიოლოგიური ძალა უზრუნველყოფს მცენარის შეგუებას განსხვავებულ ეკოლოგიურ პირობებთან. ინტროდუქციისა და ადაპტაციის პროცესი რთული და ხანგრძლივია.

ანტროდუცენტების ფართოდ დანერგვისათვის არ არის საკმარისი მცენარის ბუნებრივი გავრცელების ადგილმდებარეობის ცოდნა, შეცვლილ საარსებო გარემო პირობებში გადატანა და გამრავლება. საჭიროა მრავალწლიანი დაკვირვება იმის დასადგენად, თუ როგორია ამა თუ იმ ანტროდუცენტის შემგუებლობა შეცვლილ გარემოში. ჩვენს მიზანს შეადგენდა აჭარის ზღვისპირეთში ანტროდუქციის წარმატების განმაპირობებელი ფაქტორების შესწავლა, ანტროდუცენტების შეცვლილ გარემო პირობებთან შეგუების პროგნოზირება და ანტროდუქციის ზოგადი კანონზომიერების ჩამოყალიბება.

აჭარის ტენიან სუბტროპიკულ ზონაში ეგზოტების საკმაოდ დიდი ჯგუფი, ადგილობრივ მცენარეებთან შედარებით, გამოირჩევა სწრაფი ზრდით, მაღალი პროდუქტიულობით და ეკოლოგიური მნიშვნელობით. ისინი ალელენურ საკმაოდ მაღალ პოტენციურ შესაძლებლობებს, რაც ანტროდუქციის წარმატების დამადასტურებელ ერთ-ერთ მნიშვნელოვან ფაქტორად ითვლება.

REFERENCES

1. *V.R. Papunidze, N.S. Bagratishvili, D.M. Gvianidze, et al.* (1987), Derev'ia i kustarniki Batumskogo botanicheskogo sada (Annotirovannyi spisok). Tbilisi, 228 p. (in Russian).
2. *V.F. Verzilov* (1955), Stimuliatory rosta v zelenom stroitel'stve. M., 96 p. (in Russian).
3. *V.S. Kholiavko, D.A. Globa-Mikhailenko* (1980), Dendrologiia i osnovy zelenogo stroitel'stva. M., 248 p. (in Russian).
4. *V.I. Kefeli* (1997), Fiziologiia rastenii, **44**, 3: 471-480 (in Russian).
5. *N.K. Vekhov, M.P. Il'in* (1934), Vegetativnoe razmnozhenie drevesnykh rastenii letnimi cherenkami. L., 284 p. (in Russian).

Received June, 2012

Palaeobiology

New Spiral-Horned Antelope in Dmanisi Fauna

Abesalom Vekua

Academy Member, Institute of Palaeobiology, Georgian National Museum, Tbilisi

ABSTRACT. **Discovery of the lower jaw of a fossil man in Dmanisi in 1991 is the most outstanding event in palaeontology since the times of fascinating discoveries of early pithecanthropus in Kenia. Rather old age of the Dmanisi man is confirmed by diverse vertebrate fauna and numerous artefacts. Geological age of fossilbearing sediments and of the fauna (1.85 mln yrs) is substantiated by data of bio- and magneto-stratigraphy, also by isotopic dating of the basalts directly underlying the sediments with accumulation of early hominid remains.**

Excavations in Dmanisi continue. The list of vertebrate fauna is being filled up by new forms. At present more than thirty representatives of Proboscideans, Predators, Ungulates, Rodents and reptiles have been determined on Dmanisi site. Artiodactyla, among which deer prevails, are represented most richly and diversely. Excavations of the last season revealed remains of antelopes. Among them an incomplete scull of a large antelope is worthy of attention, which undoubtedly belongs to spiral-horned antelopes (tribe Oiocerini, Sokolov) according to the character of torsion of its horn cores. Isolated teeth and bones of extremities have been attributed by us to the same group tentatively but, based on the sizes of bones and morphological features of the teeth, an error is almost excluded. *© 2012 Bull. Georg. Natl. Acad. Sci.*

Key words: *fauna, spiral-horned antelope.*

Homonymously twisted horn appendages, massiveness of horn cores, their form and several characteristic features of structure of the post-corneous sector of the occipital part, as well as, perhaps, peculiarity of structure of molars devoid of any additional elements clearly testify to the belonging of spiral-horned antelope to Oiocerini.

It is natural that Dmanisi antelope reveals obvious similarity with representatives of tribe Oiocerini Sokolov [1] by structure, form and character of homonymous twisting of horn appendages. But the family Bovidae contains several forms with clearly homonymously twisted horn cores. Among the latter, first of all tribe Oiocerini from the Caprine subfamily, as well as Sinotragus and Prosinotragus from the subfamily Hippotragine of Mio-Pliocene of China should be mentioned.

Apparently, it is appropriate to note that not all authors include Oiocerini in the Caprine subfamily. For example, inclusion of Oiocerini in the group of Gazellinae seems indisputable to G. Meladze [2]. Without going into debate on this issue, we show preference to I. Sokolov's systematization of Bovidae, based on the natural characteristics of structure of skull

and horn cores of Bovidae [3].

At present the tribe Oiocerini combines three genera: Hypsodontus Sokolov (1949), Oioceros Gaillard (1902) and Paraoioceros Meladze [2].

It is interesting that I. I. Sokolov [3], having at his disposal only teeth (M^1-M^3) of Artiodactyla from Chokrak Belomechetskaya (North Caucasus), identified a new genus and species *Hypsodontus miocenica*, placing it in the group of Bovidae of uncertain taxonomic rank (incertae sedis). A little later, L. K. Gabunia [4], on the grounds of studying additional fossil material, including horn core from Belomechetskaya, and after comparing the corn appendages and teeth of Hypsodontus with the material of Dioceros from Tung-Gura [5], was convinced of close similarity between Belomechetskaya and Tung-Gura forms. Moreover, taking into account differences of some features of horn core structure, he decided to retain its genus name Hypsodontus.

Detailed comparison of Dmanisi antelope with Hypsodontus seems unnecessary. Differences between comparable forms are striking. Hypsodontus is characterized by comparatively small sizes, its horns are thin, straight, short, set vertically, without keels, weakly homonymously twisted, with rounded cross-section. Teeth of hypsodontus are mesohypsodontic, without additional tubercles and styles. M_3 is of primitive structure, with unforked vallecula.

Some similarities of Dmanisi antelope with Oioceros sp. from the Pontic deposits of Bazaleti (East Georgia) are clearly observable, manifested mainly in the structure of half-twisted and half-convoluted horn cores [2]. However, similarity between comparable antelopes is restricted to this. Dmanisi form is larger, its horns are more massive, longer, horn cores are devoid of longitudinal grooves, and horns branch off stronger.

Dmanisi antelope cannot be brought to resemble another East Georgian antelope of Upper Sarmatian age – Paraoioceros improvisus [2]. Sarmatian antelope is close to the Dmanisi Upper Pliocene one by large sizes, homonymous twisting of horn cores, but differs from the latter by the presence of three powerful keels, longitudinal grooves, triangular cross-section of cores and sharp branching off of horn cores.

Spiral-horned antelopes – Sinotragus and Prosinotragus – from the Mio-Pliocene of China [6], though they reveal some similarities with Dmanisi antelope by the presence of homonymously twisted horn cores, still considerably differ from the Georgian antelope by three-keeled horn cores, and accordingly, by triangular cross-section of cores (Sinotragus), horns bent backwards arcwise and slightly convoluted cores (Prosinotragus).

Family Bovidae Gray, 1821

Subfamily Caprinae Gill, 1872

Tribe Oiocerini Sokolov, 1953

Genus Pontoceros Ver., Alex., David et Baig., 1971

***Pontoceros surprine* sp. nov. Vekua, 2012-03-12** (Fig. 1-4).

The name of the species is derived from English surprine – unexpected.

Material. Incomplete skull (D5552) with horn cores. Facial and incisal parts on the skull are broken. Post-corneous part of skull is relatively well-preserved. The skull is rather large. Fragment of right horn (D5702).

Diagnosis. Antelope of large sizes (width of skull in the region of bulla tympani – 142 mm), horn cores are massive, set steeply, are weakly bent backwards, homonymously twisted into one full turn. Horn core has one sharply projected keel, originating from rear external surface of horn core. Cross-section of the core is almost round.

Geological age. Upper Pliocene, the end of Middle Villafranche.

Description and comparison. The skull is of large size (maximal width of post-corneous part of the skull in the region of bulla tympani is 142 mm), with relatively high brain section (height of occiput is 76.3 mm). Horn cores are massive without inner cavity even at the base of cores. Horns are slightly convoluted and twisted homonymously into open spiral at one full turn and have only one sharply projected

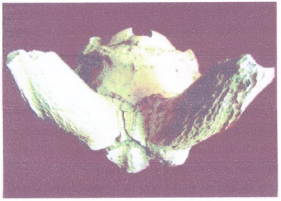

Fig. 1. Dmanisi. *Pontoceros surprine* sp. nov. Skull. Dorsal view.

Fig. 3. Dmanisi. *Pontoceros surprine* sp. nov. Skull. Occipital view.

Fig. 2. Dmanisi. *Pontoceros surprine* sp. nov. Skull. Lateral view.

Fig. 4. Dmanisi. *Pontoceros surprine* sp. nov. Skull. Ventral view.

rear external keel. Cross-section of horns is nearly round, horns are bent backwards, weakly branching off. Fracture of skull axis is about 50 degrees. There are no longitudinal grooves on the surface of horn cores. The length of the post-corneous part of the skull is medium. Basioccipitale is rather wide, of elongated-rectangular form, with a slight front contraction. Longitudinal rollers are developed on the lateral sides of bone, and observable groove is stretched between them. Frontal and rear pairs of tuber are raised.

Post-corneous part of the skull is rather broad (142 mm), relatively high (76.3 mm.). Parietal surface of skull is evenly convex, supraoccipitale occupies a noticeably broad area of dorsal surface of the post-corneous part of the skull and is directed forward with a narrow vertex of triangle.

Parietal crista is sharply projected and restricts occipital surface. Suturalambdoidalis is nearly straight with a weak curve and passes directly behind the horn cores. Fracture of skull axis is medium (in the limits of 50 degrees). Dorsal surface of brain case is located at an angle of 55 degrees towards the occipital surface.

Fragment of upper part of horn core (D5702) is massive, right-sided, judging by direction of keel, with homonymous twisting. There is the second keel-like longitudinal thickening, which can be tentatively taken for a keel, but this is not certain.

Upper jaw teeth are mesohypsodontic. Molars are devoid of supplementary styles. Styles and crests are weakly projected on the external side of teeth. Correlation of lower premolars with whole length of teeth row is medium – 42.7.

Lower molars are absolutely devoid of supplementary element. There is even no trace of external front fold on the back molars. Correlation of lower molar row with whole length of teeth row is 39.9.

According to Sokolov [1], an overwhelming majority of fossils and modern forms included in the tribe of spiral-horned antelopes have clearly heteronymously twisted and convoluted horn appendages. Moreover, they are provided with some well-observable keels and cross-section is generally triangular. That is why systematization of Oiocerini is based solely on the form of horn cores, character of twisting and convolution, presence of inner cavity, keels and so on.

An interesting antelope with clearly homonymously twisted horn cores from Upper Pliocene deposits in the area of Nogaisk is described and singled out as a new genus and species Pontoceros ambiguus by a group of authors (Vereshchagin, Alekseeva, David, Baigushcheva, [7]). It is natural, that we bring precisely Dmanisi antelope close to this antelope, although there is no complete similarity between these antelopes under comparison. In spite of the closesness of the Nogaisk and Dmanisi antelopes by homonymous torsion of horn cores, Dmanisi form cannot be identified with P. ambiguus. That is why we identify a new species of genus Pontoceros.

Dmanisi species differs from P. ambiguus by more massive, short horn cores, somewhat larger sizes, presence of one raised keel, rounded cross-section, lack of grooves on cores and cavities in the bases of horn appendages. According to authors' description, horn cores of *P. ambiguus* are three-keeled, slender, cross-section is triangular. There are longitudinal fissures on the horn surfaces and cavities at the base of horn appendages.

Detailed comparison of Dmanisi antelope with P. ambiguus convinces me that the described antelope from Dmanisi obviously belongs to a new, hitherto unknown species of tribe Oiocerini.

It should be noted that we categorically reject inclusion of Lower Pleistocene antelope Sinoreas from Akhalkalaki (Southern Georgia) in the group of genus Pontoceros. According to all characteristic features of the structure of horn cores (character of torsion, number of keels, cross-section etc.), Sinoreas from Akhalkalaki sharply differs both from Pontoceros ambiguus and from the new form of Pontoceros from Dmanisi.

We do not identify Akhalkalaki antelope with Sinoreas. Therefore its definition is given questionable and its attribution to the genus Pontoceros is obvious misunderstanding.

In the Lower Pleistocene deposits of Apollonia (Greece) fragments of horn cores of antelope with obvious homonymous twisting of horn appendages were found. The famous paleontologist Dmitri Kostopoulos [8], describing these remains, compares them with Nogaisk antelope and comes to the logical conclusion on the affinity of the antelopes under comparison. At the same time he identifies a new subspecies Pontoceros ambiguus mediterraneus Kost., 1997 on the grounds of some morphological features.

Naturally, we undertook a detailed comparison of Dmanisi antelope with its Greek counterpart According to the descriptions of the author, the Greek antelope is a rather large form with homonymously twisted massive long horn cores. There are three keels pronounced in different degrees with obvious longitudinal grooves on the horns. The antelope from Apollonia manifests considerable similiraty with the Nogaisk antelope by all the listed morphological fea-

Table. Measurenents of the skull of Pontoceros

Skull	*Pontoceros surprine* Dmanisi	*Pontoceros ambiguus* Nogaisk. Vereshchagin et al.1971	*Parastrepsiceros sokolovi* Kvabebi Georgia.	*Pontoceros ambiguus mediteraneus,* Apollonia, Greece. Kostopoulos, 1979
Width of the back horn of the skull	57.4	-	95-110	-
Width of brain box	117	-	-	-
Width of skull mastoid	126	-	-	-
Height of the occipital	76.3	-	72.82	-
Maximum width of the skull	Ca. 142.5	-	113-130	-
Distance from horn to occipital	100.6	-	93-110	-
Length of the horn	Ca.150	260	332	205
Distance between the external edges of the horns	139	_	127-138	-
Distance between the inside edges of the horns	35.7	50-55	22-26	-
Diameter of antero-posterior base of the horn core	50.0	46	44-56	40.5
Width of the horn core	55.2	48	53-63	43.2
Number of the horn keel	1	3	2	3
Form of the transversal cut (crosscut) of the horn	Round	Triangle	Triangle	Triangle

tures but by the same features it obviously differs from the Dmanisi one. First of all, Dmanisi antelope has somewhat shorter and more massive horn appendages in contrast to the Greek and Nogaisk antelopes, has only one sharply projected keel (accordingly, they have different cross-sections), horns are devoid of longitudinal fissures and are slightly bent backward.

We are aware that inclusion of Dmanisi antelope in the group of the genus Pontoceros is conditioned by the scarcity of fossil material both from Dmanisi and from Apollonia and Nogaisk. We are sure that with accumulation of fossil material on antelopes from Dmanisi, we will be obliged to find out some new genus name. At the level of present day information, we have decided only to single out a new species of Dmanisi antelope in the group of Pontoceros - *P. surprine*.

General remarks. There are only some isolated finds of remains of spiral-horned Bovidae on the territory of Georgia. All of them are timed to various stratigraphic horizons. Of the Pleistocene of Akhalkalaki Sinorea sp.? is described [9]. In Pontic deposits of Bazaleti Oioceros sp. is determined [10], from Akchagil deposits of Kvabebi spiral-horned *Parastrepsiceros sokolovi* is described [11], and in Sarmatian deposits of Yaghludja remains of Paraioiceros improvisus are found [2]. Finally, an interesting form is discovered in Dmanisi.

Systematization of spiral-horned antelopes, especially from tribe Oiocerini, is complex and intricate, which is caused by the incompleteness of fossil material. Some researchers attribute Oiocerini to Caprinae subfamily [1], while others to Hippotraginae [6], and Meladze [2] includes them into group of Gazellinae.

In Meladze's opinion (1985), Oiocerini became detached from the common stem, perhaps from the genus Hypsodontus, in the Middle Miocene epoch, spreading widely in Eurasia.

პალეობიოლოგია

ზვეულრქიანი ანტილოპა დმანისის ფაუნაში

ა. ვეკუა

აკადემიის წევრი, საქართველოს ეროვნული მუზეუმი, პალეობიოლოგიის ინსტიტუტი

დმანისის უძველესი ჰომინიდების ნაშთების აღმოჩენა (1991 წ) ბოლო დროის უმნიშვნელოვანესი მოვლენაა პალეოანთროპოლოგიაში. ქართველი მეცნიერების უახლესი გამოკვლევები დმანისის ჰომინიდების შესახებ მსოფლიო სამეცნიერო წრის ყურადღების ცენტრში მოექცა. დღეს უკვე დავას არ იწვევს დმანისის აღმოჩენების გეოლოგიური ხნოვანება 1,85 მლნ წელი, რაც დადასტურებულია პალეობიოლოგიური, მაგნიტოსტრატიგრაფიული და ეზოტოპური კვლევის მეთოდებით. დმანისის პალეოანთროპოლოგიურმა აღმოჩენებმა ძირფესვიან შეცვალეს ადრე არსებული წარმოდგენები უძველესი ადამიანის წარმოშობის, მიგრაციის გზებისა და ტემპების შესახებ. დღეს უკვე დადგენილია, რომ აფრიკიდან წამოსული ჰომინიდი (**Homo ergaster**) მშრომელი ადამიანი პლეიოცენის ბოლოს შემოვიდა სამხრეთ კავკასიაში და ბინადრობდა სამხრეთ საქართველოს ტერიტორიაზე.

წინამდებარე სტატია ეხება დმანისის ფაუნის ახალ ელემენტს — ზვეულრქიან ანტილოპას, რომელსაც ჩვის ჰომინიმური ზეცა ახასიათებს. გამოთქმულია მოსაზრება ზვეულრქიანი ანტილოპის სისტემატიკური ადგილისა და ცხოვრების ნირის შესახებ

REFERENCES

1. *I. Sokolov* (1953), Opyt estestvennoi klassifikatsii polorogikh (Bovidae), M. 295 p. (in Russian).
2. *G. Meladze* (1985), Obzor gipparionovoi fauny Kavkaza. Tbilisi, 175p. (in Russian).
3. *I. Sokolov* (1949), DAN SSSR, **27**, 6: 1101-1104 (in Russian).
4. *L. Gabunia* (1973), Belomechetskaia fauna iskopaemykh pozvonochnykh. Tbilisi, 137 p. (in Russian).
5. *G. Pilgrim* (1934), American Museum Novitates, **716**: 1-29.
6. *B. Bohlin* (1935), Palaeontologia Sinica, ser. C, **9**: 1-20.
7. *N. Vereshchagin, L. Alekseeva, A. David, V. Baigusheva* (1971), Pleistotsen Tiraspolia. 167-169, Kishinev (in Russian).
8. *D.S. Kostopoulos* (1997), Geodiversitas, **19**(4): 845-875.
9. *I. Sokolov, A. Vekua* (1966), Soobsh. AN Gruz. SSR, **43**, 1: 147-150 (in Russian).
10. *G. Meladze* (1967), Gipparionovaia fauna Arkhneti i Bazaleti. Tbilisi, 168p. (in Russian).
11. *A. Vekua* (1968), Soobshch. AN Gruz .SSR, **51**, 3: 120-137 (in Russian).

Received May, 2012

საქართველოს მეცნიერებათა ეროვნული აკადემიის მოამბე, ტ. 6, №3, 2012
BULLETIN OF THE GEORGIAN NATIONAL ACADEMY OF SCIENCES, vol. 6, no. 3, 2012

Linguistics

The "Regular" Type of Georgian Verbal Super-Paradigm

Giorgi Chikoidze

Archil Eliashvili Institute of Control Systems of Georgian Technical University, Tbilisi

(Presented by Academy Member Mindia Salukvadze)

ABSTRACT. The work is dedicated to the Georgian verb super-paradigm. The sums of the paradigms that are derived from one and the same lexical unit are meant under the name. The "regular" subset that is the most widespread and has less complicated structure, members of which consist of causative, active transitive and passive paradigms is used to regulate this rather numerous set. It is shown that the main actants of these paradigms behave correspondingly with certain semantic roles (CS, AG, OB, AD). One of the non-regular classes (INTR) the main difference of which is that OB role can be substituted by IC role (Intermediate Causer) is also considered in the paper. Ascertainment of the structure of these units first of all depends on surface appearance of verb-actant relations, which is realized by verb affixes and by the cases of actants. © *2012 Bull. Georg. Natl. Acad. Sci.*

Key words: *super-paradigm, action chain, semantic role.*

The super-paradigm is a set of Georgian verb paradigms derived from one and the same verbal lexeme. As a result these paradigms have a common semantic kernel and as a rule are derived from one and the same morphologic root.

The semantics of super-paradigm is based on the quite stable relations between participants of process/state defined by the semantic kernel of super-paradigm; nevertheless the grammatical form of actants expressing one and the same participant in the context of different members (paradigms) of super-paradigm are different. The main purpose of this work is demonstration and classification of correlations between choice of actants, grammatical form (in the first instance, of its case) and the semantic nuances which characterize the role and function of the corresponding participant in the context of the given paradigm. The peculiarities of these contexts which define the choice of actant, grammatical features essentially depend, in their turn, on the position of the given paradigm in the sequence of paradigms belonging to one and the same super-paradigm.

As to the ordering of the member-paradigms in the frames of their super-paradigm, it is based on semantic relations between these members and, in the first place, on the cause-consequential ones, according to which the position of each member in this "Action Chain" [1] should be situated after those by which the corresponding paradigm is conditioned

and before those ones which it itself conditions.

Analogous relations of causation and influence take place between the participants of process/state representing the semantic kernel of the super-paradigm. As a result they are also ordered and create something like "Actor Chain" [2], where each preceding link influences the following ones and, in the first instance, its immediate "right" neighbour.

These relations are, at least in the case of the "regular" super-paradigms, even more obvious than those between links of "Action Chain'. So, for example, if we consider super-paradigm:

1) A_1-ma aašenebina A_2-s A_3-i A_4-istvis/-s ('A_1 caused A_2 to build A_3 for A_4')

2) A_2-ma a(a/u)šena A_3-i A_4-istvis ('A_2 has built A_3 for A_4')

3) A_3a(/u)šenda A_4-istvis/-s ('A_3 was built for A_4'),

it becomes quite obvious that A_1 influences immediately A_2 stimulating him "to build A_3"; that endeavours of A_2 are immediately directed at A_3, which "is being created" by him; and that the final result of these "endeavours" (A_3) is oriented to A_4, which will become "the proprietor" of the latter. The most general scheme of these relations can be represented by (1)

$$A_1 \rightarrow A_2 \rightarrow A_3 \rightarrow A_4 \qquad (1)$$

where $(A_i \rightarrow A_{i+1})$ implies that A_{i+1} undergoes some kind of immediate influence from A_i.

The potential structure of a super-paradigm as an "Action Chain" can be represented as a sequence of three components:

$$CAUS \rightarrow PROC \rightarrow RES \qquad (2)$$

where the first member (CAUS) includes the actions which initiate actions of PROC and the latter ones produce as a result the state or process-RES. No one of them is obligatory: so, for example,

midis ('he goes'),

is represented by PROC only, though somebody/something causing this process can be pragmatically imagined without any difficulty. It is important to mention here that this verb has no RES-component either, because the latter implies something more than completion of the process expressed by the perfective form

mivida ('he came there');

Unlike this, the RES component must represent a "full-fledged" new process/state which emerged as a result of completion of the preceding PROC, particularly, as a result of its completion (but not as this "completion" itself).

The opposite example may be supplied by super-paradigms generated from verb lexemes like

qepa ('to bark'), c'uxili ('disturbance'), etc., which include all three parts of (2); so the super-paradigm corresponding to the c'uxili ('disturbance') is;

1. CAUS: 1.1) šeac'uxebina p'etrem p'avles ivane ('Peter caused Paul to disturb John')

2) šeac'uxa p'avlem ivane ('Paul has disturbed John')

2. PROC: šec'uxda ivane ('John became disturbed')

3. RES: c'uxs ivane/ ic'uxa ivanem/ uc'uxia ivanes ('John is/was turned out to be disturbed')

The chains (1) and (2) (of "actors" and of "actions") are correlated with each other, their development is in some sense, mutually parallel. Their interdependence is represented on the surface level by the verb affixes explicitly pointing to the actants representing some of the "actors" (A_1 of (1)), on the one hand, and the cases of these and some other A_i "actants", on the other.

Each paradigm of super-paradigm explicitly is addressed by its affixes one or two links of "Actor Chain" (1), and it is this choice that most obviously demonstrates the correlation between links of "action" and "actor" chains. Particularly, in the case of the pair of addressed "actors" the leading part belongs to the "upper" actor, that is, to the nearest to the "head" of the chain (1) with the minimal value of i.

The above mentioned regular super-paradigms "šeneba" ('to build') can be used as illustration of this aspect of correlation between two chains - (1) and (2): 1) affixes of first (causative) paradigm verbs

addresses the participant A_1, who has "caused" the process of "building", and his nearest right neighbour A_2, who immediately leads the process of "building"; 2) just the latter of them (A_2) is the "head" of sub chains of both active paradigms, addressed (ušenebs) and non-addressed (ašenebs); at the same time one of the following A_2 participants (A_3, A_4) can be chosen as the second member of this sub-chain of (1); 3) both passive paradigms (a(/u)šenda) have A_3 as "lead" participant, representing the object of immediate influence of A_2, which at the end of the process will be "given" to A_3, nearest right neighbour of A_3 and possible second link of sub-chain of passive paradigms.

So, if we accept the correspondence of causative paradigm to CAUS of (2), both actives "to PROC and both passives – to RES, we will have the obvious correlation between (1) and (2):

$$\text{CAUS} \leftrightarrow A_1, \text{PROC} \leftrightarrow A_2, \text{RES} \leftrightarrow A_3 \qquad (3)$$

Moreover, "Actor Chain" of some super-paradigm includes those and only those actors which are explicitly addressed at least by affixes of one of its paradigm. As a result the length of chain (1) varies for different super-paradigms: particularly, four members of (1) are characteristic of regular and some other super-paradigms, but many other ones deviate from this regular characteristic, which as it seems, should be the maximal one. One of the examples with a single actor was already mentioned earlier; it is the verb "midis" ('to go'); if the causative form of "akvs" ('to have') is acceptable ('akonina' A_1-ma A_2-s A_3-i " A_1 caused A_2 to have A_3), then this super-paradigm would have three participants, otherwise it would be only:

A_1-s akvs A_2-i (A_1 has A_2).

Nevertheless most super-paradigms have "Actor Chains" identical to (1), so that the shortening of this chain may be considered as some deviation from regularity, moreover the boundary between "regularity" and "non-regularity" is often not fully clear from this point of view (particularly, there often turns out to be a contradiction between purely grammatical and pragmatical considerations: e.g. c'vims – ac'vimebinebs/ ac'vimebs where causative forms are quite felicitous grammatically, but quite dubious pragmatically).

Up to now we considered the influence of verb affixation on the structure of super-paradigm, without taking into account the distinctions between kinds of this affixation, that is between roles of subjective (SUB) and objective (OBJ) types of verb affixes. The priority of the former one shows in the position of the actor to which SUB-affixes are most often addressed: it is the "head" position of the actor's sub-chain immediately addressed by verb affixes.

The most regular deviations from this rule represent the inversive verb forms, particularly, those of the III series; moreover it is the exchange of the positions of SUB and OBJ affixes that constitutes the main feature of this inversion. For that all other forms of regular super-paradigms satisfy this rule:

CAUS: (da)-v-axat'vine me (A^1_1) mas (A^2_2) – 'I(A^1_1) caused her/him (A^2_2) to draw'

PROC: da-v-(u)-xat'e me (A^1_2) is (A^2_2) (mas A_3) – 'I (A^1_2) drew it (A^2_3) (for her/him (A_4))'

RES: da-v-(i/e)-xat'e me (A^1_3) (for her/him A_3)';

in all these examples the "head" (first) position is occupied by the first person "me" ('I'), because it is addressed by the most obvious SUB affix (-v-); the lower index of A^j_i symbols corresponds to the basic position of A_i actor in "Actor Chain" (1) and the upper one (j) points to its position in sub-chain corresponding to the given verb form, that is including actors which are explicitly addressed by affixes of this form.

At the same time the III series forms of the same verbs demonstrate inversion of SUB and OBJ affixes, that is just OBJ affixes point at the first link of the sub-chain (A^1_1) and SUB – to the second one (A^2_{1+1}): e.g.

da-mi-xat'avs me (A^1_2) is (A^2_3) – 'it seems that I (A^1_2) have painted it (A^2_3)';

da-v-u-xat'i-v-ar me (A^2_2) mas (A^1_2) – 'it seems he (A^1_2) has painted me (A^2_2)';

the active actor ("painter") is addressed in the first example by the OBJ affix -mi- and the object of painting process (A^2_3)- by double SUB affixes -v- which additionally turns out in the auxiliary verb "var" ('I am') incorporated by the verb of the second example.

Other deviations from this rule are less regular, but for that matter, quite rare. So, some super-paradigms derived from lexical units with "emotional" semantics include paradigms which are inversive in all three series;

m-ʒuls/še-m-ʒulda/m-ʒulebia me (A^1_1) is (A^2_1) – 'I (A^1_1) hate/ begin to hate / it seems hate him (A^2_4)';

v-ʒul-v-ar/še-v-ʒuldi me(A^2_4) mas (A^1_1) – 'I (A^2_4) am / begin to be hatful for him (A^1_1)';

Some paradigms derived from lexical units with semantics oriented to (mostly "unconscious") states demonstrate analogoues inversive behaviour:

m-eʒineba/ m-ʒinavs me (A^1_1) – 'I (A^1_1) want to sleep/ sleep'.

Nevertheless the greatest part of verb paradigms (with the exception of the above mentioned forms of III series) follows the rule, according to which to SUB affixes may be ascribed higher priority than that of OBJ affixes:

$$SUB \rightarrow OBJ \rightarrow Z \qquad (4)$$

where Z symbolizes the lack of any explicit address to some actor by means of verb affixes.

Lastly, it is worth mentioning that we simplify (4) by ignoring the difference between direct and indirect objective affixation.

We have considered up to this point the expression of "action → actor" relation from the verbal point of view, but not less, perhaps even more, meaningful is the substantival aspect of this relation, particularly, the case values, which mark corresponding actants in all three series of verb paradigm and are the most important feature of these relations.

The main case values marking actants corresponding to "Actor Chain" (1) are:

e(rgative) – 'motxrobiti', n(ominative) – 'saxelobiti', d(ative) "micemiti'.

Just they mark the actants immediately addressed by SUB or OBJ affixes; the same actants, when they are not addressed explicitly, may be additionally marked by g(enitive) – 'natesaobiti', i(nstrumental) – 'mokmedebiti' and most often by some preposition combined with the corresponding case value (g+tvis, d+ze, …). The prepositional forms in general will be represented by the symbol – p, and other case values – by the first letter of their Latin terms. One more symbol (z) points to the lack of a corresponding actant form; which is conditioned by the lack of the corresponding verb form (e.g. by the lack of the II series forms; thus, for example, the verb paradigm jdoma ('to sit') has the forms of I ('zis'– 'is sitting') and III (mjdara – 'it turns out that she/he was sitting') series only.

It may be said that the complex language sign, the content of which corresponds to the action – actor relation, has expression, which on the level of the single paradigm as a whole is represented by a pair of correlated triples, the first of which includes the characteristics of verb affixes addressing the given actant (SUB, OBJ) and the other is represented by case markers of the actant, in the all series of the given paradigm. The full scheme of this expression can be given by (5).

$$VA_1, CV_1 – VA_2, CV_2 – VA_3, CV_3 \qquad (5)$$

where VA means Verbal Affixes (SUB, OBJ), CV – implies Case Value and the indexes point to the verb series (I, II, III respectively).

The values of VA_i and CV_i are strongly correlated and their interdependence supplies the possibility to restrict and accordingly to simplify (5). In the first instance, SUB affixes point to the "head" position of sub-chain corresponding to the given paradigm only and only two triples of CV may be combined with it:

n, e, d and n, n, n,

though the first of them changes in the inversional III series the SUB affixes by OBJ ones:

ašeneb-s is (A^1_2, n) mas (A^2_3, d) – 'he (A^1_2) is building (A^2_3)',

aušen-a man (A^1_2,e) is (A^2_3, n) – 'he (A^1_2) has built it (A^2_3)',

but

a-u-šenebia mas (A^1_2, e) is (A^2_3, n) – 'it turns out that he (A^1_2) has built it (A^2_3).

The first and second examples belonging to the I and II series have suffixes –s and –a of SUB type, but prefix -u- of III series form belongs to the OBJ type.

The behaviour of "head" position of causative paradigm (aašenebina man mas is) is identical with this of active one demonstrated above.

The use of this version of SUB is exhausted in the frames of regular super-paradigm by marking "head" positions of two paradigms, causative (A^1_1) and active (A^1_2). In terms of the (1) these versions of SUB address the left ("head") part of this chain, which represents the most active participants of the situation mirrored by regular super-paradigm: first of them (A_1) causes the activity of the other (A_2), which in its turn is directed immediately to A_3 and it is this influence of A_2 and A_1 that represents the core of super-paradigm semantics as a whole. Proceeding from this it seems sensible to consider A_1 as a causer (CS) of the situation and A_2 as an agent (AG), the influence of which on the A_3 as the object (OB) of AG's activity, which leads the process (PROC) that defines the essence of regular paradigm semantics.

The priority of SUB affixations supposed by (4) additionally justifies itself by marking the relation between verb and OB (A_3) placed in the "head" position, which it takes in the context of passive verb paradigms:

v-ixat'ebi / da-v-ixat'e / da-v-xat'vul-v-ar me (OB) – 'I'm being drawn / am drawn / it seems I'm drawn;

though in this context SUB is present in all three verb series (that is without exclusion of the third one), on the one hand, and is combined with the constant case value – n, which does not change by e in the second series and retains itself in the third series also, on the other hand:

ixat'eb-a is (OB-n) – daixat'-a is (OB-n) – daxat'ul-a is (OB-n) – 'she/he is being drawn / (it seems) is drawn.

In what follows we shall address these two modes of marking by their most characteristic components corresponding to the II series:

(SUB, e) and (SUB, n),

instead of

SUB, n – SUB, e – OBJ, d

And

SUB, n – SUB, n – SUB, n,

which give their full expression according to (5).

The "tail" link of (1), that is – A_3, does not take the "head" position in sub-chains of any paradigm of regular sub-paradigm and accordingly is never addressed by SUB affixes: its verb marker is OBJ which combines with d actant markers in the I and II series, but in the III series becomes "ignored" by the verb affixes (z) and is marked by some versions of prepositional actant form (pp) only:

u-xat'avs is (A_2, AG, n) mas (A_3, OB, d) mas (A_4, AD, d) – 'he/she paints something for somebody';

da-u-xat'a man (A_2, AG, e) is (A_3, OB, n) mas (A_4, AD, d) – 'he/she has painted something for somebody';

da-u-xat'avs mas (A_3, AG, d) is (A_3, OB, n) mistvis (A_4, AD, g+tvis) – 'it seems she/he has painted something for somebody';

The role of AD(dressee) of A_4 is quite obvious in this context (though in some other contexts it can be less definite).

The marking of this verb-actant (A_4, AD) may be characterized by the simplified expression of (5):

(OBJ, d – z, pp),

where the left part corresponds to I, II series and the right one – to the III series.

We have reached the "tail" of (1) by the last example (A_4, AD), at least in the case of the regular super-paradigms. This "tail" link of (1) can take the second position of the corresponding sub-chains (A_2, A_4 and A_3, A_4) only. We shall now consider the means of marking which characterize such second positions of the rest of the chain (1) that is of A_2 and A_3, because A_1 can belong to the first position of sub-chain and of the chain (1) as a whole. "By that we shall proceed in the direction opposite to the previous one: from the "tail" – to the "head".

Thus, in the first instance, after A_1 will be addressed A_3 (OB), which can be placed in the second position immediately after A_2 only: A_2A_3 is a sub-chain of the active paradigm which does not address A_4 (AD) explicitly. Receding to the back position A_3 (like the other links of (1)) becomes addressed by the OBJ affixes in I, II series

m-xat'avs / da-m-xat'a is /man (A_2 AG) me (A_3,OB) – 'she / he is drawing / has drawn me (A_3, OB)';

At the same time OB retains SUB addressation in the inversive III series:

da-v-uxat'i-v-ar mas (AG) me (OB) – 'it turns out that she/he has drawn me'.

As to case values, A_3 changes them in the I series only that is it becomes marked by d (instead of n):

(ixat'eba is (OB, n)) → xat'avs is (AG) mas (OB, d) – '(it is being painted) → she / he is painting it'. Thus "retreat" to the back position reduces the priority of OB markers: SUB→OBJ (I, II series) and n→d (I series). The former of these changes is inevitable (verb cannot address two different actants by one and the same type of affixes); as to the latter one, it may be supposed that language in this case (as in many others) avoids coincidence of forms of different members in one and the same context.

More drastic transformations follow AG's replacement to the second position of sub-chain corresponding to the causative paradigm: its marking becomes identical with that of AD (A_4):

OBJ, d – OBJ, d – Z, g +tvis.

It may be supposed that this coincidence has some semantic basis: obviously, AG functions in this causative context as an addressee (as a "sink") of stimulus information, which is immediately pointed at AG.

This combination of functions fulfilled by one and the same participant (A_2) in different contexts (causative, active paradigms) remembers the concept of "blending" [3], on the one hand, and underlines the fact that the surface characteristics of verb-actant relations have immediate deep semantic correspondences, on the other. It is the latter point that supports the supposition that these surface markings can be considered as an expression of a complex language sign.

Thus far we have considered the behavour of this sign in the frames of the super-paradigms, which were accepted as regular:

causative paradigm (CAUS)→ active transitive (PROC) → passive (RES).

The general "Actor Chain" (1) was interpreted in terms of semantic roles:

$$CS \rightarrow AG \rightarrow OB \rightarrow AD \qquad (6)$$

(the concrete interpretations of these terms here are quite different from those of [4], which nevertheless is the original general concept of "semantic role").

Each paradigm chooses some sub-chain of (6) pointing at its links by verb affixes (SUB,OBJ); causative paradigm – CS, AG; active – AG, OB/AD; passive – OB, (AD). Each position of these sub-chains can be characterized by combinations of surface markers: case values of actants representing semantic roles of (6) and verb affixes explicitly pointing at them. The most characteristic for super-paradigm surface structure are markers which show in the context of I and II (non-inversive) series: 1) the actants of "tail" positioned roles (AG^2, OB^2, AD) are addressed

by OBJ verb affixes and marked by n (OB) or d (AG, AD) case values.

According to the correlation between case values and positions of corresponding roles we can suppose the following scheme of priorities for the former ones;

$$e \rightarrow n \rightarrow d \rightarrow pp \qquad (7)$$

where the "head" position of e-value is justified by marking of "head" position role actants only; the third place of d-value is conditioned by its use mainly for marking second position actants; unlike them, n-value serves for marking of both positions of subchains and it is this that determines its intermediate place between e/d-values; lastly, the pp-value never marks actants of the role which does not belong to the sub-chain of the given paradigm, that is such that is not directly addressed by the verb affixes of this paradigm (though the same role may be expressed by an actant addressed by the verb affixes in the context of some other paradigm of the same super-paradigm, and, as a result, marked by e/n/d-values):

es saxli (OB, n) ašenda mistvis(AD, g+tvis) čems mier (AG, g+tvis)→me (AG,e) avušene mas (AD,d) es saxli (OB, n)

I have built something (for) him ↔ something was built by me (for) him!

The considerations given so far were mainly based on the most numerous class ("regular") class of Georgian super-paradigms. Of course this type, in spite of its multiplicity, does not exhaust the diversity of the whole set of these verbal super-units.

The choice of precisely this class is justified, besides its numerosity, by the relevant simplicity of its structure and, in the first instance, by transparency correspondence between the semantic roles (7) and their surface marking. One of the most essential features of this class is the stability of OB-role's behaviour: it is almost always present in non-elliptic utterances built on the basis of some verb belonging to the regular super-paradigm and, moreover, the surface marking of OB actants is remarkably stable in all these contexts: its case marker is mainly n, though sometimes – d, but never – pp, even in the contexts where OB is not immediately addressed by verb affixes.

The most essential deviation from the regularity of the super-paradigms, which may be considered next, is just the lacking of this central role of the regular ones, that is OB-role. This class, proceeding from this important quality, will be mentioned in what follows as an "intransitive" (INTR).

On example of this class (c'uxili- 'sorrow/worry') was given above. According to this single example it may be said already, that the main structure of this type of super-paradigm looks as: causative paradigm 1 – causative paradigm 2 (active, transitive) – passive – active intransitive paradigm; by that the first pair (causative 1, 2) fulfills the CAUS function of scheme (2), first passive corresponds to PROC and the last one – to the RES.

The behaviour of the "Actor Chain" "head" (A_1) is the same as in the previous case: it has obviously the status of "causer" (CS):

šeac'uxebina man (CS) mas (A_2) is (A_3) – 'She/he caused him to trouble somebody';

but the second position of this causative paradigm sub-chain (unlike the regular case) does not fulfill the AG role, which should be a "tail" of active part of the role chain : it influences one more participant (A_3), which, in its turn, is interpreted as active and at the same time represents the "tail" of activity (AG):

šeac'uxebina A_1-ma (CS) A_2 -s (IC) A_3 (AG)→ šeac'uxa A_2-ma A_3 – 'He/she has troubled somebody'; the result of the two proceeding ("causative") steps is that A_3 (AG) firstly "gets" in the state of "trouble" under immediate influence of A_2: šec'uxda is A_3 (AG) – "somebody gets troubled" and then the same A_3 (AG) "is troubled"/"has been troubled":

c'uxs is A_3 (AG) / ic'uxa man A_3 (AG).

The last two steps represent the PROC and RES studies of the whole super-paradigm proceeds: the first of them is formed as passive paradigm (šec'uxda)

and its single actant (A_2) is marked according to the usual rule of passives (SUB; n,n,n), as though it continues to be under the influence of A_2 (IC) exerted on it in the previous paradigm, where it was placed in the second position and as the result was marked as usual in this position by (SUB, d,n,n) that had the usual marking of OB in this position. It may be said that in these two steps (intermediate causation and caused by it the process of "getting in the final state") AG demonstrates the features of "blending" with OB, which nevertheless manifests itself as an explicit AG and the resulting ("tail") study of the whole process.

The preference given here to AG as a component of the "blend" may look somewhat doubtful and to solve this problem we propose the general principe, according to which the AG role should be ascribed to the active Ai nearest to the "tail" of (1) and "activity" as such should be defined by the type of surface marking of corresponding verb-actant relation in particular, it must be as a rule of "top priority", that is – (SUB, e). A_3 is marked in such way in a resulting state (c'uxs), which, according to this, is interpreted by the language as active ('somebody feels uneasy').

The final state (RES) of INTR class super-paradigm may have a quite "passive" interpretation also, as it is e.g. in the case of ʒili ('to sleep'), where obviously the "passive", "unconscious" participant's actant is marked by (OBJ,d), but, in spite of this, it is at the end considered as AG, thanks to the marking which it has in the preceding study (SUB,e):

iʒinebs is – daiʒina man – dauʒinia mas – 'she/he is asleep – it seems, that he has fallen asleep; and this process of "dropping to sleep" is interpreted as active, because this paradigm is the last one with actant marked by (SUB, e).

It can be supposed in general that INTR super-paradigm differs from regular ones, besides its lacking the OB role, by an additional paradigm with first position actant addressed and marked by (SUB,e).

The "tail" link of (1) can be again interpreted as AD; sometimes it corresponds to the AG's "proprietor", in some other contexts it may be the object to which the AG's activity is directed; an example given below demonstrates the case characterized by the possibility of both interpretations:

auqepa man(IC) mas (AD) ʒaɣli – 'he caused a/his dog to bark (on him/)'.

Thus, the main characteristics of the INTR class of super-paradigms can be represented by the following interpretation of the general chain (1):

$$CS \rightarrow IC \rightarrow AG \rightarrow AD$$

The "head" and "tail" links (CS, AD) of this scheme are identical with these of regular super-paradigm class. The differences between these classes are concentrated in its middle component, where AG is shifted from the second position (A_2) to the third (A_3) and the "gap" is filled out by the new role IC (Intermediate Causer). The scheme makes obvious both main features of INTR super-paradigms: lacking of OB role and a triple cascade of active roles (CS, IC, AG), the middle of which fills up the lack of OB.

Of course, the pair of super-paradigm classes considered above does not exhaust the variety of this set. This work makes an accent on the supposed centre of this set (regular) and demonstrates with a single example of INTR class the possible character of deviations from "regularity". The main merit of these examples is demonstration of the supposed basis on which the structure of super-paradigm can be built; "Actor chain" (1), "action Chain" (2), and correspondence between them (3). Moreover, the most important aspect of the proposed analyses is the preference of the features of surface representation, that is, of the means of marking of verb-actant relations corresponding to the predicate-role dependences.

This work is a continuation and development of Georgian super-paradigm study and of their untraditional concept justification, the beginning of which is given in [5] and [2].

ენათმეცნიერება

ქართული ზმნური სუპერ-პარადიგმის "რეგულარული" ტიპი

გ. ჩიკოიძე

საქართველოს ტექნიკური უნივერსიტეტის არჩილ ელიაშვილის მართვის სისტემების ინსტიტუტი

(წარმოდგენილია აკადემიკოს შ. ალექსიძის მიერ)

ნაშრომი ეძღვნება ქართული ზმნური სუპერ-პარადიგმების განხილვას. შემოკლებული სახელის ქვეშ იგულისხმება ზმნური პარადიგმების ერთობლიობა, რომელიც ნაწარმოებია ერთი და იმავე ლექსემისაგან. ამ საკმაოდ მრავალრიცხოვანი სიმრავლის მოსაწესრიგებლად გამოყენებულია მისი ერთეულების ყველაზე გავრცელებული და შედარებით მარტივი სტრუქტურის მქონე "რეგულარული" ქვესიმრავლე, რომლის წევრები შედგებიან კაუზატური, აქტიური გარდამავალი და პასიური პარადიგმებისგან. ნაჩვენებია, რომ ამ პარადიგმების ძირითადი აქტანტები იქცევიან გარკვეული სემანტიკური როლების შესაბამისად (CS, AG, OB, AD).

განხილულია აგრეთვე ამ ერთეულთა ერთ-ერთი არარეგულარული (INTR) კლასი, რომლის მთავარი განსხვავება მდგომარეობს OB როლის IC (შუალედური კაუზატორის) როლით შეცვლით.

ამ ერთეულთა სტრუქტურის დადგენა, პირველ რიგში, ეყრდნობა ზმნურ-აქტანტური მიმართებების ზედაპირულ გაფორმებას, რომელიც ხორციელდება ზმნური აფიქსების და აქტანტების ბრუნვების მეშვეობით.

REFERENCES

1. *R.W. Langaker* (1991), Concept, Image and Symbol: The Cognitive Basis of Grammar. Berlin-New York.
2. *G.D. Chikoidze* (2007), Proceedings of the 6th Tbilisi International Symposium on Logic, Language and Computation. Berlin-Heidelberg. 85-96.
3. *G. Fauconnier, M. Turner* (1996), Blending as a Central Process of Grammar. In: A.Goldberg (ed.), Conceptual Structure, Discourse and Language, CSLT (distributed by Cambridge University Press), 113-130.
4. *C.J. Fillmore* (1968), The Case for Case. In: E. Bach & RT Harms (Eds.), Universals of Linguistic Theory. New York.
5. *G.D. Chikoidze* (2010), Sistematizatsiia znachenii nekotorykh klassov iazykovykh edinits. Institut Sistem Upravleniia. Tbilisi, 519 p. (in Russian).
6. *R.D. Van Valin, Jr, R.J. Lapolla* (1997), Syntax, Structure, Meaning and Function (Cambridge Textbooks in Linguistics Series). Cambridge.

Received August, 2012

Economics

The Impact of Services Sector on Export Performance of Manufacturing Firms in Transition Economies

George Berulava

P. Gugushvili Institute of Economics, I. Javakhishvili Tbilisi State University

(Presented by Academy Member Leo Chikava)

ABSTRACT. The objective of the current paper is to explore the impact of services inputs on export performance of manufacturing firms in transition economies. The results of the study provide a new understanding of the consequences of trade liberalization in services sector. In particular, positive impact of services sector efficiency on export performance of manufacturers is revealed. Thus, advancing liberalization reforms in telecommunications, electric power, railway transport, road transport, and water distribution sectors as well as in banking sector will stimulate expansion of export activities of manufacturers. Along with services impact, we find that firm specific characteristics such as introduction of new products, investments in research and development, employment of advanced technologies, and employee skills are key drivers of export performance in manufacturing sector in transition economies. Firm's size and foreign investments do matter as well. The results of the study have several policy implications. The first insight is that an efficient service sector infrastructure represents a strategic and underexploited resource of export enhancement that can be influenced by policy makers. To stimulate export performance of manufacturing industries policy makers must emphasize further reforms and liberalization of their services sectors. These reforms must be focused on providing adequate access to services for downstream industries and thus on reducing their costs of doing business. Moreover, government should create favorable conditions for attracting foreign direct investments and encourage investments in innovation, research and development, employment of advanced technologies. A final policy point is that reducing trade related costs through trade and customs procedures facilitation would also increase exports. © *2012 Bull. Georg. Natl. Acad. Sci.*

Key words: *services sector, transition economies, export performance, manufacturing industry, panel data analysis.*

Exporting is an important type of economic activity that many consider crucial to the growth of productivity and living standards. The experience of the East Asian tigers provides evidence that exporting is an important component of the growth strategy in emerging markets [1]. Ensuring a favorable environment for exporting thus represents one of the key challenges for transition economies on their path to economic development.

Discussions of factors that determine success of

export performance have been ongoing for many years. Both the factors that are under the control of firm and external factors have been studied extensively in the academic literature. However, the role of services sector as one of the external factors in promoting export performance of downstream sectors remained relatively unstudied. The existing research of the consequences of services sector liberalization is limited mainly to the analysis of the impact of services sectors on the productivity in downstream industries [2-5].

In this paper we extend the existing research by emphasizing the relationship between the services sectors and the export performance of downstream industries. In particular, the objective of the study is to explore the impact of services inputs on export performance of manufacturing firms in transition economies.

The results of the study are intended to improve our understanding of the consequences of services sector policy, and thus they extend the existing theoretical framework. However, the findings of the current research are important not only for theoretical but also for practical considerations. They provide grounds for recognizing key determinants of manufacturers' export performance in transition economies. In that way, the research contributes to the ongoing political debate on economic development issues and provides insights for targeting of public policies.

This paper focuses on the role of the services sector in influencing export performance of manufactures in transition economies. The literature indicates that countries in transition can benefit from increased exports. An increase in exports might boost productivity through "learning by exporting" of individual companies; or it may allow additional imports of high tech products. Either avenue would stimulate economic growth.

Though the productivity-export link has been studied very extensively in recent years, some aspects of this relationship remain relatively unexplored. For instance, the now large heterogeneous firms' literature initiated by Melitz [6] suggests that the more productive firms are the ones that export. Melitz assumes that there is a fixed cost in selling in export markets and only the more productive firms will choose to export, while less productive firms will decide to serve the domestic market. In this stream of research, high-productivity of firms that self-select into export markets is considered as an outcome of firm's deliberate strategy. However, the productivity of firms can be caused also by factors external to the firm and which are not under its control. The recent empirical research of the relationship between export activity and external factors influencing productivity is focused mainly on the study of the effects of business climate variables. For instance, Clarke [7] in a study of African exporters finds that in addition to enterprise characteristics, policy-related variables also affect export performance. In particular, the author suggests that restrictive trade and customs regulations as well as poor customs administration can discourage manufacturing enterprises from exporting. Balchin and Edwards [8] find that the business climate is closely associated with firm-level manufacturing export performance in Africa. The empirical evidence on the effects of business climate and infrastructure on manufacturers' export supply capacity is also documented in [9-12].

Similarly, liberalization of the services sectors can be considered as one of the external factors that positively influences costs and productivity of downstream firms' and thus promotes their export activities. Services can be viewed as a factor of production along with labor, capital and other inputs. The enhancement of services inputs can reduce production costs, increase the marginal productivity of other inputs and raise output. The impact of services sector liberalization on the productivity in downstream sector is well documented in academic literature [2-5]. These studies indicate that the availability of high-quality and low cost services contributes to the reduction of costs and increase of productivity of downstream manufacturing firms. Taking into account

the fact that services sector efficiency is an important determinant of manufacturing firm productivity and productivity is a crucial factor of exporting, one may hypothesize that services sector liberalization through the improvement of productivity of the firms in downstream industries can increase their exports.

Again relying on Melitz [6], services sector liberalization can positively influence not only the export intensity of manufacturers but also their decisions to participate in export markets and the number of export markets that they serve. To be more precise, theory suggests that a more efficient services sector through increasing the productivity of firms and reducing the fixed costs of exporting can boost the number of firms in downstream industries that "self-select" into export markets. Thus, services sector liberalization, by increasing the efficiency, variety and quality of services markets, can then increase exports.

Though theory indicates that better services should increase exports (both intensively and extensively), the empirical links are not well studied. Further, those studies that do exist are based on African or Latin American data, so there is a lack of literature based on transition country data. In this research we try to fill this gap by examining the relationship between performance of services sector and export performance of manufacturing firms in transition economies.

Based on the literature review, the main research hypothesis of the study can be formulated as follows: ***the enhancement of services sector positively and significantly influences both the decision of manufacturers to participate in export markets ("extensive margin") and their export intensity in any market ("intensive margin").***

Research Methodology. In order to test the research hypothesis and to estimate the impact of services inputs on export performance of manufacturers we use the following panel data regression model:

$$EI_{it} = \gamma' SI_{it} + \psi' C_{it} + \varepsilon_{it}$$

where γ', and ψ' are vectors of parameters to be estimated

EI- export intensity (exports/total sales).

SI- vector of services input variables that reflect performance of three services sectors – telecommunications, electricity, finance. In this study we use two groups of services input variables. The first group reflects the subjective measures that are based on firm's valuation on a scale from 1 to 5 as to how much of a constraint they consider telecommunications, electricity and finance for their business. The second group of variables are EBRD (European Bank for Reconstruction and Development) indices of policy reforms [13], which reflect the overall liberalization of services sector. In particular in this study we employ: EBRD overall index of infrastructure reform, which reflects reforms in telecommunications, electric power, railway transport, road transport, and water distribution sectors; and EBRD index of banking sector reform.

C-set of control variables: firms size; employment of advanced technologies; dummy variable, which reflects whether the firm in the last three years invested in research and development; dummy variable, which reflects whether the firm in the last three years introduced new products or services; dummy variable for foreign ownership; industry type; employee skills is measured by percent of employees with tertiary education; degree of competition; regulatory quality; dummy variable which reflects whether the firm is located in the capital; European Union membership.

ε_{it} is an error term, which consists of two error components: α_i - the unobservable individual (time-invariant) effect which may be correlated with the observed variables SI_{it} and C_{it}; and ν_{it} - the remainder disturbance, which varies with individuals and time and can be thought of as the usual disturbance in the regression. α_i and ν_{it} are assumed to be *i.i.d.* $(0,\sigma_\alpha)$ and *i.i.d.* $(0,\sigma_\nu)$, respectively.

In this model productivity doesn't enter in the equation directly. We proxy the productivity by firm-

specific characteristics, like size, foreign ownership, employee skills, etc. and services inputs variables.

However, some issues can arise while estimating the model. First, since the export intensity is a truncated variable the sample selection bias issue can arise while estimating the model. The second problem is related to potential endogeneity of service input variables as well as some other independent variables.

To deal with selection bias problems the two-stage estimation process will be employed in this study [14-16]. First, we formulate a model for the probability of exporting. At this stage we employ the following selection variable: EF – export facilitation index constructed using principal component factor analysis from the *Doing Business* database (www.doingbusiness.org). The index consists of the following elements: number of all documents required to export goods; time necessary to comply with all procedures required to export goods; cost associated with all the procedures required to exporting. The estimation is conducted using standard probit regression.

At the second stage, we correct for self-selection by incorporating a transformation of the predicted individual probabilities or the inverse Mills ratio (obtained from the first stage probit regression estimation) as an additional explanatory variable to regression equation.

To address the problem of endogeneity of the services input variables, which are very likely to be correlated with individual specific effect (a_i), the export intensity equation will be estimated by applying Hausman-Taylor IV estimation procedure [17].

The main source of the data for the research is the micro-level unbalanced panel data from the Enterprise Surveys database (Business Environment and Enterprise Performance Survey (BEEPS) Panel - https://www.enterprisesurveys.org/). The surveys were conducted by the EBRD and the World Bank Group (the World Bank) in 2002, 2005, 2007, and 2008/09 for firms in 29 countries in the European and Central Asian region. The panel provides totally 29,386 observations. Since the objective of our study is the export performance of manufacturing firms, we limit the sample only to manufacturing sector. This gives us the final sample size of 11,293 observations at the firm level, which corresponds to 10263 firms. On average there are 1.1 years of data per firm available.

Results. Five different specifications of the model are estimated. Each of five services input measures enters the model one by one (The discussion of the first-stage probit equation estimation results is omitted here. The full version of the study can be found in [18]).

Table presents results of the estimation of the impact of services input variables on the export intensity of manufacturers. Hausman-Taylor estimation procedure employed at this stage allows controlling for endogeneity of services input variables caused by their correlation with unobserved individual level heterogeneity. All the five equations have Wald chi-square significant at 1% level. The inverse Mills ratio is significant at $p < 0.01$ level and positive, which reflects the significance of the first-stage selection equation. In conformity with the main research hypothesis electricity and telecommunications sector have significant ($p < 0.01$) impact on export intensity of manufacturers. According to data from Table the obstacles created by these two service sectors for the business activities of individual manufacturers have negative impact on their export performance. The obstacles formed by finance sector also have negative impact on manufacturer's exporting. However, this impact is not statistically significant.

Similarly, the overall liberalization of service sector (EBRD index of infrastructure reform) and reforms in banking sector (EBRD index of banking sector reform) have significant (at 5% level) and positive effect on export performance of downstream firms. Thus deep reforms and liberalization in such service sectors as electric power supply, railways, roads, tel-

Table. Export Intensity Models.

Variables	Coefficients				
	I	II	III	IV	V
Dependent Variable: Export Intensity (EI)					
Electricity as an obstacle	-2.281*** (.6238)	-	-	-	-
Telecommunications as an obstacle	-	-6.093*** (.7216)	-	-	-
Finance as an obstacle	-	-	-.1498 (.5666)	-	-
EBRD index of infrastructure reform	-	-	-	9.297** (3.885)	-
EBRD index of banking sector reform	-	-	-	-	9.3904*** (2. 837)
Innovation during last 3 years	11.894*** (1.563)	11.929*** (1.472)	12.724*** (1.575)	4.116*** (1.069)	11.358*** (1.513)
R&D during last 3 years	5.878*** (1.492)	5.348*** (1.452)	2.817* (1.479)	2.281 (1.434)	5.630*** (1.608)
Technological level of company (high-speed internet connection)	8.989*** (2.185)	7.674*** (2.082)	6.053*** (2.277)	7.823*** (2.511)	5.737*** (2.183)
Employee skills	.0527** (.0265)	.048* (.0259)	.034* (.0267)	.014 (.0274)	.0669** (.0303)
Foreign ownership	24.513*** (2.205)	23.741*** (2.127)	23.604*** (2.300)	11.606*** (2.035)	23.725*** (2.310)
Size (small firm)	-44.511*** (3.88)	-44.052*** (3.747)	-43.043*** (3.933)	-16.047*** (3.626)	-45.776*** (4.409)
Size (medium firm)	-16.066*** (1.67)	-15.981*** (1.665)	-16.370*** (1.729)	-9.592*** (1.724)	-17.406*** (1.832)
Location in Capital	-8.914** (3.856)	-2.335 (3.439)	-9.131** (3.875)	11.451*** (3.94)	-10.029** (4.012)
European Union country	6.336*** (1.518)	6.078*** (1.561)	6.733*** (1.607)	-	-
Competition	10.851*** (1.136)	10.689*** (1.093)	9.902*** (1.135)	4.173*** (.4676)	9.457*** (1.094)
Regulatory quality	4.556*** (1.212)	5.235*** (1.264)	4.520*** (1.242)	-4.515 (4.907)	-5.564 (5.772)
Inverse Mills ratio	21.651*** (3.525)	19.990*** (3.235)	19.054*** (3.598)	6.510** (2.844)	19.499*** (3.619)
sigma_u	90.479	99.150	100.946	87.660	96.306
sigma_i	13.732	13.355	13.804	13.731	13.892
rho	.9774	.9821	.9816	.9760	.9796
Number of obsevations	2598	2598	2511	2507	2507
Wald chi-sq (df)	769.02*** (22)	825.44*** (22)	760.75*** (22)	698.87*** (21)	727.90*** (21)

Standard errors are in parentheses. *** — significant at $p < 0.01$ level; ** — significant at $p < 0.05$ level; * — significant at $p < 0.1$ level.

ecommunications and water supply as well as in banking sector substantially improves export activity of manufacturing firms. These findings, in general, provide support for the main research hypothesis of the study that the enhancement of services sector positively and significantly influences export performance of downstream industries.

The effects of firm specific characteristics – innovations, research and development, employment of advance technologies, employee skills, size and foreign ownership - are generally significant (in most specifications at 5% level) and have expected signs. Introduction of new product and services, investment in research and development as well as employment of advanced technologies (high-speed, broadband internet connection) increase competitiveness of the manufacturing firms at global markets and thus encourage export intensity.

Firm size and foreign ownership also have positive and significant impact on the expansion of export activities. Large firms have more advantages in accessing to finance, necessary for establishing distribution networks at global markets. Generally larger firms have more resources for investments necessary for attaining of competitive advantage globally. This is especially true for transition economies. Foreign ownership, in turn, facilitates transfer of advanced managerial expertise, skills and technologies that makes firm more competitive at international markets. Employee skills variable is also expected to have a positive impact on export performance. This variable measured as a percentage of employees with tertiary education, is supposed to enhance firm's productivity and thus to improve its competitiveness at export markets. The results in Table show that employee skills have positive effect on export intensity; however, this effect is not significant in all specifications.

Among the environmental variables competition, regulatory quality and membership in European Union are important predictors of export performance of manufacturers. Study results show that competition measured as a pressure on companies to develop a new product and reduce costs encourages export intensity of manufacturers (significant at $p< 0.01$). Regulatory quality has positive and significant at 1% level effect (non-significant in models IV and V) on export intensity. Better business environment reduces costs of doing business, improves competitiveness and thus makes it easier to expand business activities at export markets. The non-significant coefficients of this variable in models IV and V can be explained by correlations with respective EBRD indices used in these specifications. The same is true for the variable which reflects membership in European Union. Industry effect is controlled but not reported in the Tables.

Conclusions. Generally, the key finding of the study is that improvement in the services sectors would enhance the export performance of manufacturers in transition economies. In particular, the study results suggest that reducing constraints and obstacles originating from inefficiencies in electricity, telecommunication, infrastructure and banking will encourage export performance of downstream industries. Thus, advancing liberalization reforms in telecommunications, electric power, railway transport, road transport, and water distribution sectors as well as in banking sector will stimulate expansion of export activities of manufacturers. Our results also suggest that services reform impacts more strongly on the intensity of existing exporters than it does in encouraging new exporters or new export markets.

This paper looks at firm specific factors that affect the export performance of manufacturers in transition economies as well. Consistent with the results in existing research, we find that firm specific characteristics such as the introduction of new products, investment in research and development, employment of advanced technologies, and employee skills are key drivers of export performance in the manufacturing sectors of transition economies. Introduction of new products and services, investment in research and development as well as employment of advanced

technologies (high-speed, broadband internet connection) increase the competitiveness of the manufacturing firms in global markets and thus improve export performance.

We find that size of the firm and foreign investment do matter as well. These factors significantly and positively affect not only the decision to export, but also export intensity of manufacturers. Large firms have more advantages in accessing to finance, which is necessary to establish distribution networks in foreign markets. Generally they have more resources for the investment necessary for attaining of competitive advantage globally. This is especially true for transition economies. Foreign ownership, in turn, facilitates transfer of advanced managerial expertise, skills and technologies that makes the firm more competitive in international markets. We also find that other factors such as trade facilitation, regulatory quality, the degree of competition, membership in European Union also positively affect exports.

The results of the study have several policy implications. The first insight is that an efficient service sector infrastructure represents a strategic and underexploited resource of export enhancement that can be influenced by policy makers. To stimulate export performance of manufacturing industries policy makers must emphasize further reforms and liberalization of their services sectors. These reforms must be focused on providing adequate access to services for downstream industries and thus on reducing their costs of doing business. Moreover, government should create favorable conditions for attracting foreign direct investments and encourage investments in innovation, research and development, employment of advanced technologies. A final policy point is that reducing trade related costs, through trade and customs procedures facilitation, would also increase exports. Private entrepreneurs should also expect that their investments in innovation, research and development, employee skills and advanced technologies will be beneficial for their export activity.

Acknowledgements. I gratefully acknowledge the financial support from Economics Education and Research Consortium (EERC), the World Bank and the Government of Austria. I would like to thank the panel of experts, who took part in the 1-st, 2-nd, 3-rd and 4-th "The Economic Impact of Liberalization of Barriers in Services in the Europe and Central Asia Regions" workshops, for valuable comments and suggestions. Especially, I am heavily indebted to Oleksandr Shepotylo, Vladimir Vakhitov and David Tarr for detailed discussions, comments, and guidance. I am responsible for all remaining errors.

ეკონომიკა

მომსახურების სექტორის გავლენა სამრეწველო ფირმების საექსპორტო საქმიანობაზე გარდამავალ ეკონომიკებში

გ. ბერულავა

ი. ჯავახიშვილის ეკონომიკის ინსტიტუტი, ი. ჯავახიშვილის სახ. თბილისის სახელმწიფო უნივერსიტეტი

(წარმოდგენილია აკადემიის წევრის ლ. ჩიქვას მიერ)

ამ სტატიის მთავარი მიზანია მომსახურების სექტორის სამრეწველო საწარმოების საექსპორტო საქმიანობაზე გავლენის შესწავლა გარდამავალ ეკონომიკებში. კვლევა მომსახურების სექტორის ლიბერალიზაციის შედეგებზე ახალ შეხედულებას გვთავაზობს. კერძოდ, კვლევის მიერ დადგენილია მომსახურების სექტორის ეფექტიანობის დადებითი გავლენა მწარმოებლების საექსპორტო საქმიანობაზე. გარდა ამისა, აღმოჩენილია ინოვაციის, კვლევასა და განვითარებაში ინვესტიციების, ახალი ტექნოლოგიების, მომსახურე პერსონალის უნარ-ჩვევების მნიშვნელოვანი გავლენა საწარმოების საექსპორტო საქმიანობაზე გარდამავალ ეკონომიკებში. ფირმის ზომა და უცხოური ინვესტიციები აგრეთვე თამაშობენ მნიშვნელოვან როლს.

REFERENCES

1. World Bank (1996), *The East Asian Miracle: Economic Growth and Public Policy*, World Bank Policy Research Reports (Oxford University Press).
2. *J.M. Arnold, B. Javorcik and A. Mattoo* (2011), Does services liberalization benefit manufacturing firms: evidence from the Czech Republic, *Journal of International Economics*. **85**, 1: 136-146.
3. *J.M. Arnold, A. Mattoo and G. Narciso* (2006), Services inputs and firm productivity in Sub-Saharan Africa: evidence from firm-level data, *The World Bank, Policy Research Working Paper 4048*.
4. *F. Eschenbach and B. Hoekman* (2006), Services policy reform and economic growth in transition economics, *Review of World Economics*. **142**, 4: 746-764.
5. *A.M. Fernandes and C. Paunov* (2012), Foreign direct investment in services and manufacturing productivity growth: Evidence for Chile, *Journal of Development Economics*. **97**, 2: 305-321.
6. *M.J. Melitz* (2003), The impact of trade on intra-industry reallocations and aggregate industry productivity, *Econometrica*. 71: 1695-1725.
7. *G. Clarke* (2005), Beyond tariff and quotas: why don't African manufacturing enterprises export more? *The World Bank, Policy Research Working Paper WPS3617*.
8. *N. Balchin and L. Edwards* (2008), Trade-related business climate and manufacturing export performance in Africa: a firm-level analysis, *Paper presented at the 2008 Conference of the African Econometric Society (AES). Pretoria, South Africa*. Available at:http://www.africametrics.org/documents/conference08/day2/session5/balchin_edwards.pdf.

9. *A. Escribano and J.L. Guasch* (2005), Assessing the impact of the investment climate on productivity using firm-level data: methodology and the cases of Guatemala, Honduras, and Nicaragua, *The World Bank, Policy Research Working Paper 3621*.
10. *D. Dollar, M. Hallward-Driemeier and T. Mengistae* (2006), Investment climate and international integration, *World Development*. **34**, 9: 1498-1516.
11. *T. Iwanow and C. Kirkpatrick* (2008), Trade facilitation and manufactured exports: is Africa different? *World Development*. **37**, 6: 1039-50.
12. *A. Portugal-Perez and J.S. Wilson* (2010), Export performance and trade facilitation reform: hard and soft infrastructure, *Policy Research Working Paper 5261, The World Bank Development Research Group, Trade and Integration Team*.
13. EBRD (2009), Transition report 2009: transition in crisis? European Bank for Reconstruction and Development. Available at: http://www.ebrd.com/downloads/research/transition/TR09.pdf
14. *J.J. Heckman* (1979), Sample selection bias as a specification error, *Econometrica*. **47**, 1: 153–161.
15. *E. Helpman, M. Melitz, and Y. Rubinstein* (2008), Estimating trade flows: trading partners and trading volumes, *Quarterly Journal of Economics*. **123**, 2: 441-487.
16. *O. Shepotylo* (2009), Export diversification across industries and space: Do CIS countries diversify enough? *Discussion Papers 20, Kyiv School of Economics*.
17. *J.A. Hausman and W.E. Taylor* (1981), Panel data and unobservable individual effect, *Econometrica*. 49: 1377-1398.
18. *G. Berulava* (2011), Services Inputs and Export Performance of Manufacturing Firms in Transition Economies, *EERC Working Paper Series 11/17e*, 23 p.

Received June, 2012

მეგზური ავტორთათვის

1. წარმოდგენილი სტატია დაბეჭდილი უნდა იყოს A4 ფორმატის თეთრ ქაღალდზე ორი ინტერვალით, ზედა და ქვედა არეები – 20-20 მმ, გვერდითი არეები - 30-30 მმ. სტატიის სიგრძე არ უნდა აღემატებოდეს 12 ნაბეჭდ გვერდს, ფორმულების, ცხრილებისა და სურათების ჩათვლით.

2. სტატია წარმოდგენილი უნდა იყოს ინგლისურ ენაზე მთავარი რედაქტორის სახელზე. სტატიას უნდა ახლდეს აგრეთვე:

- ცნობები ავტორის (ავტორების) შესახებ, მოცემულ შრომაში მისი წვლილის აღნიშვნით;
- აკადემიის წევრის წარდგინება ან ორი კვალიფიციური რეცენზია სხვადასხვა ინსტიტუტებიდან (თუ ავტორი არ არის აკადემიის წევრი); მიმართვა რედაქციის სახელზე გამოქვეყნების თხოვნით იმ დაწესებულებიდან, სადაც შესრულებულია შრომა;

სტატიას განიხილავს სარედაქციო საბჭო და გადაწყვეტს მისი გამოქვეყნება-არგამოქვეყნების საკითხს.

3. სტატია უნდა გაფორმდეს შემდეგი სახით:

- მეცნიერების დარგი;
- სტატიის სათაური;
- ავტორის (ავტორების) სრული სახელი, გვარი;
- სამუშაო ადგილი, საფოსტო მისამართი, ელექტრ. ფოსტა;
- ნაშრომის წარმომდგენი აკადემიის წევრის გვარი;
- რეზიუმე;
- საკვანძო სიტყვები;
- ტექსტი. ტექსტის ბოლოს დაფინანსების წყაროს და მადლობების ჩამონათვალი;
- ინგლისური ტექსტის შემდეგ რეზიუმე ქართულ ენაზე (გაფორმებული იმავე თანმიმდევრობით, როგორც ინგლისური ტექსტი), მოცულობა ერთ გვერდამდე;
- დამოწმებული ლიტერატურის სია უნდა დალაგდეს ტექსტში ციტირების მიმდევრობის მიხედვით (ლიტერატურა ტექსტში აღნიშნული უნდა იყოს ციფრებით კვადრატულ ფრჩხილებში);
- ნახაზები და ცხრილები მოცემული უნდა იყოს ცალკე გვერდებზე. ფოტოები – ორიგინალის სახით;
- სურათებს უნდა ახლდეს წარწერები;

სტატიის ბოლო გვერდზე უნდა იყოს ყველა ავტორის ხელმოწერა (გარკვევით).

4. ელექტრონული ვერსია: CD-ROM, შრიფტი – Times New Roman. ტექსტი: Supply – Word, Word Perfect, RTF. ცხრილები და ნახაზები წარმოდგენილი უნდა იყოს ცალ-ცალკე ფაილად, ნახაზები უნდა შესრულდეს TIFF, EPS, მაღალი ხარისხის PDF, JPEG, ცხრილები: Word, Word Perfect, RTF. ფორმულები Equation 3.0, Equation 5.0;

5. სტატიის ტიპოგრაფიული თუ ელექტრონული სახით გამოქვეყნებაზე ავტორმა უნდა განაცხადოს თანხმობა;

მიღებული სტატიის გასწორებული ვერსია, ან დაწუნებული ნაშრომი ავტორს არ უბრუნდება.

სარედაქციო საბჭო არ განიხილავს ნაშრომს, რომელიც მოთხოვნების მიხედვით არ იქნება გაფორმებული.

ავტორს შეუძლია ნიმუშად გამოიყენოს ჟურნალის რომელიმე ნომერი.

6. რუსული ტექსტის ტრანსლიტერაცია მოცემულია ლათინური ასოებით კონგრესის ბიბლიოთეკის სისტემის მიხედვით.

7. ნაშრომის გამოქვეყნება უფასოა.

GUIDE FOR AUTHORS

Manuscripts should be presented in the following form:

1. Two double-spaced copies of the manuscript, printed on a white paper A4, marginated 20 mm below and above, 30 mm on the sides, must be provided. The length of the manuscript should not exceed 12 printed pages, including all text with figures, tables, and equations.

2. Manuscripts should be written in English and sent to the Editorial Board. Attached to the manuscript should be:

- Short information about the research work by the author(s), including specific contribution to the published work;
- Qualified references from different Institutions;

Articles will be evaluated by the Editorial Board and may be rejected or subjected to further review.

3. Manuscript order:

- Classification;
- Title;
- Full name(s), surname(s) of the author(s);
- Affiliation(s), postal address, e-mail;
- Abstract;
- Key words;
- Text, including acknowledgements and funding sources;
- References in the order of citation (square brackets used);
- Figures and Tables must be given on separate pages. Pictures and photos must be original;
- Figure legends;
- The last page of the manuscript must be signed by the author(s).

4. Electronic version: CD-ROM in Times New Roman. Text: Supply Word, Word Perfect, RTF. Figures and Tables must be submitted as separate files, not imbedded in manuscript text. Provide figure images in TIFF, EPS, high resolution PDF, JPEG. Tables: Supply Word, Word Perfect, RTF. Include one Table per file. Do not use tabs or spaces to separate columns in Word or Word-Perfect Tables.

5. The author will be asked to give consent to publish the manuscript in print and electronic version. Corrected version is not returned to the author(s). The Editorial Board reserves the right not to consider the paper, if the instructions are ignored. For symbols and style conventions, authors should consult current issues of the Journal.

6. Transliteration of the Russian text into Roman letters should be given according to the LC system.

7. Publication is free of charge.

Starting with the year 2009 each Volume of the Bulletin of the Georgian National Academy of Sciences appears in three Issues annually

Subscription Information:

Correspondence regarding subscriptions and manuscript publications should be sent to:

Georgian National Academy of Sciences,
52, Rustaveli ave, 0108 Tbilisi, Georgia
Phone:+995-32 99-75-93
Fax/Phone: +995-32 99-88-91
E-mail: Bulletin@science.org.ge

The online edition of the *BULLETIN* is available from the website of the Academy at:
http://www.science.org.ge
http://www.science.org.ge/moambe/moambe.html

რედაქციის მისამართი: 0108, თბილისი-8, რუსთაველის პრ. 52. ტელ.: 299-75-93

INDEX 76181

GEORGIAN NATIONAL ACADEMY OF SCIENCES

0108 Tbilisi, Georgia
52 Rustaveli ave
Tel.: (+995 32) 2 99 88 91;
Fax/Tel.: (+995 32) 2 99 88 23
E-mail: bulletin@science.org.ge
academy@science.org.ge

საქართველოს მეცნიერებათა ეროვნული აკადემია

0108 თბილისი,
რუსთაველის პროსპ. 52
ტელ.: 2 99 88 91; ფაქსი: 2 99 88 23
ელ. ფოსტა: bulletin@science.org.ge
academy@science.org.ge